ERDC/CHL TR-16-9

US Army Corps
of Engineers®
Engineer Research and
Development Center

ERDC
INNOVATIVE SOLUTIONS
for a safer, better world

Coastal Inlets Research Program

Assessment of Modifications for Improving Navigation at Hilo Harbor, Hawaii

Zeki Demirbilek, Lihwa Lin, Okey G. Nwogu,
Kent K. Hathaway, William C. Butler, Jessica H. Podoski,
and Thomas D. Smith

June 2016

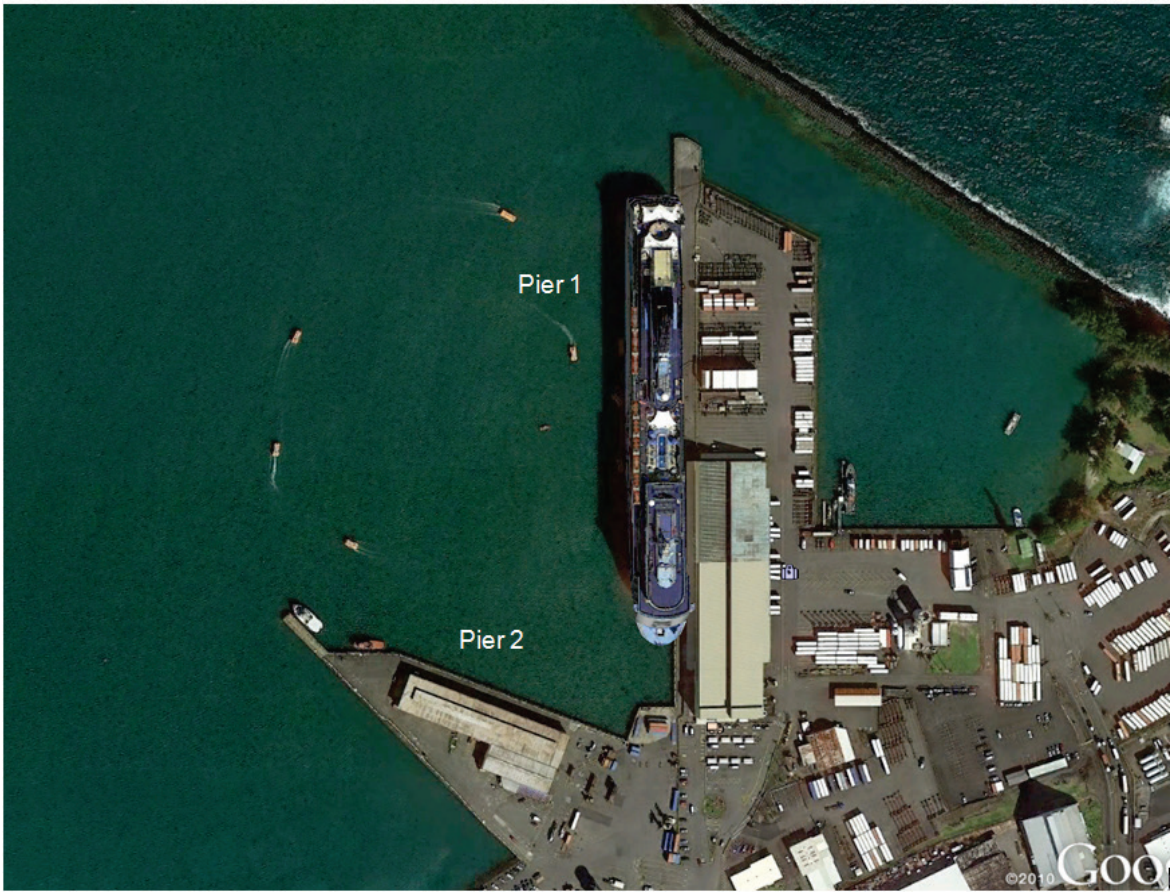

Coastal and Hydraulics Laboratory

The U.S. Army Engineer Research and Development Center (ERDC) solves the nation's toughest engineering and environmental challenges. ERDC develops innovative solutions in civil and military engineering, geospatial sciences, water resources, and environmental sciences for the Army, the Department of Defense, civilian agencies, and our nation's public good. Find out more at www.erdc.usace.army.mil.

To search for other technical reports published by ERDC, visit the ERDC online library at http://acwc.sdp.sirsi.net/client/default.

ERDC/CHL TR-16-9
June 2016

Assessment of Modifications for Improving Navigation at Hilo Harbor, Hawaii

Zeki Demirbilek, Lihwa Lin, Kent K. Hathaway, and William C. Butler

Coastal and Hydraulics Laboratory
U.S. Army Engineer Research and Development Center
3909 Halls Ferry Road
Vicksburg, MS 39180-6199

Okey G. Nwogu

University of Michigan
Department of Naval Architecture and Marine Engineering
2600 Draper Road
Ann Arbor, MI 48109-2145

Jessica H. Podoski and Thomas D. Smith

U.S. Army Corps of Engineers, Honolulu District
Building T223
Fort Shafter, HI 96858

Final report

Prepared for U.S. Army Engineer District, Honolulu
Building T223
Fort Shafter, HI 96858

Under Project 454634, "A1100-FY16 Rosati-Waves Navigation Structures"

Abstract

Numerical wave and flow modeling studies were conducted to evaluate modifications to improve navigation at Hilo Harbor, HI. Analysis of field data, hydrographic surveys, and numerical and ship simulation modeling calculations are described in this report. The existing mooring and turning basin area adjacent to the Federal channel cannot safely accommodate the size of vessels presently using the harbor. A second issue affecting navigation in Hilo Harbor is the *surge* problem, which occurs mostly during winter swells when ships are in the berthing areas, describing*a pulling away of ship* movement from the piers, a form of long-period wave phenomenon commonly known as *harbor oscillation*.

CMS-Wave and BOUSS-2D models were used to investigate potential Alternatives to address navigation conditions in Hilo Harbor, with field data from 2007 and 2013–14 for calibration of the numerical models. Alternatives considered included modifying the breakwater, incorporating structures in the interior harbor, and deepening and expanding the mooring basin to provide more space for safe mooring and maneuvering of ships. Results of this study indicated that the addition of a spur to the western-most tip of breakwater would provide the greatest reduction in wave and currents in the harbor.

Contents

Figures and Tables

Figures

Tables

Preface

This study was conducted for the U.S. Army Engineer District, Honolulu (POH), under Project Number 454634, "A1100-FY16 Rosati - Waves Navigation Structures." The technical monitor was Jessica Podoski.

This study of Hilo Harbor, HI, was performed between August 2014 and November 2015 by the Coastal and Hydraulics Laboratory (CHL) of the U.S. Army Corps of Engineers (USACE), Engineer Research and Development Center (ERDC), at the request of the POH.

The USACE Coastal Inlets Research Program (CIRP) provided partial support for this study. Overall program management of the CIRP is provided by Headquarters (HQ), USACE. CIRP is administered at CHL under the USACE Navigation Research and Development Technology (RD&T) Program. At the time of this study, Jeffrey A. McKee, Chief, Navigation Branch, HQ, was the HQUSACE Navigation Business Line Manager overseeing the CIRP program. W. Jeff Lillycrop, CHL, was the ERDC Technical Director for Civil Works and Navigation RD&T. Charles E. Wiggins, CHL, was the Associate Technical Director for Navigation. Dr. Julie Rosati, CHL, was CIRP Program Manager during the period of this study. Jessica H. Podoski and Thomas D. Smith, POH, provided oversight for the study.

At the time of publication, James Gutshall was Chief, HNH, CHL; Tanya M. Beck was Chief, HNC, CHL; Dr. Jackie Pettway was Chief, HN, CHL; and Ty Wamsley was Chief, HF. José E. Sánchez was Director, CHL.

COL Bryan S. Green was Commander of ERDC, and Dr. Jeffery P. Holland was Director of ERDC.

Unit Conversion Factors

Multiply	By	To Obtain
acres	4,046.873	square meters
cubic yards	0.7645549	cubic meters
feet	0.3048	meters
knots	0.5144444	meters per second
miles (U.S. nautical)	1.852	kilometers
miles (U.S. statute)	1.609347	kilometers

1 Introduction

1.1 Background

This report describes a numerical modeling and field data collection study conducted to investigate harbor navigation problems experienced at the Hilo Deep Draft Harbor, located in the County of Hawaii, Hawaii. It is part of a cost-shared Feasibility Study by the U.S. Army Engineer District, Honolulu (POH), to improve navigation by evaluating proposed modifications to the interior harbor in collaboration with the non-Federal sponsor, Harbors Division of the Department of Transportation (DOT), State of Hawaii. The harbor consists of an entrance channel 1,500-feet (ft) (460-meter [m])-long, 500 ft (150 m) wide, and 35 ft (10.5 m) deep. The turning basin is approximately 2,500 ft (760 m) long, 1,500 ft (460 m) wide, and 35 ft (10.5 m) deep. The harbor is sheltered by a 10,080 ft (3,073 m) (2-miles [3.2 km])-long breakwater that extends across the northeastern half of the harbor. A need to modify the harbor to improve navigation within the interior of the harbor has been identified by POH and the State of Hawaii.

Hilo Harbor is located in a protected coastal area but is completely exposed to meteorological and oceanographic forcings in the Pacific Ocean from the north and east sides. As such, the harbor is affected by locally generated seas, swells, and distant storms. The POH and State DOT work together to maintain the breakwater, navigation channel, and interior of harbor to maximize the harbor's utilization because it is vital to the economy of Hawaii. Piers 1 and 2 (Figure 1-1) are two heavily used areas of Hilo Harbor. The limited space does not allow extending these piers to accommodate larger vessels and more cargo. Demand by users to accommodate a larger size and number of ships led the DOT recently to consider building two more piers along the south shoreline west of the existing Piers 1 and 2.

The users of Hilo Harbor have also reported the presence of a *surge* problem sometimes occurring while ships are moored at Piers 1 and 2. Users have also requested enlarging and deepening of the *waiting* or *mooring* or *turning* basin area located north of the navigation channel and Pier 1 near the Federal breakwater. Expansion of this temporary

Figure 1-1. Layout of Hilo Bay, HI.

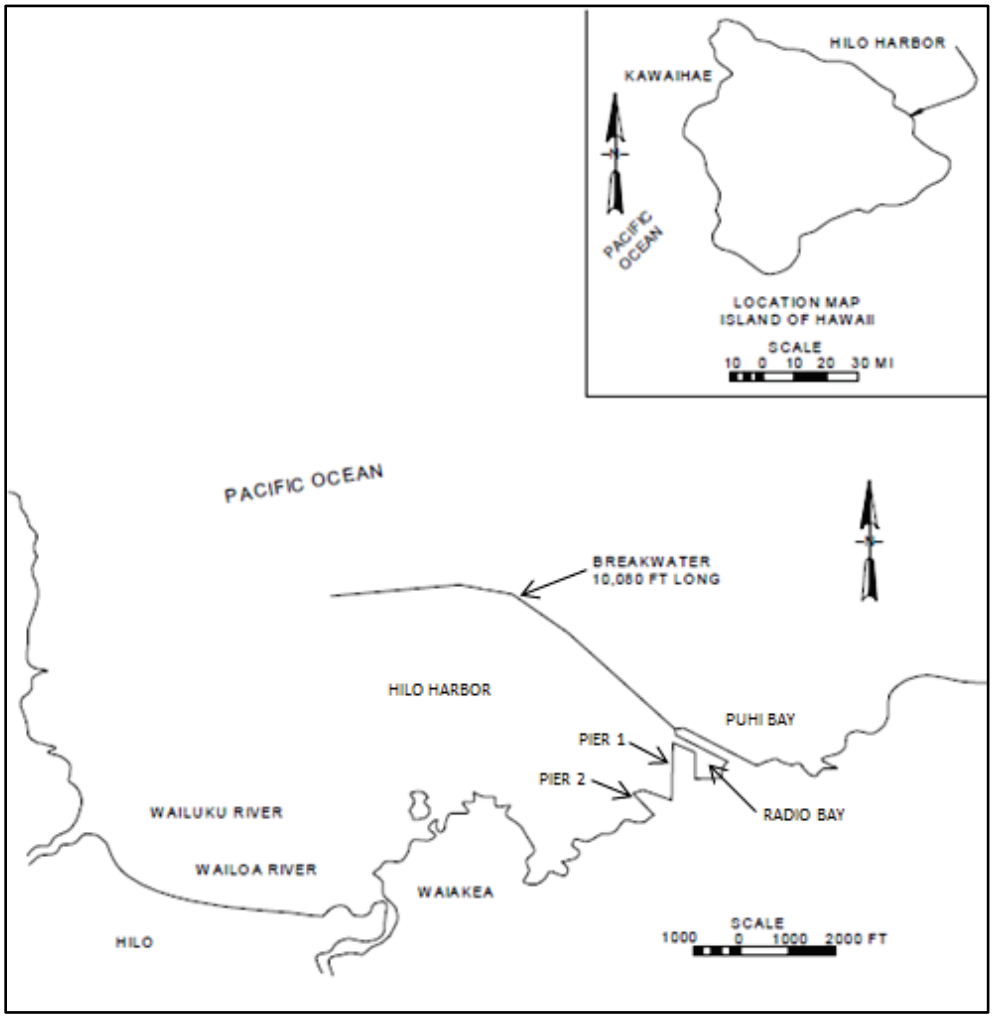

A berthing area is desired for the safety of moored vessels and also for maneuvering space necessary for larger ships accessing Piers 1 and 2. Such vessels have to *back off* when leaving the piers and need sufficient space/area to make a turn into the navigation channel to head out.

POH contacted the U.S. Army Corps of Engineers (USACE), Engineering Research and Development Center (ERDC), Coastal and Hydraulics Laboratory (CHL), to assist in development of a study plan to address navigation issues in Hilo Harbor. Navigation issues include (a) wave energy propagation from offshore into Hilo Bay to the harbor through the dredged navigation channel, (b) modification of the wave energy by reefs seaward of the breakwater, (c) transmission of wave energy into the harbor because of the porosity of the breakwater, (d) overtopping of the

breakwater, (e) effects of reefs and the breakwater on wave energy in the inner harbor close to the two piers, and (f) excessive wave energy reaching the mooring/turning basin near the piers. These issues were investigated with a combination of numerical modelling and field data, including analysis of modifications to improve navigation at Hilo Harbor.

Development of Hilo Harbor was initially authorized under the River and Harbor Act of 1907. Subsequent work was authorized under the River and Harbor Act of 1912 and 1925. The harbor was completed in 1929. The layout of Hilo Bay including the protected harbor area is shown in Figure 1-1. The harbor entrance is flanked on the west by shorelines and on the east by the breakwater and reefs. A tsunami in 1946 damaged nearly 6,000 ft (1,830 m) of the breakwater and created a 1,100 ft (335 m) breach. The breakwater was restored to its original design in 1948. A combination of storm waves and tsunamis in the 1950s, 1960s, and 1970s caused further damage to the structure, which was again repaired in 1972 to the original design. In 1976, Hurricane Kate damaged the breakwater, and continued sporadic damage and transmission through the structure prompted new repairs, including the addition of a concrete rib cap with a single layer of tribars placed on a 1V:1.5H slope on the seaward side of breakwater near Radio Bay (Figure 1-1). These repairs were completed in the 1980s. Figure 1-2 shows a cross section of the repaired reach, and Figure 1-3 shows a photograph of the rib cap and tribar repair section in July 2005 (viewed from the center of the crest, east to west).

Figure 1-2. Rib cap and tribar repairs of ocean side of breakwater in 1980s.

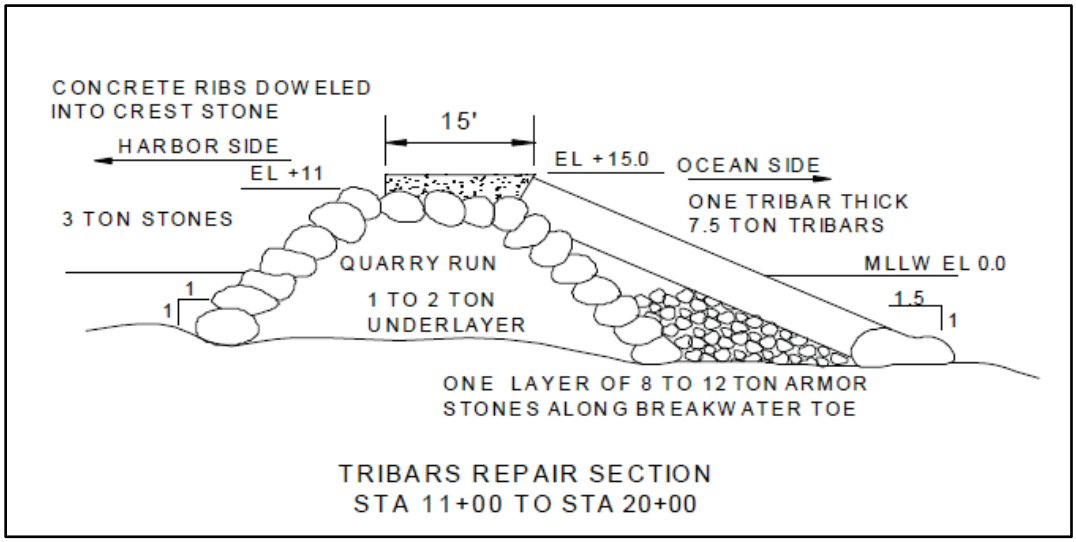

Figure 1-3. The breakwater with rib cap and tribar (view from east to west).

Periodic inspections of Hilo Harbor were conducted over the subsequent years, and repairs were made as warranted. In addition to lidar data, three-dimensional (3D) side-scan surveys of the breakwater structure and bathymetry in the vicinity landward and seaward the breakwater were conducted to obtain depths and a detailed condition assessment of the breakwater. Numerous walking inspections along the breakwater over the years revealed broken tribars, cracked armor stones, settling, voids, missing armor stones, and perched or flipped armor stones in different reaches of the structure. The information from these inspections and detailed surveys was crucial to subsequent repairs and numerical modeling studies at Hilo Harbor. For example, data from these sources were combined with the lidar bathymetric and topographic data for a water-quality study performed in 2007–2009.

Field data collected in 2007, 2013, and 2014 were used in the present study to calibrate numerical models. Water level and wave measurements were obtained in the summer of 2007 at three gauges deployed inside the harbor. A pressure-transducer was placed near the north tip of Pier 1 that collected water level data from late December 2013 through early May 2014. Detailed bathymetric surveys of the interior harbor and reef were conducted in 2012, along with tripod surveys of the breakwater. Detailed lidar and tripod survey data were used in this numerical wave modeling study for evaluation of the proposed modifications to Hilo Harbor.

The main tasks of the Hilo Harbor study were to (1) process existing hydrographic survey data of the interior harbor, (2) process existing wave and current data for numerical modeling applications, (3) process and analyze data from a pressure sensor deployed by the University of Hawaii (UH) at the berthing area of Hilo Harbor, (4) perform numerical wave modeling simulations inside and outside the harbor to evaluate merits of each of the proposed modifications, (5) develop hydrodynamic conditions for the ship simulator study, and (6) document study results by a technical report. The ship simulator support tasks were added later to this study, which included development of winds, waves, water levels, and currents to conduct the ship simulation for training mariners. Only a summary of conditions generated for the ship simulator are included in this report. The goal of the numerical modeling study was improvement of navigation between the harbor entrance and Piers 1 and 2. Proposed Alternatives were evaluated to determine the impacts of waves on navigation using a Boussinesq model, Bouss-2D (B2D), and the Coastal Modeling System (CMS)-Wave model. Details of the modeling study, data requirements, tasks, results, and major findings are provided in this report. An overview of the study plan is presented in this chapter.

1.2 Objectives

The objective of this investigation was to analyze the role and effects of wind, waves, water levels, and currents on navigation, and efficacy of the Alternatives for improving the utilization of Hilo Harbor. Specific issues investigated included (a) modeling wave transformation outside and inside the existing harbor, (b) evaluating the proposed Alternatives, (c) analyzing the surge problem in and around Piers 1 and 2, (d) evaluating impacts of enlarging and deepening the mooring and maneuvering area, (e) calculating wave transmission and overtopping of the breakwater, and (f) developing hydrodynamic conditions for the ship simulator study.

1.3 Study area

Hilo Harbor is a deep-draft port located in Hilo Bay on the Island of Hawaii at the mouth of two rivers, the Wailuku River and the smaller Wailoa River. There is also a small-boat harbor in Radio Bay located at the easternmost end of the harbor near the root of the breakwater and behind Pier 1. Radio Bay is used primarily by recreational and transient vessels, U.S. Coast Guard vessels, and small research vessels owned by the UH at

Hilo. Google maps (Figures 1-4 and 1-5) show the location of the study site and layout of the present harbor, respectively.

A large reef system outside the breakwater (Figures 1-4 and 1-5) extends to the 40 ft (13 m) depth contour before transitioning to deeper depths offshore. Reefs are also present in the interior of the harbor between the navigation channel and breakwater to the north and between the channel and shorelines to the south. The breakwater is extremely effective in protecting the harbor from incident waves and currents from the southeast to northwest sector. Wind waves are affected significantly by the bathymetry of the reefs present inside and outside the harbor. Water depth decreases over rough and rugged reefs outside the harbor approaching the interior harbor and adjacent shorelines, causing waves to refract and break. These breaking waves generate currents that affect maneuvering of in- and out-bound vessels and induce harbor siltation.

Figure 1-4. Hilo Harbor, HI (photo from Google Earth).

Figure 1-5. Hilo Harbor Piers 1 and 2 and
Radio Bay Marina (photo from Google Earth).

The State of Hawaii DOT is the non-Federal sponsor of the Hilo modeling study initiated by POH as part of the Operation and Maintenance (O&M) project for Hilo Harbor. Originally constructed by the State of Hawaii in 1929, Hilo Harbor received a Section 102 authorization in 1986 for dredging the existing basin to create a 39 ft (12 m) deep entrance channel and a 38 ft (11.5 m) deep turning basin to allow bulk sugar carriers to load to their maximum safe drafts. However, the project was terminated in 1991 based on lack of economic justification. Hilo Harbor was originally designed for freight with approximately 90% domestic traffic and 10% international. The port now accommodates different users and vessels, even though some of the original infrastructure was not designed to handle these new users. There is need for enlarging the harbor because it has been operating over capacity in recent years. The port basically works around the scheduling of cruise ships to accommodate the use of Pier 1 for both the cargo vessels and cruise ships. Cargo carriers using Pier 2 adjust their time in port based on the cruise ship schedule.

The harbor is a major commercial and industrial center for the Island of Hawaii and is the primary location of commercial waterborne traffic for the eastern side of the island. Vessels access Piers 1 and 2 through a well-maintained 500 ft (150 m) wide and 35 ft (10.5 m) deep navigation channel.

The 1,500 ft (460 m) wide and 35 ft (10.5 m) deep mooring area for ships to use as a waiting area or for turning/maneuvering is located north of the channel, very close to the breakwater. The navigation channel, mooring area, and interior harbor complex with infrastructure are all protected by a nearly 2-mile- (3.2 km) long breakwater that extends across the northeastern half of the harbor.

The port is critically important to the economy of Hawaii as it is one of the primary locations of commercial waterborne traffic and a major commercial and industrial center for the Island of Hawaii. Larger and deeper-draft vessels cannot access the harbor because of present navigation and infrastructure constraints that limit commercial waterborne commerce. The port is the only passenger terminal on the Island of Hawaii, and improvements to the Federal channel and turning basin will help to bring in more passenger vessels and larger and deeper-draft cargo carriers. State DOT officials anticipate that Hilo Harbor will become a regular port of call for the new-generation cruise vessels that are more than 1,000 ft (305 m) in length.

1.4 Problems affecting harbor operations

The existing mooring and turning basin area adjacent to the Federal channel cannot safely accommodate the size of ships presently using the harbor under prevailing conditions (Figure 1-6). This includes large cruise and cargo ships berthing at Pier 1 and the larger fleet that is projected to use the harbor in the future. The majority of the deeper-draft ship calls are cruise ships with drafts in the 25 to 30 ft (7.5 to 9 m) range, and ships with drafts of 33 to 35 ft (10 to 10.7 m) require a high tide and ideal calm conditions. Harbor pilots often take unwarranted risks and operate under less than ideal conditions while turning large cruise ships from 700 ft (210 m) to 950 ft (290 m) in length. New-generation cruise ships are longer than 1,050 ft (320 m) and have expressed an interest in making Hilo Harbor a regular port of call. Such ships presently are unable to use this facility due to current Federal channel and turning basin constraints. The landward end of the Federal channel is approximately 600 ft (183 m) from Pier 1 and the inner harbor, creating a limited area where ship maneuverability is already risky, even for shorter vessels.

Figure 1-6. Hilo Harbor Piers 1 and 2, Radio Bay Marina, and breakwater (photo from Google Earth).

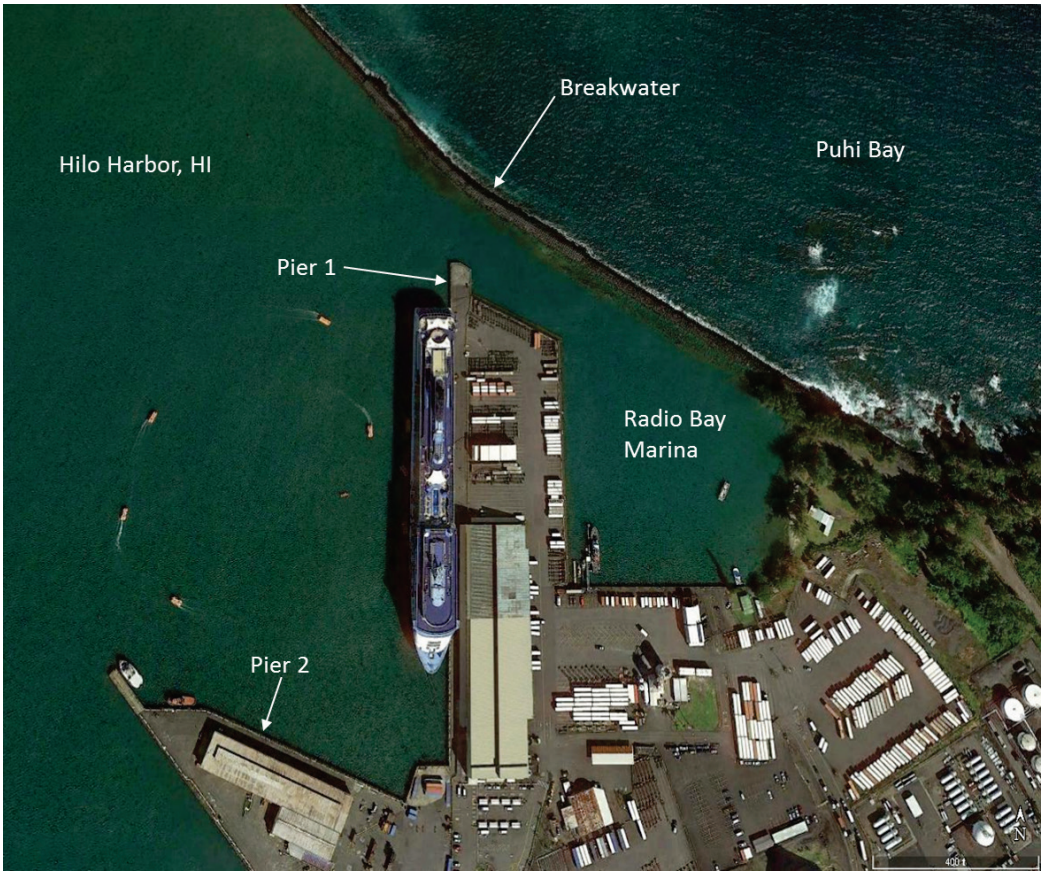

A second issue affecting navigation in Hilo Harbor is surge or long-period harbor oscillation, which occurs mostly during winter swells when ships are in the berthing areas. The surge is more pronounced with deeper-draft vessels, and over the years, surge has been blamed for several groundings in the Federal channel. The reported surge problem is local to Pier 1 and Pier 2 and is more prominent during high winter swell conditions and significantly hinders use of berthing areas. However, the surge problem is not manifested by standing wave characteristics typically seen with harbor oscillations that occur often in harbors. The mariners use the term *surge* for Hilo Harbor to describe *a pulling away of ship* movement from the piers. This type of ship response can also be caused by wind forcing acting on the superstructure of cruise ships, and it is not necessarily caused by long-period infragravity (IG) waves, the well-known cause of classical harbor surge problems. The cause of this surge problem at Hilo Harbor is unknown, but most likely it is due to IG waves, which are culprit of similar problems in other harbors. Without some modifications to the interior harbor, the surge problem will continue to affect navigation of commercial

vessels and cause damage to vessels and berthing facilities. For this reason, the classical harbor surge induced by IG waves, and influence of the widening and deepening of the mooring and maneuvering areas, was investigated in the present numerical modeling study in an attempt to address the surge issue in this harbor.

The surge has also been blamed for vessel groundings and damages to both vessels and piers. Although there have been groundings of large dry bulk carriers in the past in the Federal channel, there is no evidence that these groundings resulted from surge conditions, or vessels attempting to compensate for severe weather, or vessels maneuvering in the restricted turning basin. The groundings had occurred with wind out of the north creating incident waves directed down the entrance channel. The widening and/or deepening of the entrance or navigation channel would reduce these incidents without further exposing the harbor and infrastructures to increased wave energy and sedimentation. Because Pier 1 is shared by cargo and cruise operators, there is a lack of space for growing cargo and cruise passenger activities at Hilo Harbor, and there are concerns for passenger safety when combined with cargo operations. Several Alternatives to decrease the severity of these problems include expanding the harbor turning basin, widening or deepening the Federal channel, and adding space and maneuverability for present ships and anticipated future larger vessels.

The State DOT is also interested in extending the basin closer to Pier 1 to increase the capacity of the port to handle more ships and cargo. The DOT is considering three additional proposed piers and berthing areas to the west of Pier 2 to be known as Piers 3, 4, and 5. Because the limits of the turning basin adjacent to Pier 1 are too small for present and future vessels, the potential for ship grounding is very high. Turning cruise ships longer than 900 ft (275 m) presents a problem for the pilots and captains. Larger ships docked alongside Pier 1 require performing maneuvers in the mooring area to the north near the breakwater. Therefore, the risk of ship groundings is very high as vessels have to back out of the berth until they are too close to the shallow depths near the breakwater. Some cruise ships use an azipod thruster system for enhanced control and maneuvering to continue to use the harbor when vessels are dangerously close to the breakwater. Tug boats have to be used to assist with maneuvering the bulkers or tankers by crabbing the bow 90 deg starboard to help the ship sail straight out through the main channel. The crabbing (or turning) of

vessels pushes the stern of the vessel closer to the breakwater, creating a suction force that can pull a vessel further toward the shallow reef and potentially cause grounding.

The harbor pilots need more room for larger vessels to safely utilize Piers 1 and 2. Enlarging and deepening the turning basin would improve navigation safety, but doing so would also require expanding the terminal end of the Federal channel near Pier 1. Larger channel dimensions would be necessary to accommodate the world fleet that continues to increase in length and draft. The expected improvements in port operations with Alternatives evaluated herein include (a) increased safety of vessel operations, (b) reduced potential for damage to vessels from surge conditions, (c) reduced potential for damage to moored vessels and/or harbor infrastructure, (d) reduced potential for cancellation and delays of services due to high surge conditions, and (e) an increase in the size and capacity of vessels bringing tourists, goods, and services to the port. As the busiest port on the Island of Hawaii and one of the busiest in the State outside of Oahu, this harbor will continue to expand as an important port in the State's economic base. The improvements will be significant as they will provide safer vessel operations and allow use of the harbor by larger vessels, thereby increasing the cargo volume of the port. The harbor improvements will also increase the opportunities for ports of call by larger passenger vessels in the cruise ship industry.

1.5 Problem statement

Improving berthing and surge problems at Hilo Harbor Piers 1 and 2 would require a reduction in wave energy reaching these areas of the interior harbor. The reefs inside the harbor help greatly to dissipate wave energy getting into the harbor while comparatively more wave energy exists in the channel and other areas of the harbor that are not influenced by reefs. Structures can be used to intercept and prevent waves impacting these areas, or waves can be diverted from these impacted locations.

Limited wave, current, and water level data were obtained in 2007 at three locations inside the harbor during the calm summer months. It was necessary to deploy a gauge near the north end of Pier 1 to collect more wave, current, and water level data from December 2013 to May 2014. Additionally, water level data were available from a NOAA tide gauge located west of Pier 2. These datasets were used in validating and calibrating numerical models to investigate the existing harbor

configuration and proposed structural modifications for improving navigation in the harbor basin.

1.6 Harbor modifications

Figures 1-1 through 1-6 show general features of the existing Hilo Harbor, including the small Radio Bay Marina behind Pier 1, and other coastal and land features present in Hilo Bay. The sketches of modifications in consideration to Hilo Harbor included adding a few structures to the interior harbor and enlarging and deepening the mooring/turning basin area. Each proposed modification is shown in a B2D model grid with schematics or sketches in Figures 1-7 through 1-12. Each sketch depicts the type of modification and its location in the harbor. Implementation of these sketches as Alternatives is described in Chapter 4. General information about each modification is provided here.

Figure 1-7 shows the main features of the existing harbor from a B2D grid, including bathymetric variation outside and inside the harbor with reefs, the breakwater, and two piers. The sketches of modifications are displayed without providing details of bathymetry.

Figure 1-7. Bathymetric features of existing harbor.

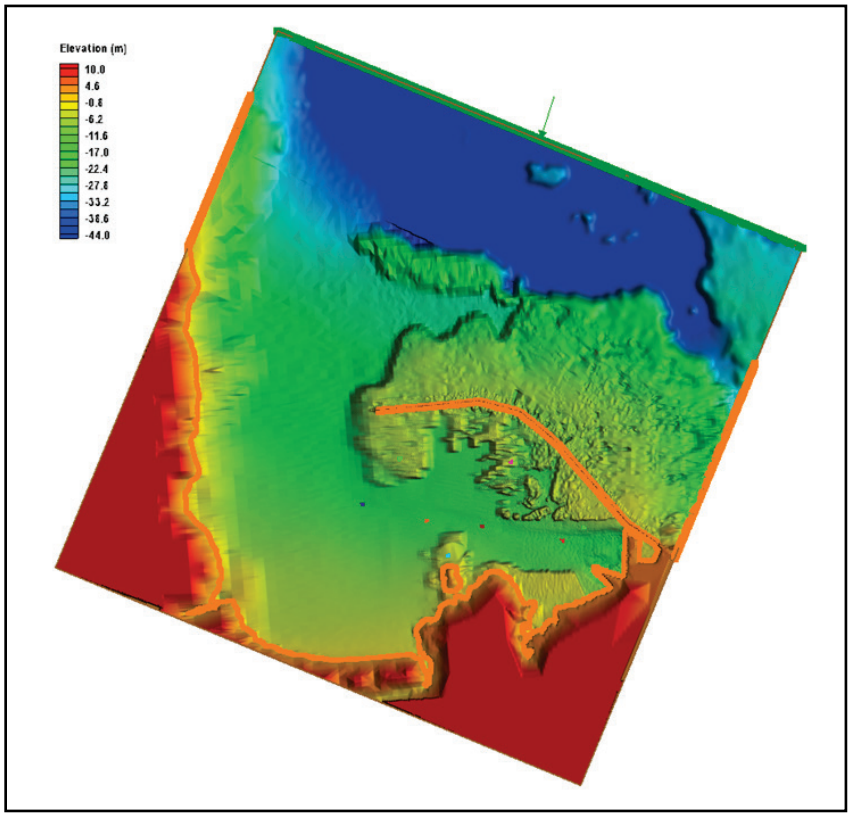

The proposed modifications include strategic placement of detached breakwaters and short spurs inside the harbor. Sketches of these structures are shown in Figures 1-8 through 1-11. The first modification (Figure 1-8) considers a short structure while longer structures are used in the second and third modifications (Figures 1-9 and 1-10). These detached breakwaters and spurs are situated between the Federal breakwater and the north edge of navigation channel, which are expected to intercept and reduce the wave energy that reaches the mooring area, turning basin, and Piers 1 and 2. For safety reasons, these are located at a distance of approximately ~200 ft (61 m) from the north edge of channel bank. These structures may be moved southward into the channel to further reduce wave energy at the piers, but doing so would pose an increased risk to ships transiting the channel.

Figure 1-8. Proposed modification with a short (820 ft) interior structure.

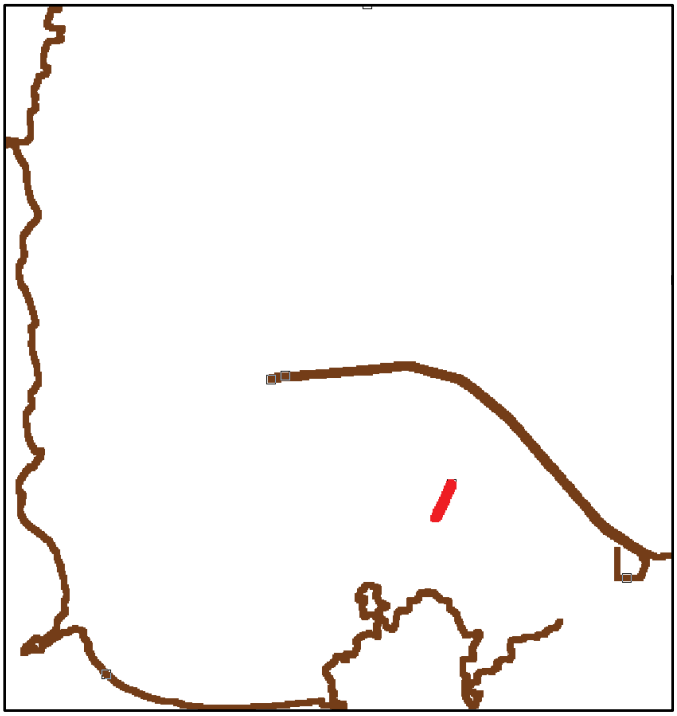

The second and third modifications use medium and long interior breakwaters and spurs as shown in Figures 1-9 and 1-10. The location, length, and orientation of these structures can be adjusted if necessary.

One of the modifications involved adding a structure (spur) to the tip of the Federal breakwater (Figure 1-11). Different attachment points, lengths, and angling of the spur were considered to determine desired dimensions

of the spur that would produce maximum benefits to mooring/turning basin and Pier 1 and 2 areas. Figure 1-12 shows dual structures on the north and south sides of the channel.

Figure 1-9. Modification with a medium length (1,580 ft) structure.

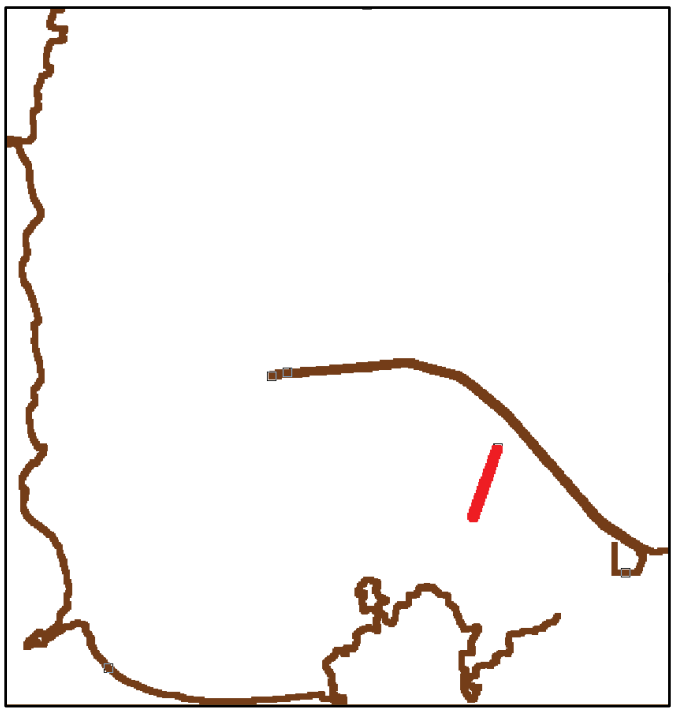

Figure 1-10. Modification with a longer (2,230 ft) structure.

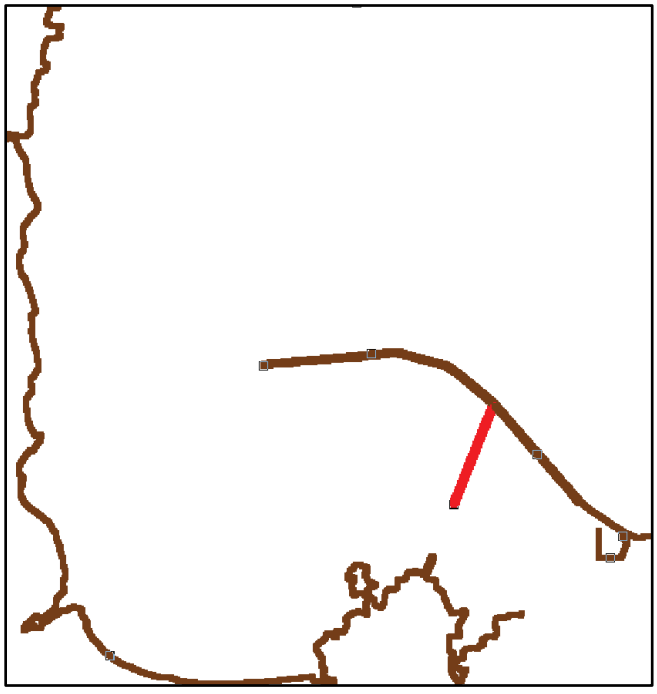

Figure 1-11. Modification with a spur added to the tip of breakwater.

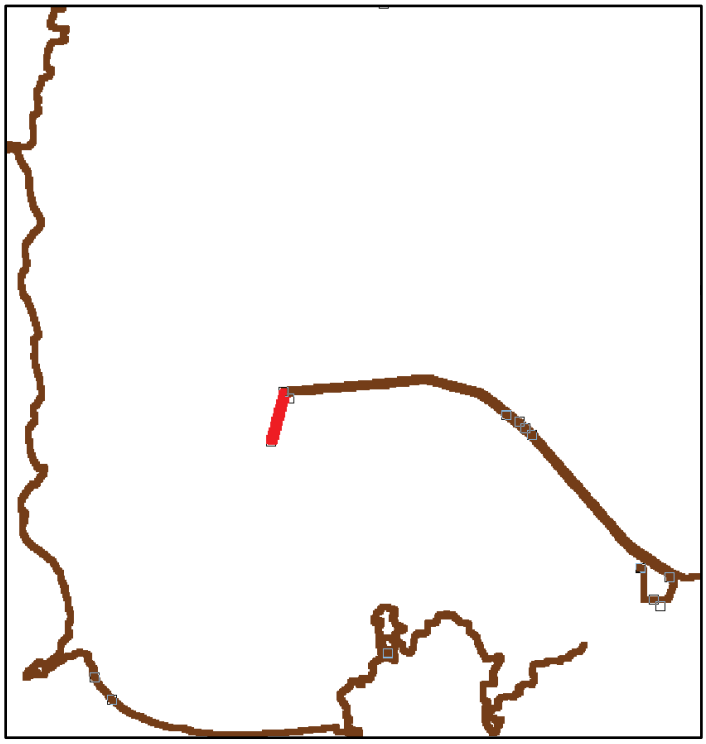

Figure 1-12 Modification with dual structures north and south of channel.

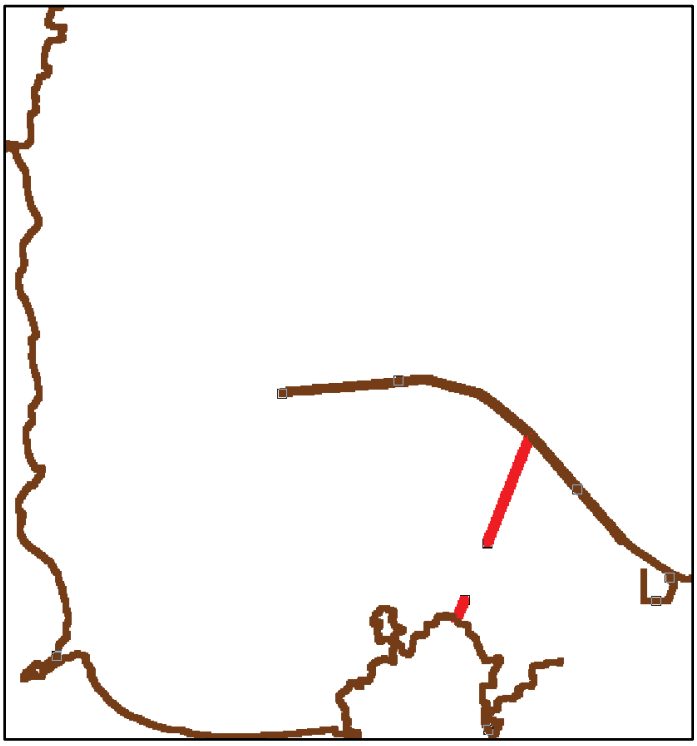

The modification involving the enlarging and deepening of the mooring and turning basin area is shown in Figure 1-13, with the bathymetry change. This area is northwest of the tip of Pier 1, located north of the channel and between the breakwater and edge of the channel. The deepening and enlargement of this area are intended to provide an expanded mooring and turning basin for ships.

Figure 1-13. Enlarged and deepened mooring/turning basin area.

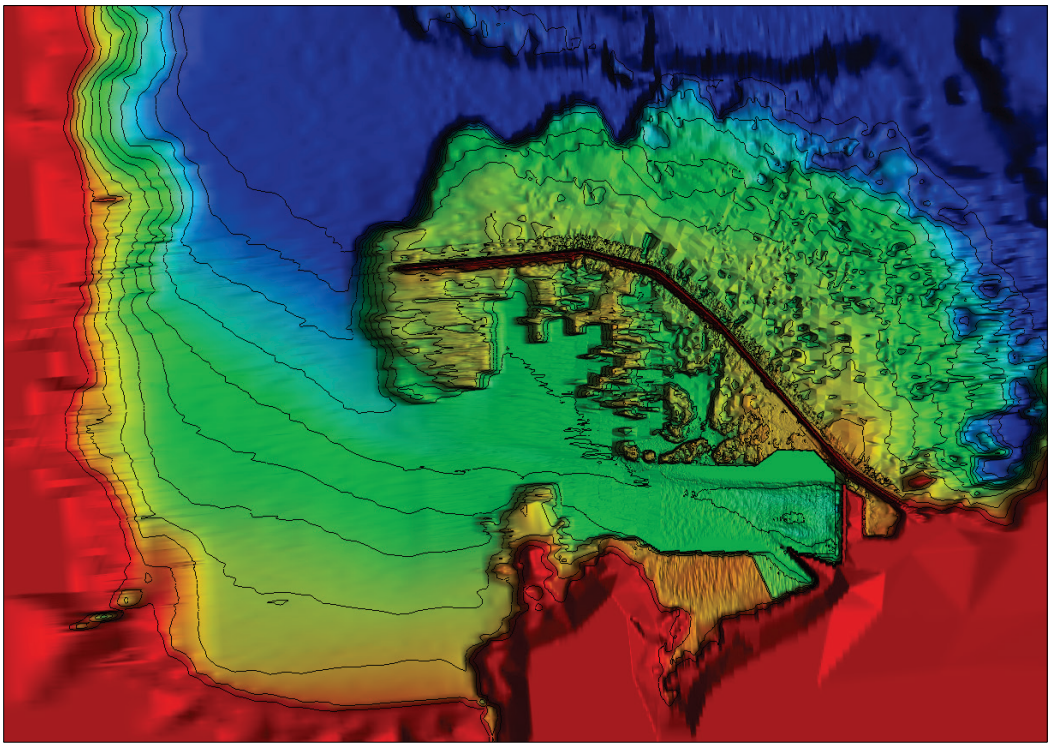

Last, a conceptual modification shown in Figure 1-14 was considered for changing the Pier 1 area by re-orientating the pier in an east-west direction. This modification would greatly facilitate the access of larger future ships to the Pier 1, where two new separated docks provide additional berthing slips. With this new layout, ships of lengths up to 2,000 ft (610 m) could easily get in/out of the Pier 1, and more vessels could use three sides of the docks for berthing. This conceptual configuration is provided here only for potential future expansion of the harbor and will not be discussed further. Additional information about the implementation of the proposed modifications is provided in Chapter 4 with B2D modeling.

Figure 1-14. Modification with realignment of east-west berthing slips at Pier 1.

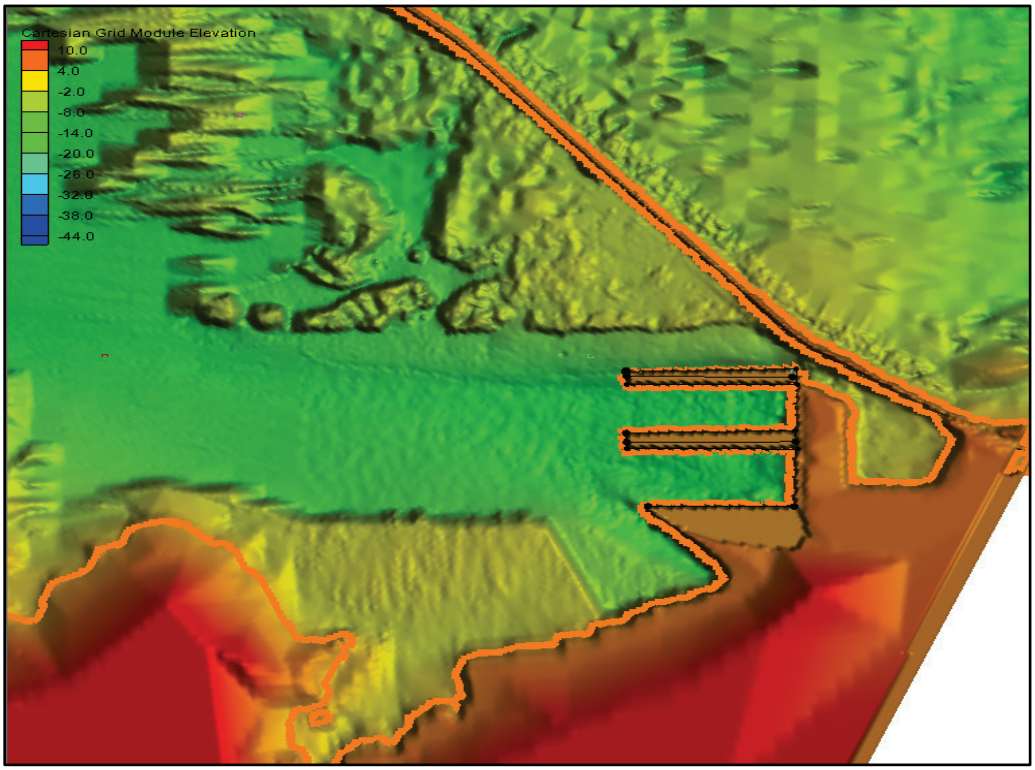

1.7 Study plan

The study plan consisted of the following activities: (1) processing existing hydrographic survey data of the harbor, (2) analyzing existing wave and current data from the 2007 field experiments to provide input for the numerical models, (3) processing and analyzing data from a pressure sensor deployed by the UH at the berthing area of Hilo Harbor, (4) performing a detailed numerical wave modeling for the regions inside and outside the harbor to evaluate benefits of the proposed modifications, (5) developing forcing conditions (winds, water levels, waves, and currents) for a ship-simulator training study conducted at the CHL in December 2014, and (6) documenting these study tasks in this technical report.

Hydrographic surveys of the harbor interior, entrance, breakwaters, reefs, and nearshore areas within the 40 ft (13 m) depth contour provided bathymetric data for numerical modeling. Other bathymetry data were obtained from different sources, including digital elevation maps and previous numerical modeling for deep water areas. Available water levels, wave, and current data from gauges in the harbor and vicinity were used for validation and/or forcing conditions in this numerical modeling study. Models were used for wave transformation between the offshore, entrance,

and interior of the harbor. Field measurements were used for calibration and validation of numerical models. The infrastructure modifications in the interior of the existing harbor were evaluated in terms of improvement to navigability and usage of the harbor, including investigation of the harbor surge problem that pulls vessels away from the berthing areas. Wave estimates inside and outside of Hilo Harbor were calculated by investigating wave processes outside and inside the harbor in evaluating proposed Alternatives (modifications) for improving navigation in the interior harbor. A matrix of conditions (water levels, winds, waves, and currents) was simulated with CMS-Wave and CMS-Flow for generating inputs to a ship-simulator testing study conducted in December 2014.

1.7.1 Approach

Because waves and winds were the main concerns to users of Hilo Harbor, a goal of each proposed modification was to reduce wave energy at and around Piers 1 and 2 and the mooring basin. The characteristics of waves passing through the entrance are largely controlled by reefs outside the Federal breakwater and to a lesser extent, by the shoreline west of the harbor entrance. Large waves can exist outside Hilo Bay north of the harbor entrance over the fringing reefs seaward of the breakwater and along the northwest and west shorelines. The long Federal breakwater is very effective in sheltering the harbor from large incident waves and currents. Only waves passing through the entrance between the western-most tip of breakwater and west shoreline can reach the south shorelines and move into the interior of harbor. The reefs covering large areas inside and outside the harbor (Figure 1-7) extend offshore to approximately the 40 ft (13 m) depth contour. The cross-shore and east-west extent (width) of these reefs varies. The outside reefs extend approximately 1 mile (1.5 km) to the east and 0.25 mile (0.4 km) to the west of the entrance channel. The inside reefs cover a large part of the harbor interior, and if waves propagating over these reefs break, they generate wave-induced currents that can affect navigation at Hilo Harbor.

Reefs are also present in the interior harbor except in the navigation channel and Piers 1 and 2, affecting waves inside the harbor complex. Reefs inside and outside the harbor are of great help to navigation in Hilo Harbor by controlling the level of wave energy affecting ship traffic. Potential causes of reported problems at Piers 1 and 2 were investigated by evaluating wave processes with and without proposed structural Alternatives. Impacts and effectiveness of the proposed structural

modifications on navigation in the channel and harbor were investigated. The field data collected in 2007, 2013, and 2014 were used in model calibration. Numerical model results were utilized to examine the merits of changes and their impacts on different areas of harbor. Alternatives included changes to the breakwater, mooring/turning basin, Piers 1 and 2 areas, and along the southeast and south shorelines.

1.7.2 Tasks

A summary of numerical modeling study tasks follows.

Task 1: Development of grids and boundary conditions

The B2D and CMS-Wave grids for selected Alternatives were developed. One grid for CMS-Wave was used for the existing harbor and Alternatives, whereas different grids were used for B2D. The incident waves were specified along the northern grid boundaries of both models. The north and east boundaries of the model grids were in open water, and west and south boundaries were mixed boundary types (e.g., part water and part land). Included in the model grids were the nearly 2-miles-long (3.2 km long) breakwater, harbor entrance, navigation channel, two piers, and other features present inside the Hilo Harbor. The modifications applied to the harbor affect the amount of local wave energy at and around where the change is made and can affect wave energy in other parts of harbor as well. Some Alternatives may require more than one change to be effective for improving vessel navigability, mooring, maneuvering, and shoaling of navigation channel. Wave conditions used in simulations are provided in Chapters 3 and 4. Detailed structural features of the breakwater, the land features present on the east and west sides of harbor entrance; east, west, and south shorelines; and the reefs in the harbor interior were included in the model grids. The reflectivity of structures and land boundaries were also included in the model grids. Three B2D grids for different incident wave directions were used with the default values of computational model parameters. These were adjusted based on the outcome of model-to-data calibration results. The incident waves were applied to the B2D grids as directional sea states with the values of significant wave height, peak period, and peak wave directions obtained from the CMS-Wave simulations.

Task 2: Preparation of models and test runs

CMS-Wave was used for deep-water wave modeling to transform incident waves from the buoys and ERDC Wave Information Study (WIS) station to the B2D model boundary and used as input conditions for B2D simulations. CMS-Wave was used with CMS-Flow to develop wave and current fields for a ship simulator study. B2D was used for wave modeling needs inside the existing harbor and proposed modifications. Wave estimates were calculated along the navigation channel, in the mooring/turning basin, at two piers, and at other areas inside and outside the harbor complex. The potential for harbor oscillations (IG waves) was investigated. A number of wave conditions were considered in the model preparation and testing. Surge is most severe during the October to March time period, with waves from north-northwest, north, north-northeast, northeast, and east directions. Waves from May to September are mostly from the east-southeast, east, northeast, north-northeast, and north directions. During the last 5 years, the range of wave parameters incident from north-northwest, north, north-northeast, northeast, and east directions included peak periods of $8 < Tp < 16$ sec and significant wave heights of $3.3 < Hs < 16.4$ ft ($1 < Hs < 5$ m). For the ship simulator study, a different set of wave conditions was modeled. In this case, the USACE Coastal Data Information Program (CDIP) data for 2012 and 2013 were used. The time windows for these conditions were specified by the ship captains and pilots attending the ship simulator training. The values of wave parameters simulated ranged from 9 to 15 sec, with maximum wave heights of 9.8 to 15.4 ft (3 to 4.7 m) and wave directions from north and east. These wave conditions and associated winds were simulated for the spring tides when currents were expected to be strong.

Task 3: Status meetings

Periodic telephone conference call meetings were held to discuss the status of the numerical modeling study work progress. Included were information about data needs, model setup, assumptions, model limitations, results of tests, and conditions for model production runs.

Task 4: Production runs

Two types of production runs were performed. The first set was for investigation of the reported navigation problems and evaluation of

Alternatives to improve navigation. The second set of production runs was for the support of the ship simulator study. CMS-Wave was used for both sets of productions runs, and B2D was used for the first set. Hilo Harbor was one of the largest modeling domain sizes considered with the B2D model that required a very large number of simulations, with run times ranging from 6 to 35 hrs.

Task 5: Post-processing and analysis of modeling results

Results from both wave models and CMS-Flow were post-processed and presented in tables, figures, snapshots, and animation files. Spatial and temporal outputs generated from post-processing were evaluated by the project team for action.

Task 6: Draft report and review

Study results documented in the draft report were delivered to POH for review and design consideration. CHL incorporated POH review comments into this final technical report. All derivative products generated from the numerical modeling effort were provided to POH with this final report, including examples of input/output files.

2 Data

Field data including bathymetry, coastlines, water levels, currents, surface winds, and river discharges were assembled to prepare inputs to the wave and hydrodynamics models.

2.1 Bathymetry and coastline data

Coastline digital data for this study were extracted from the National Geophysical Data Center (NGDC, http://ngdc.noaa.gov), and a geo-referenced image file was downloaded from Google Earth 5.0 (http://earth.google.com).

The offshore bathymetry data were obtained from GEOphysical DAta System by the NGDC (http://www.ngdc.noaa.gov/mgg/bathymetry/relief.html) and an ADCIRC grid used in a previous water-quality modeling study for Hilo Harbor in 2007. The land elevation data were obtained from U.S. Geological Survey (USGS) Geographical Digital Elevation models (DEM, http://data.geocomm.com/dem/). POH provided the bathymetric survey data from the 2013–14 field monitoring and data collection study and detailed multibeam survey data of breakwaters and parts of interior harbor. These bathymetries were used in the Bay and nearshore area.

2.2 Wave data

Wave data for Hilo Harbor modeling were available from five sources: (1) the National Data Buoy Center (NDBC) Buoys 51004 and 51100, (2) the Coastal Data Information Program (CDIP) Buoy 188, (3) the Wave Information Studies (WIS) Station 82527, (4) a pressure transducer (UH-HB) installed and maintained at Pier 1 by the UH, and (5) an acoustic Doppler current profiler (ADCP) installed by ERDC CHL (CHL H1) in 2007. Figures 2-1 and 2-2 show the areas of interest encompassing Hilo Bay (yellow box area) and locations of available metocean data stations.

The NDBC Buoy 51004 is located in deep water 210 nautical miles (n.m.) (389 km) southeast of Hilo, and has collected wave data since November 1984, with directional wave measurements starting September 2009. The NDBC Buoy 51100 is located 240 n.m. (245 km) north-northeast of Hilo in deep water and has collected directional wave data since April 2009. The CDIP 188, also a deep-water buoy, is located 4 n.m. northeast of Hilo and has collected directional wave data since

Figure 2-1. Location of NDBC and CDIP buoys and WIS, NOAA, and USGS Stations.

Figure 2-2. CMS modeling domain with UH-HB and CHL H1, H2, H3 gauges.

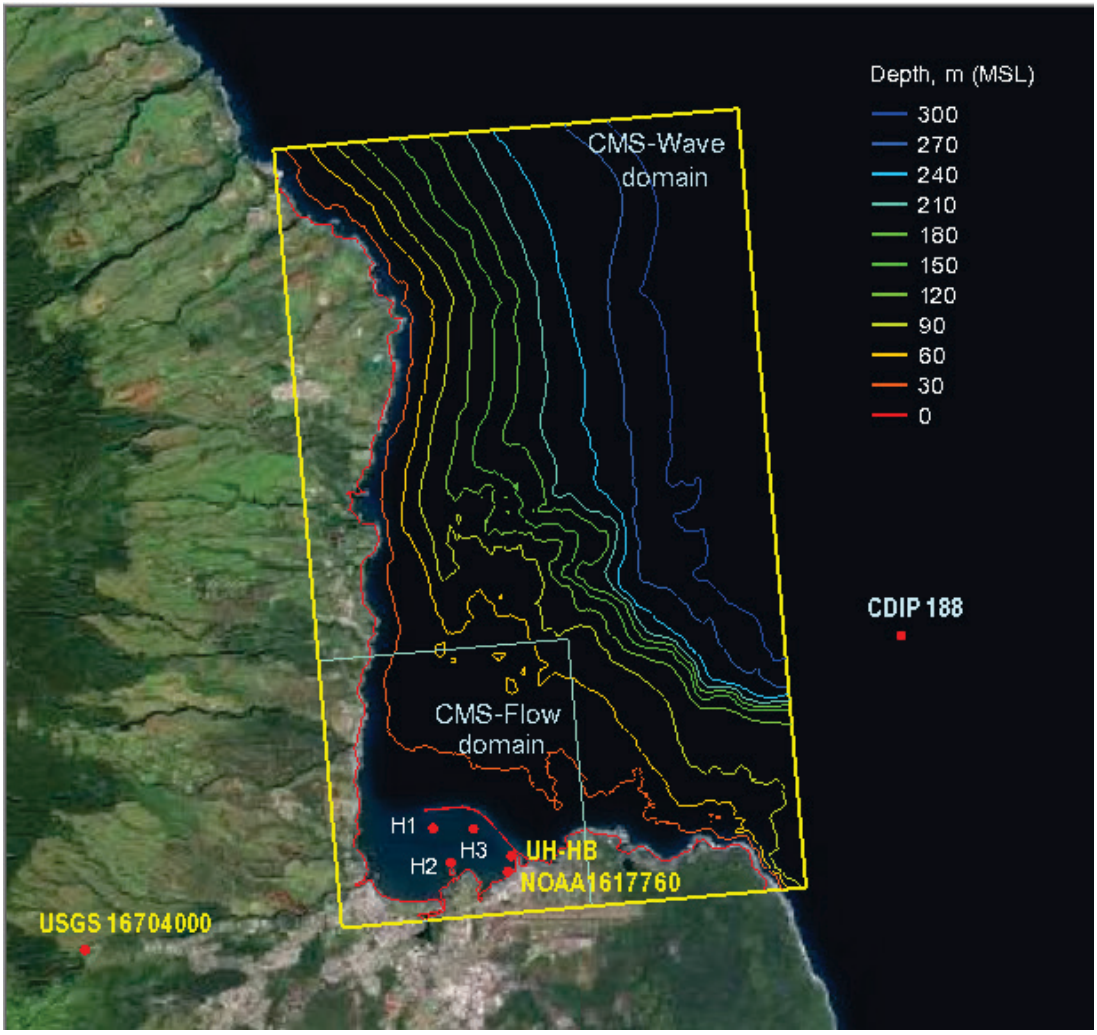

March 2012. WIS 82527 is approximately 20 n.m. northeast of Hilo and has a 32 yr hindcast wave record (1980–2011). The UH-HB gauge was deployed specifically for this Hilo Harbor project at the north end of Hilo Harbor Pier 1 and has collected data from late December 2013 through April 2014. The CHL H1 gauge was deployed 0.25 n.m. south-southeast of the east end of Hilo Bay breakwater and collected directional wave data March–June 2007. Table 2-1 lists the geographical location and nominal depth of various data sources mentioned.

Table 2-1. Wave data sources.

Station	Location	Depth (m)	Data History
NDBC 51004	17.602 N, 152.395 W	5230	Nov 1984–present
NDBC 51100	23.558 N, 153.9 W	4755	Apr 2009–present
CDIP 188	19.7814 N, 154.968 W	347	Mar 2012–present
WIS 82527	20 N, 154.6 W	5963	1980–2011
UH-HB	19.73366 N, 155.054 W	9	Dec 2013–present
CHL H1	19.7391 N, 155.073 W	6	Mar–Jun 2007

Figures 2-3 and 2-4 show examples of wave and wind data collected in 2011 and 2013 by two buoys, NDBC 51004 and 51100, respectively. These plots show measured wave heights are similar at Buoys 51004 and 51100. Smaller wave heights range from 3.3 to 13.1 ft (1 to 4 m) in the summer and fall seasons, and greater wave heights from 6.5 to 19.7 ft (2 to 6 m) are observed in winter and spring months. Buoy 51004 detects more southern swell than Buoy 51100 during June to September as Buoy 51100 is sheltered by the Hawaiian Islands from southern swell. At this project site, during spring to fall seasons, more waves are from the east, which are generated by strong easterly trade winds.

Figure 2-3. Wind and wave data for 2011 from NOAA Buoys 51004 and 51100.

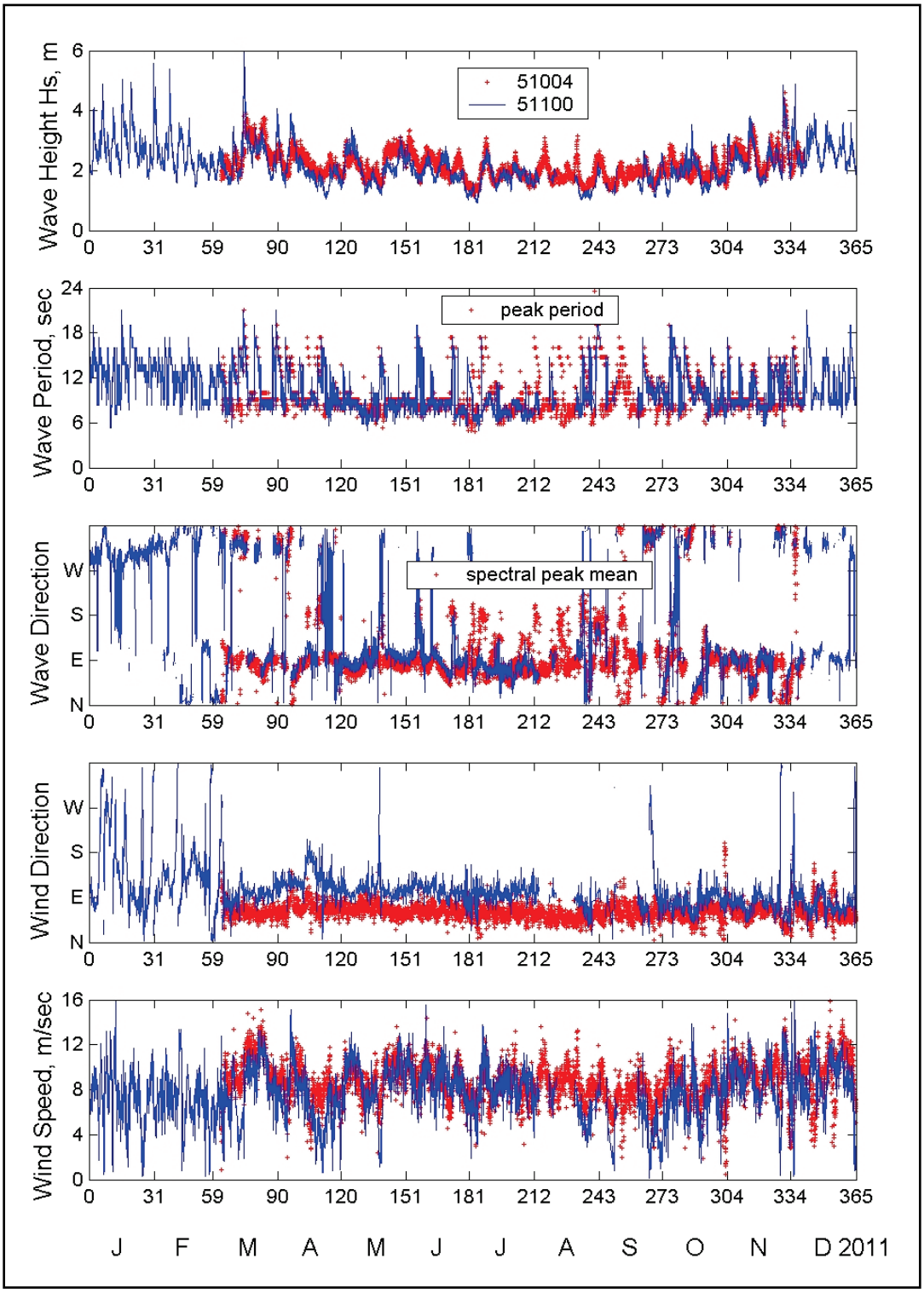

Figure 2-4. Wind and wave data for 2013 from NOAA Buoys 51004 and 51100.

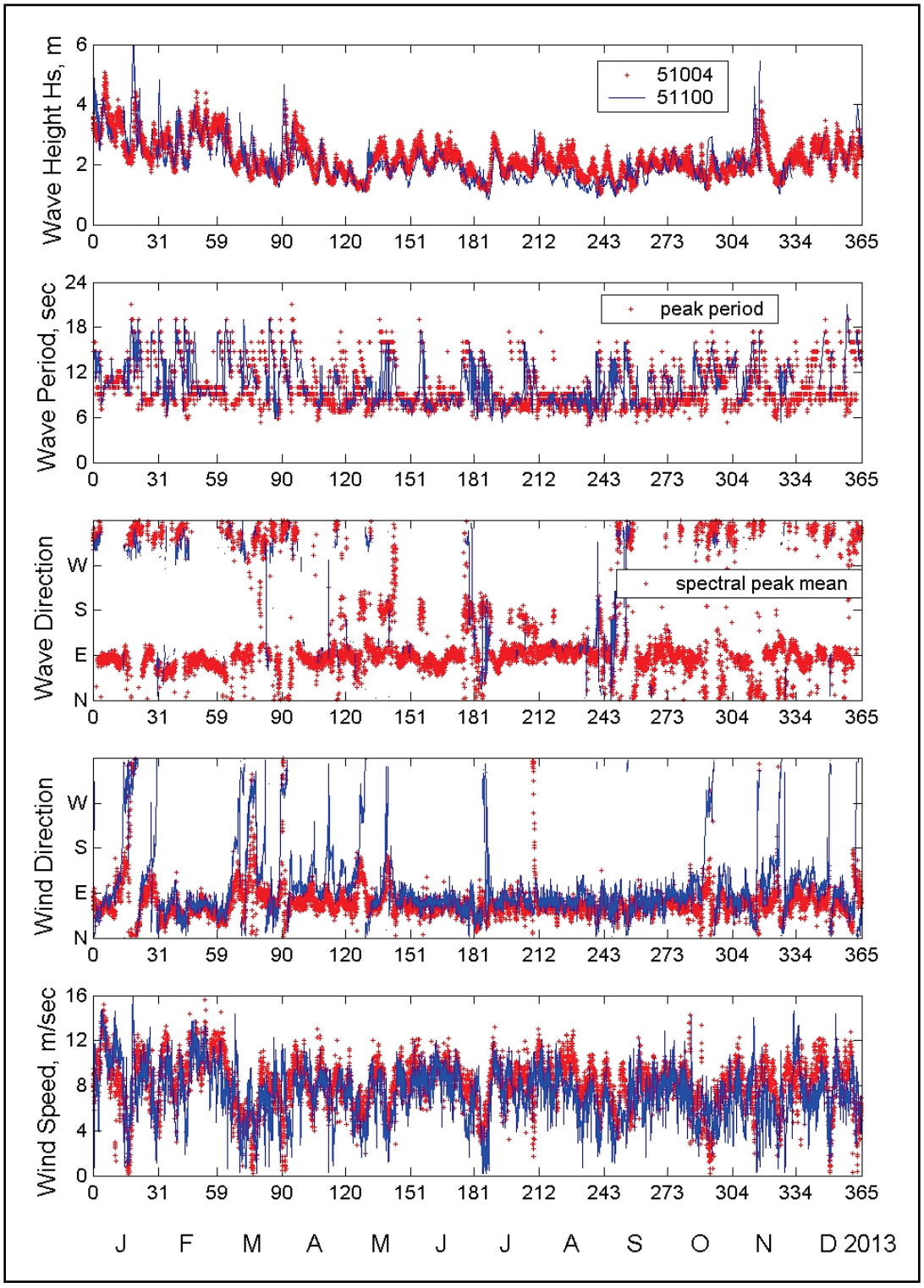

Figure 2-5 shows an example of 2013 wave data collected by two buoys located outside the Hilo Bay (CDIP 188 and NDBC 51004). Figure 2-6 shows wave data for 2011 from WIS Station 82527 and NDBC Buoy 51004.

Wave heights from CDIP 188 and WIS 82527 are generally smaller than offshore wave heights reported by NDBC 51004. This is because wave directions at the locations of CDIP 188 and WIS 82527 are mainly exposed to the north and east quadrants and are partly sheltered by the Hawaii Island to wind waves and swells emanating from the south and west directions.

Figure 2-5. Wave data for 2013 from CDIP 188 and NOAA Buoy 51004.

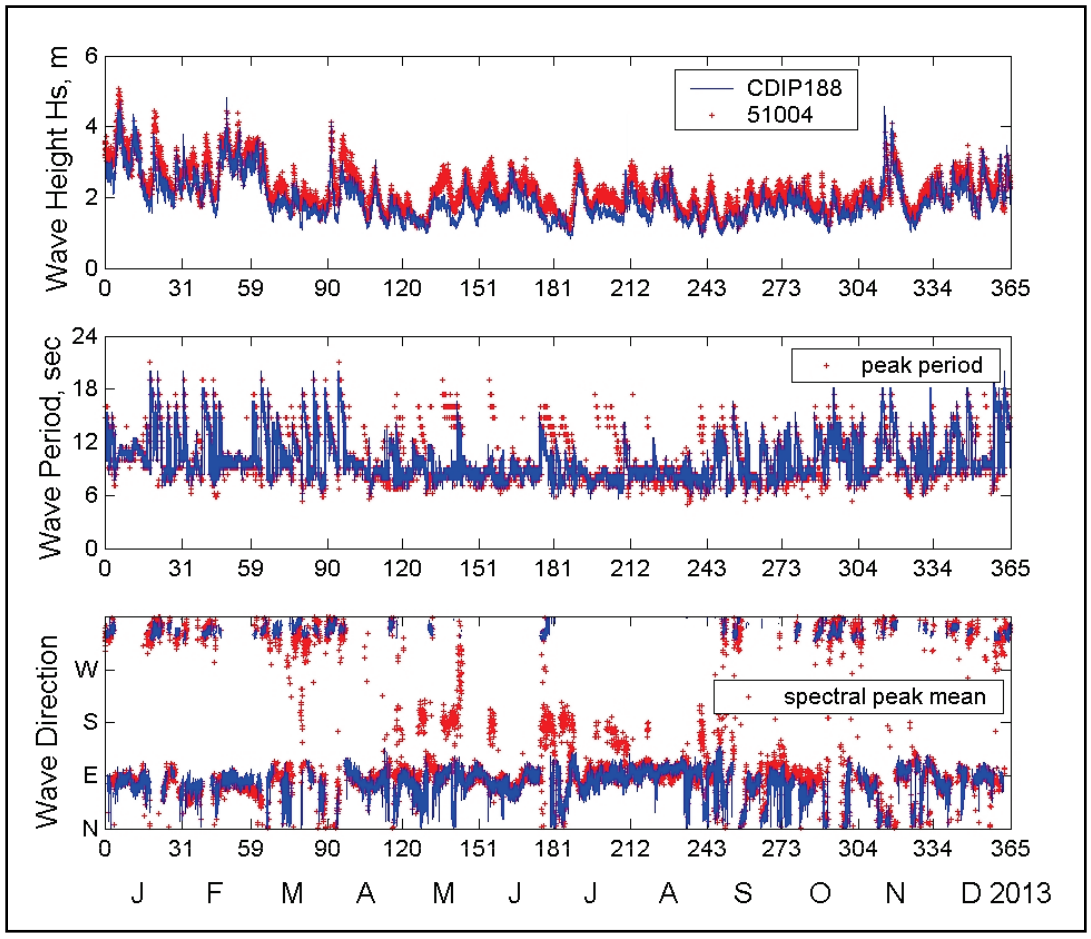

Figure 2-6. Wave data for 2011 from WIS 82527 and NOAA Buoy 51004.

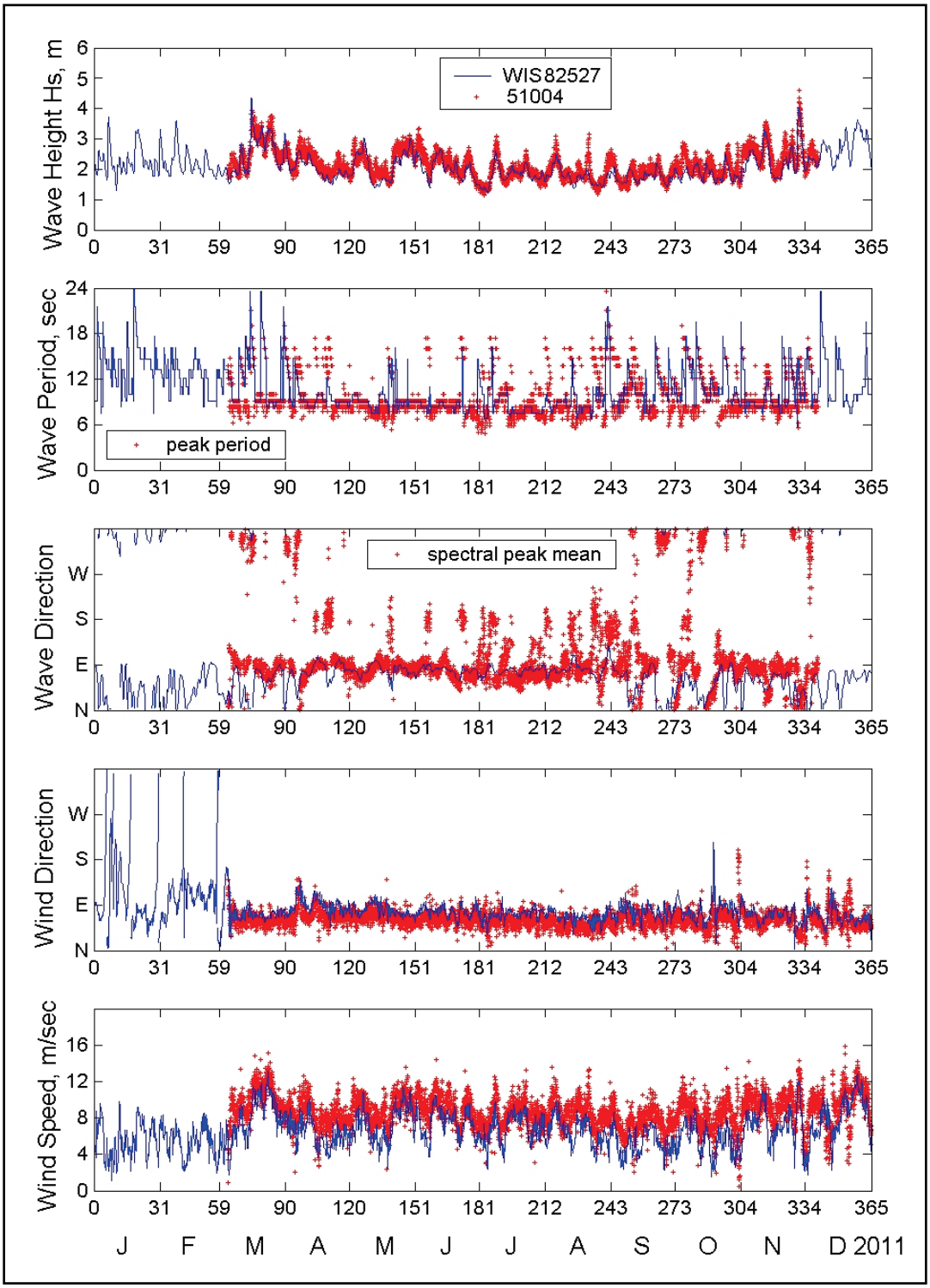

Wave data collected from January to April 2014 at the UH-HB gauge located at Pier 1, and CDIP 188 located outside the Bay, are compared in Figure 2-7. A comparison of March to June 2007 wave data from the CHL H1 gauge and NDBC 51004 is shown in Figure 2-8. These two comparisons indicate that wave heights measured inside Hilo Bay at CHL H1 and UH-HB are much smaller than offshore waves outside the Bay at the CDIP 188, WIS 82527, and NDBC 51100 and 51004, as expected.

Figure 2-7. Wave data collected for January–April 2014 at UH-HB gauge.

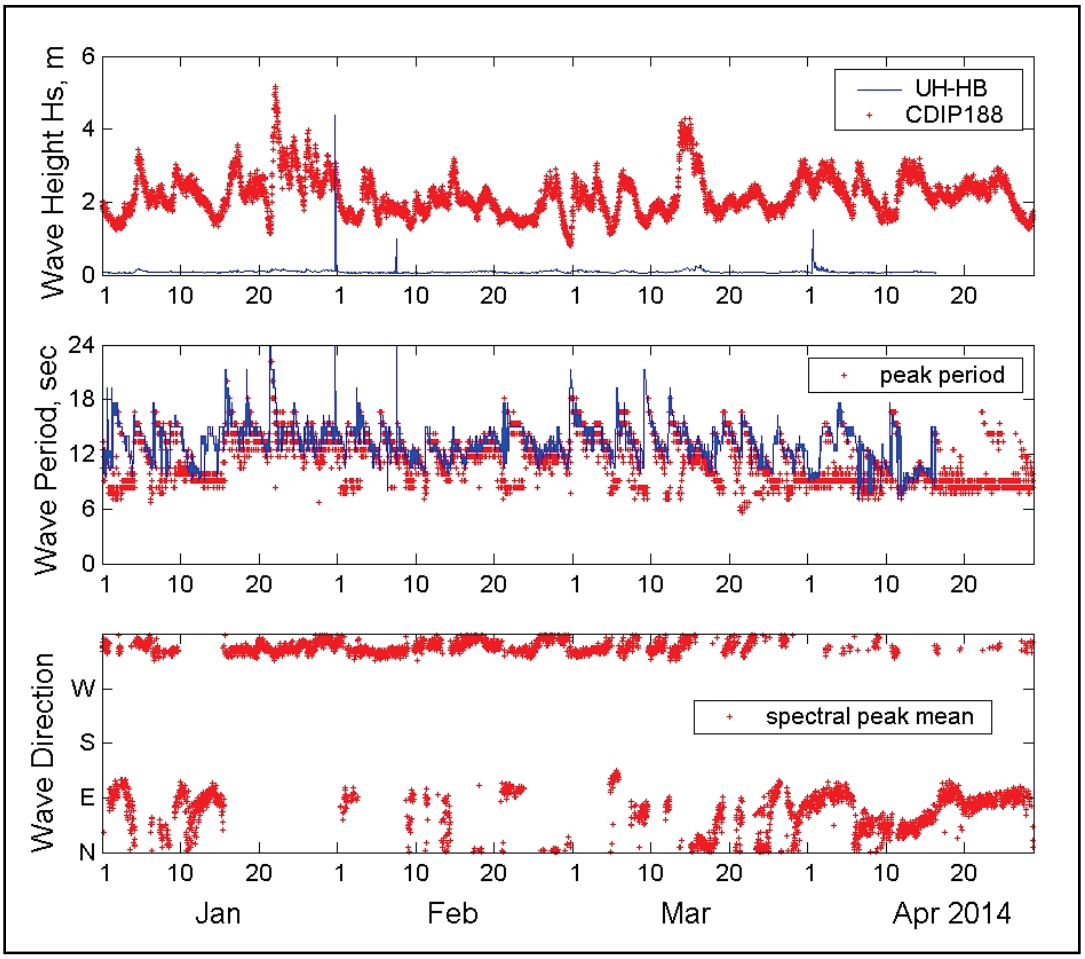

Figure 2-8. Wave data for March–June 2007 from CHL H1 and NOAA Buoy 51004.

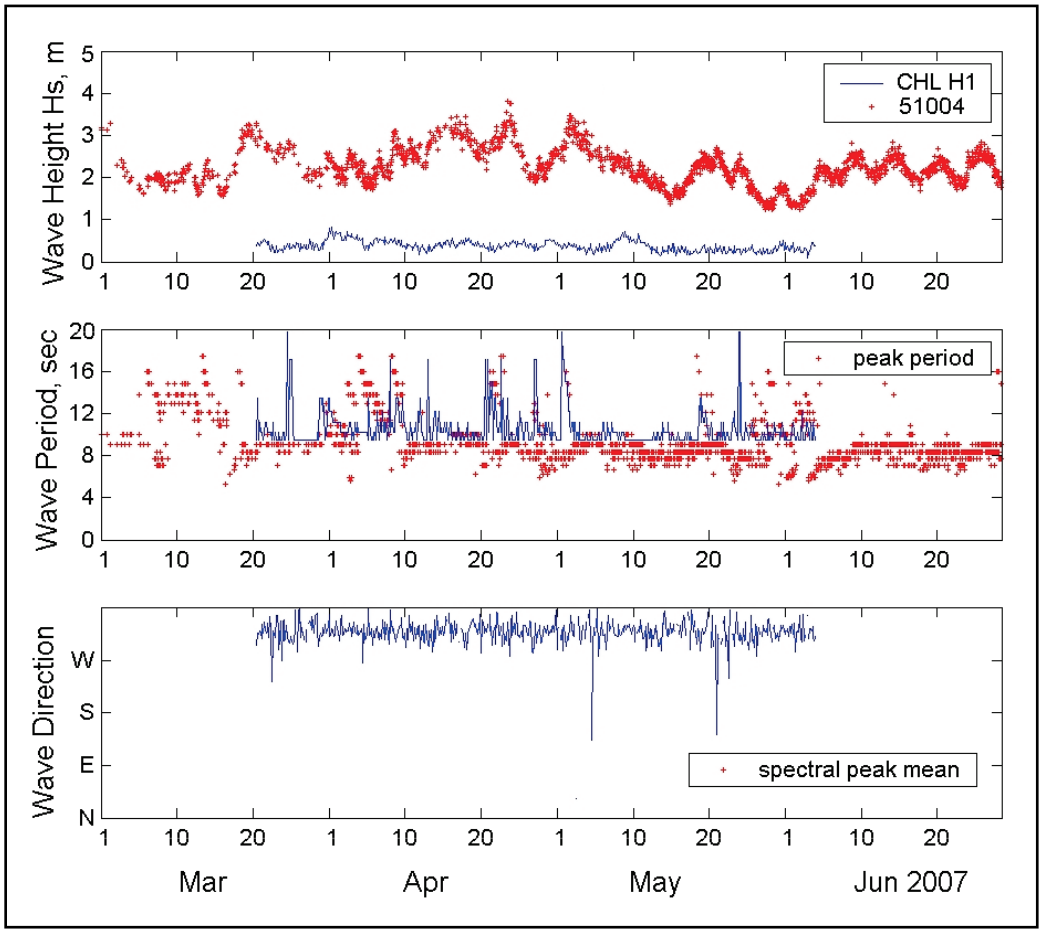

2.3 Wind data

Wind data for the Hilo Harbor modeling were obtained from the NDBC Buoys 51100 and 51004 and a tide gauge (NOAA Coastal Station ILOH1, 1617760) inside the Hilo Harbor (Figure 2-1). NOAA ILOH1 (19.73 N, 155.056 W), located at Hilo Harbor Pier 2 west end, has collected wind data since July 2008. Examples of wind data collected by NDBC 51004 and 51100 for 2011 and 2013 are shown in Figures 2-3 and 2-4, respectively. The wind data from both buoys show strong, easterly trade winds during the spring and fall seasons (March to November). Figure 2-9 shows example of 2013 wind data collected at NOAA ILOH1 and Buoy 51004. The wind magnitude at ILOH1 (Hilo Harbor) is much smaller than at the open ocean Buoy 51004, and wind direction at ILOH1 varies during the day between north and south directions due to local sea breeze at that location.

Figure 2-9. Wind data for 2013 from NOAA Station ILOH1 and NDBC Buoy 51004.

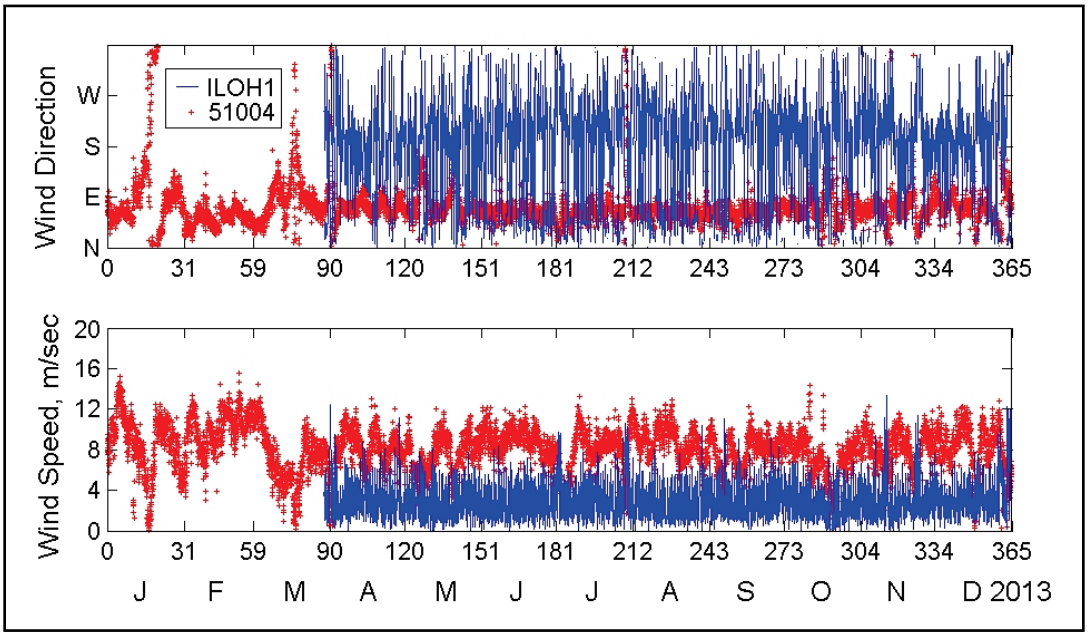

2.4 Water level data

Water level data were obtained from CHL H1 and UH-HB gauges and two NOAA Coastal Stations 1617433 and 1617760 (Figure 2-1). A tide gauge of NOAA 1617433 (20.037 N Latitude, 155.829 W Longitude) is located in the northern end at Kawaihae Harbor Pier on the west coast of the Hawaii Island, which has collected water level data since January 1996. NOAA 1617760 (19.73 N, 155.056 W) gauge is located on the west end of Hilo Harbor Pier 2, which has collected water level data since August 1994. Figure 2-10 shows hourly water level data for January–April 2014 from Stations 1617433, 1617760, and UH-HB. Figure 2-11 shows hourly water level data from CHL H1 and NOAA Station 1617760 for March–June 2007. According to Figures 2-10 and 2-11, the hourly water levels are very similar at the CHL H1, UH-HB, NOAA 1617760 (inside Hilo Bay) and at an outside tide gauge (NOAA 1617433 in Kawaihae Harbor) on the west coast of Hawaii Island.

Tables 2-2 and 2-3 provide tidal datum for NOAA gauges 1617433 and 1617760, respectively (http://tidesandcurrents.noaa.gov/stations.html). The mean range of tide (tidal range) at NOAA 1617760 (Hilo Harbor) is 1.67 ft (0.508 m), which is slightly higher than the mean range of 1.60 ft (0.488 m) at NOAA 1617433 (Kawaihae Harbor). Figure 2-12 shows comparison of water level data from Stations 1617433 and 1617760. The

Figure 2-10. Water levels at NOAA 1617433 and 1617760, and at UH-HB gauge for January–April 2014.

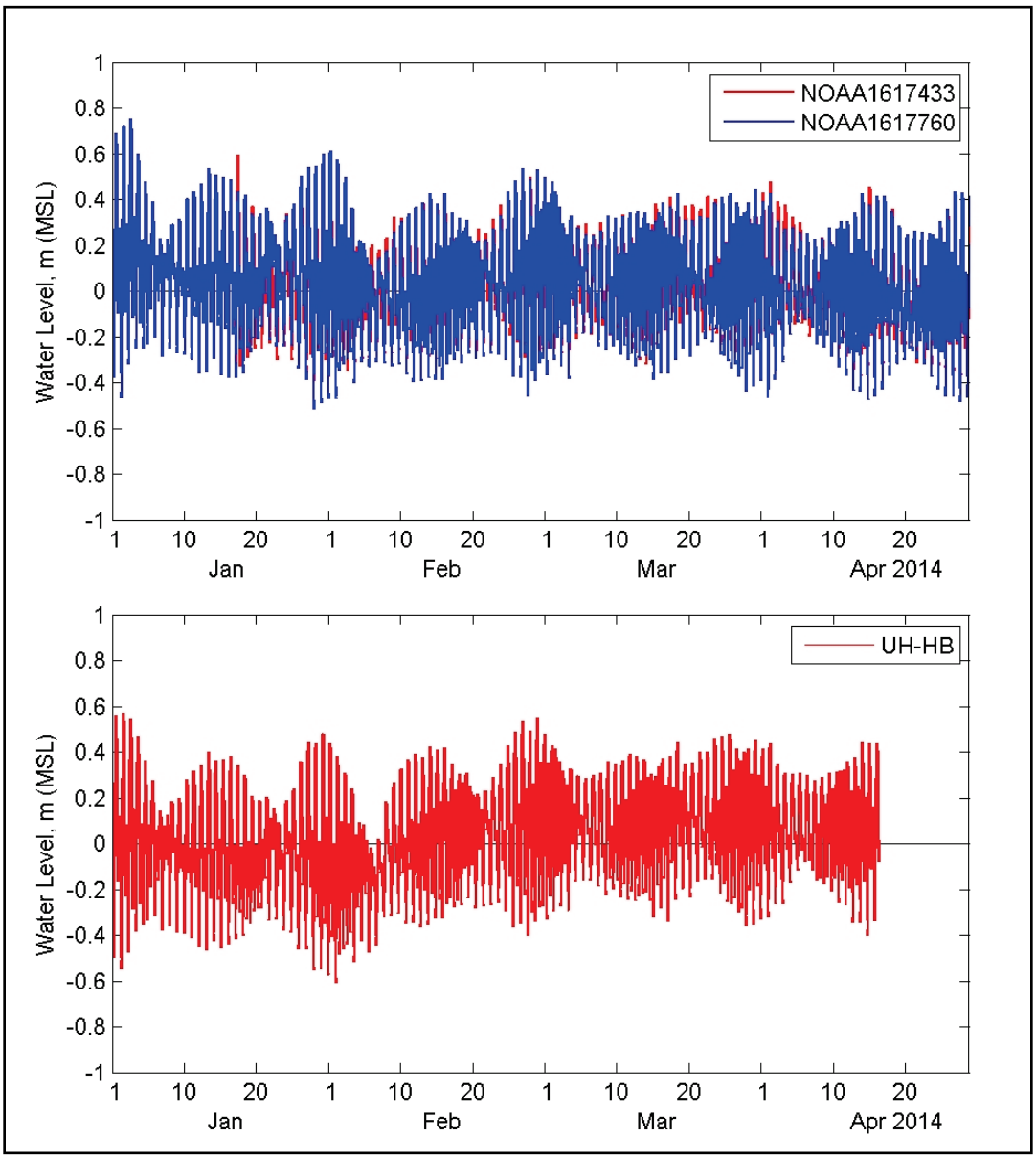

tidal signal is slightly stronger at NOAA 1617760 than 1617433, and the tidal phase at NOAA 1617760 is slightly lagging behind NOAA 1617433. In Figure 2-12, the abnormal fluctuation of water levels on 2 April 2014 was caused by a far-distant tsunami generated by the northern Chile earthquake that occurred on 1 April 2014, with an 8.2 magnitude (Mw).

Figure 2-11. Water levels for March–June 2007at Stations CHL H1 and 1617760.

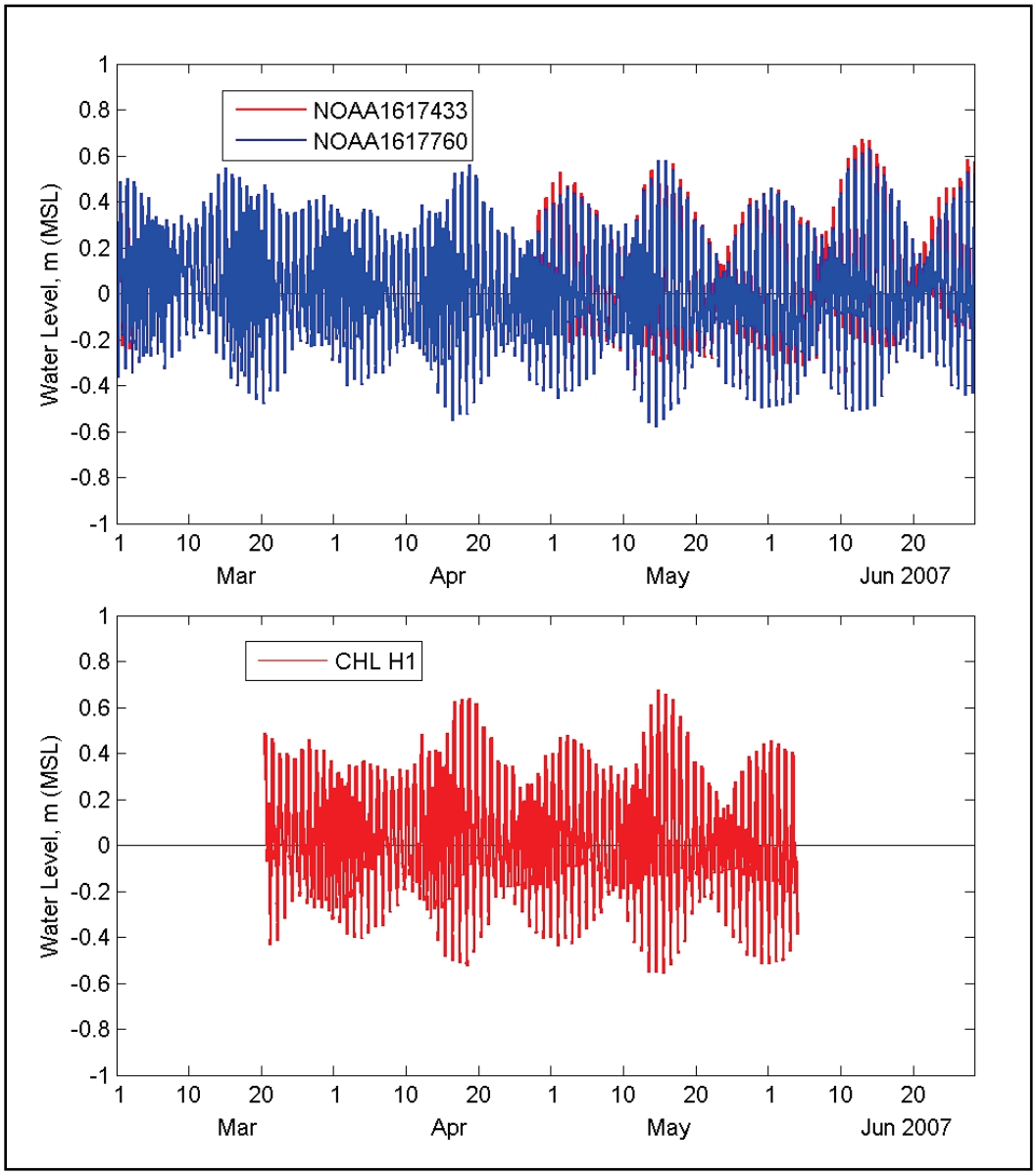

Table 2-2. Tidal datums (m) at NOAA 1617433 in Kawaihae, HI.

Mean Higher High Water (MHHW)	= 0.658
Mean High Water (MHW)	= 0.498
Mean Sea Level (MSL)	= 0.282
Mean Tide Level (MTL)	= 0.274
Mean Low Water (MLW)	= 0.050
Mean Lower Low Water (MLLW)	= 0.000
Mean Tidal Range (MHW – MLW)	= 0.448

Table 2-3. Tidal datums (m) at NOAA 1617760 (Hilo Harbor, HI).

Mean Higher High Water (MHHW)	= 0.731
Mean High Water (MHW)	= 0.599
Mean Sea Level (MSL)	= 0.349
Mean Tide Level (MTL)	= 0.345
Mean Low Water (MLW)	= 0.091
Mean Lower Low Water (MLLW)	= 0.000
Mean Tidal Range (MHW – MLW)	= 0.508

Figure 2-12. Water levels at NOAA Stations 1617433 and 1617760 for April 2014.

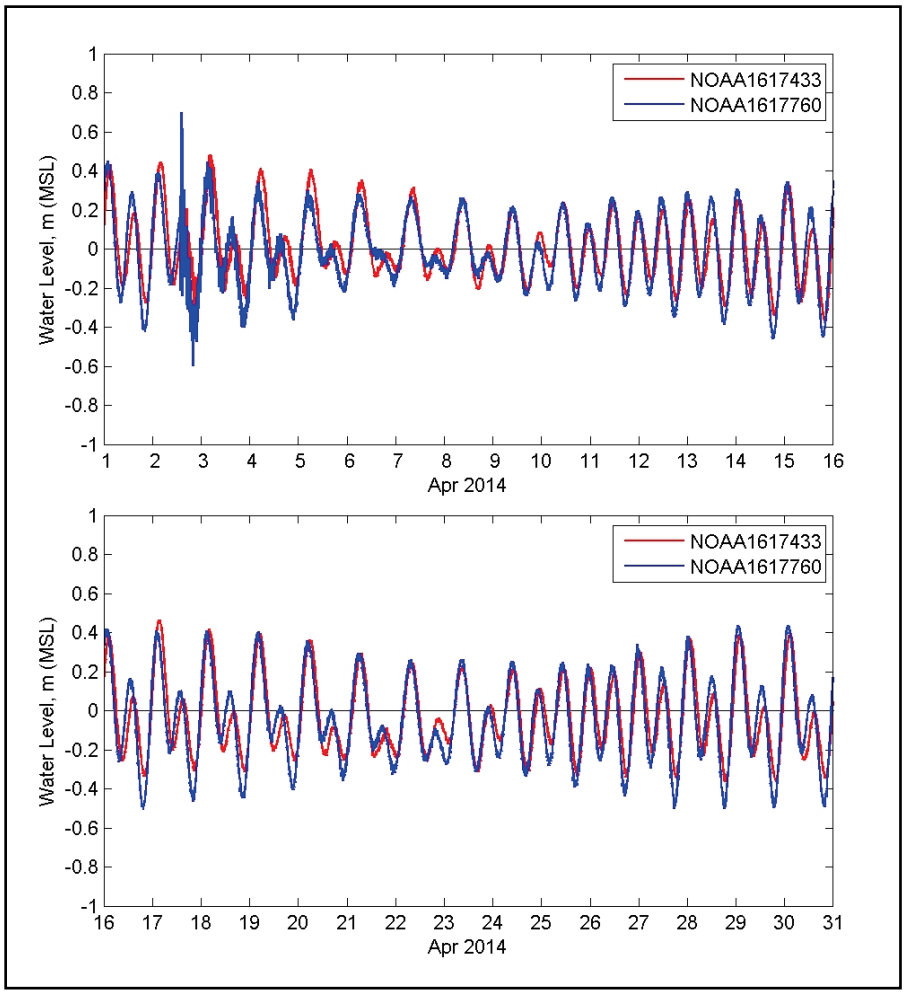

2.5 Current and discharge data

CHL deployed three gauges inside Hilo Bay from March to June 2007 to collect wave and current data. These gauges were H1, H2 (19.7317 N, 155.069 W), and H3 (19.739 N, 155.0639 W) and collected depth-averaged magnitude and direction of current. The nominal depth at all three gauges was 20 ft (~6 m). ADCP H3 operated only several days before the batteries were depleted, indicating the possibility that this unit was damaged during shipping before the deployment. No data were recovered from H3. Figure 2-13 shows current data from CHL H1 and H2 gauges for March–June 2007.

Figure 2-13. Measured current data for March–June 2007 from CHL H1 and H2.

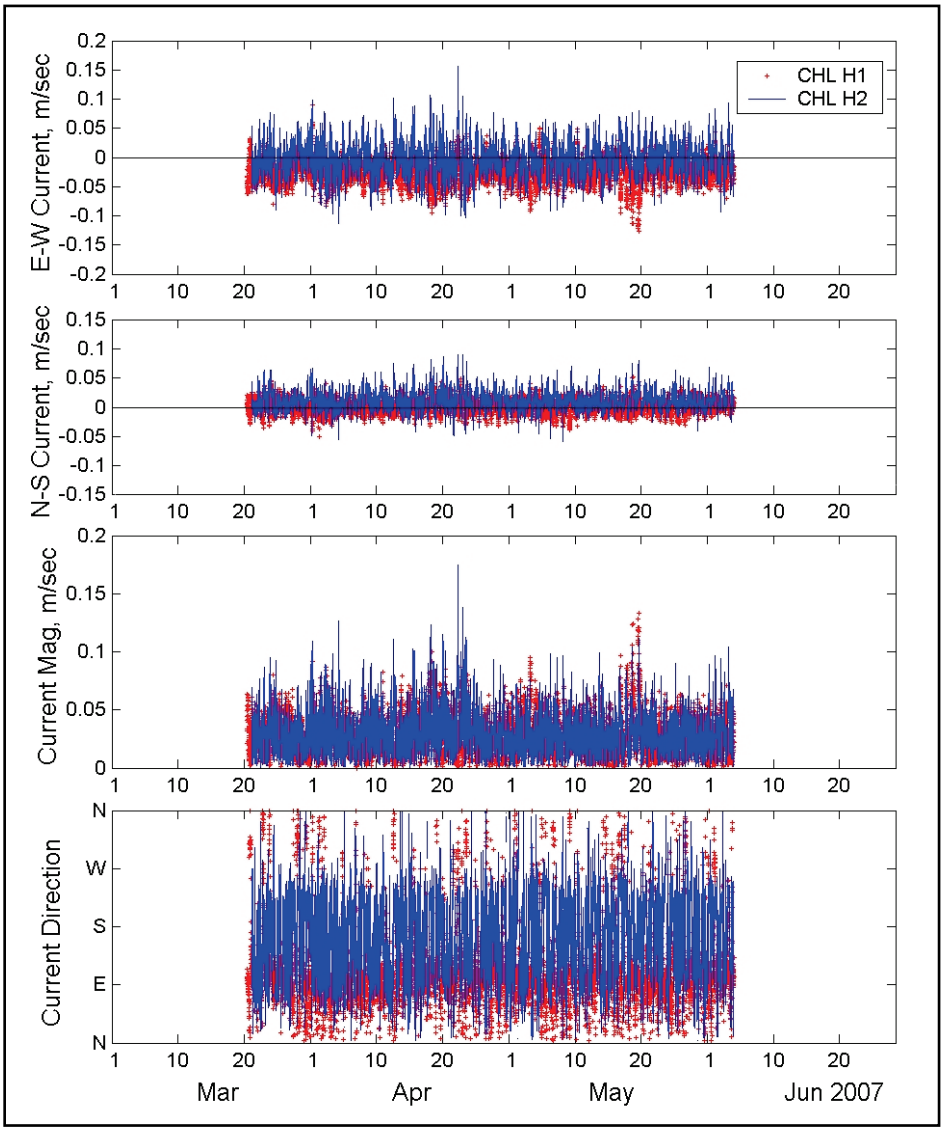

The largest river stream emptying into Hilo Bay is the Wailuku River, which has a drainage area of 150 square miles (390 square kilometers [km^2]). It is the longest and southernmost river in Hawaii. An average of 275 million gallons (~1 million cubic meters [Mm^3]) of water flow daily through the Wailuku to Hilo Bay. During intense storms, the discharge can be more than 20 times greater. Maximum discharge often reaches 3,500 cubic feet per second (ft^3/sec) (~100 m^3/sec). The daily flow rate at the lower reach of Wailuku River is available from the USGS Station 16704000 (19.7121 N, 155.151 W). Figure 2-14 shows the daily discharge data for 2012 collected at the USGS 16704000.

Figure 2-14. River flow discharges from USGS 1614000 in Wailuku River for 2012.

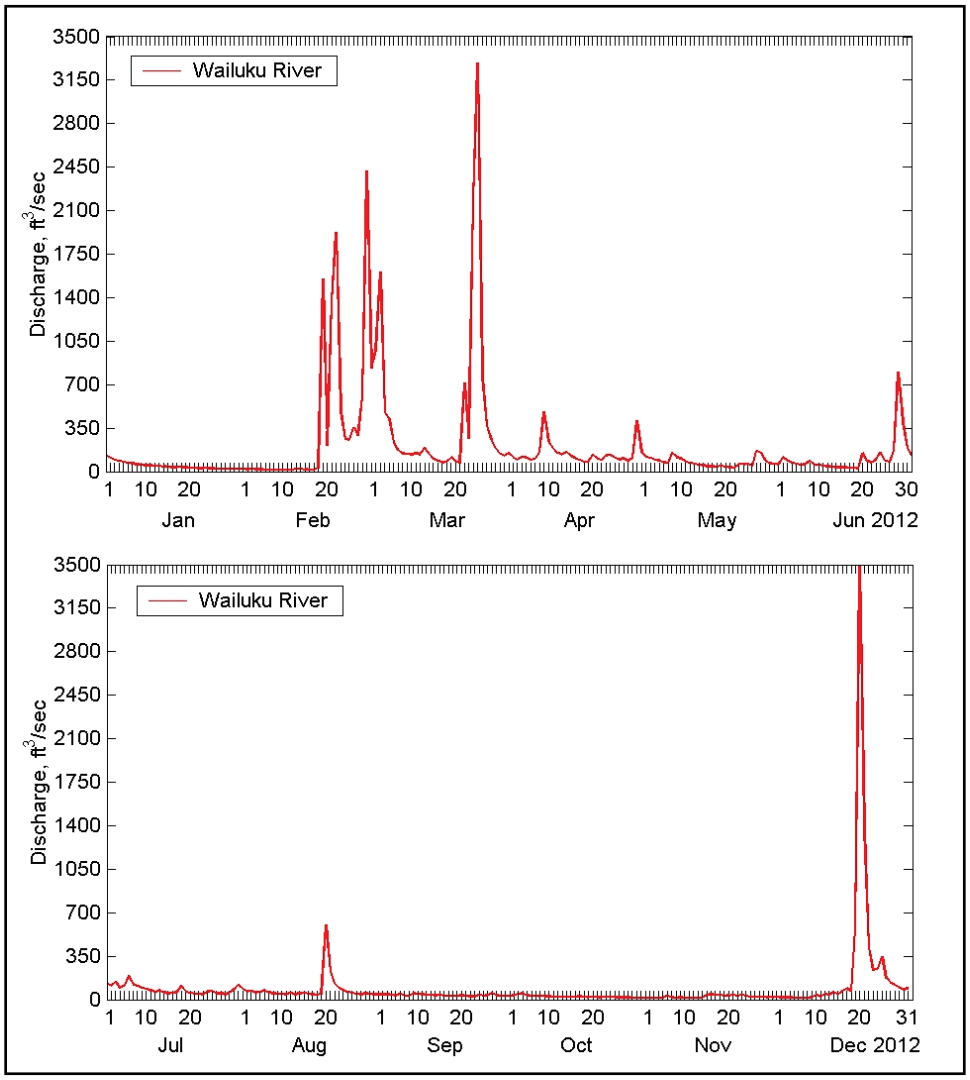

3 CMS-Wave Modeling

Wave modeling for Hilo Harbor was conducted using two types of numerical models: B2D and CMS-Wave. B2D was used in this study to investigate Alternatives representing different proposed structure changes to the inside and outside of the harbor. Because B2D is a fully nonlinear time-domain model able to represent linear and nonlinear nearshore wave processes, it is a computationally resource-demanding model. B2D is used in the present study over a small area covering details of the harbor, structures, and the immediate vicinity including reefs and shorelines.

To determine how winds, waves, and water levels affect navigation at Hilo Harbor, a good understanding of the effects of complex bathymetric features, surrounding coastlines, and protective structures on water levels, waves, and currents is required. The geometries of the existing breakwater, harbor entrance, navigation channel, mooring/waiting area, and Piers 1 and 2 play a role in navigation problems, as well as for evaluating relative merits of Alternatives with different structural modifications. Field data were used in the understanding of the existing navigation difficulties experienced inside and outside the harbor and for assessing the potential usefulness of Alternatives. The existence of hard bottom reefs inside and outside the harbor limits the type of Alternatives that can be considered. Reefs not only limit the amount of dredging by reducing channel shoaling rates but also narrow the range of Alternatives favorable for safe navigation based on relative position and alignment of structural Alternatives in relation to the entrance, navigation channel, breakwater, and reefs.

Because large domain modeling around Hilo Bay was not possible with B2D for a wide range of wave conditions, it was necessary to augment B2D modeling with a spectral wave model capable of providing estimates of waves over much larger domains and for a large number of wave conditions. The CMS-Wave was selected as a steady-state, two-dimensional (2D) spectral wave model (Demirbilek et al. 2008; Demirbilek and Rosati 2011; Lin and Demirbilek 2012, 2005; Lin et al. 2008; Lin et al. 2011) for simulating wave processes with ambient currents at navigation channels, coastal inlets, and harbors. Because of

complementary features of B2D and CMS-Wave, these models are frequently used in tandem in similar coastal studies.

CMS-Wave was used to transform offshore wave information provided by deep-water coastal buoys and other available wave information to the project site at the seaward boundary of B2D. CMS-Wave was also used to check the reliability of deployed field gauges to obtain nearshore wave data for B2D modeling. CMS-Wave is part of an integrated CMS developed at CHL for coastal inlets and regional modeling project applications. A brief description of the CMS is presented in Appendix A.

CMS-Wave can be used in half-plane or full-plane mode for wave transformation from deep to shallow water. The half-plane mode is the default because CMS-Wave can run more efficiently in this mode as waves are transformed primarily from the seaward boundary toward shore. The model is based on the wave-action balance equation that includes wind-wave generation and growth, wave propagation, refraction, shoaling, diffraction, reflection, breaking, and dissipation. The computational efficiency of the model and recent improvements to capabilities of the model allow for the simulation of large domains and a large number of wave conditions in coastal engineering applications. The nested-grid capability of the model is used here to ensure necessary grid resolution for representing fine details of the harbor geometry.

CMS-Wave was used to develop incident wave-input conditions for the B2D model. Several improvements to CMS-Wave were necessary to provide these inputs, as well as to address the project's other needs. Additional research and development (R&D) to enhance the model's predictive capabilities was funded by the CIRP. The advances included (a) simulations for tropical storms and nonstorm waves in full-plane mode with parent-child grid capability of CMS-Wave, (b) modeling of a dual-peaked wave condition (combined seas and swells from different directions), (c) developing 2D wave spectra at the offshore boundary of B2D, (d) validation of model with the NOAA buoys and CDIP gauges near the project site for improving the deep water wave generation/growth capability of CMS-Wave, (e) development of pre- and post-processing analysis codes for improving model setup, (f) developing and providing spatially varying wave parameters (height, period, direction) and wave spectra along the model boundary as B2D input conditions, and (g) developing a number of Fortran and Matlab utilities to facilitate coupling

of two wave models. This chapter describes the CMS-Wave modeling, and Chapter 4 provides details of B2D modeling.

3.1 Model domain

Two grids were generated for CMS application to Hilo Harbor, one for CMS-Wave and another for CMS-Flow. Figure 2-2 shows the CMS-Wave and CMS-Flow model domains and locations of field gauges. The CMS-Wave grid consisted of 504 × 564 grid cells, with variable cell spacing. The smallest cells were 13.1 ft (4 m) in the bay, with cell size increasing to 650 ft (200 m) in the offshore area. The CMS-Wave grid covered a rectangular domain of 6.0 miles (11 km) × 10.0 miles (18.5 km) extending eastward and northward to approximately the 1,100 ft (340 m) depth contour. The CMS-Flow grid was a subdomain of CMS-Wave, with 472 × 503 grid cells of variable cell size ranging from 13.1 ft (4 m) to 540 ft (165 m). The flow model grid covered a rectangular area of 3.2 miles (6 km) × 3.5 miles (6.4 km) that extended from Hilo Bay to the offshore depth contour of 260 ft (80 m). The CMS-Wave grid domain was greater than the CMS-Flow grid domain for transforming waves properly from offshore locations into the Bay. The CMS-Flow grid domain was sufficiently large and covered the reef present outside the Hilo Harbor. Bathymetric data for both grids were extracted from NGDC database, USGS DEM, and USACE surveys, which represented the most recent bathymetry of Hilo Bay and harbor complex.

Because CMS-Wave was used to develop input wave conditions for B2D simulations, the domains and orientation of three B2D grids (north, north-northeast, and northeast grids) are shown in Figure 3-1. The north grid in Figure 3-2 shows details of Hilo Bay bathymetry, the breakwater to the north that protects the harbor, the reefs present outside and in the interior harbor, and the two piers. To highlight the complexity of waves, Figure 3-3 is an example wave field from B2D for an incident wave from the north (north grid). This figure shows interesting spatial patterns of waves moving over the outside fringing reef system including areas of wave focusing (converging) caused by strong wave refraction, shoaling, and breaking, and waves wrapping around the tip of the breakwater and moving into the interior harbor. Similar wave height trends were also observed in B2D model results obtained with the north-northeast and northeast grids. (See Chapter 4 for additional information about B2D modeling.)

Figure 3-1. Three B2D model domains (north, north-northeast, and northeast grids).

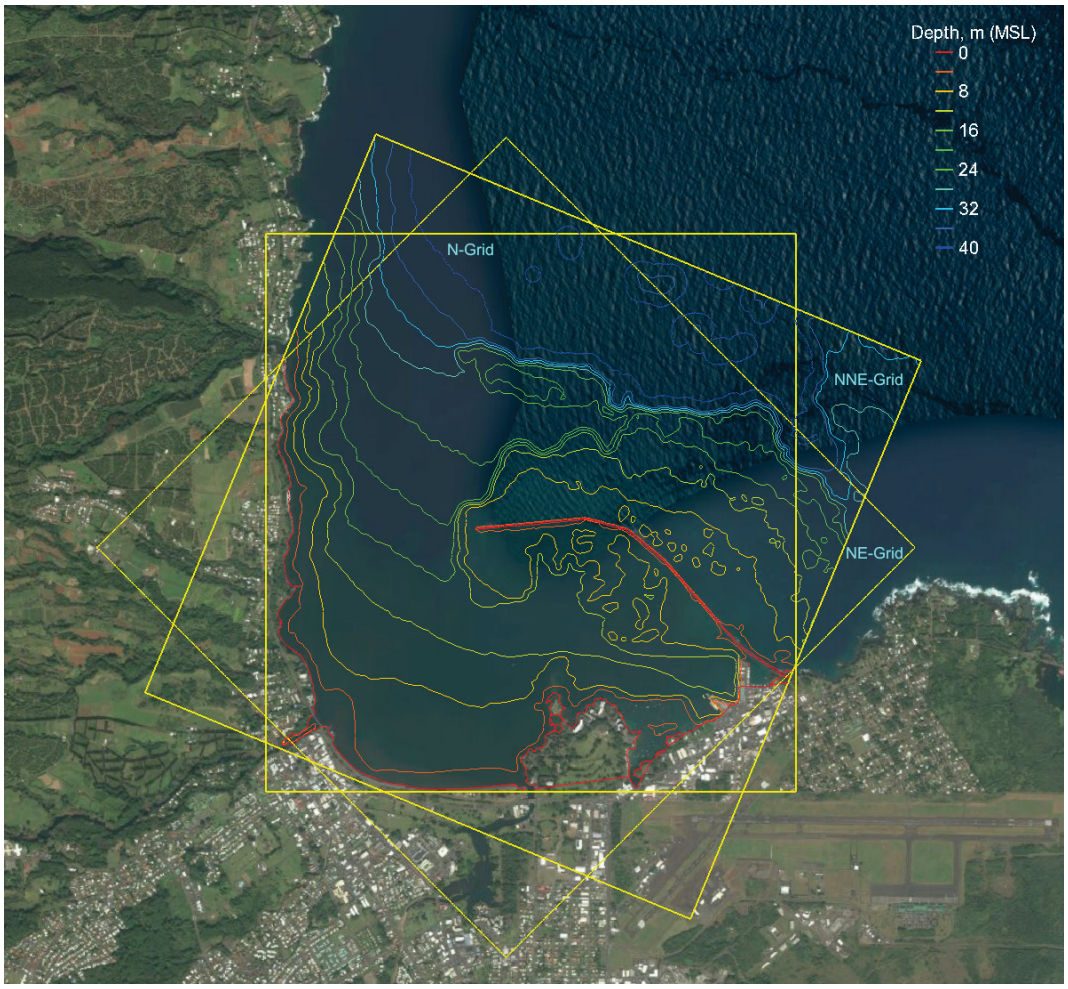

Figure 3-2. Bathymetric features of Hilo Bay in B2D north grid.

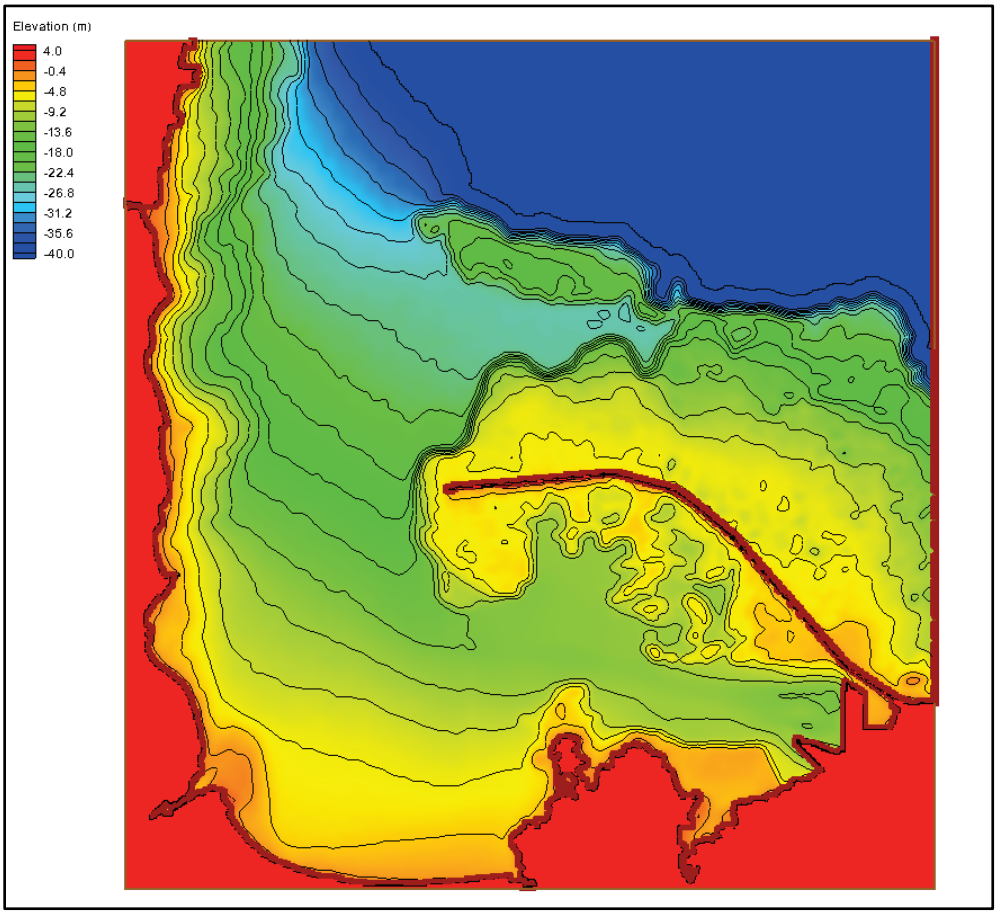

Figure 3-3. Example of wave height field from a B2D simulation.

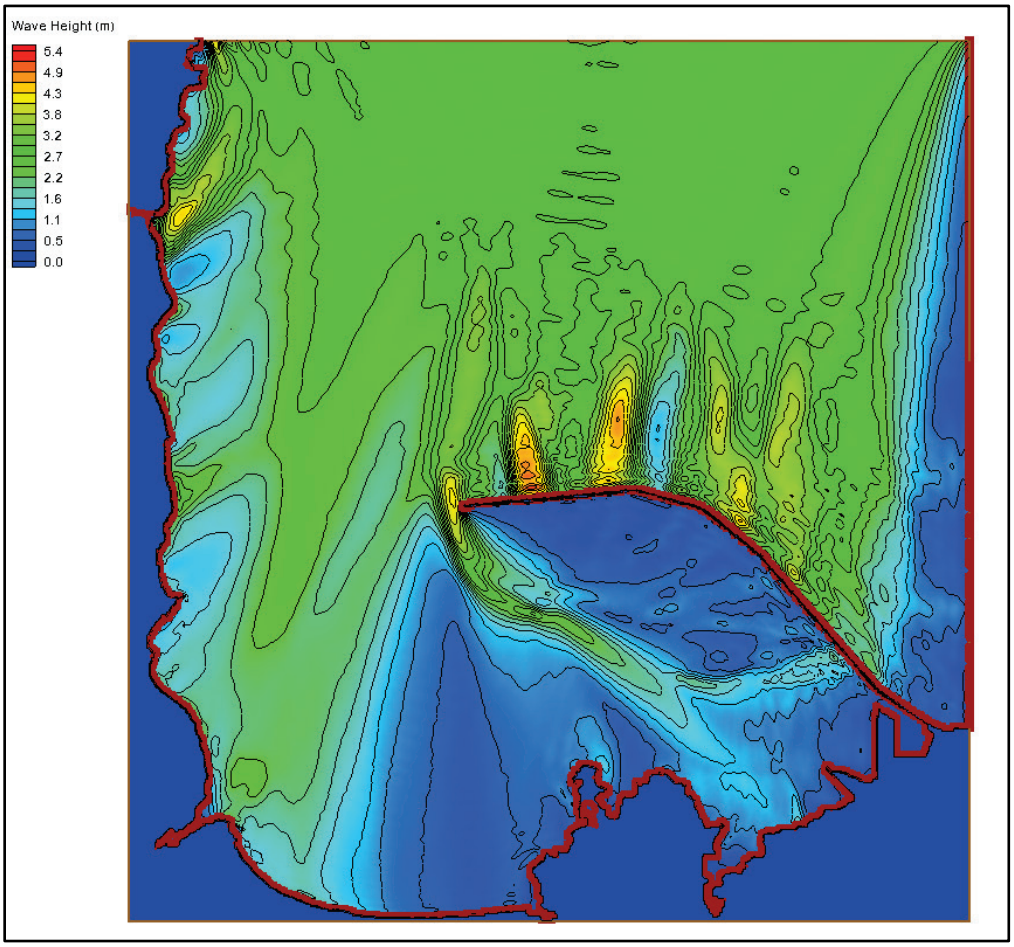

3.2 Model verification

The deep-water spectral waves were transformed with CMS-Wave using the full-plane mode to ensure accurate estimates of incident waves at the B2D grid boundary. These simulations used 35 directional bins with a 5 deg directional resolution and 42 frequency bins with frequencies ranging from 0.04 to 0.45 Hz in 0.01 Hz increments. Wave shoaling, refraction, diffraction, reflection, runup processes, and wind input were included in the simulations. CMS-Flow was coupled with CMS-Wave to calculate water level variation and current fields in the flow model domain.

The CMS-Wave and CMS-Flow models were calibrated for the period 21–31 March 2007. Incident directional waves were obtained from NDBC Buoy 51001 (23.445 N, 162.279 W), surface winds from WIS 82527, and water levels as boundary condition to the CMS were obtained from NOAA 1617433. CMS-Wave and CMS-Flow were coupled at a 3 hr interval. The effect of reef bottom on calculated water level and current estimates was

calibrated by tuning Manning's coefficients in CMS-Flow by comparing model results to data from field gauges. Figure 3-4 shows two regions with different Manning's coefficients (0.075 and 0.085) used in the flow model.

Figure 3-4. Manning's coefficients applied in CMS-Flow.

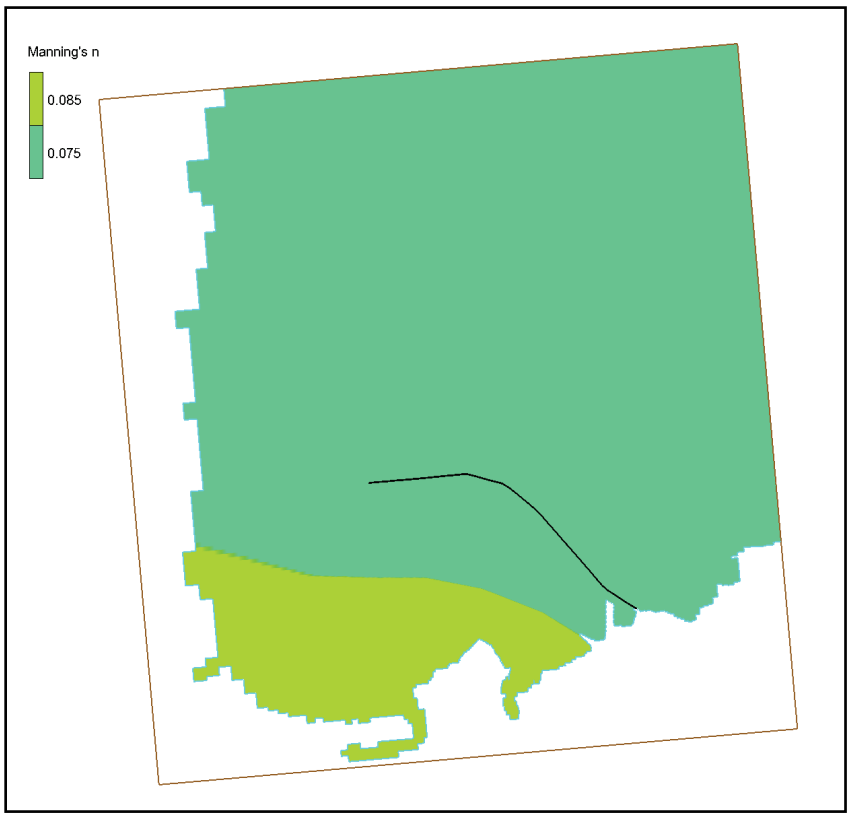

Figure 3-5 shows a comparison of calculated and measured waves for 21–31 March 2007 at CHL H1. Figure 3-6 shows calculated and measured water levels for 21–31 March 2007 at CHL H1 and NOAA 1617760. Figure 3-7 shows calculated and measured currents for 21–31 March 2007 at CHL H1 and H2. The CMS calculated current magnitude and direction at H1 agree well with data, but current magnitude at H2 is overestimated by the model. The model calculated current direction estimates at H2 had a larger bias than those at H1. The overestimated current magnitude at H2 is likely caused by the hindcast coastal wind data used in the model, which are stronger than the winds in the bay.

Figure 3-5. Measured and model waves during 21–31 March 2007 at CHL H1.

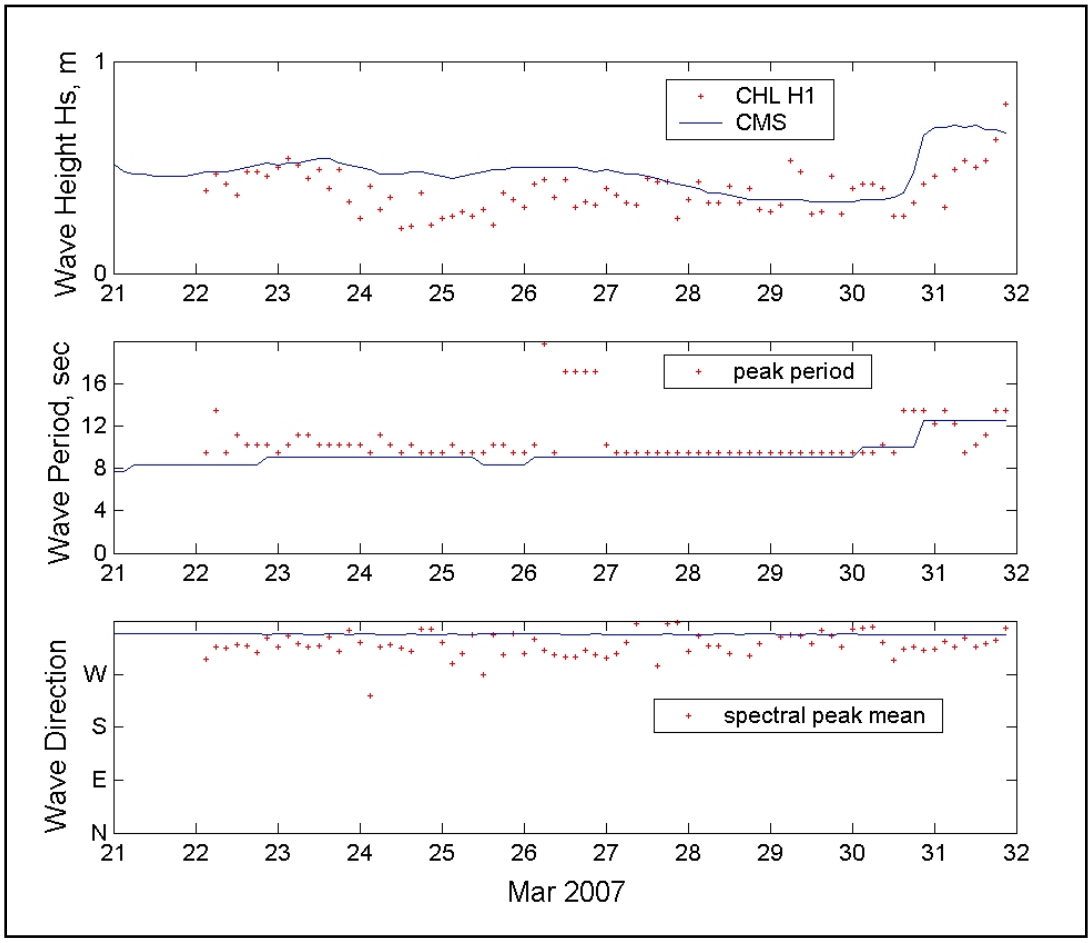

Figure 3-6. Measured and model water levels for 21–31 March 2007 at CHL H1 and NOAA 1617760.

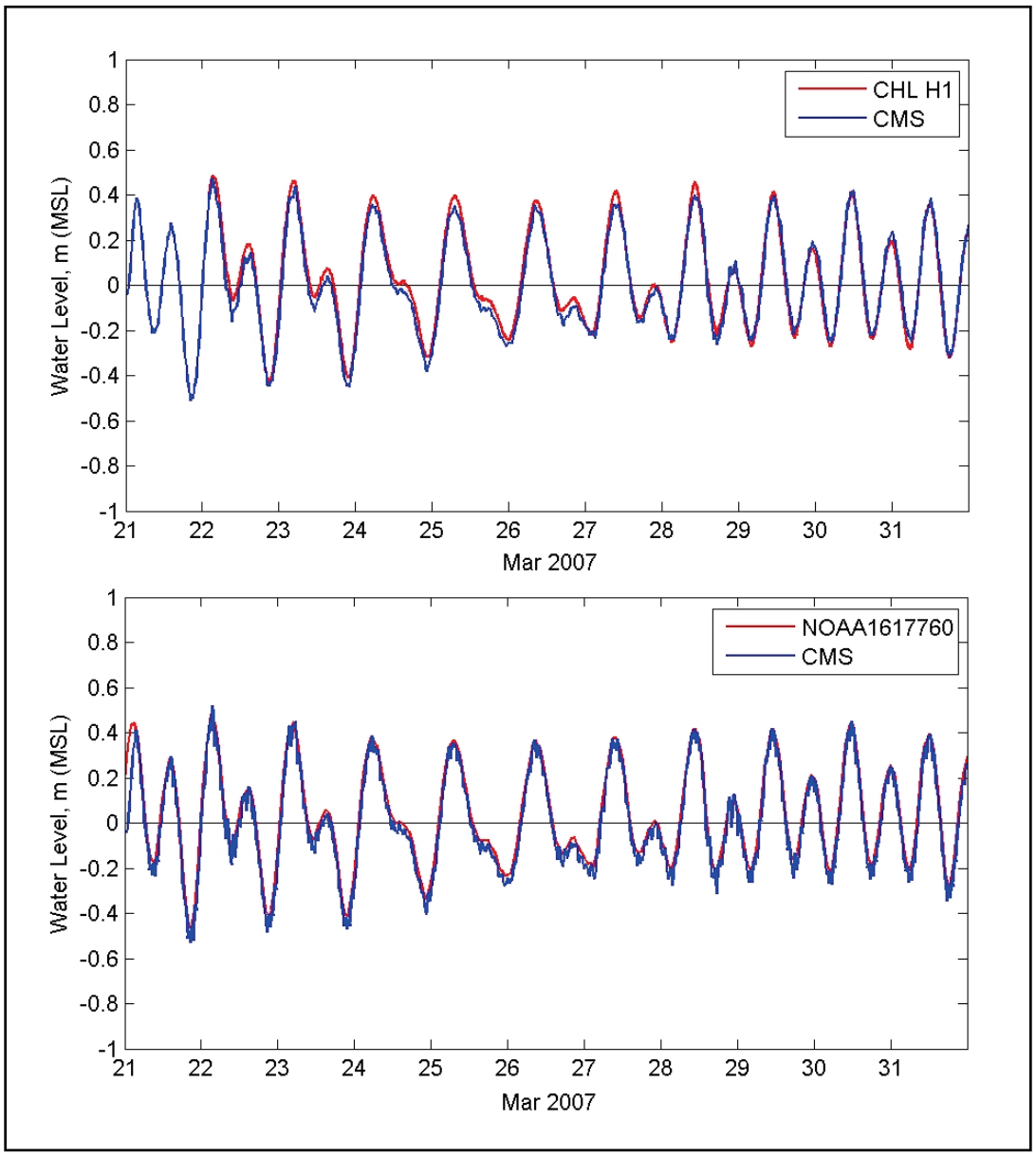

Figure 3-7. Measured and model currents for 21–31 March 2007at CHL H1 and H2.

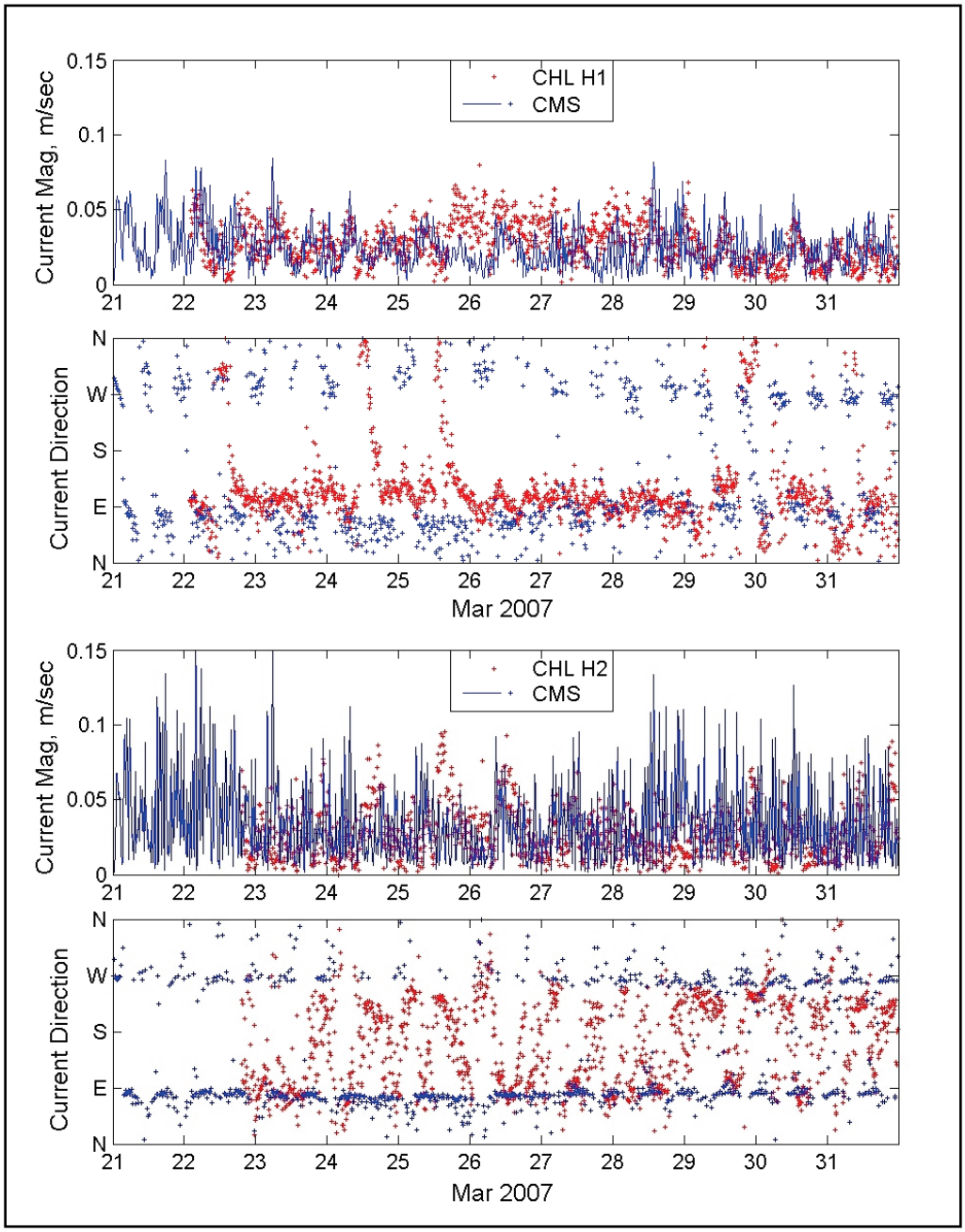

April 2007 field measurements data were used to validate CMS-Wave and CMS-Flow models. For boundary inputs to the CMS, incident directional wave data were obtained from NDBC Buoy 51001 (23.445 N, 162.279 W), surface winds from WIS 82527, and water levels from NOAA 1617433. CMS-Wave and CMS-Flow were coupled at 3 hr interval. Calculated and measured waves at CHL H1 for April 2007 are compared in Figure 3-8, water levels at CHL H1 and NOAA 1617760 in Figure 3-9, and currents at CHL H1 and H2 in Figure 3-10. These comparisons show calculated waves

Figure 3-8. Measured and model waves at CHL H1 in April 2007.

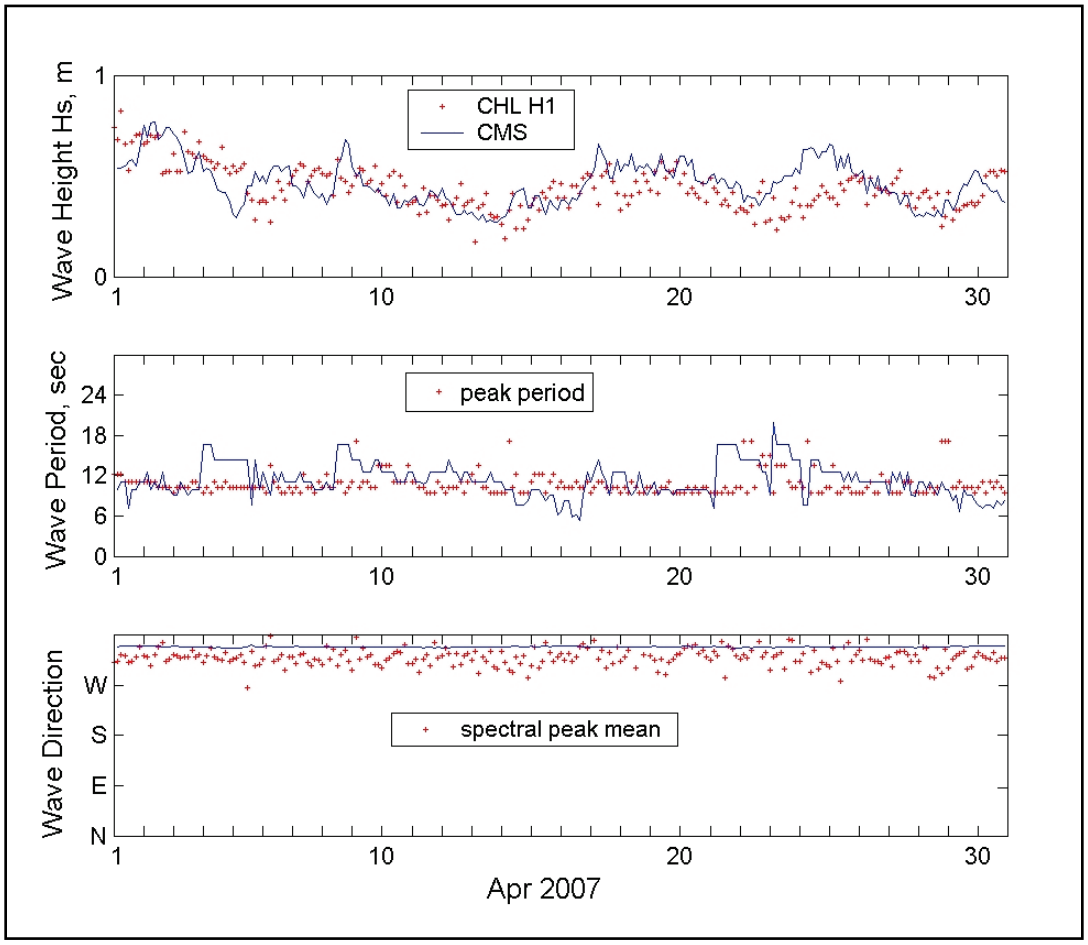

agree well with data at CHL H1. Likewise, calculated water levels agree well with data at CHL H1 and NOAA 1617433. Both calculated current magnitude and direction agree better with data at H1 than H2, which was also noted in the model calibration.

Figure 3-9. Measured and model water levels in April 2007 at CHL H1 and NOAA 1617760.

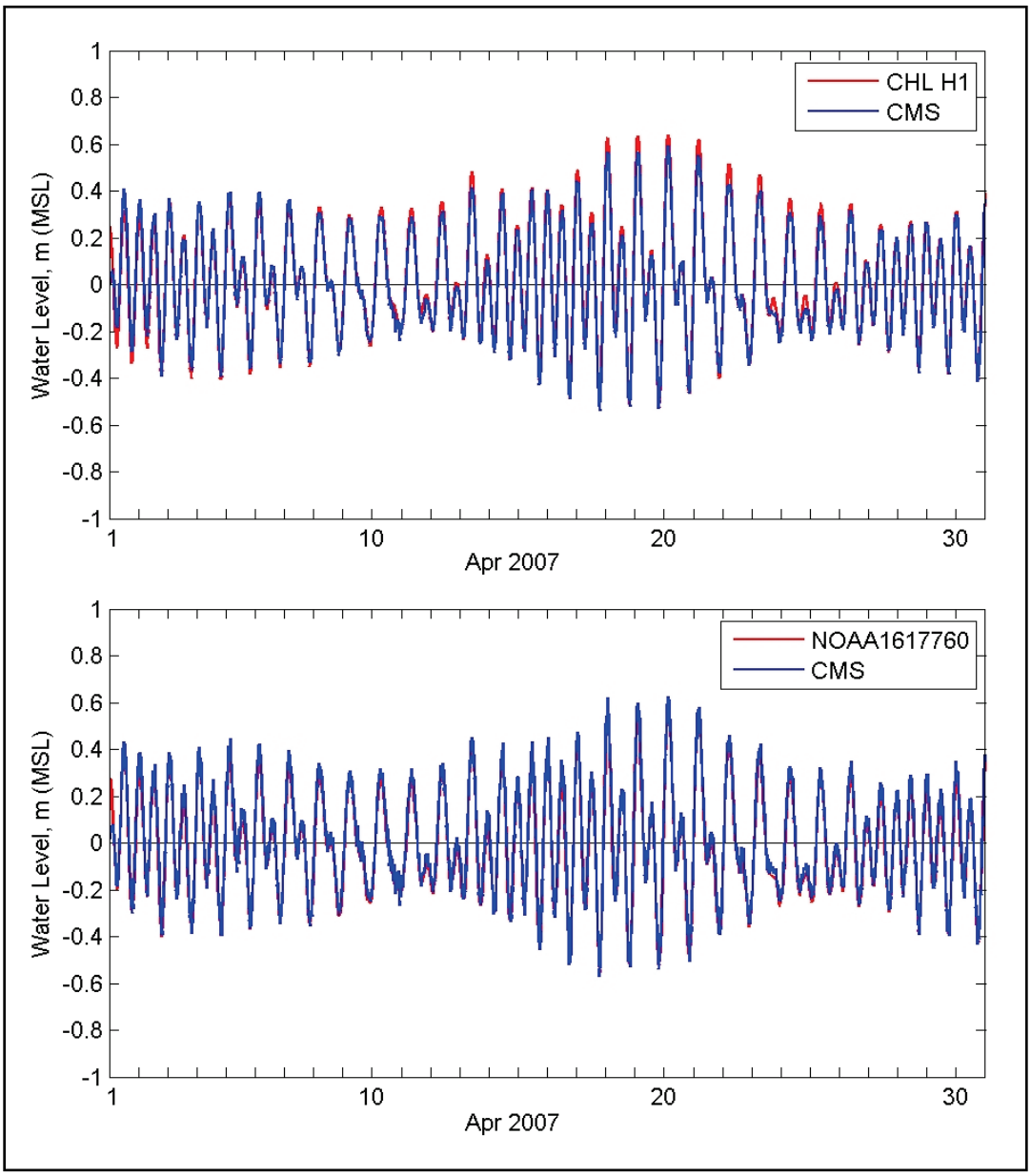

Figure 3-10. Measured and model currents at CHL H1 and H2 in April 2007.

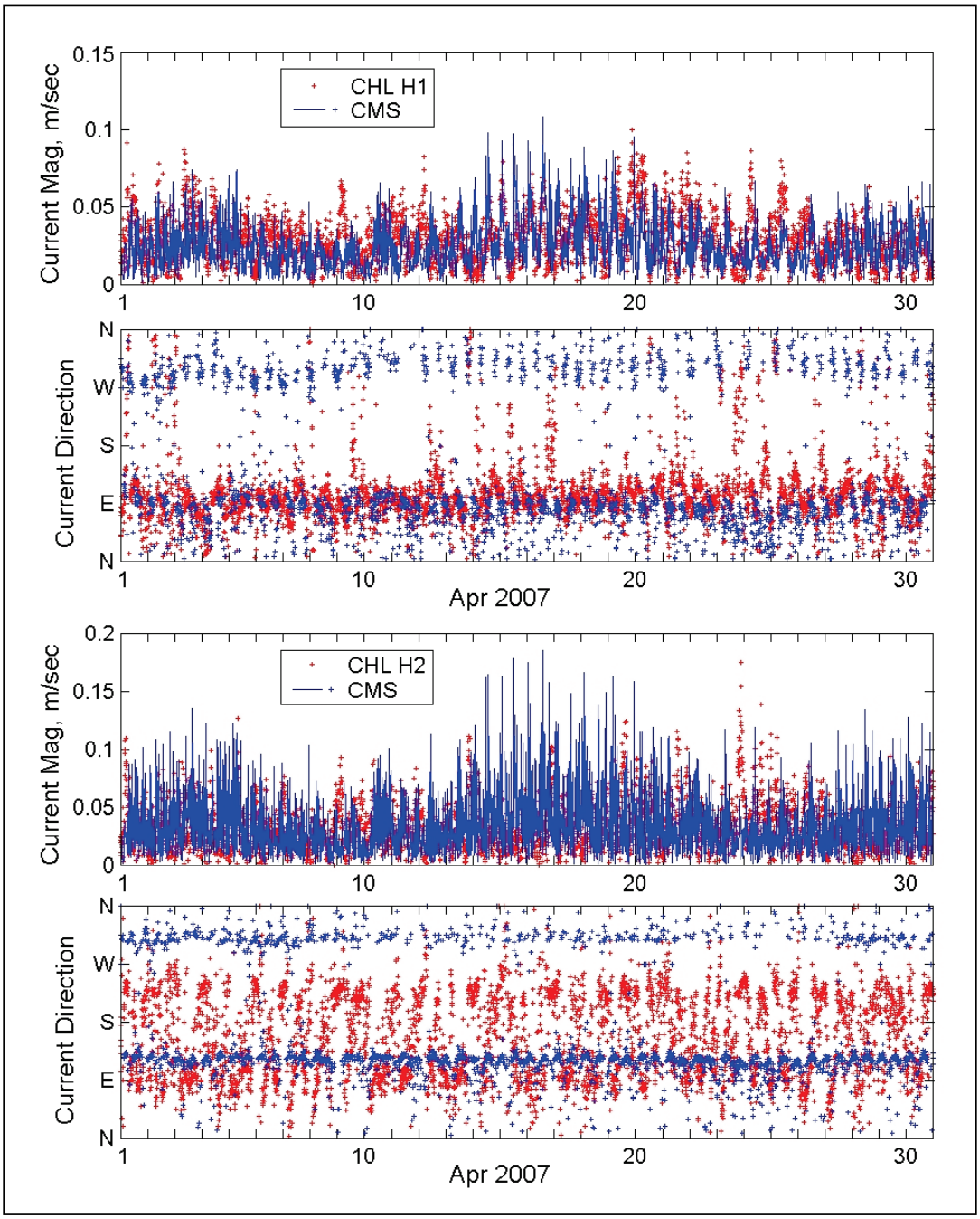

3.3 Selection of simulation conditions

The selection of simulation conditions considered events that can generate strong currents in Hilo Harbor that can potentially affect navigation. Additional analyses of the data sources described in the previous sections were performed to select representative conditions that would be consequential to harbor navigation. A set of spring tides and storm waves

was identified for these simulations, which are listed below and summarized in Table 3-1. Test runs confirmed that maximum currents occur in the Hilo Bay navigation channel for these selected forcings. From each simulation, the maximum current cycles (snapshots of maximum ebb and flood currents) were selected for typical spring tides and storm events. Model results only for these extracted snapshots (time periods) were provided to the ship simulation team.

Table 3-1. Matrix of inputs conditions for the ship simulator use.

Case	Time Period	Water Level	Wind Forcing	Incident Wave
1	6–7 May 2012	Spring tide	~ 8 m/sec, ENE	~ 2 m, 9 sec, ENE
2	14–15 November 2012	Spring tide	~ 2 m/sec, NE	~ 2 m, 14 sec, E
3	24–26 March 2012	Spring tide	~10 m/sec, NE	~ 3 m, 10 sec, NE
4	15–16 May 2011	Mean range	~10 m/sec, NE	~ 3 m, 10 sec, NE
5	27–29 October 2012	Mean range	~10 m/sec, N	~ 3 m, 12 sec, N
6	22–23 December 2012	Mean range	~10 m/sec, ENE	~ 4 m, 15 sec, ENE

Based on further analyses of available wind, wave, and water level data, the following dates were selected as simulation periods for the CMS-Wave and CMS-Flow models. For the duration of each selected event, the corresponding metocean data were obtained from available data sources. A special emphasis was on inclusion of the effects of trade winds with which mariners have reported difficulties. This is reflected in the direction selected for the events (north, east-northeast, and northeast).

The metocean conditions for the following time periods were used in CMS simulations for spring tides: (1) 6–7 May 2012, (2) 14–15 November 2012, and (3) 24–26 March 2012.

The following time periods and associated metocean conditions were used in CMS simulations for storms: (1) 15–16 May 2011, (2) 27–29 October 2012, and (3) 22–23 December 2012

3.4 Model simulations

CMS simulations were conducted for the existing harbor and a proposed dredge configuration shown by a polygon in Figure 3-11. The proposed dredge depth inside the polygon was set to 35 ft (10.7 m) MLLW or 36 ft (11.0 m) MSL. The conditions used in CMS simulations are listed in Table 3-2. All simulations were forced by water levels, waves, and winds, except for Condition 3. For Condition 3, additional run was conducted with flow discharges for Wailoa River and Wailuku River. The discharge for Wailoa River was estimated based on measured river flow discharge for Wailuku River by using the proportion of drainage areas of the two rivers.

Table 3-2 provides the inputs for each of the simulation condition corresponding to spring tides and storm events. This includes the simulation period (start and end dates of simulations), duration of simulation in hours, two harbor configurations considered (e.g., existing harbor [Alt-0] and one area of existing harbor dredged [Alt-1]), runs with river discharges, and two water levels considered (spring tide and average tide or mean range).

Figure 3-11. Location of proposed dredge area inside the polygon.

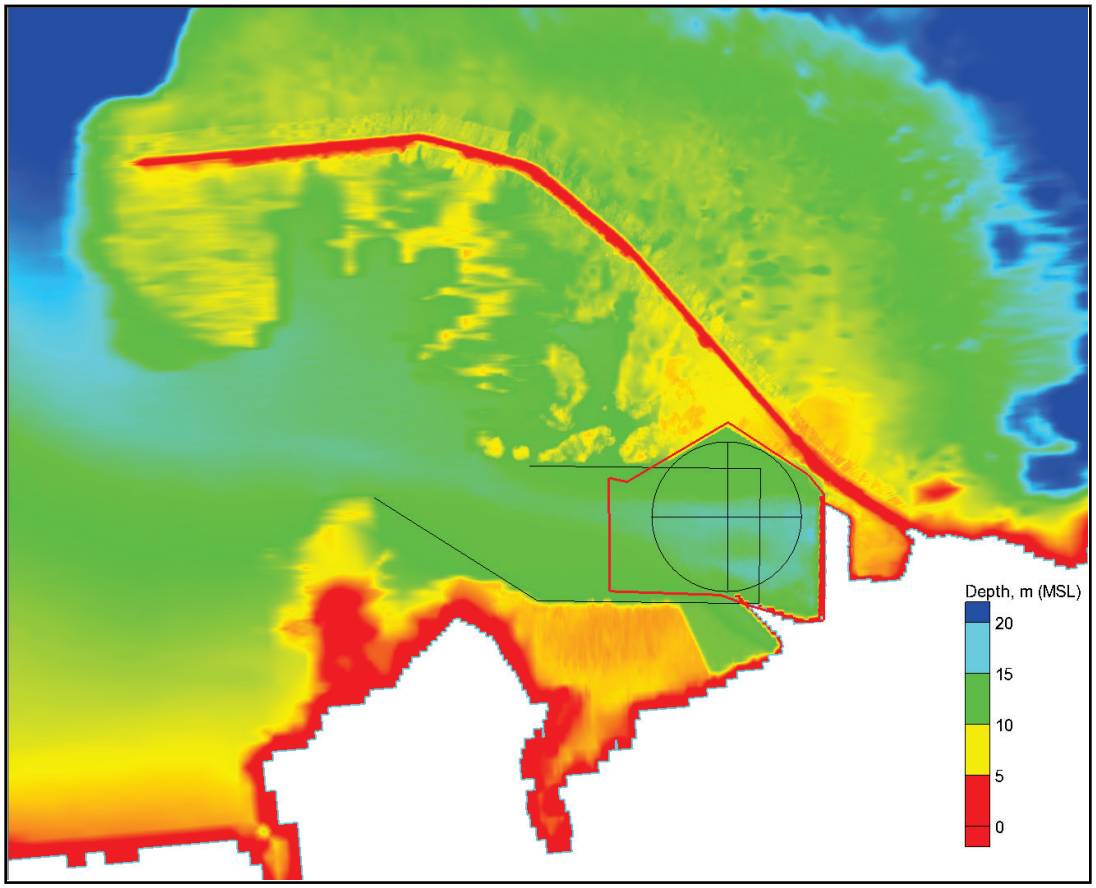

Table 3-2. Input data used in CMS simulations for ship simulator.

Simulation Dates	Duration (hr)	Configuration	Water Level
6–7 May 2012	24	Alt-0 Alt-1 (dredged harbor)	Spring tide
14–15 November 2012	24	Alt-0 (dredge)	Spring tide
24–26 March 2012	36	Alt-0 (without rivers)	Spring tide
24–26 March 2012	36	Alt-0 (with rivers)	Spring tide
15–16 May 2011	33	Alt-0, Alt-1	Mean range
27–29 October 2012	33	Alt-0, Alt-1	Mean range
22–23 December 2012	33	Alt-0, Alt-1	Mean range

3.5 Model output for ship simulator

CMS results corresponding to maximum currents in the navigation channel were extracted in a subrectangular area of the CMS-Flow grid domain (Area A in Figure 3-12). The time of occurrence of the maximum current during a simulation was determined for both the flood and ebb cycle. This was done by using two small rectangular areas (Areas B and C) to calculate the spatially averaged current magnitude corresponding to the maximum flood current (in Area B) and maximum ebb current (in Area C). The maximum current fields were saved for the existing bay configuration and also for a proposed dredge area and in the channel and turning basin. Examples of maximum flood and ebb current fields are provided in Figures 3-13 and 3-14, respectively. These were extracted from CMS run for 6–7 May 2012, where wave heights were calculated for the existing bay configuration.

Figure 3-12. Location map of areas A, B, and C used in extraction of model results.

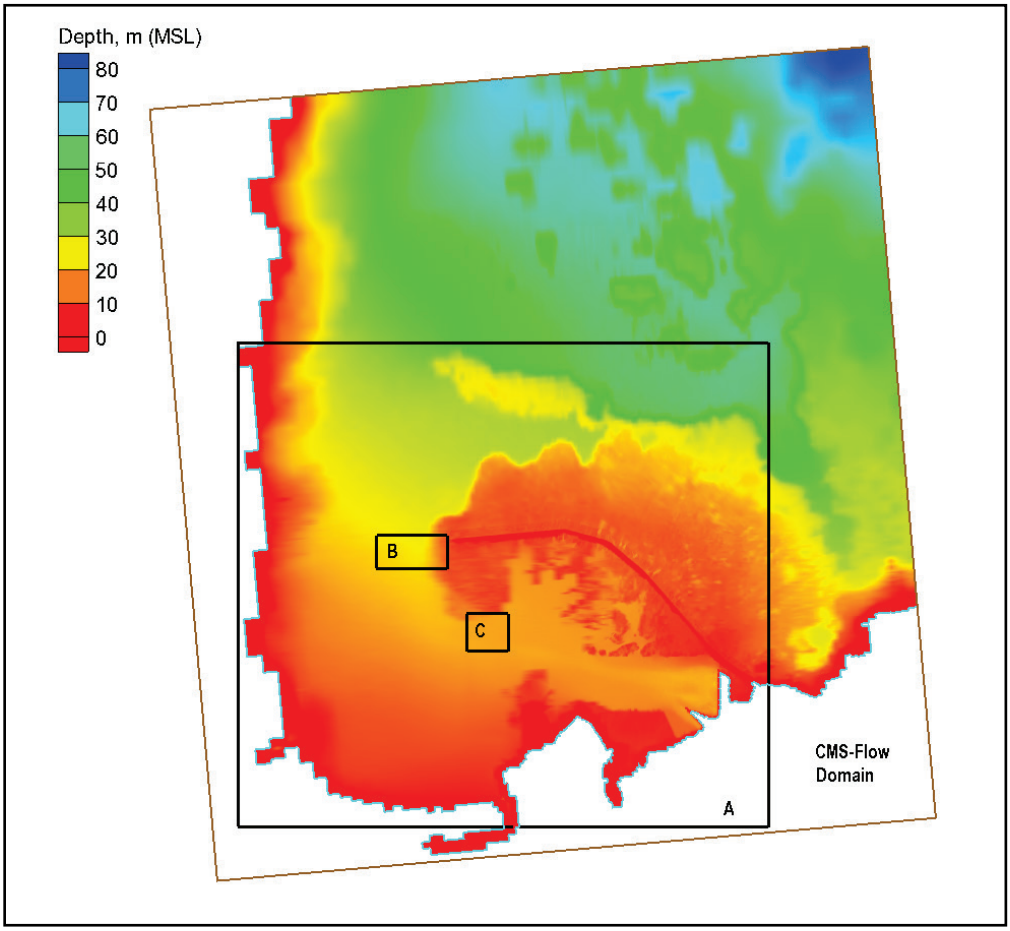

Figure 3-13. Calculated maximum flood current field at 2330 GMT on 6 May 2012.

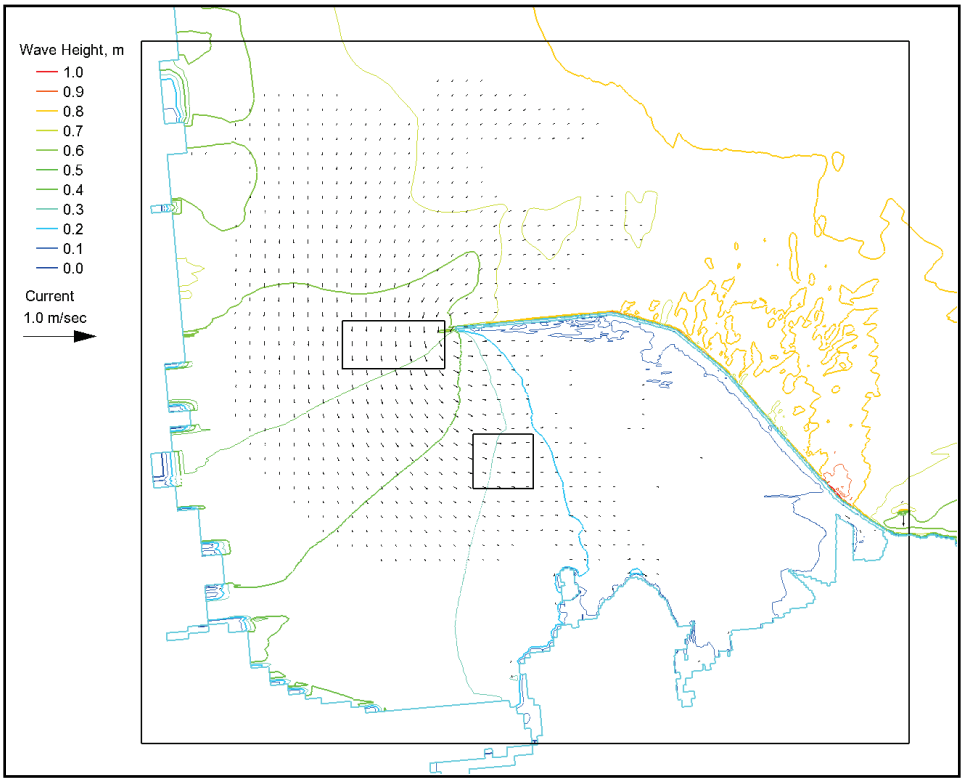

Figure 3-14. Calculated maximum ebb current field at 0630 GMT on 7 May 2012.

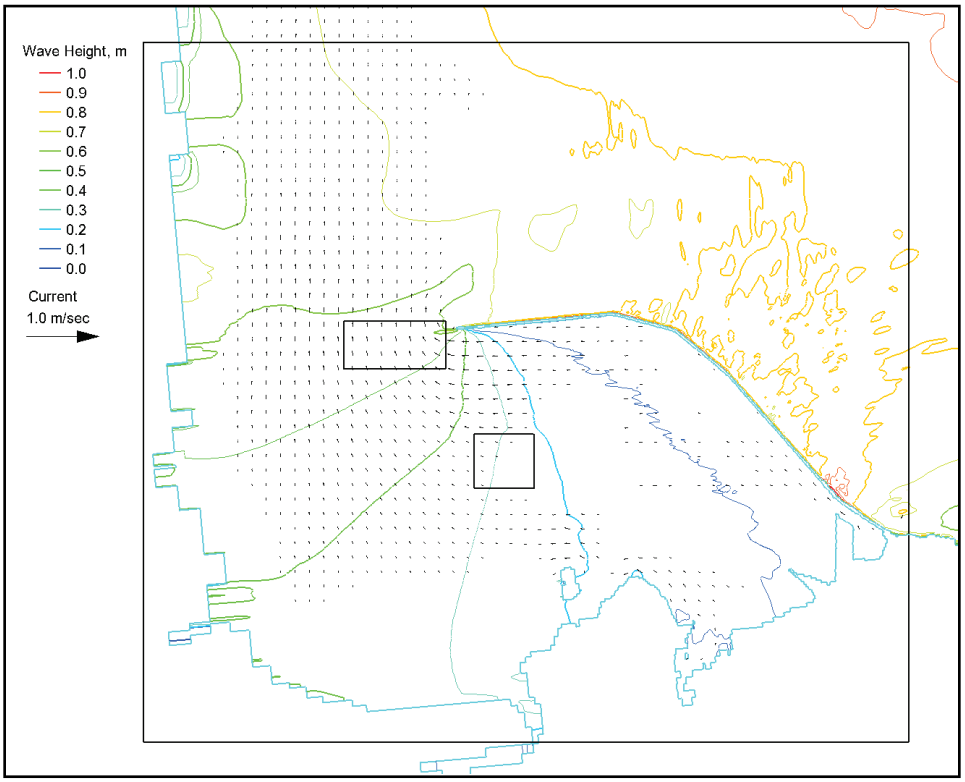

In general, the calculated maximum current magnitude in Hilo Bay along the navigation channel was small, less than 0.65 ft/sec (20 cm/sec) in Area B and less than 0.5 ft/sec (15 cm/sec) in Area C. Maximum wave height can reach 6.5 ft (2 m) to 8.2 ft (2.5 m) in Area B and 3.3 ft (1 m) to 4.9 ft (1.5 m) in Area C. Along Piers 1 and 2, the maximum current was less than 0.33 ft/sec (10 cm/sec), and maximum wave height was less than 1.6 ft (0.5 m).

The extracted water level and current results were saved in text files in a format specified by the ship simulator team. The output files include a header section followed by model calculations. The header provides information about the run and coverage of extracted results, including the extent of the rectangular output area as maximum and minimum (x, y) coordinates, number of spatial points in the output area (npts), and number of output time cycles written to output the file (n-cycles, default is 1). The data section of the output file includes n-blocks of data corresponding to n output time cycles. Each time cycle (or block) of output includes one line of the timestamp (hr), one line of constant wind speed (m/sec), and one line of constant wind direction (deg, from north). These are followed by npts lines which are model results for calculated water level, current, and wave. Values at each spatial output location in the CMS grid are provided. Model results are written in free format in 10 columns as

Columns 1 to 2: output cell coordinates, x (m) and y (m)
Column 3: water depth (m), reference to MSL
Column 4: water surface displacement, eta (m)
Column 5: total depth (m) = water depth + eta
Columns 6 and 7: currents in x and y directions, u (m/sec) and v (m/sec)
Columns 8, 9, and 10: significant wave height (m), spectral peak period (sec), and spectral mean wave direction (deg, from north).

An example of a model output file is listed below. It corresponds to the flood condition at 23:30 GMT on 6 May 2012.

The first 15 lines of the output file are

```
Explicit Time Varying WL and Current

North max_y =                2185980.00
South min_y =                2182010.00
```

East max_x =		285130.00							
West min_x =		280783.00							
Total Save Points =		201961							
Total Time Cycles =		1							
Time (hr) =		11.5							
Wind spd (m/sec) =		8.4							
Wind dir (deg,N) =		82.0							
282976.38	2182022.50	-0.53	0.57	0.04	0	0	0	0	0
283066.12	2182078.50	-1.16	1.20	0.04	0	0	0	0	0
282968.22	2182116.00	0.52	0.22	0.74	0	0	0.08	6.2	52.7
283000.97	2182118.75	3.60	0.22	3.82	0	-0.01	0.02	6.2	47.0
283032.25	2182121.50	1.78	0.22	2.00	0	-0.02	0.02	5.3	30.0

Table 3-3 provides a summary of meteorological conditions simulated for the ship simulator study using CMS-Wave and CMS-Flow. Input conditions were selected in close coordination with the POH project team and with the sponsors (State agency, pilots, harbormaster).

The summary information in Table 3-3 includes date of the selected condition simulated, duration of simulation and associated water level, wind forcing, and deep-water incident wave parameters. Each condition is simulated for two harbor configurations, the existing harbor (without mooring/turning basin dredged) and with a dredged mooring area. The 24–26 March 2012 condition was repeated with and without two river discharges to assess the effect of river flow on waves and currents in the interior harbor. The output desired from these combined CMS-Wave and CMS-Flow simulations were coordinated with the CHL ship simulator team. The results at the time of peak flood and ebb currents and corresponding winds were extracted from the CMS solution files. CMS results from these coupled simulations were processed, and the output quantities requested included spatially and time-varying winds, wave parameters, water levels, and current components. The extracted information was provided to the ship simulator team in the specified formats in text files. The CHL ship simulation team conducted a 2-week ship simulation training during the first 2 weeks of December 2014 for two groups of attendees.

Table 3-3. Summary of the extracted output files for ship simulator study.

Simulation Dates	Duration (Hr)	Water Level	Wind Forcing	Incident Wave	Config.	Output Timestamp (GMT)	Wind Field (m/sec, deg N)
6–7 May 2012	24	Spring tide	~ 8 m/sec ENE	~2 m 9 sec ENE	Exist	Max flood current @ 23:30, 6 May 2012	8 m/sec, 82 deg
					Dredge	Max ebb current @ 06:30, 7 May 2012	8 m/sec, 88 deg
14–15 Nov 2012	24	Spring tide	~ 2 m/sec NE	~2 m 14 sec E	Exist	Max flood current @ 12:00, 14 Nov 2012	2 m/sec, 237 deg
					Dredge	Max ebb current @ 19:00, 14 Nov 2012	3 m/sec, 21 deg
24–26 Mar 2012	36	Spring tide	~ 10 m/sec NE	~3 m 10 sec NE	Exist (no rivers)	Max flood current @ 23:00, 24 Mar 2012	10 m/sec, 49 deg
						Max ebb current @ 17:30, 25 Mar 2012	11 m/sec, 36 deg
24–26 Mar 2012	36	Spring tide	~ 10 m/sec NE	~3 m 10 sec NE	Exist (with rivers)	Max flood current @ 23:00, 24 Mar 2012	10 m/sec, 49 deg
						Max ebb current @ 17:30, 25 Mar 2012	11 m/sec, 36 deg
15–16 May 2011	33	Mean range	~ 10 m/sec NE	~3 m 10 sec NE	Exist	Max flood current @ 21:30, 15 May 2011	10 m/sec, 45 deg
					Dredge	Max ebb current @ 03:30, 16 May 2011	15 m/sec, 45 deg
27–29 Oct 2012	33	Mean range	~ 10 m/sec N	~3 m 12 sec N	Exist	Max flood current @ 10:45, 28 Oct 2012	10 m/sec, 0 deg
					Dredge	Max ebb current @ 14:45, 28 Oct 2012	20 m/sec, 0 deg
22–23 Dec 2012	33	Mean range	~ 10 m/sec ENE	~4 m 15 sec ENE	Exist	Max flood current @ 07:00, 23 Dec 2012	11 m/sec, 72 deg
					Dredge	Max ebb current @ 23:30, 22 Dec 2012	11 m/sec, 65 deg

4 Boussinesq Wave Modeling

As noted in Chapter 3, two numerical wave models, CMS-Wave and BOUSS-2D (B2D), were used in this study. CMS-Wave was applied to a large domain, covering deep-water offshore areas up to the shorelines. The computational efficiency of CMS-Wave permits simulation of many wave conditions to investigate the reported navigation problems and modifications or Alternatives proposed to certain areas of the Hilo Harbor. CMS-Wave was also used in development of wave conditions for the ship simulator component of Hilo Harbor project. (See Chapter 3 for details of CMS-Wave modeling.)

B2D is used in this study for the nearshore wave modeling between approximately the 130 ft (40 m) depth contour and land (shoreline). This model is appropriate for smaller domains and a limited number of wave conditions and is capable of modeling linear and nonlinear nearshore wave processes. The surge problem in Hilo Harbor is investigated using B2D since this model handles both short- and long-period waves by solving for time-domain, shallow-water nonlinear wave processes using Boussinesq-type equations. (Additional information about B2D is available from references and recent applications [Demirbilek et al. 2007a, 2008, 2009; Nwogu and Demirbilek 2001, , 2006, 2008, 2010; Nwogu 2007, 2009]). Although B2D can address a broad range of wave processes in harbor projects, long computational times in practice require limiting the extent of grids and number of simulations. In large domain harbor studies or when dealing with modeling of many conditions or Alternatives, it may be necessary to use B2D with a spectral model. Lin and Demirbilek (2012, 2005) provide details of a coupled B2D and CMS-Wave modeling approach for harbor applications. This is the approach followed here.

Both offshore and nearshore areas of Hilo Harbor are included in the B2D wave modeling grids. The extensive fringing reefs outside the harbor beyond the harbor entrance and breakwater as well as reefs in the interior of the harbor are included in the B2D modeling. Model simulations were conducted for two water levels for the existing harbor and four Alternatives. Effects of wave diffraction, reflection, refraction, shoaling, breaking, and nonlinear wave-wave and wave-current interactions are included in these simulations. The model provides estimates of wave

parameters (height, period, direction), wave-induced currents (circulation), and IG waves that are known to be a potential source of harbor surge problems (Demirbilek et al. 2005a, b, 2007b,c; Nwogu and Demirbilek 2001, 2004, 2006; Nwogu 1993a,b, 1994, 1996, 2000, 2006).

As described in the *Coastal Engineering Manual* (Demirbilek and Vincent 2015), three wave parameters are required to characterize ocean waves: significant wave height, H_s, peak spectral period, T_p, and mean wave direction, θ_p. A steady-progressive wave train can be defined by mean water depth, h, wave crest-to-trough height, H, and wavelength, L. In applications, the wave period is known rather than the wave length, and since the wavelength is related to wave period through the dispersion relationship, the above three parameters are widely used in coastal engineering practice. Three dimensionless quantities can be formed from the above parameters, which are H/h, L/h, and H/L, to characterize the shallow-water waves. Generally, waves travel faster when traveling the same direction as a current. Consequently, wave speed and hence the measured wave period depend on the existing background current or wave-induced current generated by breaking waves.

The nonlinear features of shallow-water waves in Boussinesq wave theory are defined using two fundamental parameters, H/L and H/h, which quantify the dispersion and nonlinearity of waves, respectively. As depth decreases, the wave nonlinearity generally increases with the wave height, leading to an increase in wave asymmetry and eventual breaking and deformation of the wave shape or profile. Not all features of nonlinear shallow-water wave processes can be described accurately by linear wave theory or nonlinear wave models such as B2D. However, field measurements have shown that Boussinesq wave models are capable of capturing most essential characteristics of nonlinear shallow-water waves important for oscillation (surge) problem occurring in Hilo Harbor (Demirbilek et al. 2015a,b, 2007b,c; Nwogu and Demirbilek 2001, 2004, 2006; Nwogu 2006, 2007; Nwogu 1993a,b, 2009; El Asmar and Nwogu 2006).

The same modeling domains were used for the existing harbor and Alternatives. Grids setups for the existing harbor were modified as required for each modified plan (Alternative). For consistency of extracting and comparing model results at some selected output points or along transects, the same spatial extent was used for the existing and

Alternatives. The sources of bathymetric data for model grids were described in Chapters 2 and 3.

4.1 Alternatives investigated

The modeling domains for the existing harbor and Alternatives are shown in Figures 4-1 through 4-5. The existing harbor is designated as "Alt-0" in Figure 4-1 since it is the baseline study plan. It includes reefs, the breakwater, harbor entrance, interior harbor, and shorelines. This modeling domain is approximately 2.6 miles (4.8 km) easting by 2.5 miles (4.6 km) northing.

Figure 4-1. Existing harbor geometry (Alt-0).

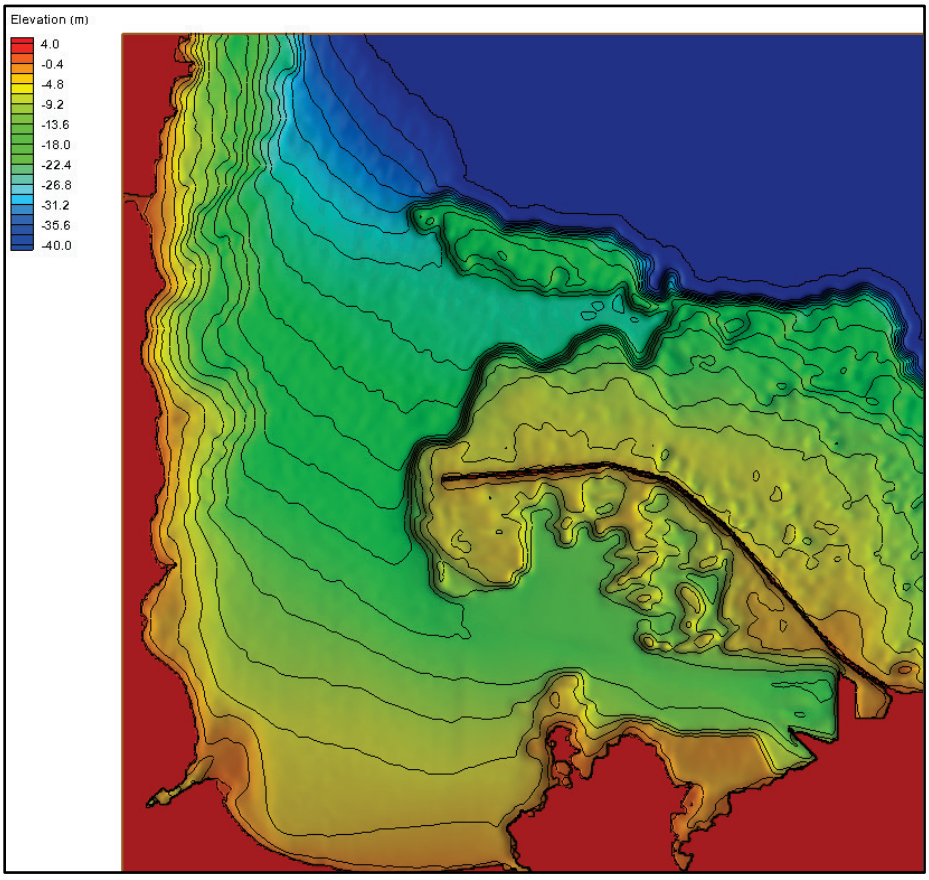

A goal of the proposed modifications is to improve conditions at the mooring and turning basin area. This area is shown by a polygon in Figure 4-2. The dredged depth of 35 ft (10.7 m) MLLW inside the polygon is

Figure 4-2. Location and size of mooring/turning basin.

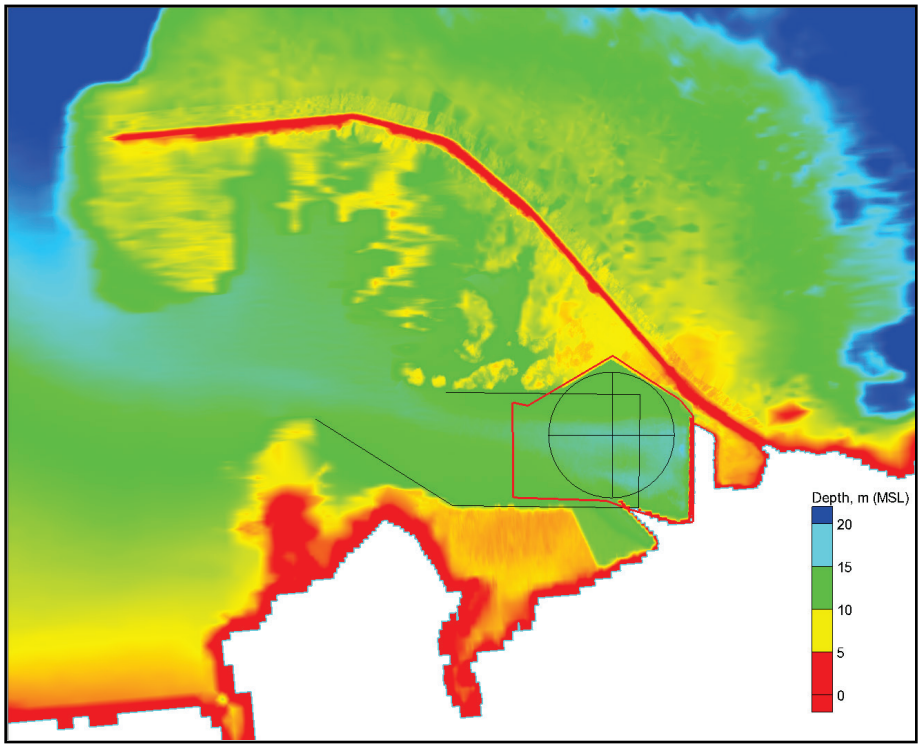

included in three B2D modeling domains. The three grids for these model domains are north, north-northeast, and northeast grids. The grids for the Alternatives were generated from the sketches provided in Chapter 1 by modifying the associated Alt-0 grid with the corresponding sketch. The numerical model grids developed for Alt-1, Alt-2, Alt-3, and Alt-4 are provided in Figures 4-3, 4-4, 4-5, and 4-6, respectively. The objective of each proposed modification is to reduce wave energy at the mooring/turning basin and Piers 1 and 2 areas. Different length spurs are used to intercept and redirect waves heading to these areas. A brief description of each Alternative and its modeling domain follows.

A short, detached surface-piercing structure (e.g., breakwater) is used in Alt-1. This modification in Figure 4-3 is depicted by a structure with a brown line located west of the mooring/turning basin area. This short structure was placed approximately 195 ft (60 m) from the north edge of navigation channel and oriented in a northeast direction. The Alt-1 structure is approximately 820 ft (250 m) long and 40 ft (12 m) wide.

Figure 4-3. Alt-1 with a short detached structure.

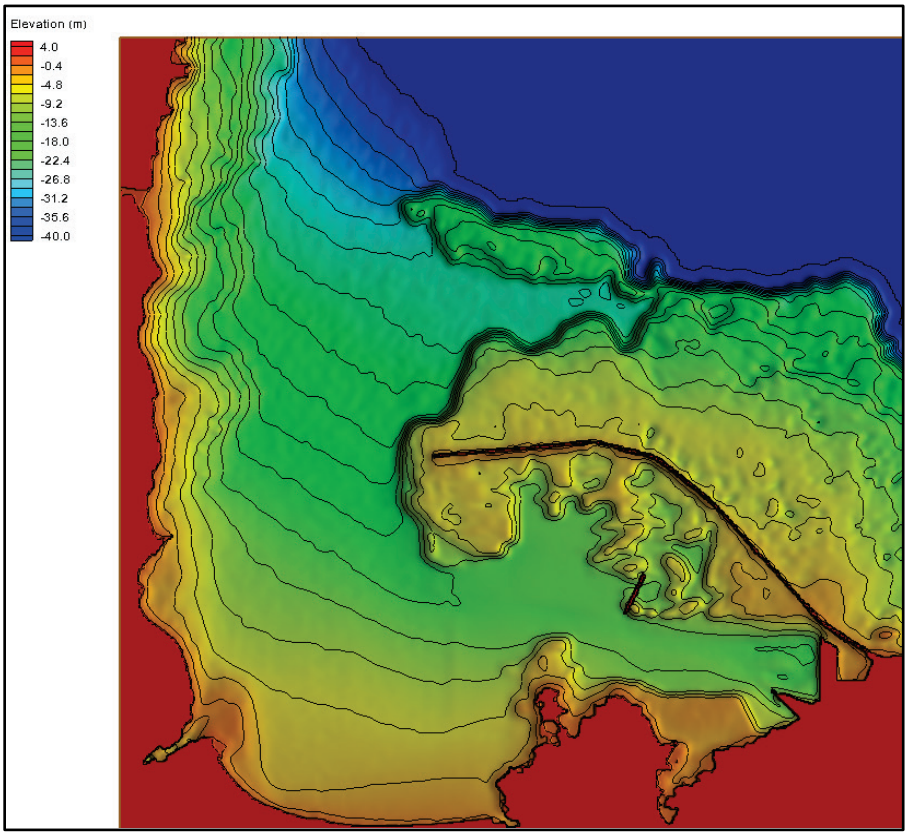

The modification for Alt-2 (Figure 4-4) includes a medium length structure nearly twice the length of the structure used in Alt-1. This structure was also positioned north of the navigation channel and aligned in a northeast direction but was moved eastward closer to the mooring basin because the shorter structure in Alt-1 did not reduce wave energy significantly at the mooring/turning basin and at the piers. The length and width of the structure in Alt-2 are 1,580 ft (480 m) and 40 ft (12 m), respectively.

Figure 4-4. Alt-2 with a medium-length detached structure.

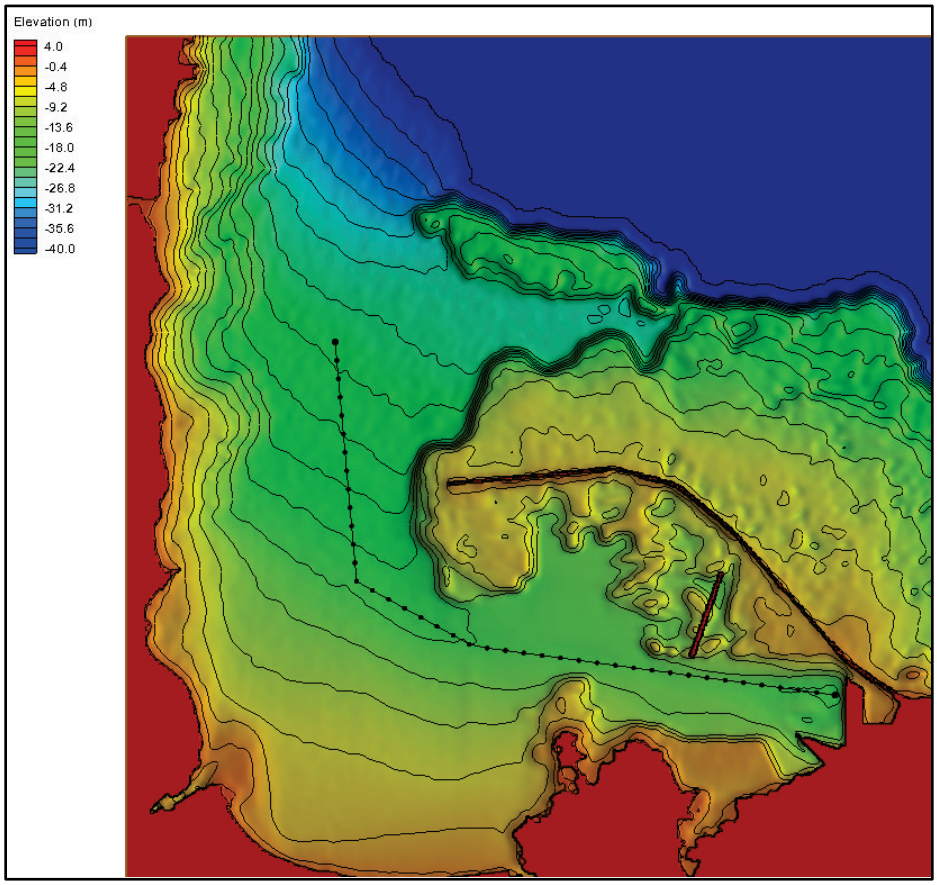

Alt-2 (Figure 4-4) and Alt-3 (Figure 4-5) geometries look similar except that a longer structure is used in Alt-3. The length and width of this structure are 2,300 ft (700 m) and 40 ft (12 m), respectively. It extends and connects to the Federal breakwater. Model test simulations indicated no significant gain in protection of the mooring and pier areas using the longer structure (Alt-3). For this reason, Alt-3 was not further investigated. Note that the channel centerline is depicted by a dotted black line in Figures 4-4 and 4-5 since it serves as a reference for the locations of interior structures, the mooring/turning basin, and the two piers.

Different lengths and locations of interior structures were used in the first three Alternatives (Alt-1, Alt-2, and Alt-3). These structures were placed inside the harbor westward of the mooring/turning basin area in an attempt to block further penetration of waves into the affected areas. Alt-4

Figure 4-5. Alt-3 with interior structures (north structure connects to breakwater).

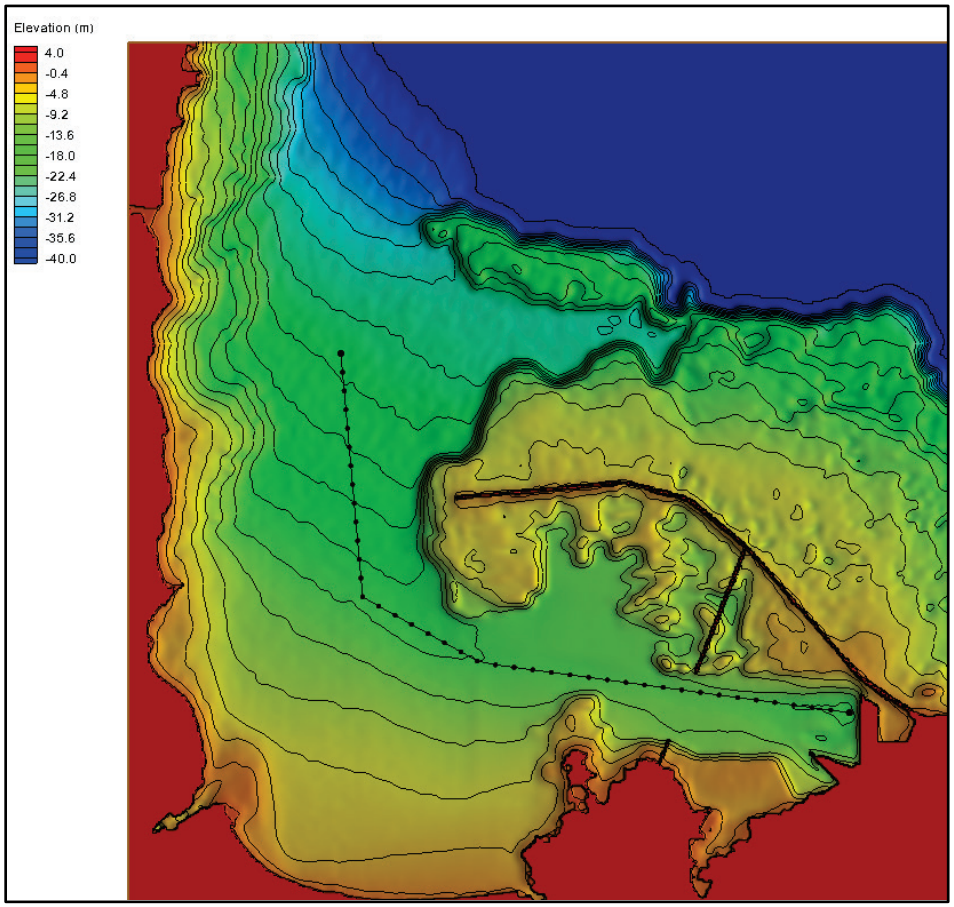

as shown in Figure 4-6 is different than the three previous Alternatives. In this case, a spur is used in an attempt to control the waves coming in through harbor entrance. This was done because model simulations indicated waves passing through the entrance turn and propagate eastward into the mooring/turning basin and the two piers in the southeast corner or interior harbor. To minimize the effects of these waves, a spur was attached to the most western tip of the Federal breakwater that effectively shelters the interior harbor complex from the incident waves from the north and east sides of the bay. Different lengths and orientations of the spur were investigated. The selected final spur is shown in Figure 4-6. It is 2,300 ft (700 m) long and 40 ft (12 m) wide and is oriented in a southwest direction.

Figure 4-6. Alt-4 with a spur near the west tip of breakwater.

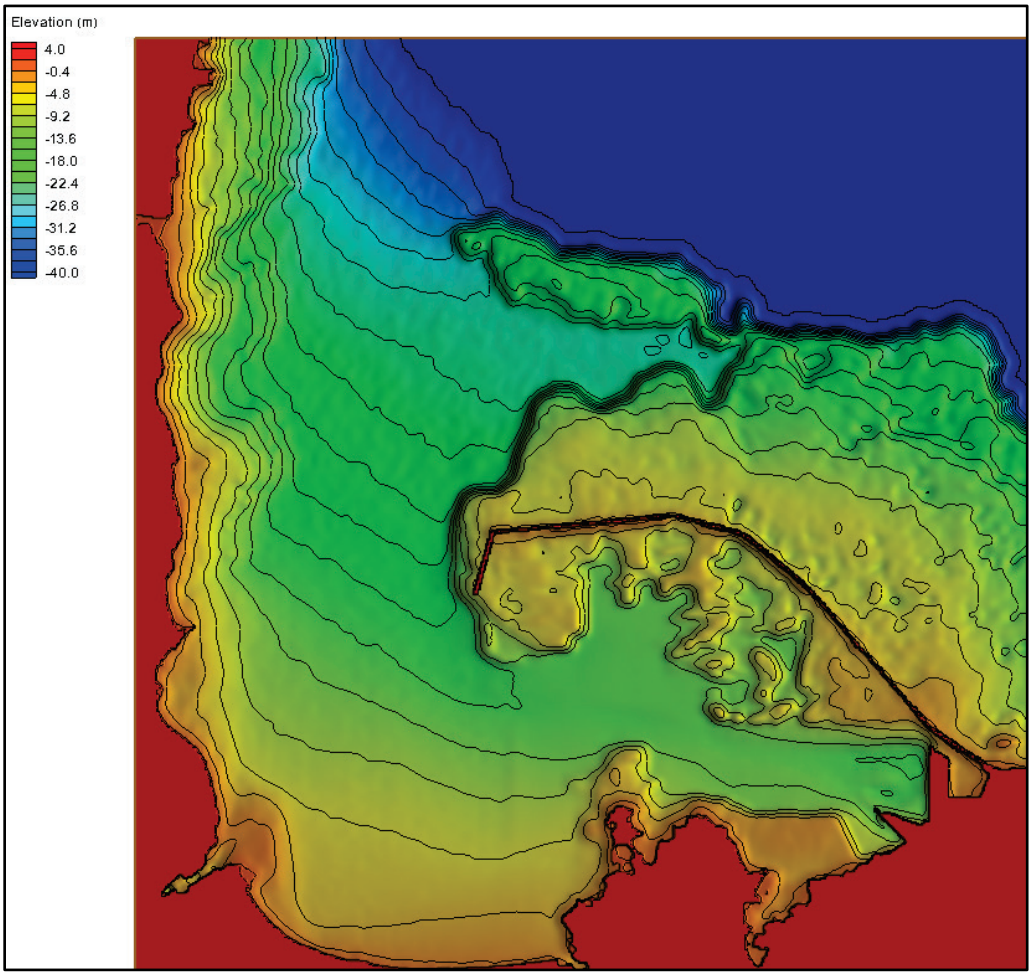

The reefs present to the north and south of the channel; the locations of added structures, channel center, and distance of structures to the north edge of channel are shown in Figures 4-4 and 4-5. The water depth along the channel varies. The boundaries of the channel and bathymetric variations inside and outside the harbor are not marked but can be seen from these figures. Water depth varies along the harbor entrance. In the north part of harbor entrance, the average depth in the channel is 49 ft (15 m), and the depth decreases gradually as ships move southward to turn into the interior harbor toward Piers 1 and 2. The depth contour range in these figures is set from -130 ft (-40 m) to +13 ft (+4 m) MLLW to show areas of interest and the boundaries of dredged navigation channel. A summary of main features of the five Alternatives investigated is provided in Table 4-1.

Table 4-1. Summary of five harbor configurations investigated.

ID	Configuration	Features
Alt-0	Existing harbor	Present harbor geometry
Alt-1	Existing harbor with a short interior structure	Positioned west of mooring area, oriented northeast, between the north channel edge and Federal breakwater
Alt-2	Existing harbor with a medium length structure	Similar to Alt-1, has a medium length structure
Alt-3	Existing harbor with a longer interior structure	Similar to Alt-2, has a longer structure that extends and joins to the Federal breakwater
Alt-4	Existing harbor with a medium length spur at the tip of breakwater	Added to near the west tip of Federal breakwater in a southwest orientation

4.2 Model grids

Three grids were used to model waves for the existing harbor (Alt-0) and Alternatives (Alt-1, Alt-2, Alt-3, and Alt-4) at Hilo Harbor. These are designated as N, NNE, and NE Grids in Figure 4-7. The three grids were necessary because incident waves come into Hilo Bay from different directions. Although the grids look similar, their orientation, coverage, dimensions, location of offshore boundary, and width of each grid domain are different. The grids are oriented with respect to true north by 0^0 (N Grid), 22.5^0 (NNE Grid), and 45^0 (NE Grid), respectively. Waves affecting the Hilo Bay within a north-northwest to east sector can be simulated using these three grids.

There are also differences between these grids at the harbor entrance and/or in the inner harbor where an infrastructure modification was introduced. With a 26 ft (8 m) cell size, the number of cells and areas covered by each grid were as follows: N Grid (603 by 578 cells, 2.6 miles [4.8 km] × 2.5 miles [4.6 km]), NNE Grid (601 by 601 cells, 2.6 miles [4.8 km] × 2.6 miles [4.8 km]), and NE Grid (613 by 626 cells, 2.65 miles [4.9 km] × 2.7 miles [5.0 km]). The incident waves from north, north-northeast, and northeast directions were normal to the offshore boundaries of N, NNE, and NE Grids, respectively (Figure 4-7). These boundaries were placed at approximately the -130 ft (-40 m) MLLW depth contour.

Figure 4-7. Modeling domain and orientation of north, north-northeast, and northeast grids.

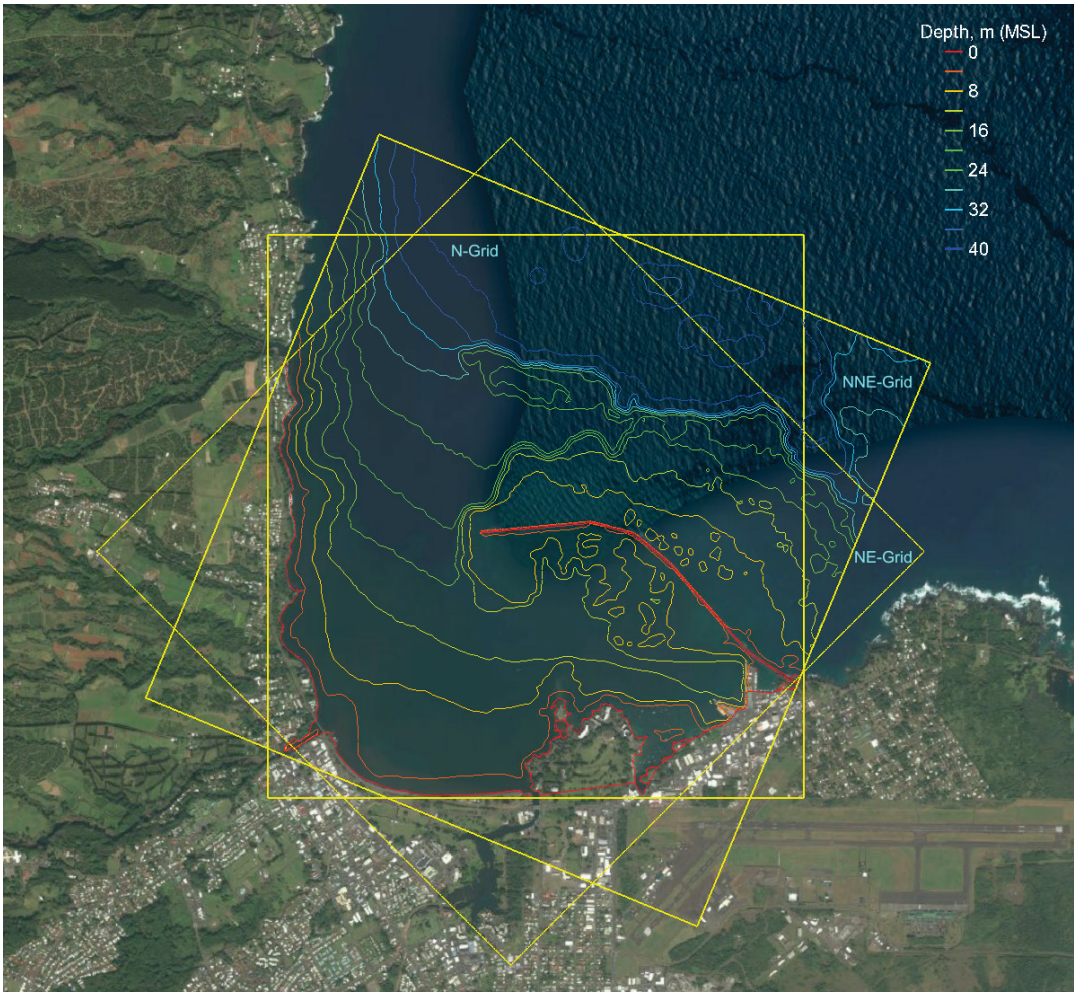

The north, north-northeast, and northeast grids are shown in Figures 4-8, 4-9, and 4-10. Grid details are provided including extent of modeling domains, shorelines, structures, and bathymetric features of each grid. The solid-red grid boundary with an arrow indicates the location of the exterior wavemaker where wave forcing is applied. For simulations using an internal wavemaker, the wave generation boundaries were pushed inward by 650 ft (200 m). The exterior wavemaker is located along the offshore boundaries of the grids approximately at the 130 ft (40 m) water depth of each grid. For simulation of wave conditions with longer peak periods (T_p > 13 sec), an interior wavemaker shoreward of the offshore boundary was used. An interior wavemaker approximately 650 ft (200 m) shoreward of the offshore boundary was used for simulations with longer peak periods (T_p > 13 sec).

Figure 4-8. North grid modeling domain.

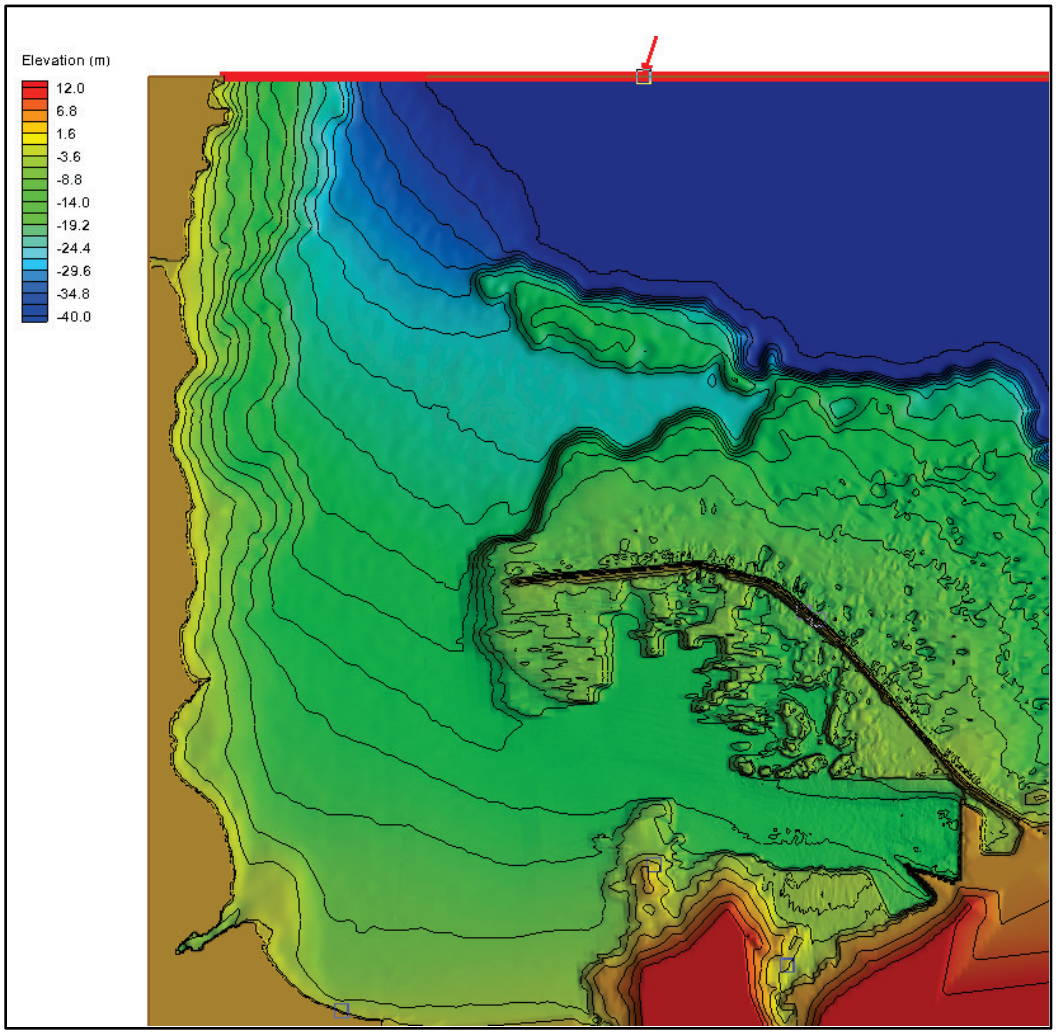

A sensitivity study was conducted on input parameters which affect computational stability of model solutions. The effects of Chezy and Smagorinsky coefficients and damping layers on model results were investigated. The width and strength of the lateral damping layers (sponge layers) applied along parts of the land boundaries to absorb oblique waves were determined with these tests. Appropriate damping widths ranged from 25 ft (8 m) to 130 ft (40 m), with values of damping coefficients from 0 to 1.0. These agree with the recommended default damping settings for B2D model (Demirbilek et al. 2015a,b, 2007; Nwogu and Demirbilek 2001).

Figure 4-9. Modeling domain covered in north-northeast grid.

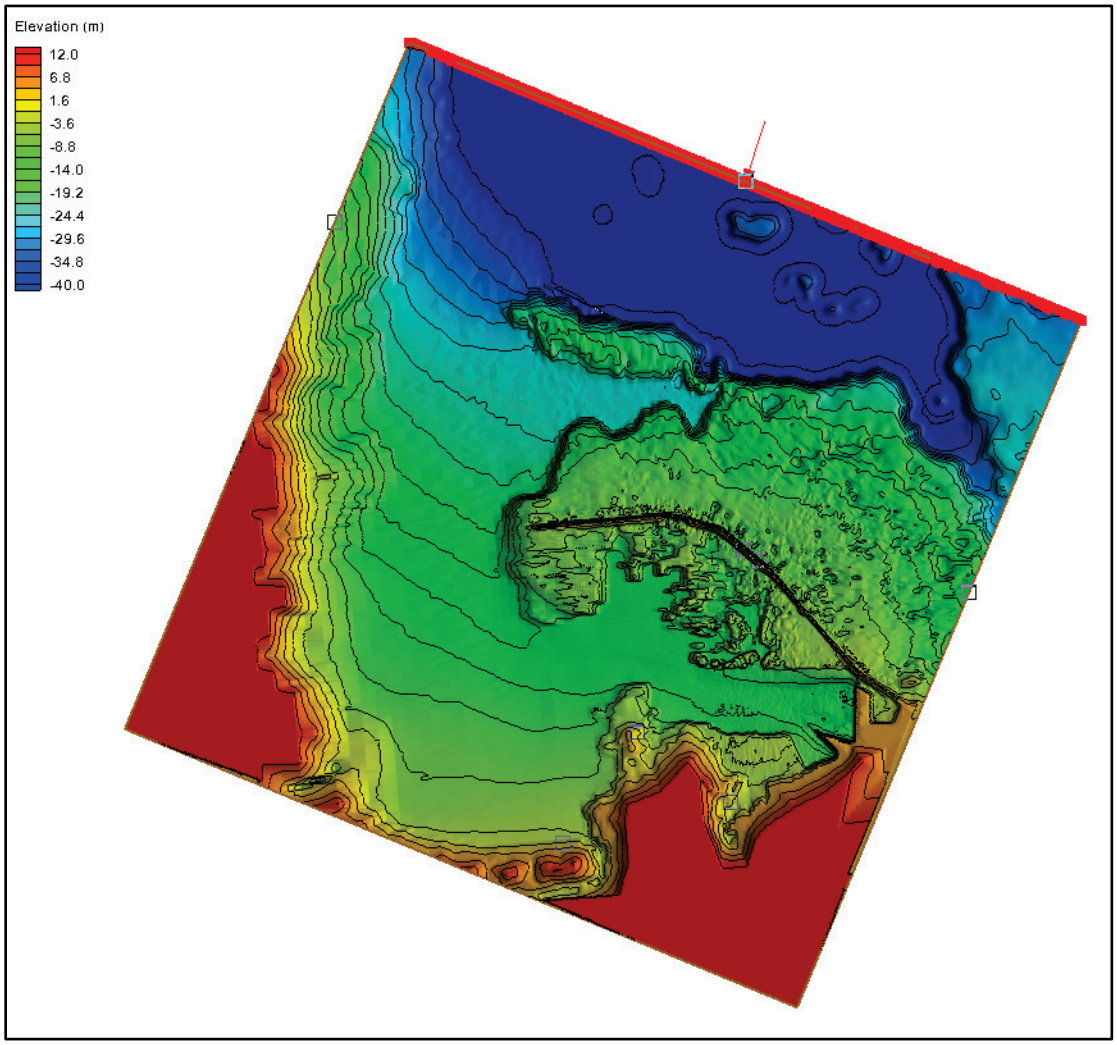

Figure 4-10. Modeling domain covered in northeast grid.

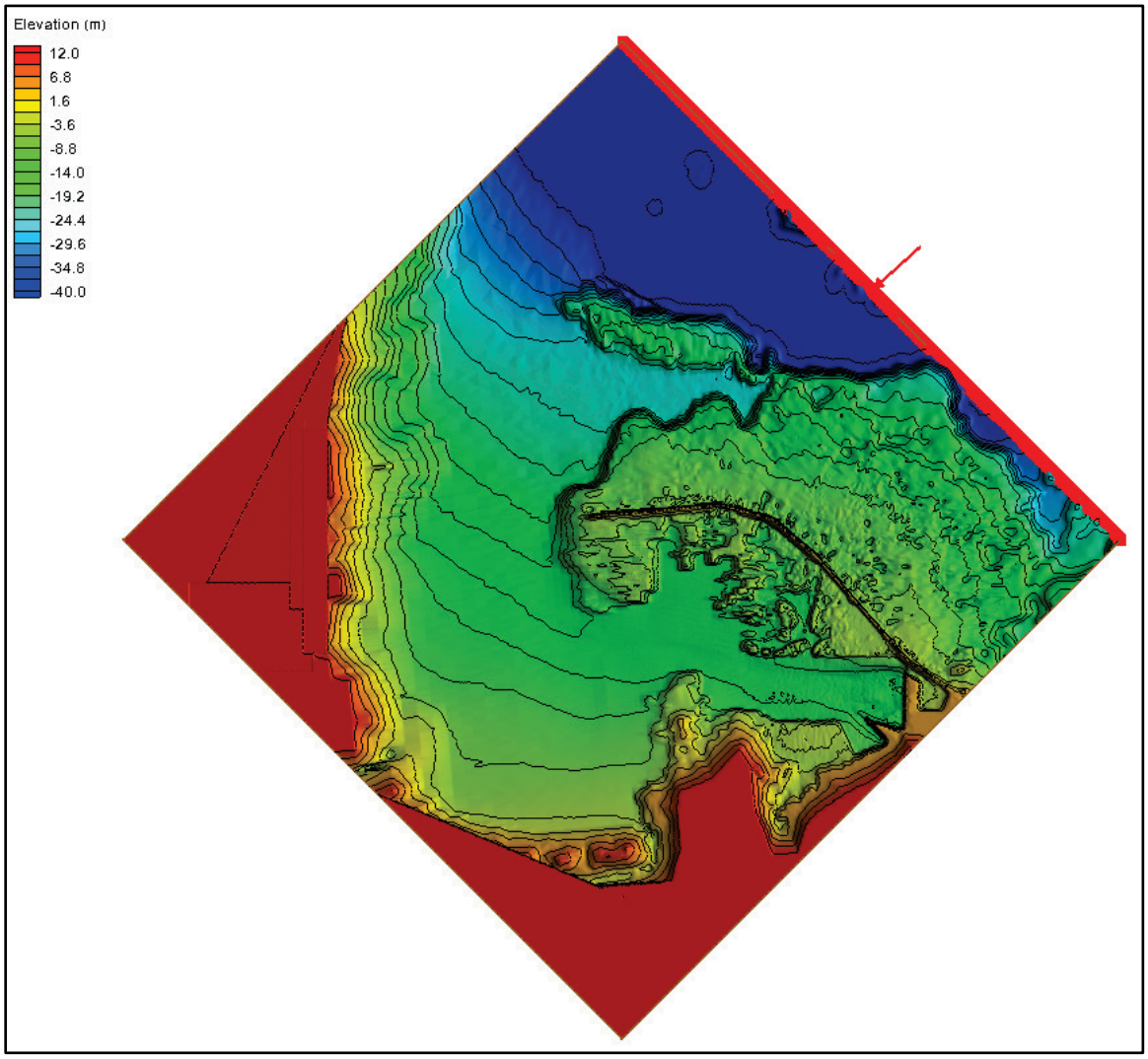

4.3 Wave input

The incident waves from the east direction are largely blocked by the Federal breakwater on the north side of Hilo Harbor. Only waves which graze or ride along the breakwater may eventually get into the harbor. Waves wrapping around the western tip of Federal breakwater and those reflecting from the west land boundary (shoreline) would get into the harbor. Waves from the east direction are simulated by placing a wavemaker along the eastern boundary of the north grid. An example simulation of the sea surface elevation for an incident wave from the east direction is shown in Figure 4-11 to illustrate the expected wave pattern outside and inside the harbor.

Figure 4-11. Example simulation for a wave from the east direction.

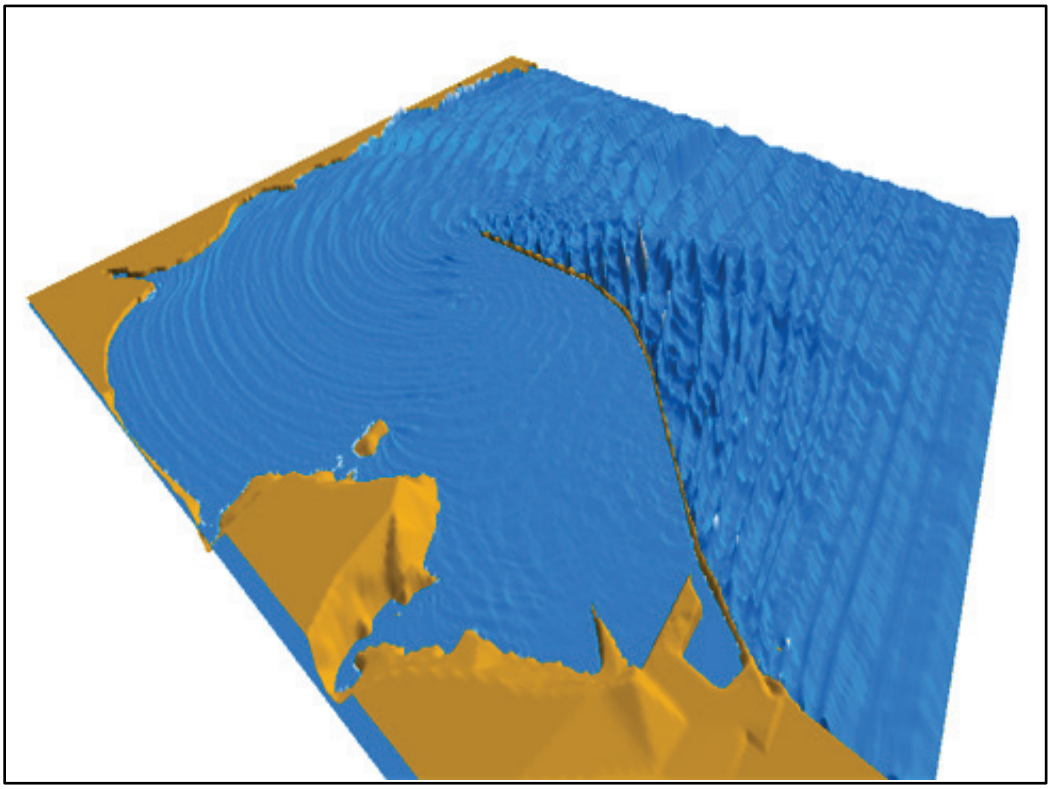

Incident wave input conditions for B2D simulations were obtained from the CMS-Wave directional wave parameters saved at the offshore boundary of each of the three B2D grids. Based on data from deep-water offshore buoys and hindcast estimates, incident waves into Hilo Bay during the months of October–March are generally from the northweast to east sector. Therefore, waves can be expected from the north-northwest, north, north-northeast, northeast, and east directions. During the months of May–September, waves are mainly from the east-southeast, east, northeast, and north directions. When the deep-water waves are transformed to the B2D grid boundaries located in comparatively shallow depths, a significant variation can be expected in the wave height, wave period, and wave direction along the wavemaker (forcing) boundaries of the B2D grids. The range for wave parameters was 3.3 ft < H_s < 16.4 ft, (1 m < H_s < 5 m), 8 sec < T_p < 16 sec, and 0 < Θ_p < 20°, respectively. The CMS-Wave-calculated wave parameters at the midpoint of the wavemaker boundaries of each grid were specified as input for the B2D simulations.

The selection of wave conditions is described next. Based on analysis of the 2014 wave climate, a number of severe wave events were reported by National Oceanic and Atmospheric Administration (NOAA) offshore buoys

which impacted navigation according to users of Hilo Harbor. Five wave conditions from different directions were selected to investigate the harbor surge problem, including storm and nonstorm conditions. IG waves inside the harbor could be causing the localized surge at the piers if the period of these waves coincides with one of the natural periods of the harbor. The storm events for investigation of the surge problem are listed in Table 4-2. UTC denotes Coordinated Universal Time.

Table 4-2. Wave conditions used in B2D simulations.

Event Date and Time	H_s (m)	T_p (sec)	θ (deg)
5Jan2014@UTC16	1.5	14.3	5
	2	14.3	5 & 20
	2.14	14.3	0, 18
	2.5, 2.8, 3.4	14.3	0
23Jan2014@UTC07	5	14.3	0 & 345
27Feb2014@UTC15	2.4	13.3	0
18Mar2014@UTC20	3.3	13.3	0
4Apr2014@UTC05	3	14.3	0 & 345

Incident waves specified at the exterior boundary undergo significant changes as they move over the fringing reefs present outside the breakwater. Model simulations showed waves were refracting, shoaling, and breaking over the reefs, and waves reaching the breakwater were diffracting and reflecting, and in some low areas, wave runup/overtopping of the Federal breakwater could be seen. Consequently, the spectra of reformed waves would be different than the spectra of incident waves specified at the offshore boundary.

The prevailing waves outside the harbor move through the entrance to propagate into the interior harbor. The harbor is well protected by the Federal breakwater on the north and shorelines to the south, southwest and west of the harbor. A low-frequency surge problem occurs in the interior harbor, caused by waves that reach Piers 1 and 2. According to ship captains, pilots, and harbor masters familiar with Hilo Harbor, the surge problem was related to deep-water storms occurring outside the harbor. Furthermore, they noted that the surge was not limited to storms

because it was also occurring during less severe (milder) weather conditions. For this reason, a few typical (day-to-day) 2014 wave conditions from different directions were also simulated to investigate surge problem in the harbor (Table 4-3).

Table 4-3. Milder wave conditions for study of surge problem.

Test Condition	H_s (m)	T_p (sec)	θ (deg)
1	1.33	14.3	40
2	1.5	10	0, 5, 22.5, 45
3	1.5	14.3	8, 15
4	1.77	14.3	28
5	2	14.3	20
6	2.63	14.3	8
7	3.44	14.3	350

The first condition (5 January 2014) in Table 4-2 was used for the setup, testing, and calibration of model. The focus of these investigations was on the model's ability to represent the evolution of wave spectra over fringing reefs and generation of the IG waves outside/inside the harbor. These capabilities were studied using a broad range of wave conditions from Tables 4-2 and 4-3. The values of bottom friction, turbulence coefficients, and boundary damping layers were determined from these simulations. Model results were analyzed to evaluate changes in the wave spectral shape and wave-energy density. Results showed redistribution of energy in the spectra to different wave frequencies at varying water depths. Results also indicated modeling some wave processes inside the harbor correctly would in part depend on damping layers, Smagorinsky, and Chezy coefficients used in the simulations. The duration of simulation also played a role in model performance.

The wave parameters (height, period, and direction) obtained from CMS-Wave were applied to the B2D boundary as unidirectional and multidirectional inputs with a user-defined directional spread (Nwogu and Demirbilek 2001; Demirbilek et al. 2015a,b, 2007a,b,c, 2008, 2009). Numerous simulations were conducted to determine the effects of bottom friction (Chezy) and turbulence (Smagorinsky) coefficients on the

transformed wave spectra at some selected output locations (probes). In these numerical experiments, values of Chezy coefficient from 20 to 30 and Smagorinsky coefficient 0 to 0.2 were used, which are the recommended defaults parameters. For applications with or without field or laboratory data, these tests confirmed that B2D could be used with default values of the numerical parameters.

The storm and nonstorm wave conditions in Tables 4-2 and 4-3 were used to evaluate the IG-generated surge problem and to evaluate Alternatives. These two sets of wave conditions cover a wide range of significant wave height, peak period, and directions. A few simulations were repeated for two water levels (0.0 ft [0.0 m] and 1.6 ft [0.5 m] MLLW). Model results showed that the water level clearly affected wave patterns on fringing reefs outside but had less influence on waves at the mooring basin and in the immediate vicinity of the two piers.

4.4 Field data

Data from two field studies were available at Hilo Harbor. The first study was conducted in March–August 2007, and wave and current data were collected using three ADCPs. A second field study collected water level measurements with a pressure transducer from December 2013 to April 2014. A brief description of these measurements follows.

4.4.1 2007 field study

The 2007 field measurements were obtained by the CHL in support of a water-quality study in Hilo Harbor. Gauge coordinates are provided in Table 4-4 and locations on a navigation chart (Figure 4-12) and B2D grid (Figure 4-13). Gauge1 (ADCP1) was deployed near the harbor entrance to collect wave data. Gauge2 (ADCP2) and Gauge3 (ADCP3) were farther inside the harbor to measure currents. Other information about instruments and field data collection is provided in Table 4-4. The ADCPs were bottom-mounted, 1,200 kHz Workhorse RD Instruments and faced upward with the sensor head approximately 1.6 ft (0.5 m) off the bottom. Gauges were held to the bottom with lead weight and equipped with four acoustic transducers for measuring currents and a pressure sensor for measuring water level. Horizontal and vertical current profiles were computed at 6.6 ft (2 m) vertical spacing. No significant storm event occurred during this data collection period.

Table 4-4. Instrument identifications and locations in 2007 field study.

Type	ID	Lat (N)	Lon (W)	SN	Deploy Times (2007)	Nominal Depth (m)	Wave (W) Current (C)
ADCP	adcp_1	19º 44.34’	155º 4.38’	1885	21 Mar – 5 Jun	6	W/C
ADCP	adcp_2	19º 44.90’	155º 4.14’	7057	21 Mar – 5 Jun	6	C
ADCP	adcp_3	19º 44.34’	155º.3.83’	2993	21 Mar - 5 Jun	6	C

Figure 4-12. Locations of three ADCP gauges in 2007 field study.

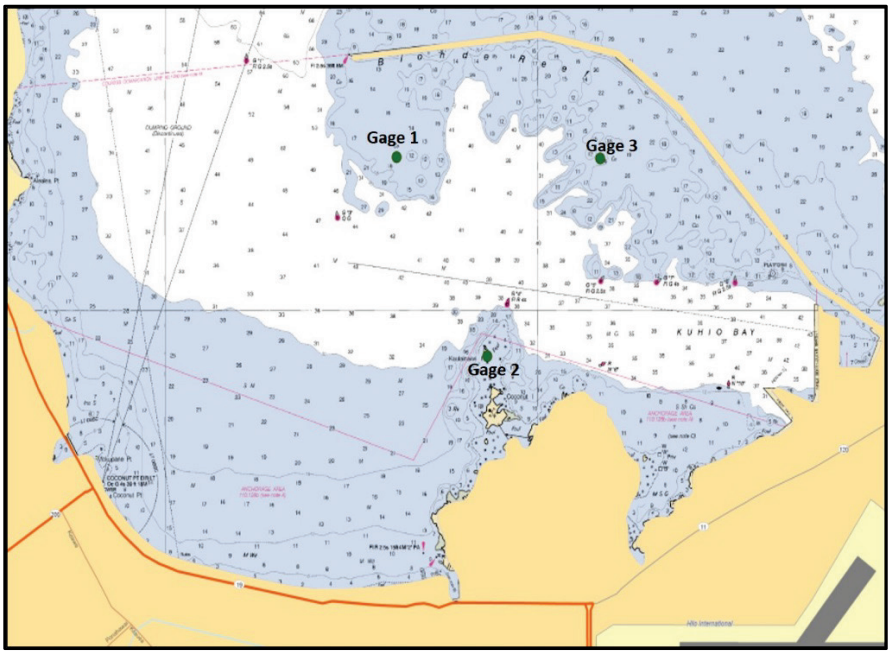

Data at ADCP1 were sampled at 2 Hz for directional wave measurements, with each hourly wave burst being approximately 34 min in length (4,096 points) and data recording beginning at the top of each hour. The current profiles were collected every 10 min from a 200-point average. Gauges were deployed on 21 March 2007 and retrieved on 5 June 2007. It was determined during field deployment testing and calibration that two ADCPs could only measure currents. ADCP1 was closest to the entrance that collected waves and current while ADCP2 and ADCP3 only collected currents.

Figure 4-13. Gauge locations in B2D grid for 2007 field study.

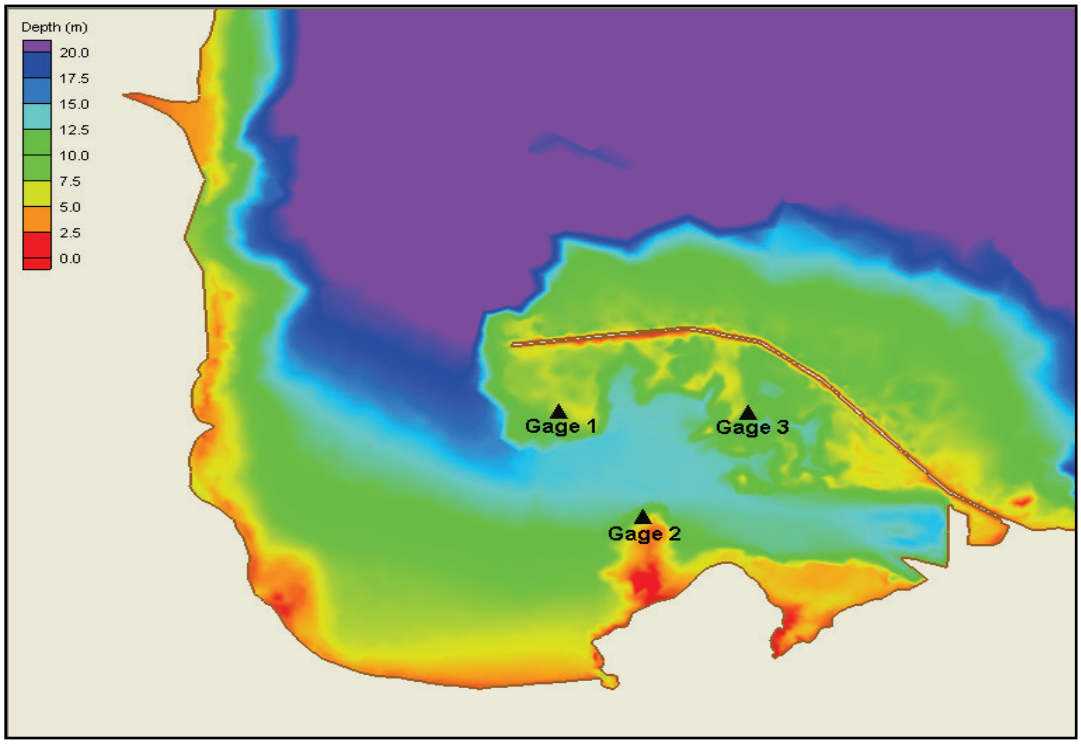

Visual observations of waves were made near the locations of ADCP2 and ADCP3. On-site analysis of ADCP1 data showed greater wave heights (~ 3.3 ft [1 m]) than the comparatively smaller waves at the two inner gauges (generally less than 1.0 ft [0.3 m]). The batteries of ADCP3 depleted on 7 April, so it operated only for 20 days. This unit was probably damaged during shipping.

Spectral processing of data was done using 4,096 points of each 34 min record to calculate directional spectra with band-averaged 128 frequency points and 90 directional bins. Figures 4-14 and 4-15 are monthly wave roses for ADCP1. Measurements for each month are fairly consistent with waves from the northeast with height never exceeding 3.3 ft (1 m). Wave height, period, and direction statistics for March–June 2007 data are provided in Figures 4-14 through 4-16.

Figure 4-14. Wave rose from ADCP1 for March–April 2007.

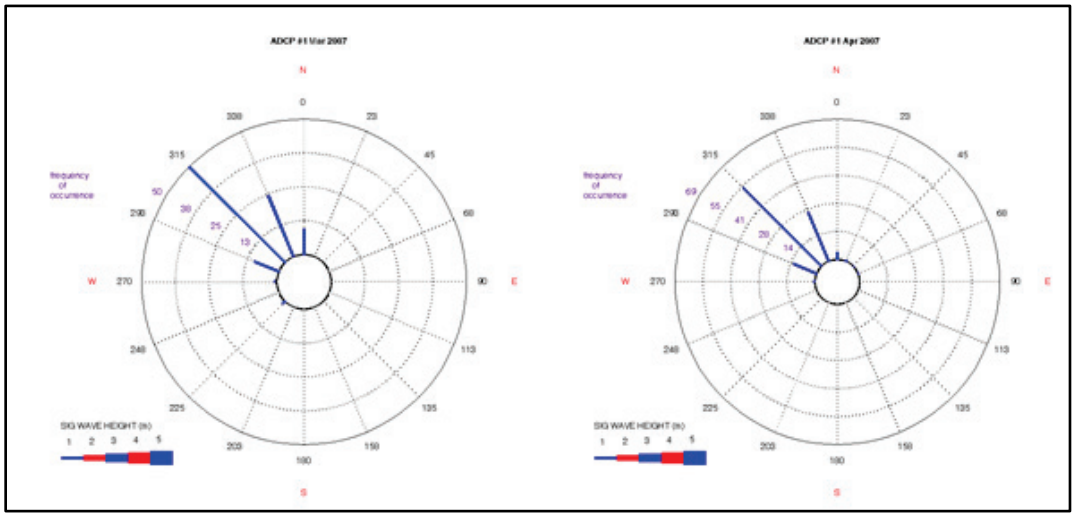

Figure 4-15. Wave rose from ADCP1 for May–June 2007.

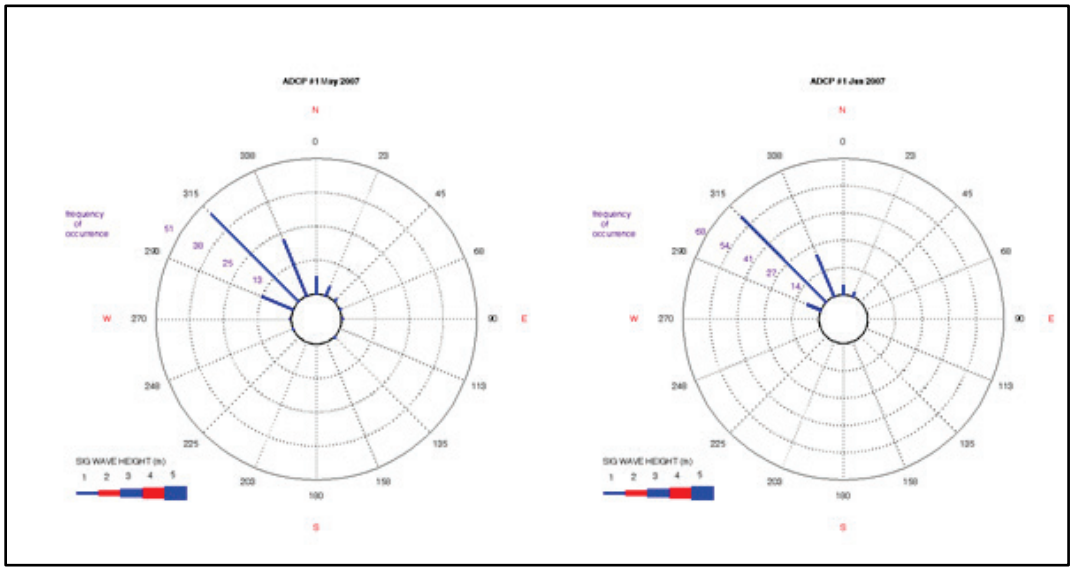

Figure 4-16. Wave height and period statistics from ADCP1 for March–June 2007.

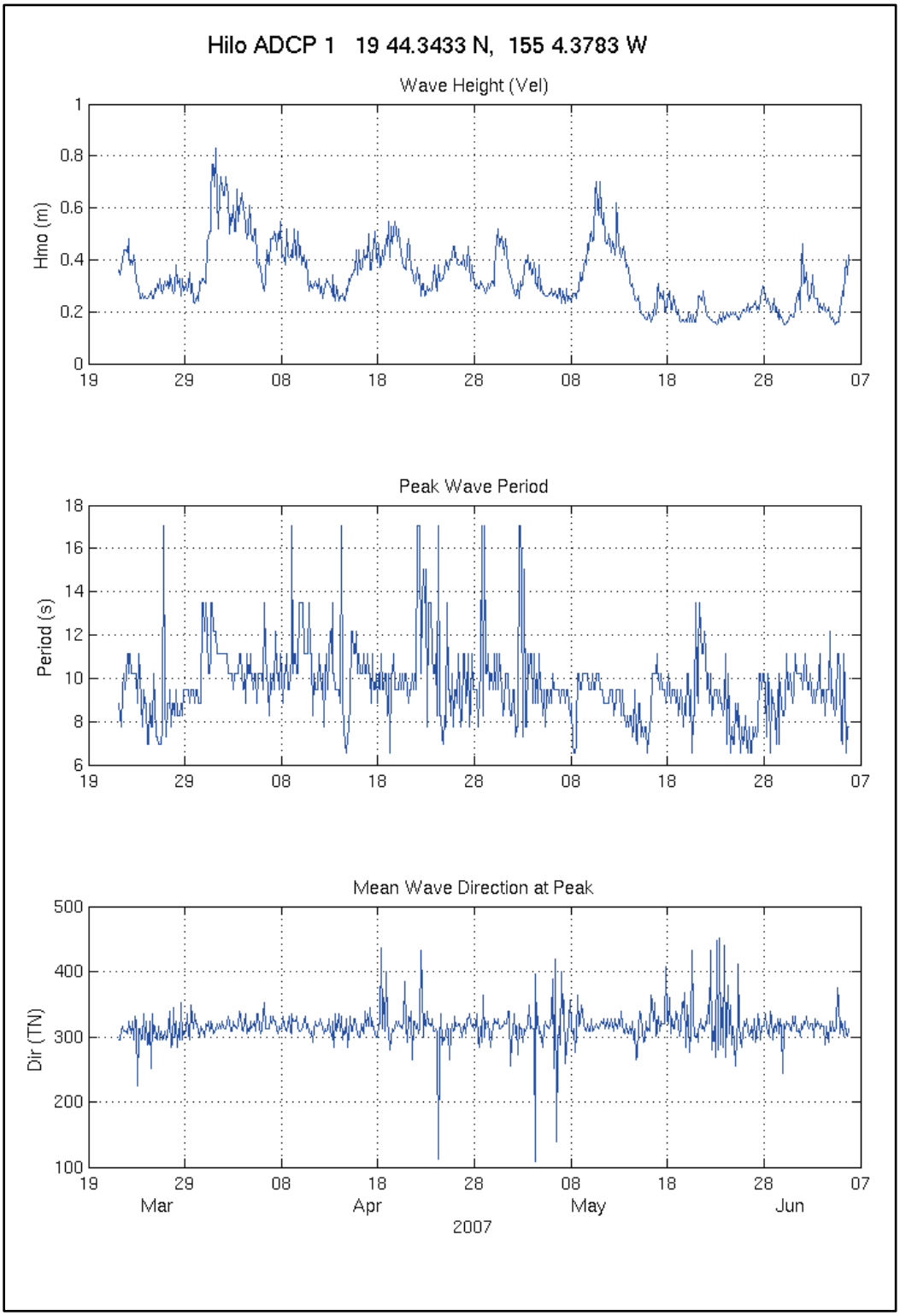

4.4.2 2013–2014 field study

Field data were collected between 21 December 2013 and 18 April 2014 by the UH. A pressure transducer as shown in Figure 4-17 was deployed near the north end of Pier 1 at (19.73365 N, 155.05428 W). This Sea-Bird 26Plus wave and tide gauge collected data at 1 Hz with sampling with a 20 sec gap between the records. The gauge was placed in a nominal depth of approximately 30 ft (9 m).

Figure 4-17. UH gauge location in 2013–2014 field study (photo from Google Earth).

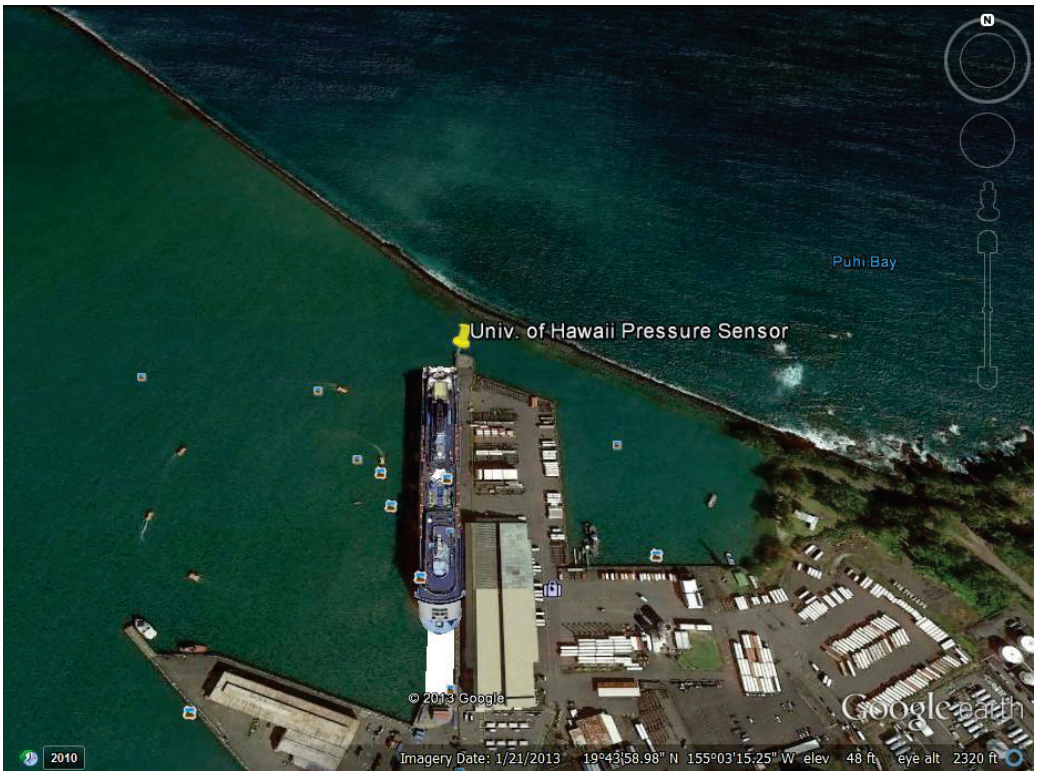

The data time series were parsed out into hour-long records for analysis. Pressure data were corrected to water surface displacement (eta) using linear wave theory with a high-frequency cutoff where the amplitude correction exceeded 10. Spectra were processed with the Welch method using a 50% overlap or 1,024 point segments and 5-point band-averaging. The IG and swell waves were split at 0.0333 Hz (~ 30 sec), and corresponding energy density spectra were stored in separate files. Hourly wave statistics (H_s, T_p) and mean water depth were computed for the IG and incident band waves and stored in monthly files. Note that peak period of IG waves was dominated by long periods, which were longer than the time-series ensemble length of 1,024 sec. Spectra plots were made of the 12 hr records to check for the low-frequency IG waves.

4.5 Model calibration and validation

The two field data sets described above were used to test and validate the B2D model. The 2007 measurements were obtained from a water quality study and limited wave data were collected only by one gauge near the entrance. No major storms occurred during this data collection period. The two highest wave conditions recorded by ADCP1 in April and May are shown in Figure 4-16. These and four events from the 2013–2014 field study were selected for model calibration and validation. These included events on 5 January 2014 at 1600 UTC, 27 February 2014 at 1800 UTC, 18 March 2014 at 1500 UTC, and 3 April 2014 at 1800 UTC.

A comprehensive model-to-data comparison was performed for the first event of 5 January 2014 at 1600 UTC. The same approach and analyses were used for three other events. The validation for the second set of events with a wide range of input conditions was performed in time- and frequency-domain. These simulations were used to investigate appropriateness of model parameters (e.g., calibration), including selection of damping layers (width and coefficient), bottom friction, turbulence coefficient, and lengths of model simulation times necessary to adequately model generation and changes in developing IG waves.

Model simulations generate temporal and spatial solution files, which include output files of the mean water level (i.e., wave setup), mean wave direction, significant wave height, mean velocity (current), and optional time series outputs of the water surface and pressure at the selected output locations (*probes*). The most appropriate grid for each incident wave condition was used in the simulations. Model results were saved over the entire grid domain and also at the nine probe locations shown in Figure 4-18. Probes 1, 4, and 6 were placed at the 2007 field gauge locations, and Probe 9 was placed at the 2013–14 field gauge location.

Post-processing and analysis of the solutions in time- and frequency-domain were performed. The B2D model interface in the Surface-water Modeling System (SMS) was used to view, extract, and post-process model results (i.e., wave parameters such as wave height, period, direction, water level, and wave-induced current) in the computational domain. Other analyses of model time-series solution files saved at the specified probes were performed using various Matlab and Fortran programs. These time- and frequency-domain analyses provide estimates of wave parameter

statistics and wave spectra. Results of two sets of validation are described in the next section.

Figure 4-18. B2D special save points (probe locations).

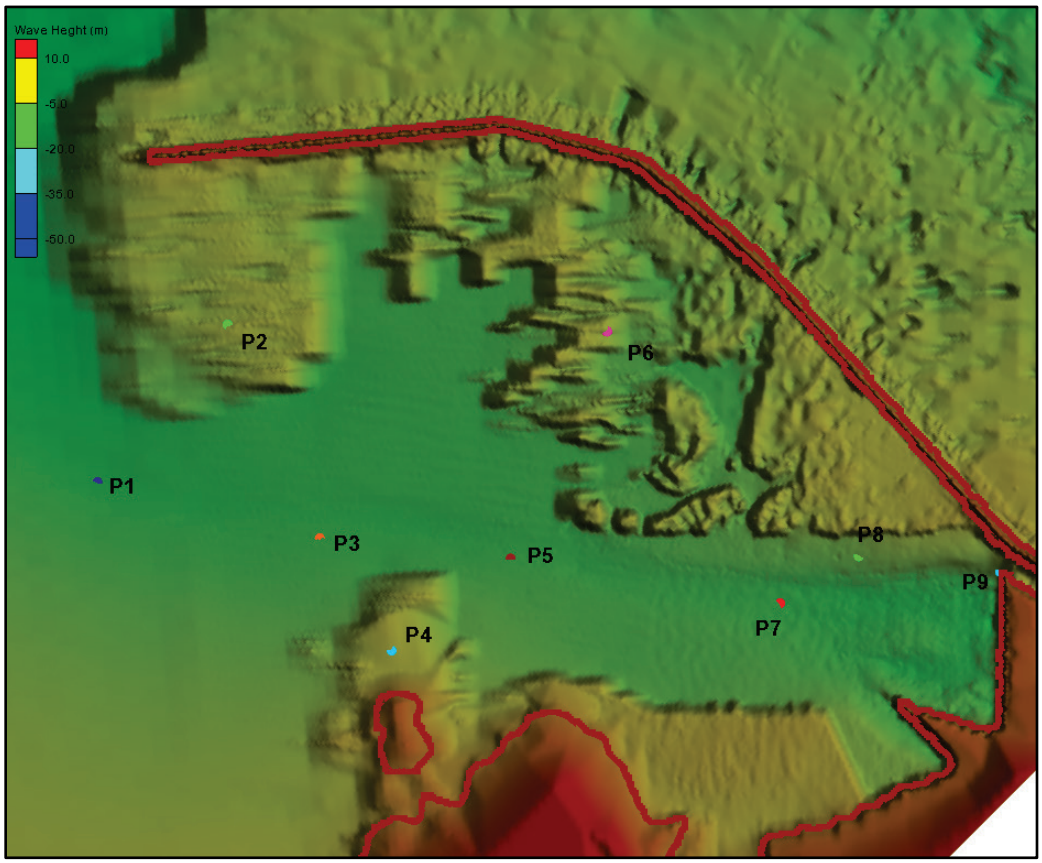

4.5.1 Calibration/validation with 2007 field data

Although no major storms had occurred during the 2007 field data collection period, Figure 4-16 shows two noticeable wave conditions in April and May 2007, which were selected for model evaluation. In these *blind tests*, B2D was intentionally set up with the recommended default parameters to determine its ability of capturing the characteristics of field measurements. The offshore wave conditions for these two test conditions were representative of the values shown in Tables 4-2 and 4-3. The offshore incident waves for April and May 2007 events were similar to the values for the 27 February 2014 event in Table 4-2 and to the fifth and sixth wave conditions in Table 4-3. The deep-water wave estimates for these two selected wave conditions were obtained from the available wave hindcast sources (e.g., WIS and WW3). The estimates for the 1 April 2007 event were H_s = 6.6 ft (2.0 m) and 7.5 ft (2.3 m), T_p = 11 and 10 sec, and θ_p =

40 and 45°, respectively. The estimates for the 12 May 2007 event H_s = 5.6 ft (1.7 m) and 5.9 ft (1.8 m), T_p = 9 and 8.5 sec, and θ_p = 55° and 40°, respectively.

The model calibration test runs indicated that the harbor interior boundaries were weakly reflective with less than 10% wave reflection, and the exterior land boundaries were slightly more reflective (15% to ~20%). For consistency, the same damping layers were assigned to the boundaries of three grids for all simulated wave conditions in Tables 4-2 and 4-3 (10% interior and 20% exterior reflection). Analysis of model results showed long-period IG waves were present near the piers and at ADCP1. The amplitude and frequency of IG waves appeared to be more sensitive to dampers assigned to land boundaries located near the piers but not as sensitive to damping layers used near the entrance where ADCP1 was located. Sensitivity tests were performed for default damping coefficients range of 0 to 1 for wave periods up to 20 sec and damping layers widths of 26 ft (8 m) to 130 ft (40 m).

The 2007 field data validation results are summarized in Table 4-4. These demonstrate the ability of the model to predict wave parameters (height, period, direction) and the presence of low-frequency (IG) waves. These results confirm and suggest that in projects where no field data are available, the model could be used with the default parameters. The model is fairly insensitive to parameter settings, and the predominant factors in modeled wave conditions are the incident forcing conditions. Additional simulations made using different values of numerical parameters showed little effect on model results. At the location of ADCP1, changes in model results were negligible (less than 5%) for different incident wave directions used in simulations. Wave estimates at this location have a limited range due to the sheltering by the breakwater and refraction of waves at the harbor entrance. Consequently, model results at this location were less sensitive to incident wave height and period specified at the B2D wavemaker boundary but sensitive to the incident wave direction. Table 4-5 shows comparison of calculated wave parameters to data at ADCP1 location.

Table 4-5. Model-to-data comparison for 2007 field study at ADCP1.

Condition Simulated	Data			B2D		
	H_s	T_p	Theta	H_s* (m)	T_p* (sec)	Theta** (deg)
1 Apr 2007	0.8	13.8	120	0.65 (16%)	17.0 (24%)	108 (-12)
12 May 2007	0.7	11	117	0.59 (12%)	13.8 (20%)	104 (-13)

Values in parentheses are percent difference (*) and bias (**) between model and data.

Because model results appeared to be sensitive to the incident wave direction, each condition was simulated for three incident wave directions (0° = north and ±10° from north). The model results shown in Table 4-5 for each event are average estimates for these three incident wave directions. The average difference along the wavemaker boundary in the calculated peak wave period and direction from three simulations was 3 sec for the peak period and 22 deg for wave direction at the ADCP1, respectively. Considering the 2 Hz sampling rate and short record length of the field data and relatively calm seas being simulated, the overall agreement between model and data was considered reasonable. Hence, no attempt was made to fine tune numerical model parameters to improve model calculated wave height, period, and direction estimates. Instead, it was decided to provide average estimates along the wavemaker boundary for three incident wave directions.

The calculated wave spectra in Figure 4-19 and Figure 4-20 contains wave energy in the IG frequency band (less than 0.05 Hz), indicating low-frequency waves exist in this part of the interior harbor away from the piers and mooring basin. Comparison of energy densities in Figure 4-19 (1 April 2007) and Figure 4-20 (12 May 2007) indicates both magnitude and frequencies of emerging IG waves inside the harbor vary with the characteristics of incident waves. More energetic IG waves with larger wave height and longer peak period occurred for the 1 April 2007 event as compared to the 12 May 2007 event. The wave direction for 1 April 2007 event was normal into the harbor (from north) at the wavemaker boundary and slightly oblique (8 deg) for the 12 May 2007 condition.

Figure 4-19. Calculated wave spectra for 1 April 2007 event.

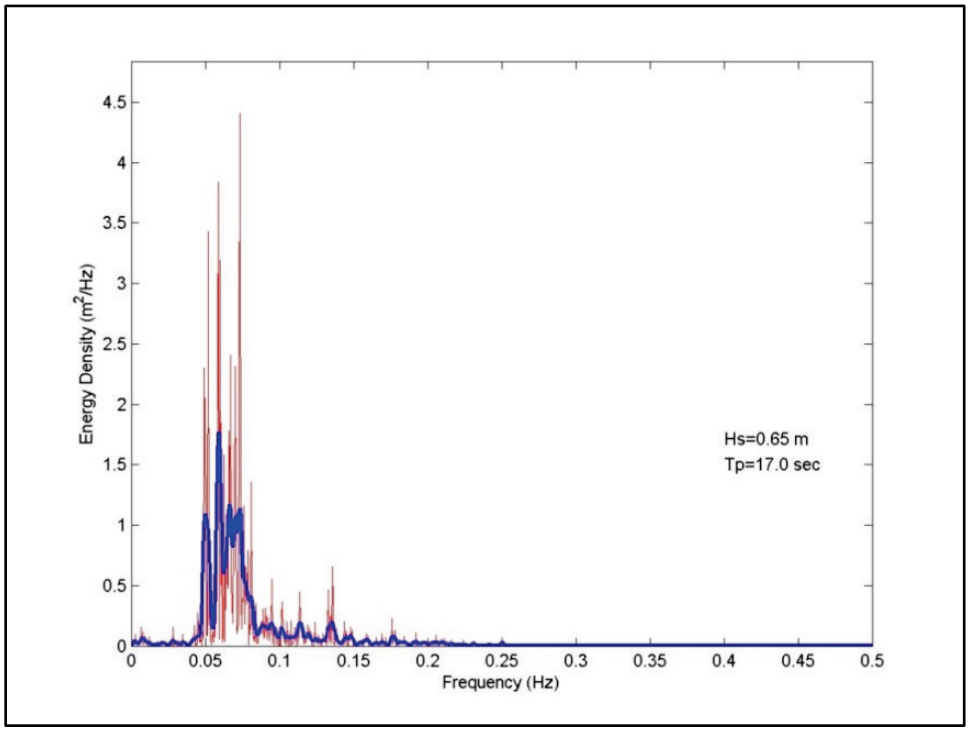

Figure 4-20. Calculated wave spectra for 12 May 2007 event.

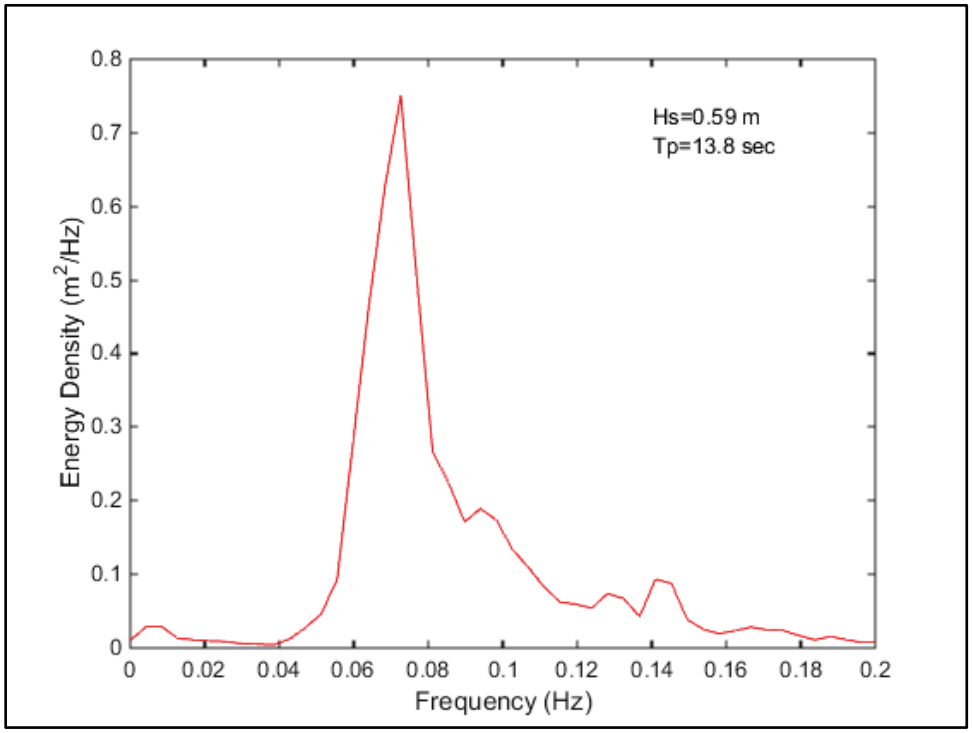

4.5.2 Calibration/validation with 2013–2014 field data

Model validation with 2007 field data showed B2D was capable of providing good estimates of design wave parameters (height, period, direction), and model predictions agreed with field data reasonably well. Results also showed the existence of wave energy in low frequencies near the harbor entrance far from the piers where the surge problem has been observed.

Additional validation tests were then conducted for four events selected from the 2013–2014 field study. These included offshore wave conditions that affected Hilo Harbor on 5 January 2014 at 1600 UTC, 27 February 2014 at 1800 UTC, 18 March 2014 at 1500 UTC, and 3 April 2014 at 1800 UTC. Since these events cover a wide range of input conditions, these were also used in the investigation of computational parameters, including the width and coefficient of damping layers, bottom friction, turbulence coefficient, and the length of simulation (run time). Figure 4-21 shows time-series of wave height, period, and water depth (water level) for January 2014 at the UH gauge.

Each condition was simulated with the B2D grid best suited for a given wave direction for the selected condition. Model results were saved over the entire grid domain and also at nine special output points (probe locations) shown earlier in Figure 4-18. The temporal and spatial output files of the mean water level (i.e., wave setup), mean wave direction, significant wave height, mean velocity (current), and time series of water surface elevation and pressure at the probe locations were post-processed and analyzed. The B2D model interface in the SMS was used to view, extract, and post-process model results (i.e., wave parameters such as wave height, period, direction, water level, and wave-induced current). Additional analyses of model time-series solution files saved at specified probes were performed using Matlab and Fortran codes. These and SMS post-processing capabilities were used to develop estimates of wave parameter statistics and wave spectra in time-domain and frequency-domain.

The results for the first event on 5 January 2014 at 1600 UTC are described in detail here. Other selected wave conditions used the same modeling approach and analyses, with similar findings in terms of characteristics of model-predicted waves inside the harbor. For the 5 January 2014 event, the month-long variation of wave height (including

swells and IG waves), peak period, and water level (depth) are shown in Figure 4-21. The largest wave heights in this figure occur between 4–7 January, and 23–30 January 2014. The peak wave period varies from 10 to 23 sec, and water level fluctuates between 28 ft (8.5 m) and 30 ft (9.0 m) during the month of January 2014.

Figure 4-21. Swell, IG waves, and depth change at the UH gauge (January 2014).

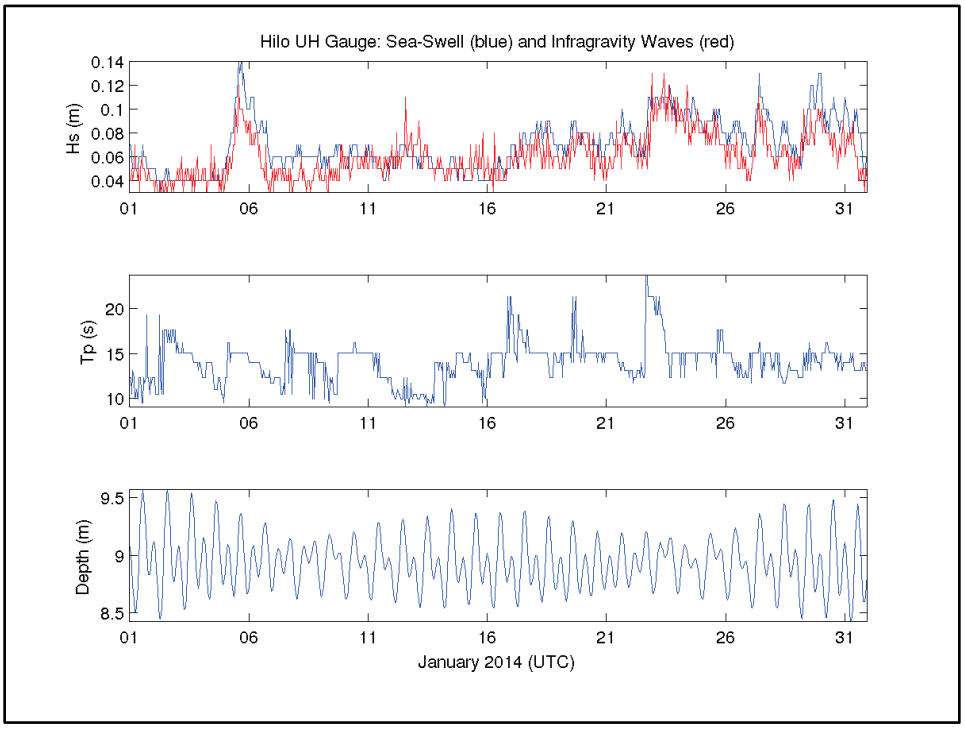

The north-northeast grid was used to simulate the condition of 5 January 2014 at 1600 UTC. The significant wave height field from this simulation is shown in Figure 4-22. Larger significant wave heights exist outside the harbor and also in the western part of the navigation channel at the harbor entrance and near the tip of the breakwater. Model results indicate waves over the reefs seaward of the breakwater converge in some areas as denoted by orange to yellowish color bands, designating areas with the largest wave heights. Larger breaking waves generate wave-induced currents seaward of the breakwater and can cause runup and overtopping of the breakwater segments with low elevation.

Figure 4-22. B2D calculated significant wave height field for 5 January 2014 at 1600 UTC.

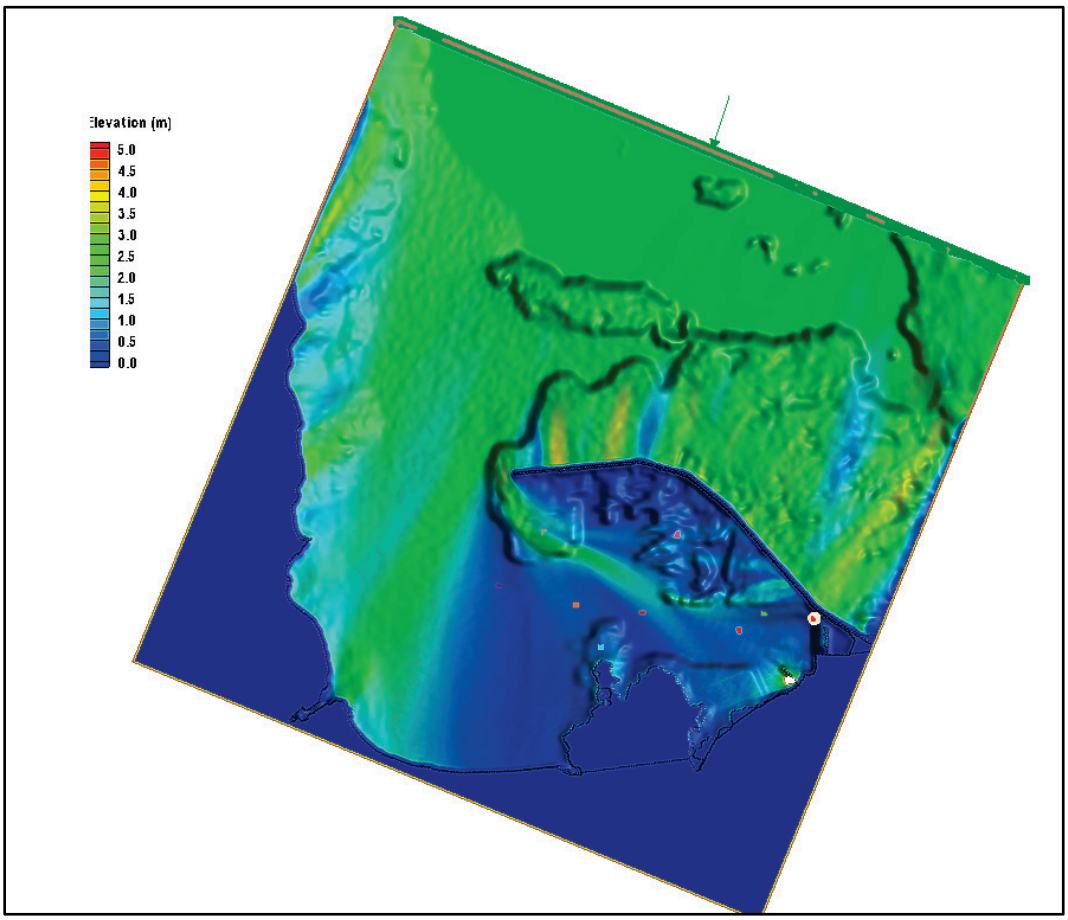

Figure 4-22 shows low and high wave height zones develop over the exterior and interior reefs, in the harbor entrance, and along the navigation channel inside the harbor. Waves wrap around the western tip of breakwater and head east and southeast toward the mooring/turning basin and Piers 1 and 2 areas. Waves that can reach the interior harbor refract away from the dredged navigation channel toward the reefs present north and south of the navigation channel. Waves with smaller heights move through the navigation channel to reach the mooring/turning basin and Piers 1 and 2 areas. The height of waves at the mooring area and Piers 1 and 2 is generally less than 1.6 ft (0.5 m).

Model-calculated time series and data from the UH gauge are shown in Figure 4-23. A segment of this time series on 5 January 2014 at 1600 UTC for 1 hr (3,600 sec) from model output and data is selected for further analysis. The model results are for much longer times than field measurements that are of finite-length records. The selected segments for

analysis covered the time period when the two records overlapped. Smoothing was applied as necessary to filter outliers in the data. Figure 4-23 shows time series from Probe 9 and data from the UH gauge analyzed at the field gauge location. Model results and UH gauge data are displayed for the raw and smoothed time series from both sources. The model-to-data agreement can change depending on how these short records are processed and on the types of analyses applied.

Figure 4-23. Comparison of model time series and data at Probe 9 for 5 January 2014 at 1600 UTC.

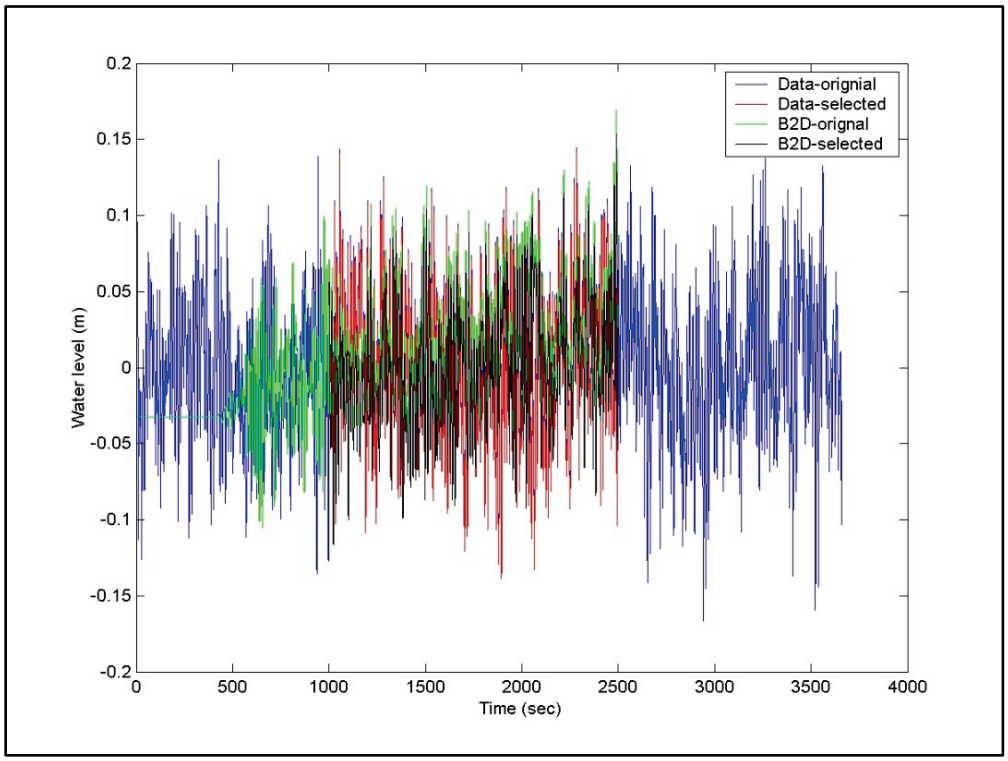

A sample spectral analysis plot is provided in Figure 4-24 to show results obtained using both raw and smoothed (filtered) continuous spectra (e.g., energy density) estimates. Note that the calculated wave height and peak period would change depending on type of spectral or time-series analyses and smoothing applied (e.g., linear summation of energy densities over frequencies vs. zero down-crossing, analysis-based peak period estimates and the number of degrees of freedom (DOFs) (e.g., 10 to 30] used in the analysis). In time-series analysis of short data records, a value between 10 and 20 for DOF is recommended.

Figure 4-24. Sample wave energy density calculated at the UH gauge.

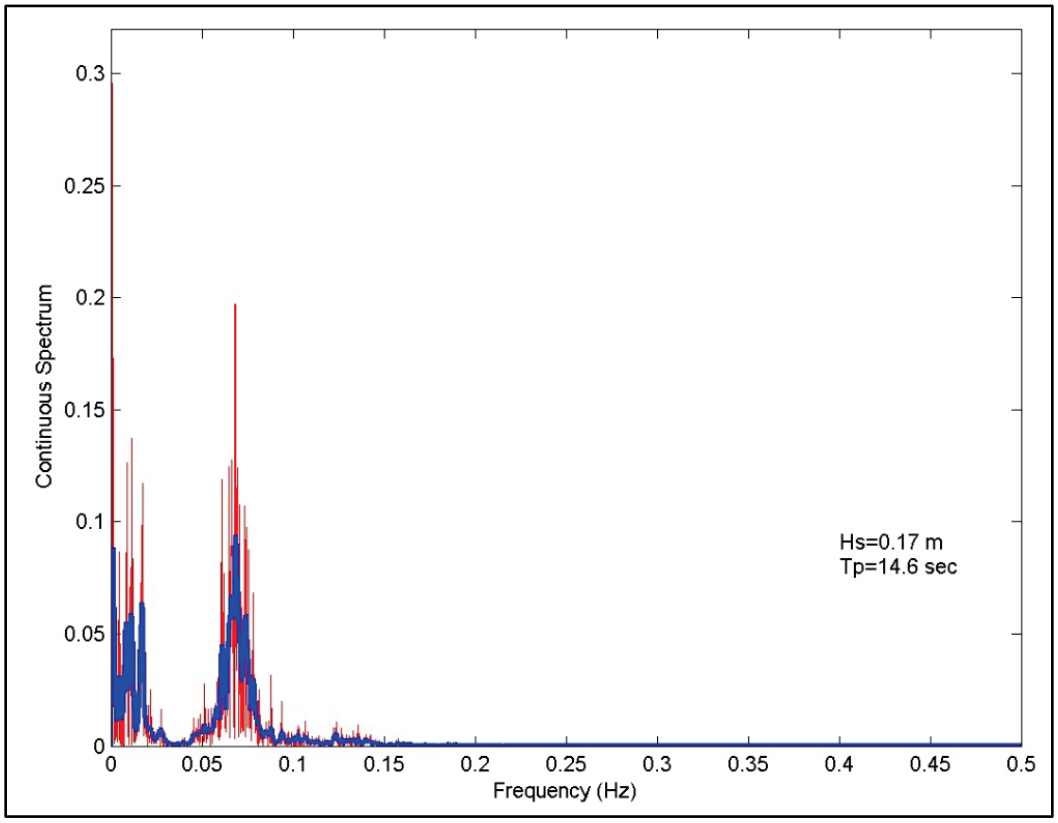

In Figure 4-25, the model-calculated energy density (wave spectra) is compared to the data (measurement from the UH gauge) spectra, including the low-frequency part of the spectra where IG frequencies occur. The model-to-data comparison was sensitive to damping layers assigned to the land and structures in the vicinity of Probe 9, one of the nine special output save locations where model time series were saved. Probe 9 was positioned at the location of the UH gauge. Probes are used in B2D to collect model-calculated results at a data collection time interval specified by the user. Overall, good comparisons are obtained in the frequency-domain and time-domain. These results demonstrate the model is capable of representing the time variation of waves in this part of Hilo Harbor and that the model captures the characteristics of emergent IG waves.

The distribution of wave energy density (spectrum) depicted in Figure 4-25 shows clearly the presence of IG waves in this southeast corner of the interior harbor. The comparison between model and data for wave energy density with and without smoothing indicated the agreement improves with smoothing applied. Noted earlier in the B2D calibration tests, model

results were sensitive to the values of damping layers used to represent partially reflective land boundaries around Probe 9. These include the two piers and east end of the Federal breakwater that are close to the UH gauge.

Figure 4-25. Wave spectra comparison for B2D and UH gauge data for 5 January 2014 at 1600 UTC.

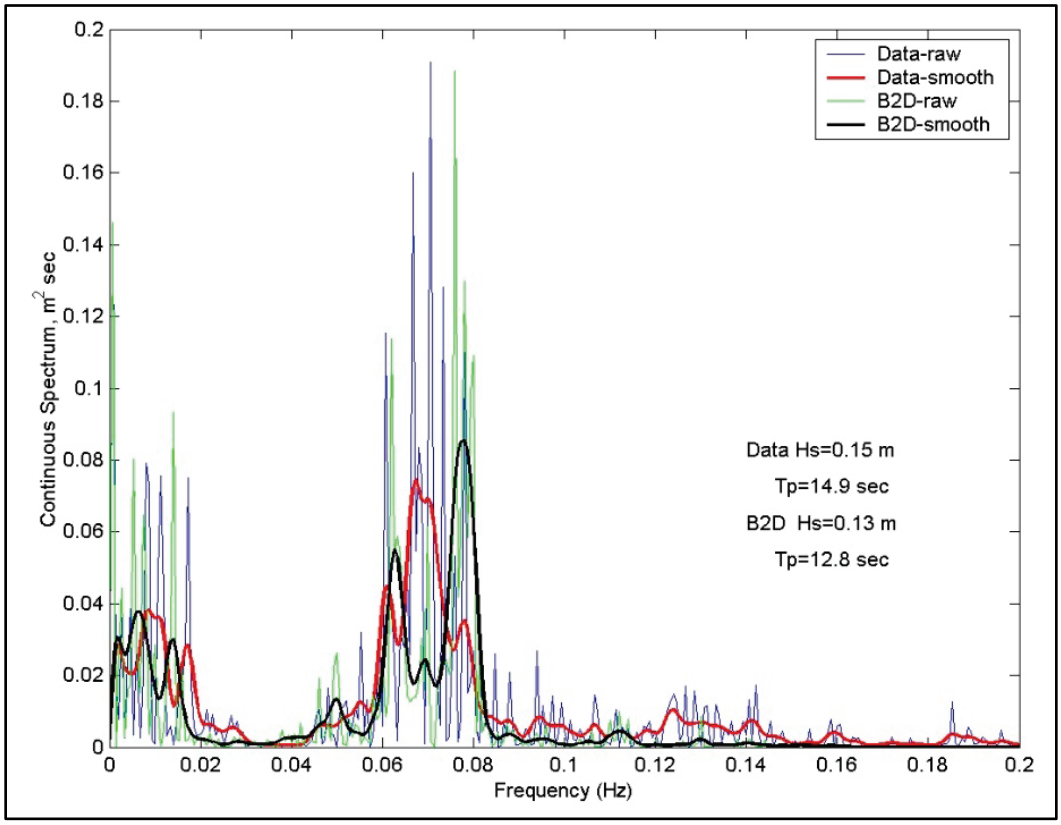

4.5.3 Chile tsunami effect on Hilo Harbor

An interesting event happened on 1 April 2014 in the Pacific Ocean near Chile in South America that affected Hilo Harbor in the days following this event. An 8.2 Mw earthquake occurred off the coast of Chile on 1 April 2014 at 2358 UTC. This earthquake generated a massive tsunami that propagated through the Pacific Ocean, reaching Hawaii 14 hr later and producing oscillations in Hilo Harbor starting on 2 April 2014 at 1348 UTC. Analysis of the UH gauge data for 1–18 April 2014 (Figure 4-26) shows the variation in wave height, peak period, and water level (depth). Figure 4-27 shows a 36 hr record starting from 2 April 2014 of the water level change at the UH gauge location before and after the tsunami. Figure 4-28 shows the large depth (or water level) change between 800 and 1,000 min during which the peak water level occurred. The water levels before

and after the tsunami from the UH gauge are shown in Figures 4-29 and 4-30, indicating a nearly 40-fold increase in water level. The 12 hr wave energy changes from 1 April to 4 April 2014 are shown in Figures 4-31 through 4-38.

The wave period was used instead of frequency in some energy distribution plots to show the tsunami's effect on the southeast corner of harbor. In the analysis of field data, the spectra were divided into three period bands: (a) long periods in minutes, (b) IG wave periods from 30 sec to 300 sec, and (c) incident wind wave periods less than 30 sec. The time series and spectral plots in Figures 4-26 through 4-38 provide indisputable evidence of short- and long-wave frequencies present in the

Figure 4-26. Wave height, period, and depth change at the UH gauge (April 2014).

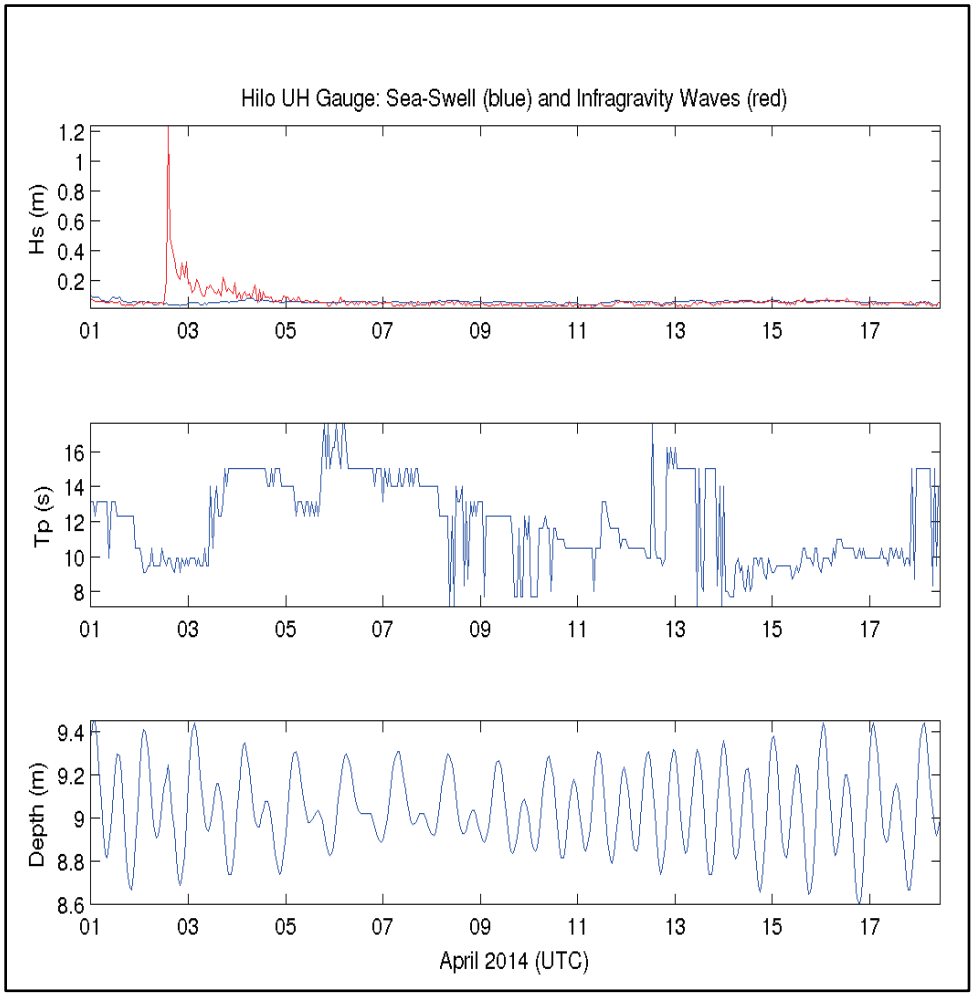

Figure 4-27. The 36 hr water level variation in Hilo Harbor.

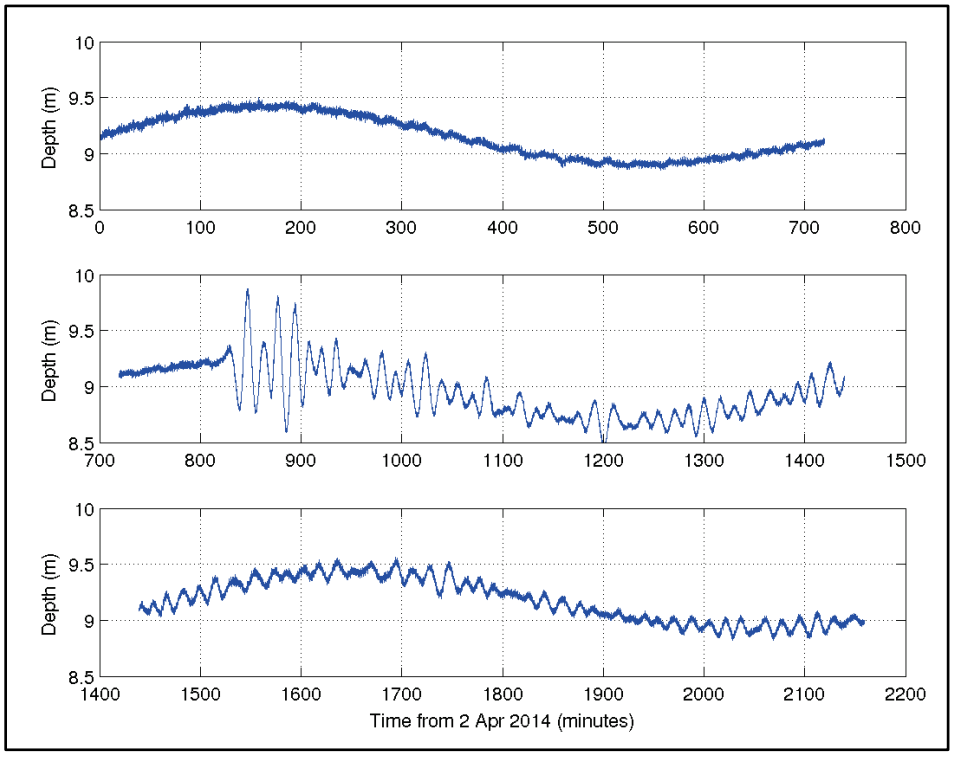

Figure 4-28. Water level change between 800 and 1,000 min from 2 April 2014.

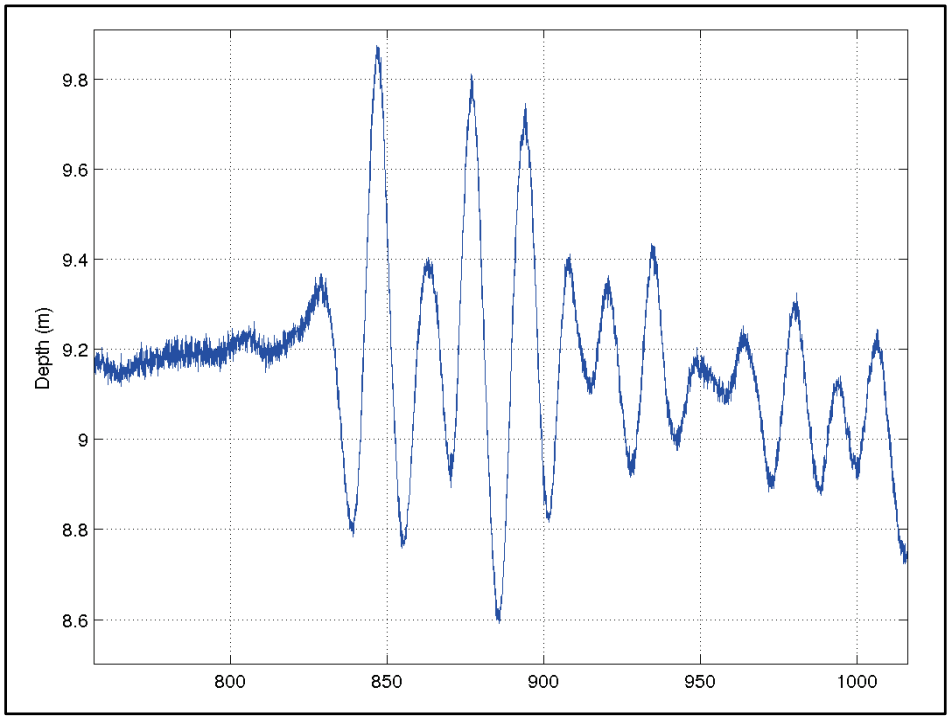

Figure 4-29. Water level change on 2 April 2014 at 0000 UTC (before tsunami arrival).

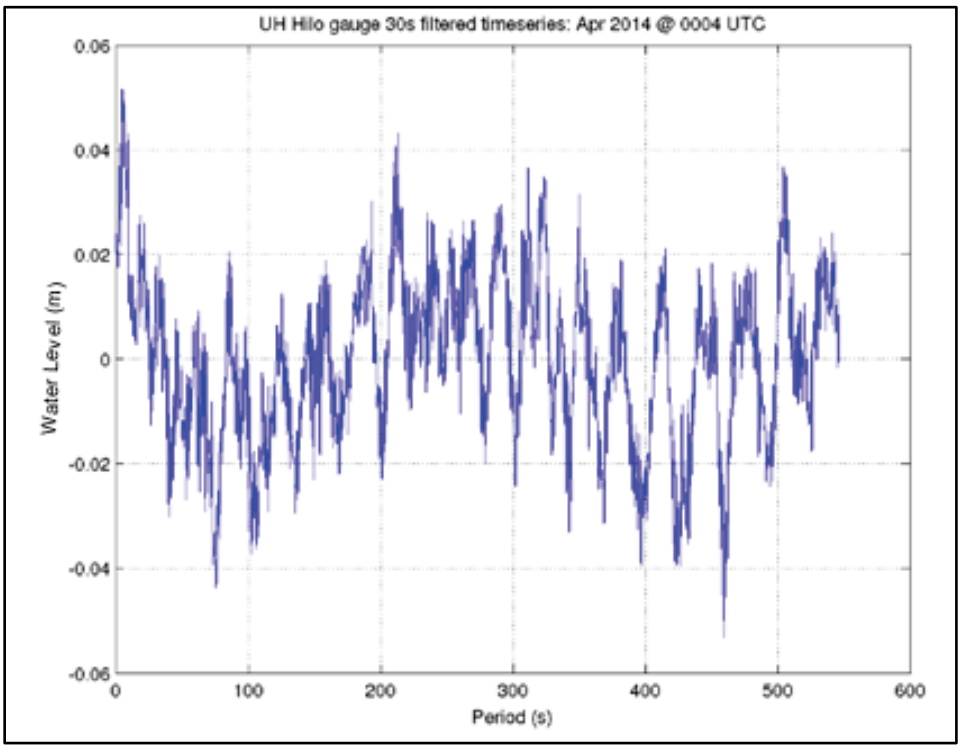

Figure 4-30. Water level change 2 April 2014 at 1200 UTC (after tsunami arrival).

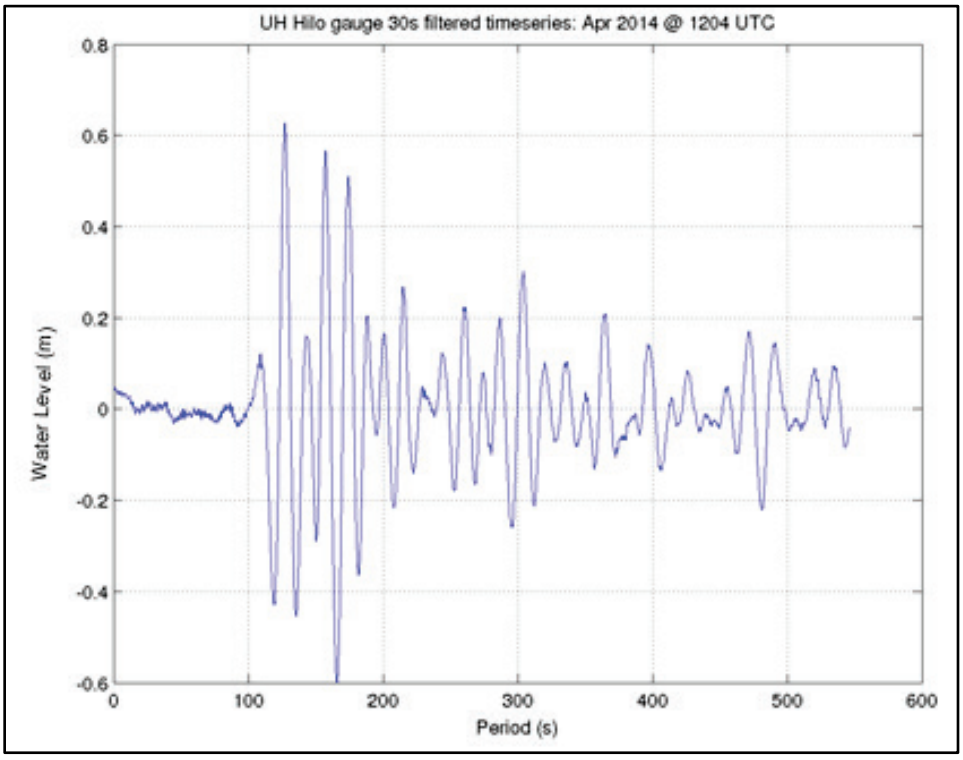

Figure 4-31. Wave energy density variation on 1 April 2014 at 0000 UTC.

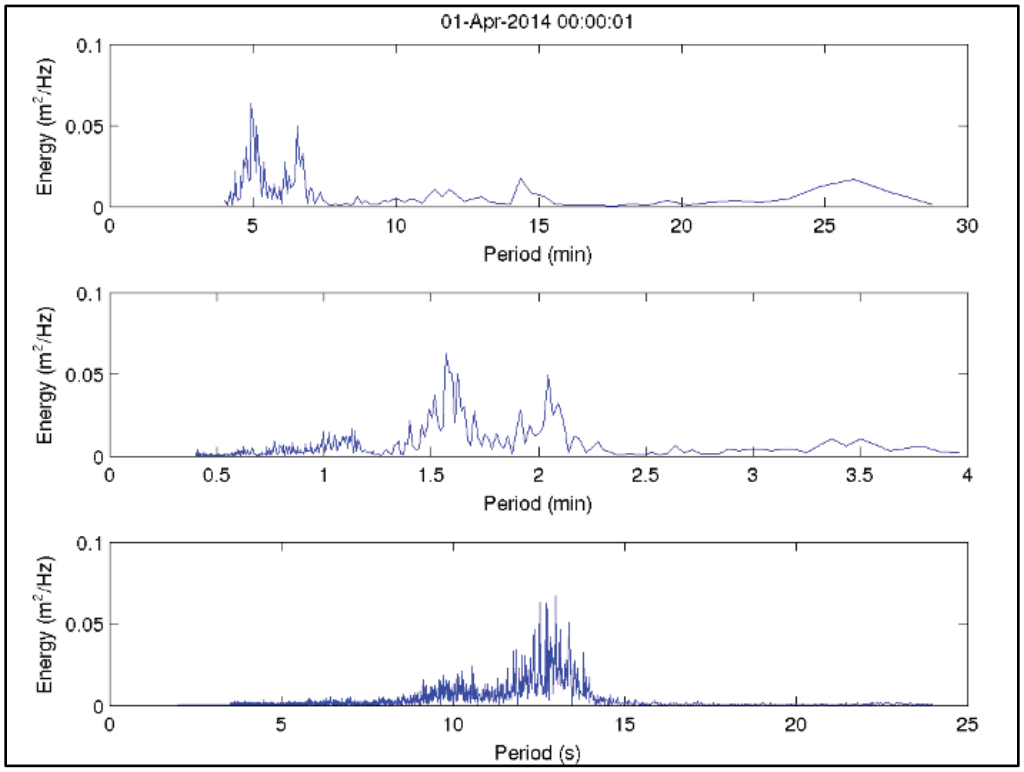

Figure 4-32. Wave energy density variation on 1 April 2014 at 1200 UTC.

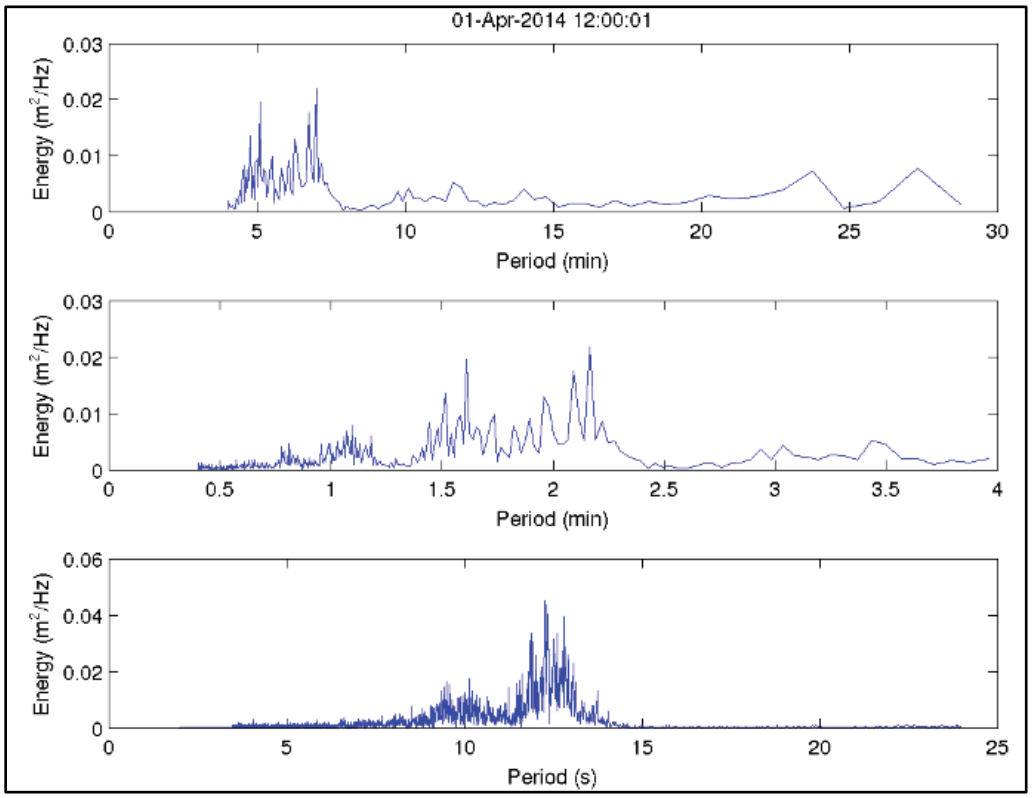

Figure 4-33. Wave energy density variation on 2 April 2014 at 0000 UTC.

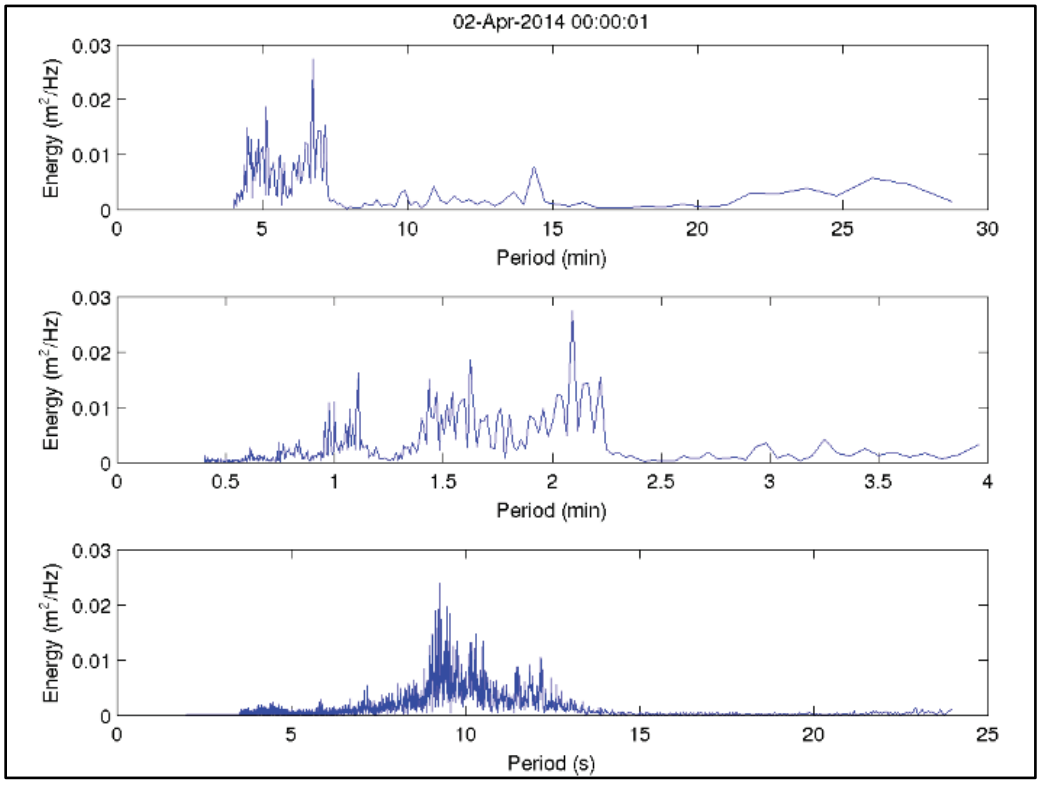

Figure 4-34. Wave energy density variation on 2 April 2014 at 1200 UTC.

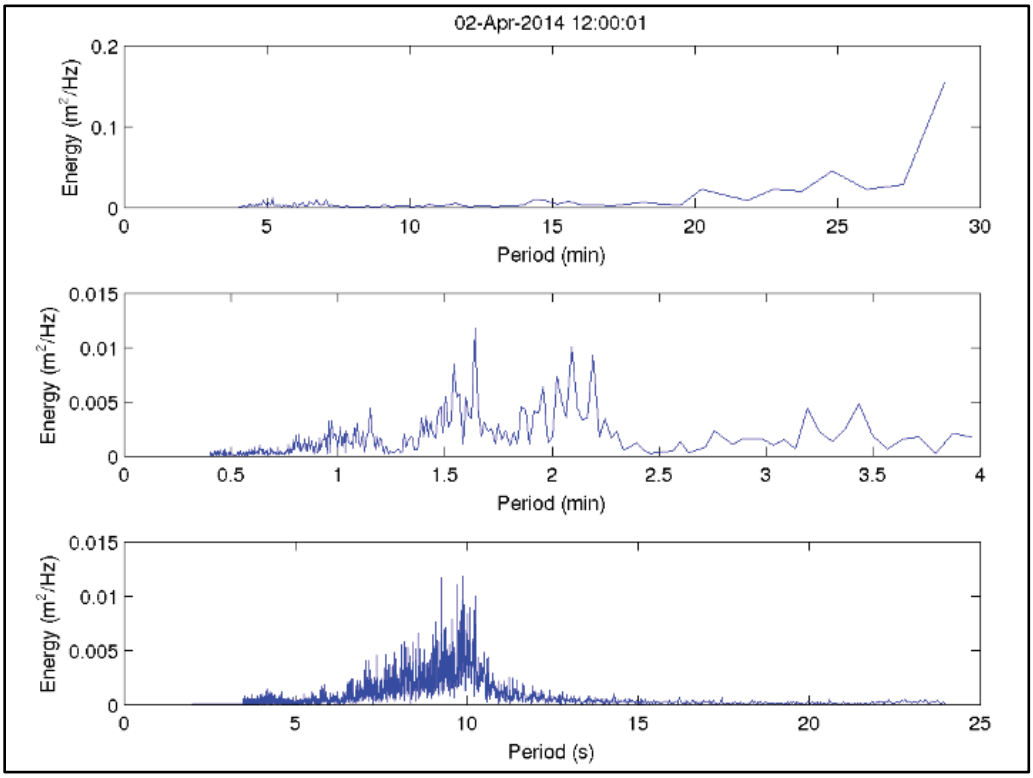

Figure 4-35. Wave energy density variation on 3 April 2014 at 0000 UTC.

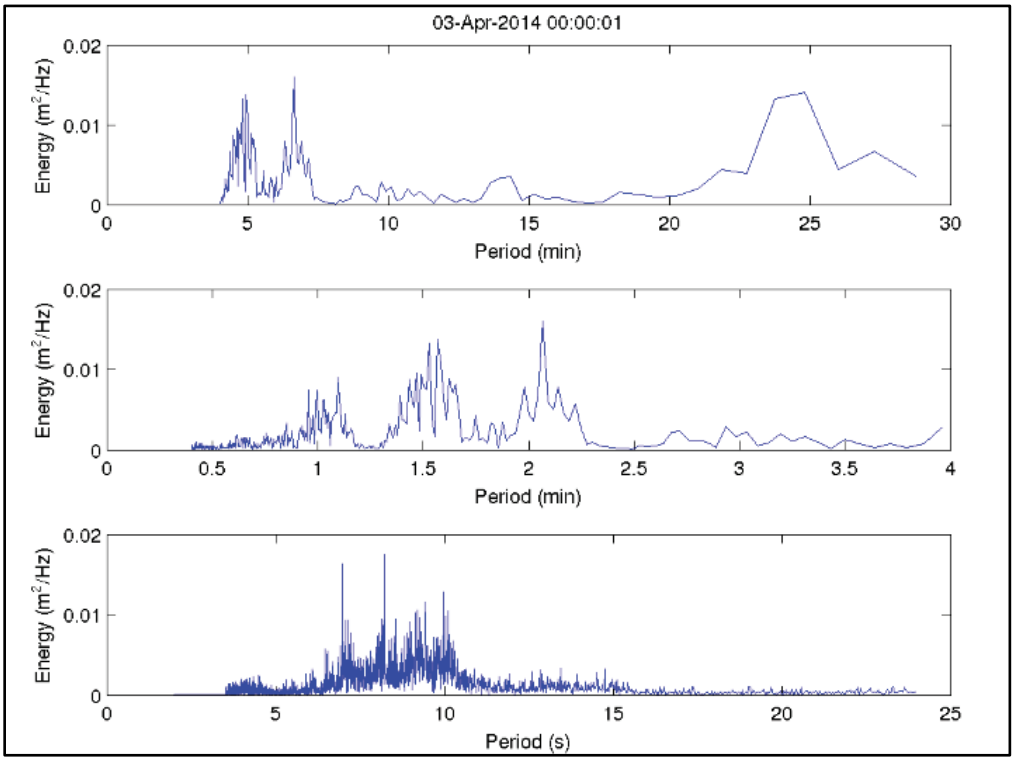

Figure 4-36. Wave energy density variation on 3 April 2014 at 1200 UTC.

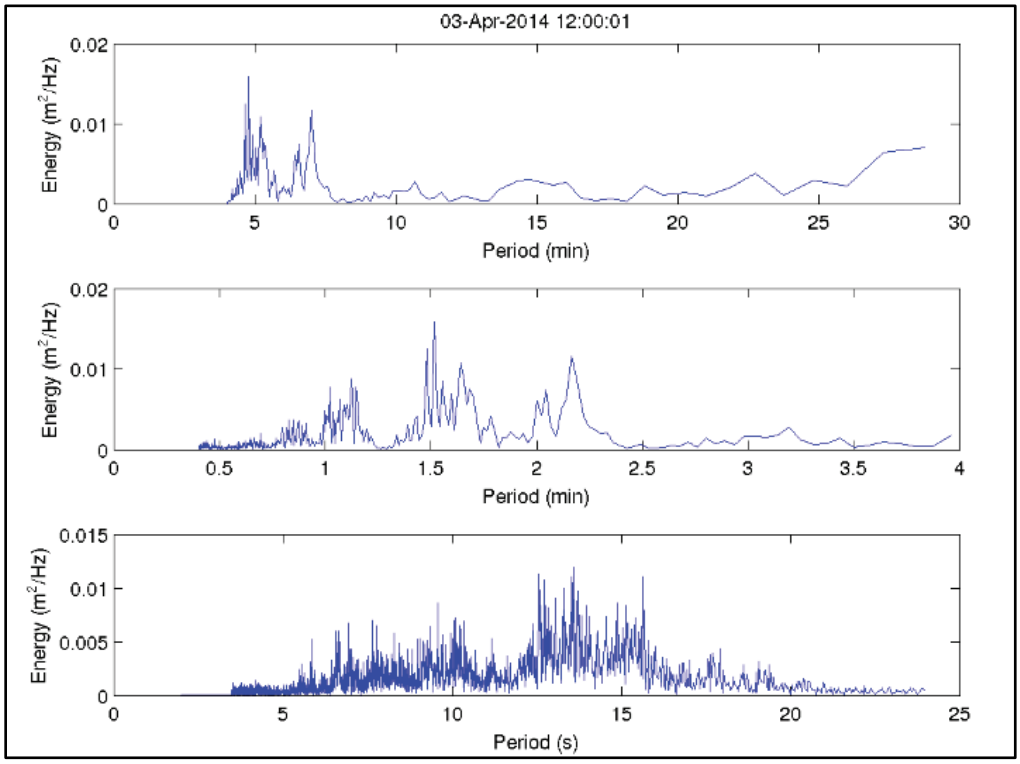

Figure 4-37. Wave energy density variation on 4 April 2014 at 0000 UTC.

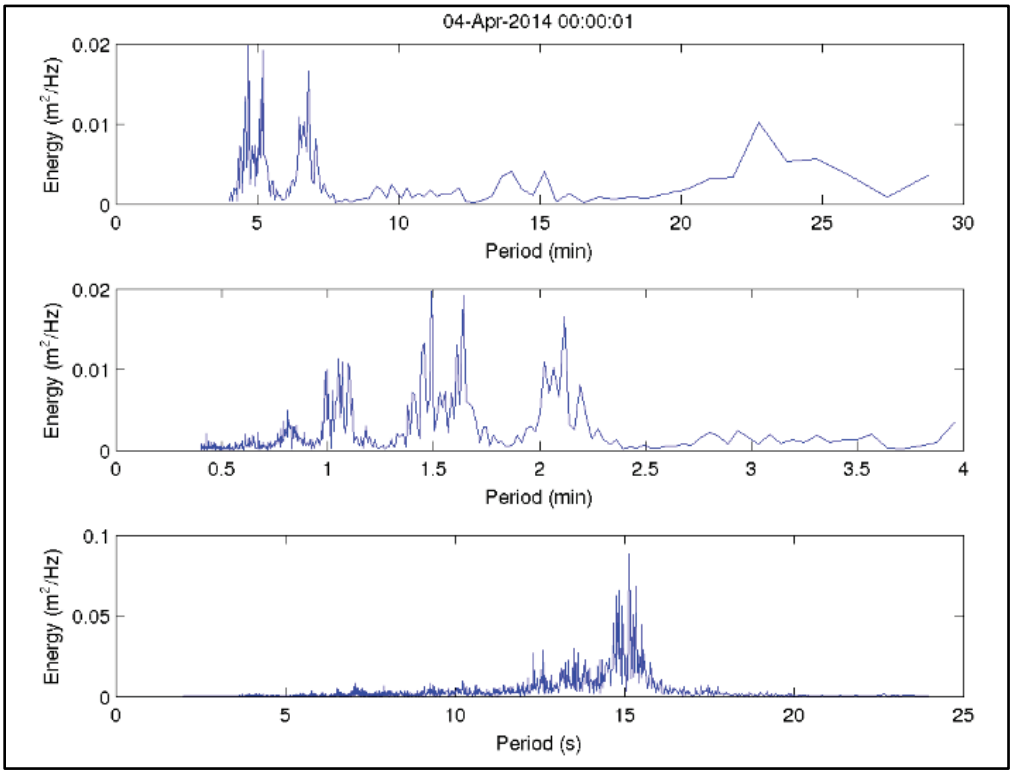

Figure 4-38. Wave energy density variation on 4 April 2014 at 1200 UTC.

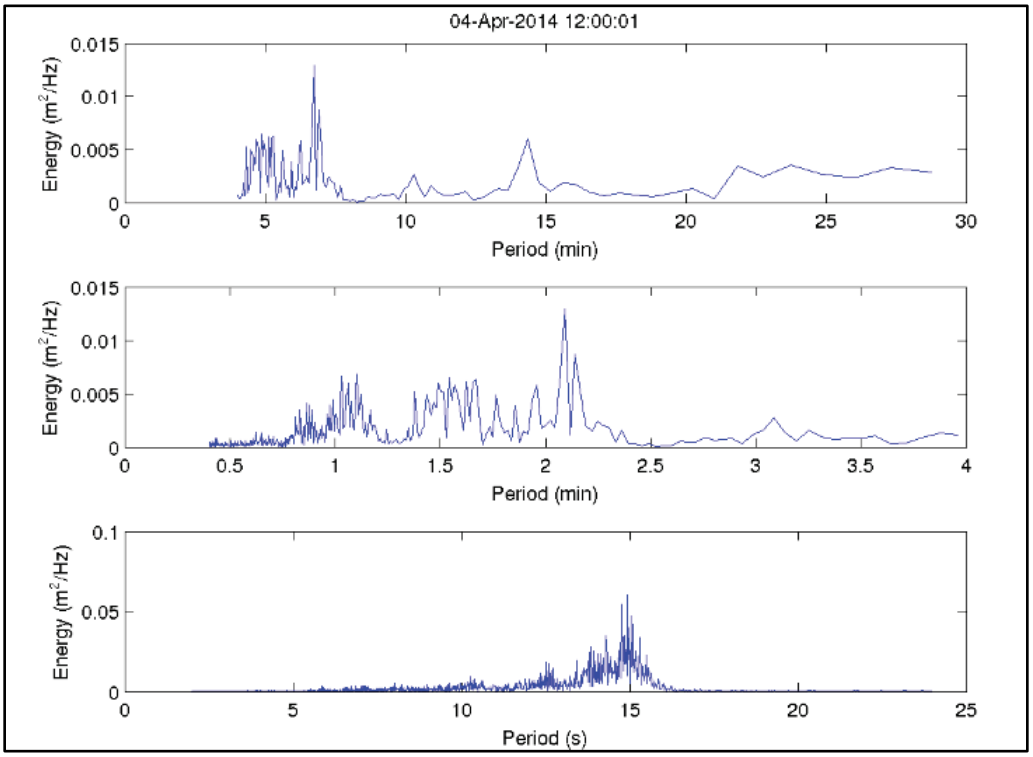

field data collected at the Pier 1 in response to the Chilean earthquake and subsequent tsunami.

The above analysis reveals how the Chile tsunami affected Hilo Harbor by generating a significant water level variation inside the harbor at the UH gauge location starting approximately noon on 2 April 2014. The analysis provides details of water level change (depth) during the next 36 hr and energy density between 1 and 4 April 2014. Although there is clear evidence of significant energy present in the IG frequency band, this does not necessarily mean the harbor would experience surge problem. There will be an increased chance of harbor surging (oscillations) only if any of the low frequencies are close to the natural periods of harbor. The IG frequencies that contain significant energy can affect ship motions, maneuvering, and moorings only when they coincide with the periods of ship motions and mooring lines. No accidents were reported during this time period.

To simulate the impact of the Chile tsunami inside the harbor and further analyze the model-to-data comparison during this event, B2D was set up for the 2 April 2014 offshore incident wave condition. Offshore incident wave parameters for this event are within the values shown in Table 4-3. The calculated spatially varying wave height field is shown in Figure 4-39. Figure 4-40 shows the distribution of energy density over all frequencies, including wind-wave and low frequencies. Both model and data contain a substantial amount of energy in the low-frequency tail of the spectra. This confirms the ability of the model to represent IG waves that develop inside the harbor by interaction among other frequencies in the spectra (e.g., wave-wave interactions). The energy densities (wave spectra) for model and data are provided with and without smoothing. An improved agreement is obtained with a 10-point smoothing.

Model results showed a weak sensitivity to the damping values assigned to partially reflective land boundaries near the UH gauge (e.g., the two piers and Federal breakwater to the north). The change in wave height and period was small (less than 5% and 10%, respectively). Overall, the best agreement between the model and data was obtained with weak dampers (e.g., 26 ft [8 m] damping width and 0.05 damping coefficient) for the two pier structures and a narrow and fully absorbing damping (26 ft [8 m] damping width and 1.00 damping coefficient) assigned to approximately 0.54 mile (1 km) of the interior surface of the Federal breakwater near

Figure 4-39. Calculated significant wave height field on 2 April 2014 at 1200 UTC.

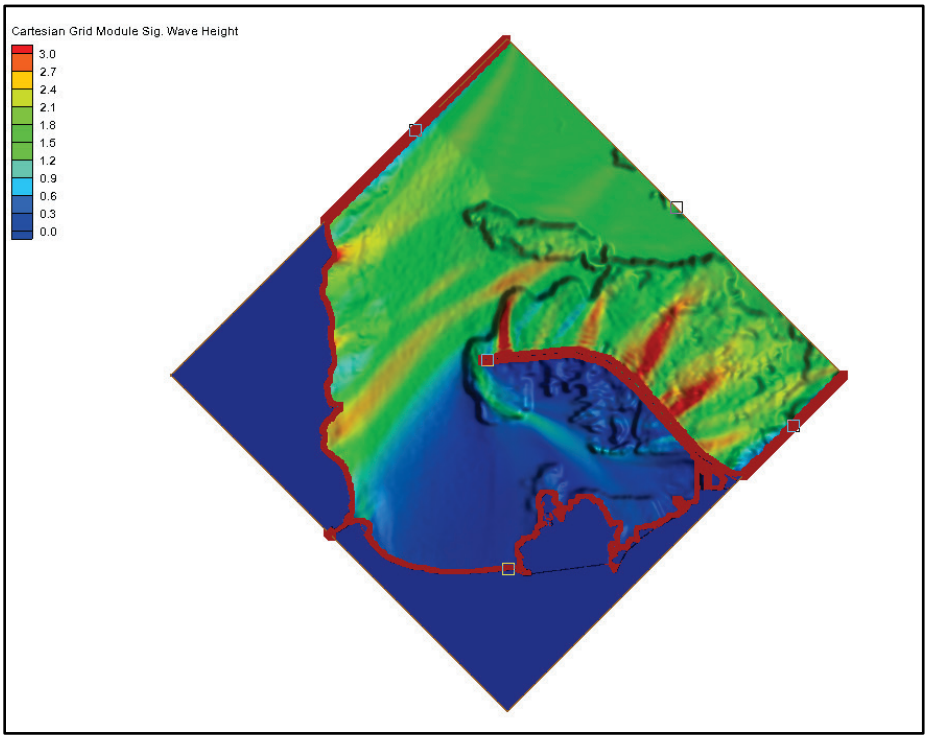

Figure 4-40. Calculated and measured wave energy densities on 2 April 2014 at 1200 UTC.

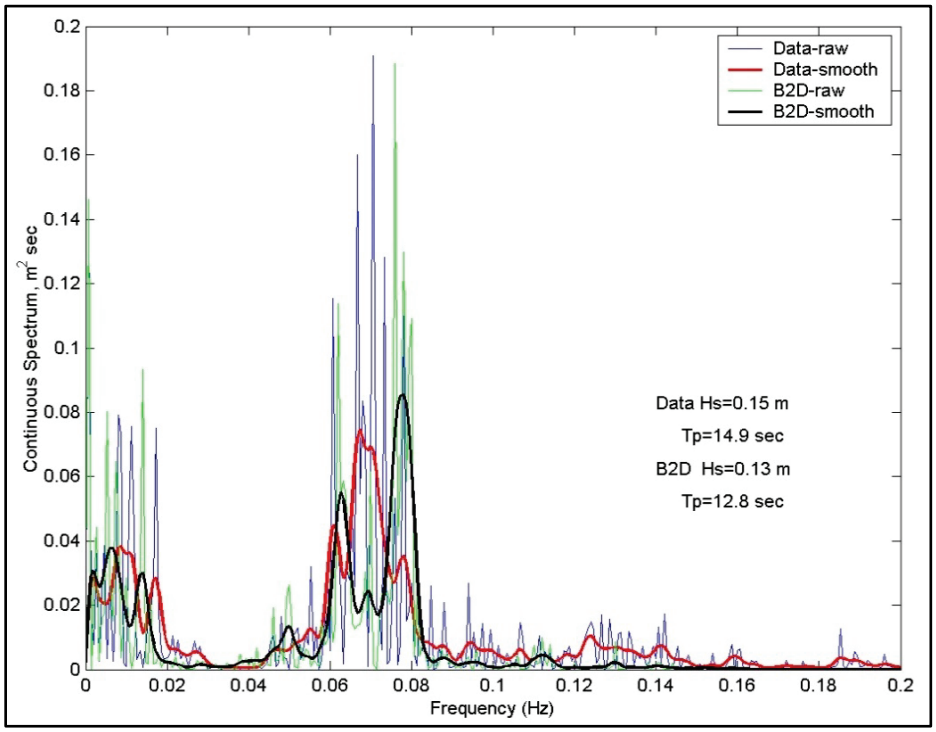

the UH gauge. Simulations were also made with no damping at the piers and interior part of breakwater near the UH gauge. The short-duration runs were successful, but wave parameters were underpredicted, and the IG waves were either small or absent.

4.6 Discussion of results

A wide range of wave conditions in Tables 4-2 and 4-3 was used to investigate mariners' concerns in Hilo Harbor. Structural modifications were considered to reduce waves in the harbor, expanding the size of the turning basin to potentially improve operational limitations. The modifications to improve conditions at the turning basin and piers were described earlier in this report. Additional discussion of the present numerical modeling study results follows.

4.6.1 Wave estimates in Hilo Harbor

The meteorological convention is used in this study. This means waves and winds are defined with the *from* direction convention, as measured clockwise with respect to true north, with north as 0°. As noted in the model calibration/validation section earlier, the incident wave direction had the greatest impact on estimates of waves inside the harbor. Modeling results indicated incident waves from true north $\pm 10^0$ were most consequential at the turning basin and piers. The waves from north by northeast (22.5^0), northeast (45^0), and east directions (90^0) had a lesser impact on these areas. The snapshots of model animations for various incident directions revealed additional interesting characteristics of wave propagation within the harbor complex, indicating which incident waves reach the turning basin and piers. The calculated wave height fields are provided in Figures 4-41 to 4-48 for three B2D grids (north, north-northeast, and northeast grids). The zoomed images depict details of the spatial transformation and movement of waves inside the harbor complex.

Figures 4-41 and 4-42 show calculated wave height fields for the north grid correspond to a large oblique incident wave (Hs = 7.02 ft [2.14 m], Tp = 14.3 sec, $\theta = 18^0$). Figure 4-41 represents the entire wave height field while Figure 4-42 reveals features of wave propagation inside the harbor. Results indicate wave dissipation occurs over the reefs outside the breakwater. There is a significant amount of wave shoaling, refraction, and breaking that produce a few high and low wave heights zones over the

Figure 4-41. Wave height field over the entire domain for an oblique wave (north grid).

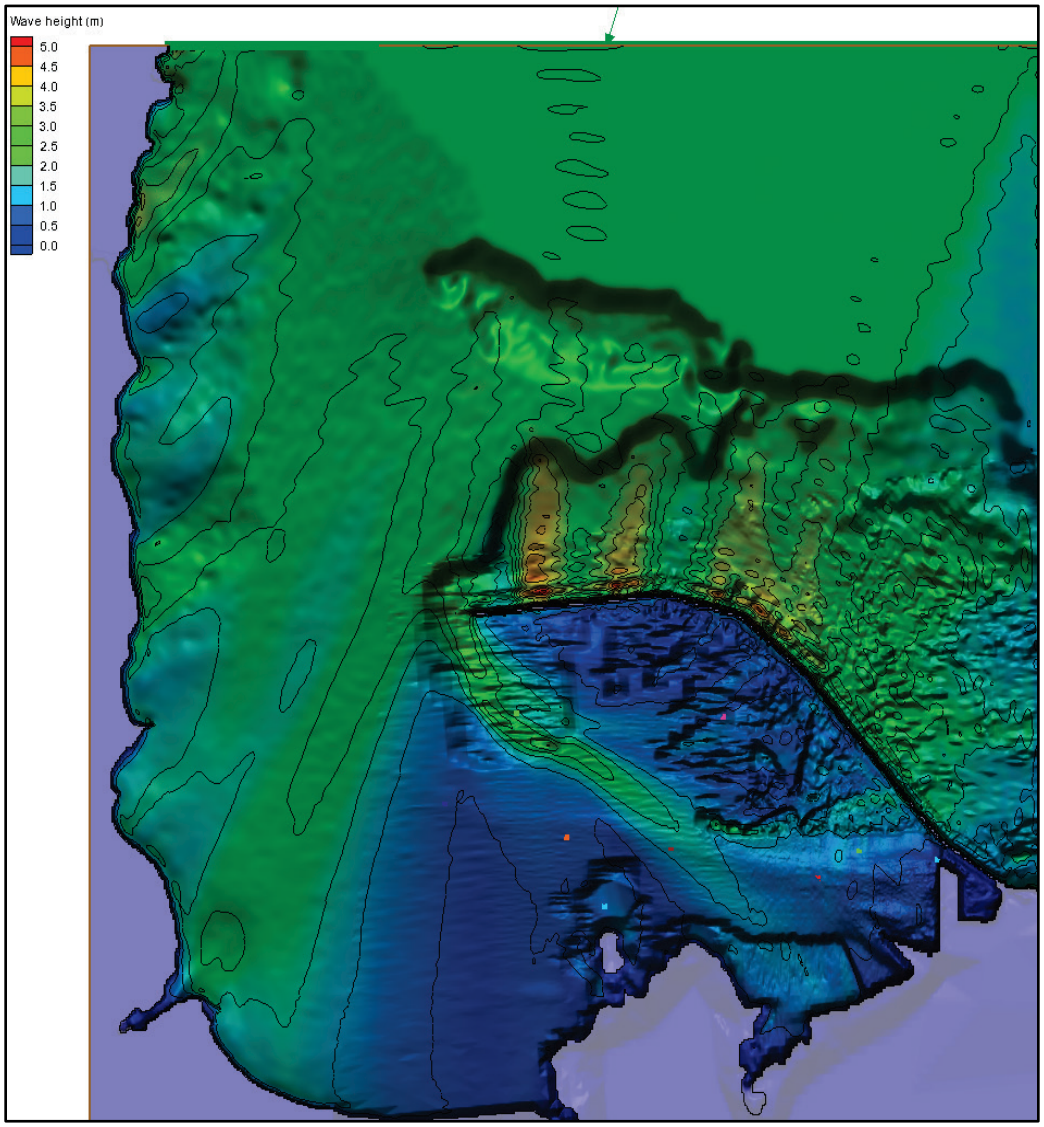

rapidly changing bathymetry of the reefs. The zoomed image shows that after a wave passes through the entrance and is diffracted at the tip of breakwater, it follows the channel halfway into the harbor and then splits up and refracts toward the channel sides and reefs on both sides of the channel. The height of outward refracting waves over the reefs and shallower parts of harbor north and south of the channel is smaller as compared to waves in the channel. The wave heights in the turning basin and Pier 1 range from 1.6 ft (0.5 m) to 2.6 ft (0.8 m) and from 0.3 ft (0.1 m) to 1.3 ft (0.4 m), respectively. These estimates varied slightly with different model parameters with a maximum change in wave height of ±20%.

Figure 4-42. Wave height field inside the harbor for an oblique wave (north grid).

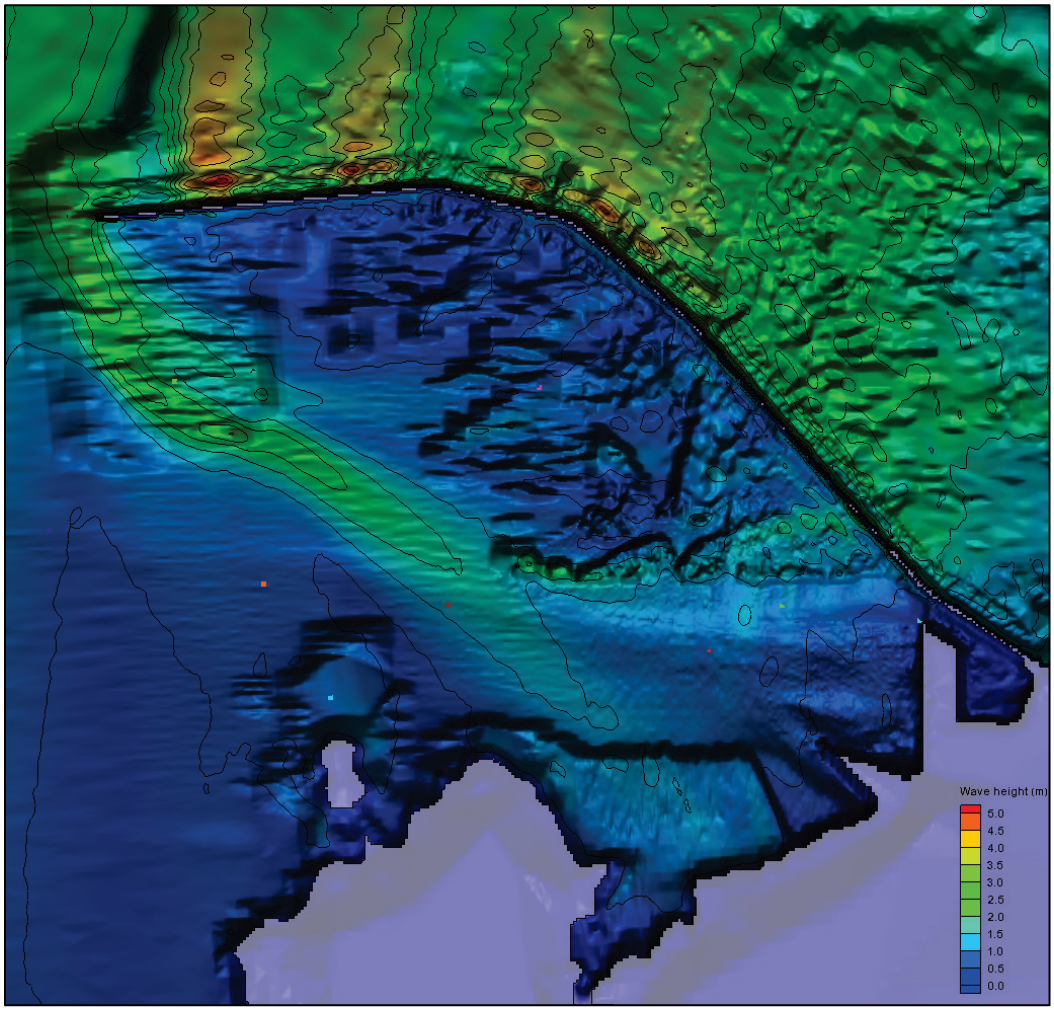

The oblique wave condition was next simulated with the north-northeast grid. As shown in Figures 4-43 and 4-44, a similar pattern of wave height is obtained outside the breakwater and in the entrance. However, comparatively more wave energy arrives along the west shoreline and greater energy reaches the southwest side of harbor. The zoomed image (Figure 4-44) also shows that waves move in and propagate through the channel and refract outward from the channel toward the reefs and shallower areas of the harbor north and south of the channel. Less wave energy reaches the turning basin because more wave energy is heading southeast toward the proposed Piers 3 and 4 areas. The maximum wave height in the turning basin and Pier 1 is reduced to 2.1 ft (0.65 m) and 1.0 ft (0.3 m), respectively. These estimates changed ±10% to 20% with the model setup and parameters that were used.

Figure 4-43. Wave height field over the entire domain for an oblique wave (north-northeast grid).

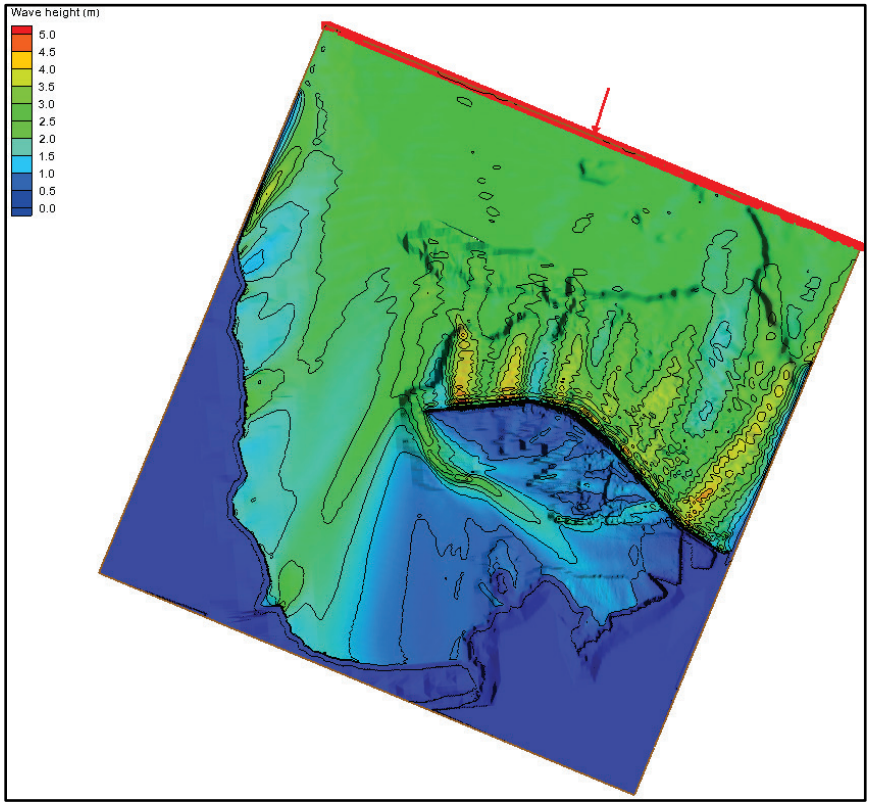

Figure 4-44. Wave height field inside the harbor for an oblique wave (north-northeast grid).

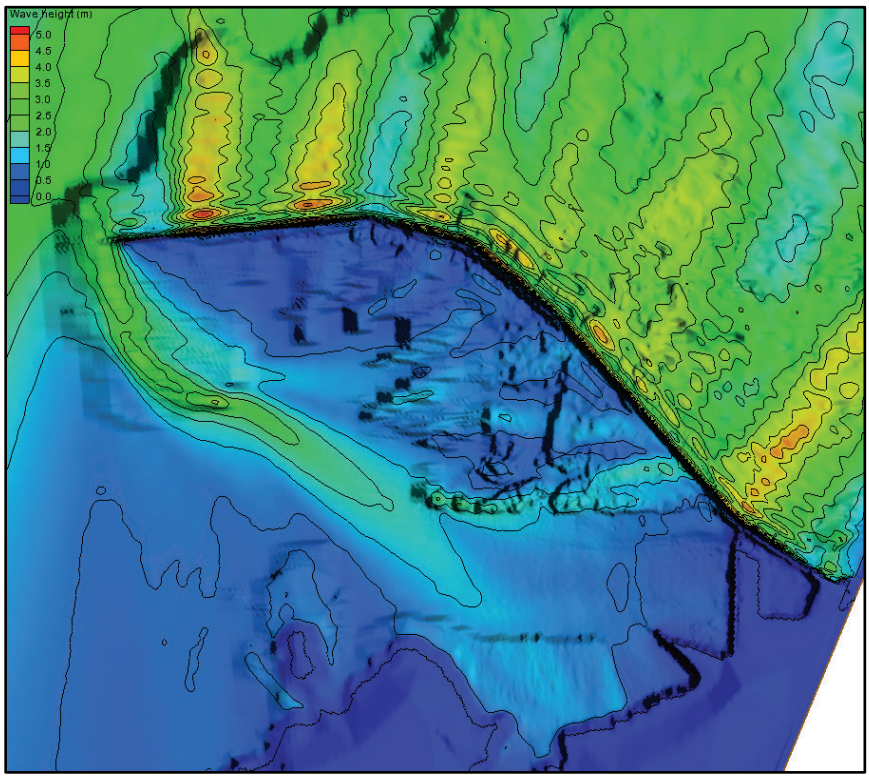

Figures 4-45 and 4-46 show the spatial change occurring in wave phase outside and inside the harbor, respectively. Shown are the bending of wave fronts and changing distance between wave crests, representing direction and spatial motion of waves in harbor. Figure 4-46 displays the variation of sea surface elevation at the piers and resulting water pile up occurring in front of the south end of Pier 1. Such a piling of water is significant to ships moored at the pier as it creates a gradient in surface elevation that may affect vessel hydrodynamic forces, motions, and mooring line forces. An imbalance in water level between the bow and aft of a ship can produce a substantial increase in forces on mooring lines and pulling forces applied to bollards. These high-strength structural elements are built into pier decks to fasten mooring lines. The bollard design is beyond the scope of this report. Related information is available from manufacturers and design manuals.

Figure 4-45. Spatial change of wave phase outside the harbor (north-northeast grid).

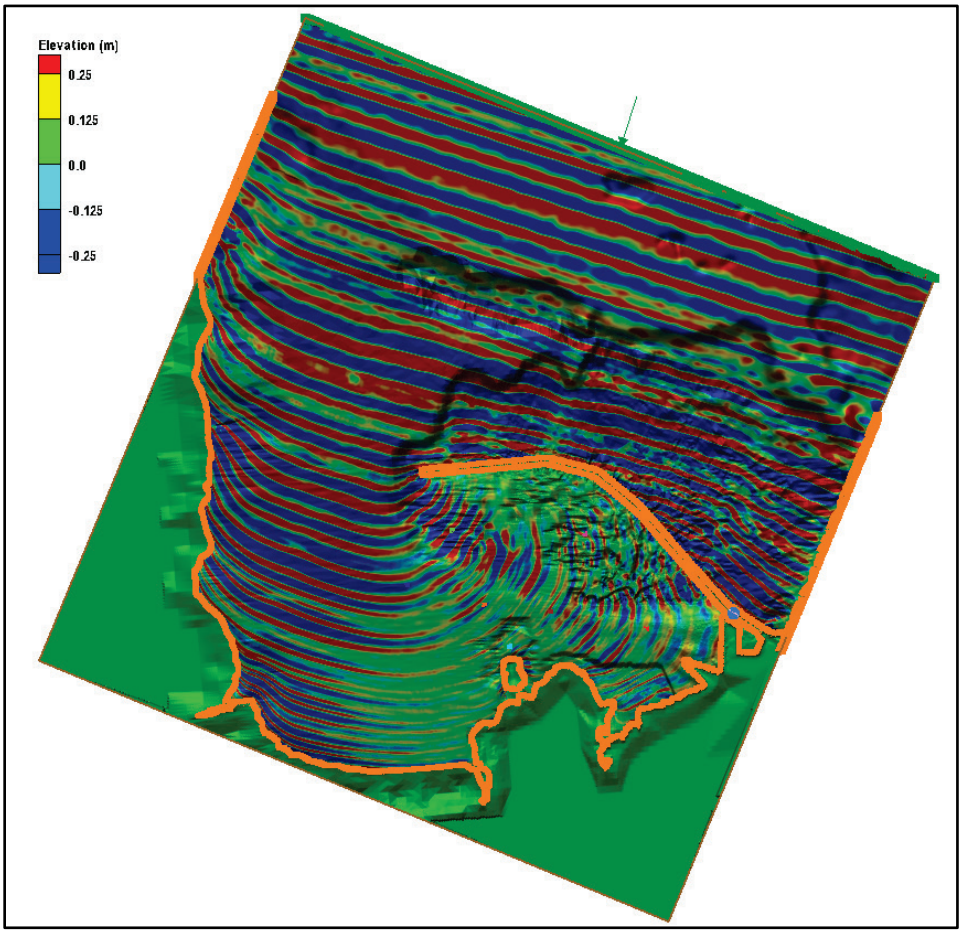

Figure 4-46. Spatial change of wave phase inside the harbor (north-northeast grid).

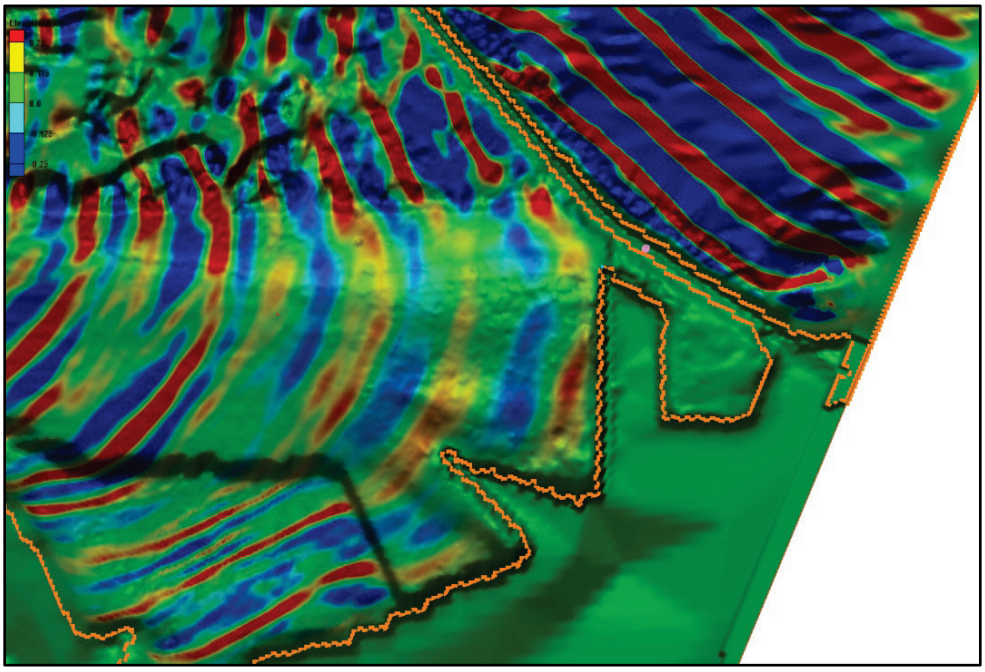

The waves generated by the trade winds blowing from the north-northeast to northeast directions affect the operations and usage of Hilo Harbor. Results for a northeast wave (H_s = 5.74 ft [1.75 m], T_p = 14.3 sec, and θ_p = 48^0) are shown in Figures 4-47 and 4-48. The east coast of the island is the west grid boundary included in the modeling domain and is extended southward to represent the southwest area of the harbor. Results indicate larger wave heights are calculated along these coastlines. The average wave height along the west grid boundary is 6.6 ft (2 m) to 8.2 ft (2.5 m) obtained in some localized areas. For this wave from the northeast direction, less wave energy gets into and penetrates into the harbor. Consequently, wave height at the turning basin and piers is reduced.

The average wave height in the entrance south of the breakwater tip is approximately 3.3 ft (1 m), and decreases in the navigation channel moving southeast. The average height in the turning basin and along the face of Pier 1 is 2.1 ft (0.65 m) and 0.6 ft (0.2 m), respectively. Spatial variation of the wave height field is depicted in Figure 4-48. The wave heights in the turning basin and Pier 1 range from 1.6 ft (0.5 m) to 2.6 ft (0.8 m) and from 0.3 ft (0.1 m) to 1.3 ft (0.4 m), respectively. These estimates changed slightly for different values of model parameters and type of damping applied. The maximum change in wave height at the southeast side of harbor was less than ±20%.

Figure 4-47. Wave height field over the entire domain for an oblique wave (northeast grid).

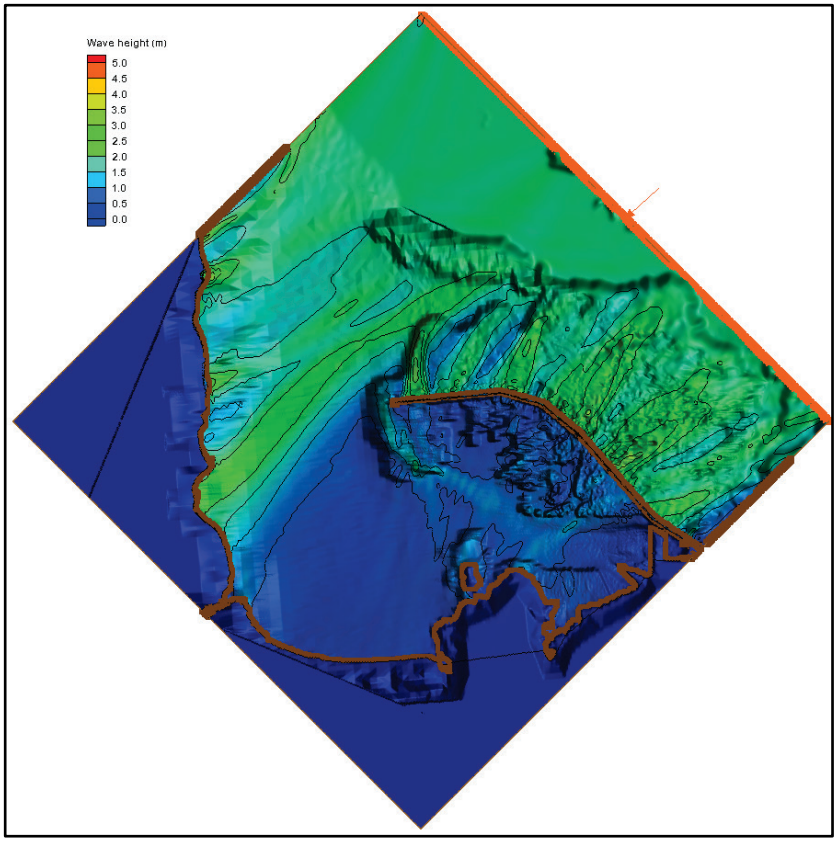

Figure 4-48. Wave height field inside the harbor for an oblique wave (northeast grid).

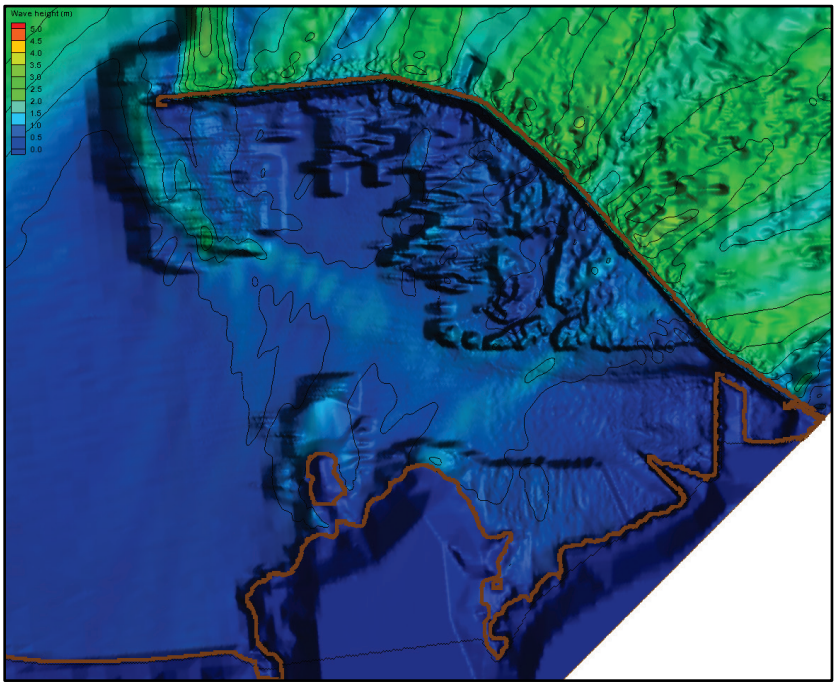

4.6.2 Results for Alternatives

One or more of the B2D results or other engineering parameters derived by post-processing model results can be used in the evaluation of structural modifications for improvement of harbor utilization and navigation safety. The model outputs include wave height, period, direction, wave-induced current, and time series data. The basic engineering parameters derived from model estimates can be checked against the functional requirements for navigation to determine pros/cons of any proposed Alternative. In harbor studies, the wave height is most often used as the primary parameter to evaluate the merits of Alternatives. In this study, wave energy reduction in the harbor is the ultimate goal for improving the conditions for the existing harbor, which is the baseline in evaluation of Alternatives investigated. B2D simulations were performed for four harbor configurations (i.e., existing harbor plus three Alternatives).

The results provided in the previous section indicated that the largest waves in the harbor were caused by waves incident from ±10° around true north (e.g., slightly oblique waves between north and north-northeast directions). For this reason, model simulations for evaluation of Alternatives considered a severe storm event from a nearly north direction. The waves parameters input to the wavemaker were H_s = 8.6 ft (2.63) m, T_p = 14.3 sec, and $\theta_p = 8^0$, and MSL = 0 m. In the discussion of results, first the 2D color contours of the wave height for each Alternative are provided in Figures 4-49 through 4-53. These images of the overall wave fields depict the spatial variation of waves over the entire modeling domain, showing some low and high wave energy areas outside and inside the harbor, navigation channel and adjacent areas, turning basin, and at the two piers. Estimates of the maximum, minimum, and average values of wave height for each Alternative in these two areas of interest are provided. For comparison of Alternatives, attention is on the innermost 0.5 miles (1 km) of navigation channel as it passes through the turning basin. Details of the calculated wave height variation along a transect passing through the turning basin are described later. Results for each Alternative in the navigation channel, turning basin, and two piers will be used in the evaluation of Alternatives. These best represent the impacts of proposed structural modifications on waves in these areas. Figure 4-49 shows wave height variation along the navigation channel, starting from north of the entrance to the west face of Pier 1. Maximum wave height along the channel centerline transect was 8.2 ft (2.5 m).

Figure 4-49. Wave height variation along navigation channel for Alt-0.

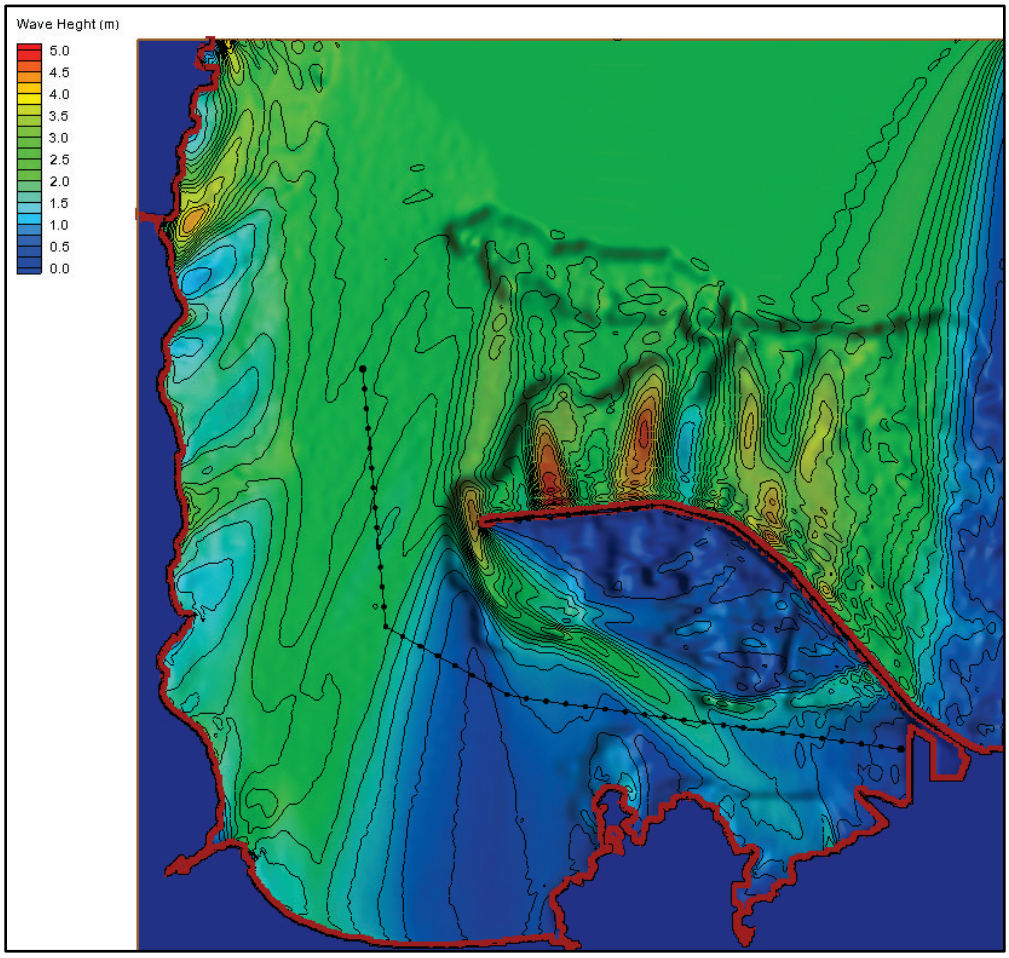

The short structure in Alt-1 was located west of the turning basin in an attempt to reduce waves affecting vessels maneuvering in the basin. Iterations on positioning of this 40 ft (12 m) wide and 820 ft (250 m) long structure indicated that the maximum reduction was obtained with part of the structure placed in the channel. Doing so would pose a risk to the ships using the channel and the turning basin and was not considered further. It was necessary to place the structure close to the edge of navigation channel at 37.7 ft (11.5 m) depth and at a relatively safe distance west of the turning basin. Figure 4-50 shows the wave field for Alt-1. The effect of structure on waves is localized to the vicinity of structure and appears to have diverted waves slightly toward the southeast direction. The comparison of Figures 4-49 and 4-50 shows an increase in wave height around Pier 2 and proposed Piers 3 and 4 and a wave height reduction in the turning basin and at Pier 1.

Figure 4-50. Wave height variation along navigation channel for Alt-1.

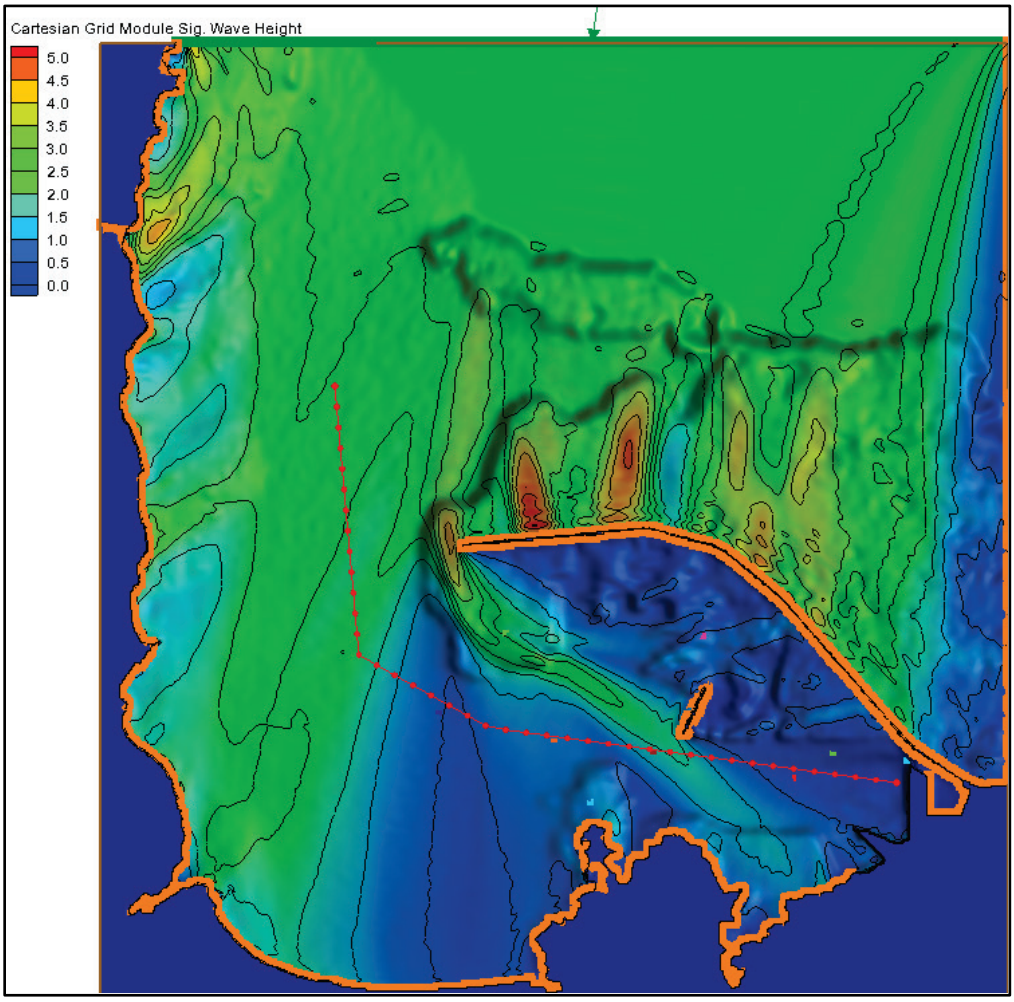

Figure 4-51 provides the results for Alt-2, where a twice-longer structure (1,575 ft [480 m) length, 40 ft [12 m] width) than the one in Alt-1 was used initially. The structure was placed west of the turning basin near the north edge of the channel at 31.1 ft (9.5 m) depth. Similar to the results for Alt-1, Figure 4-51 shows the structure is clearly redirecting waves to the southeast direction, which helps to reduce waves in the turning basin and at Pier 1. In Alt-2, a longer (2,300 ft [700 m] long) structure connecting to the breakwater was also tested. Overall, with the longer Alt-2 compared to the original Alt-2, similar results were obtained, and there was no significant change in waves in the turning basin and Pier 1 areas.

Figure 4-51. Wave height variation along the navigation channel for Alt-2.

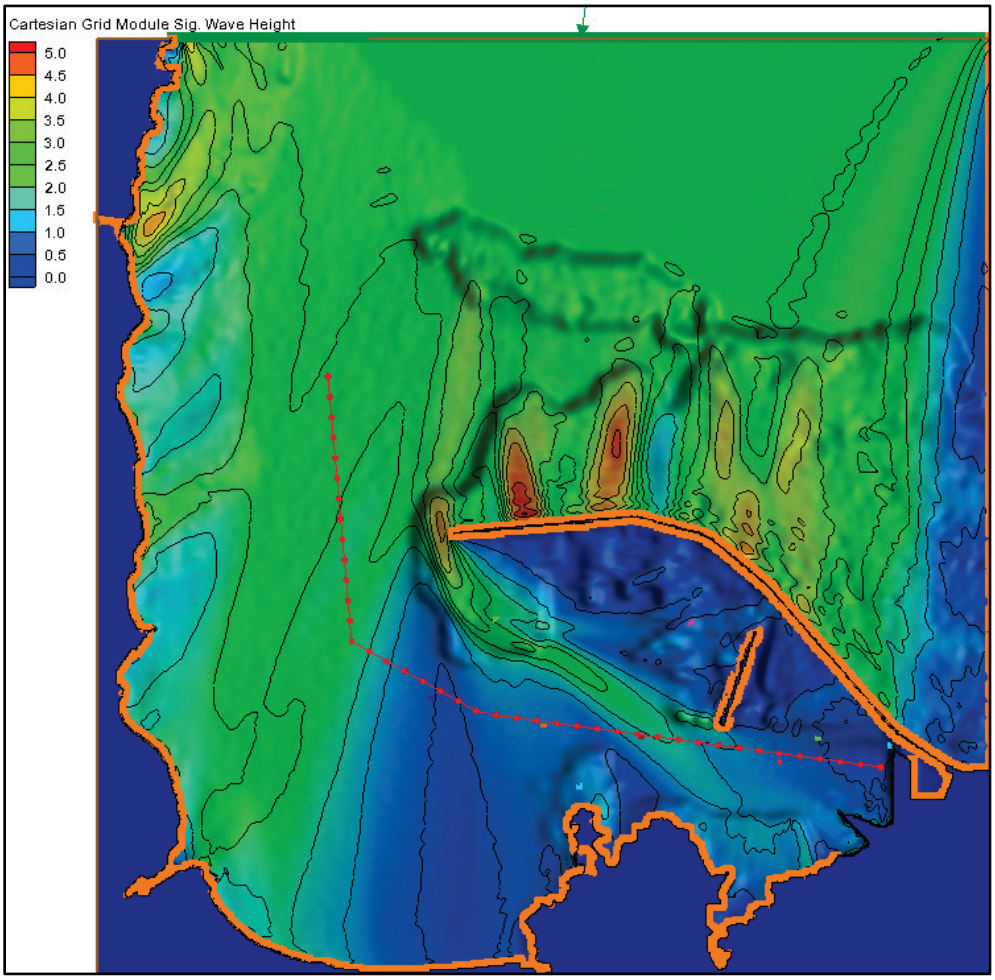

As shown in Figure 4-52, two structures were used in Alt-3 to better control waves in the southeast side of Hilo Harbor. The lengths of the north and south structures were 2,300 ft (700 m) and 410 ft (125 m), respectively. The tips of the north and south structures on the channel side were at 30 ft (9 m) and 33 ft (10 m) depth, respectively. Alt-3 results provided in Figure 4-52 were similar to the Alt-2 results in Figure 4-51. Because the addition of a short south structure increased waves in the turning basin and at Pier 1, this Alternative was not considered further.

Figure 4-52. Wave height variation along the navigation channel for Alt-3.

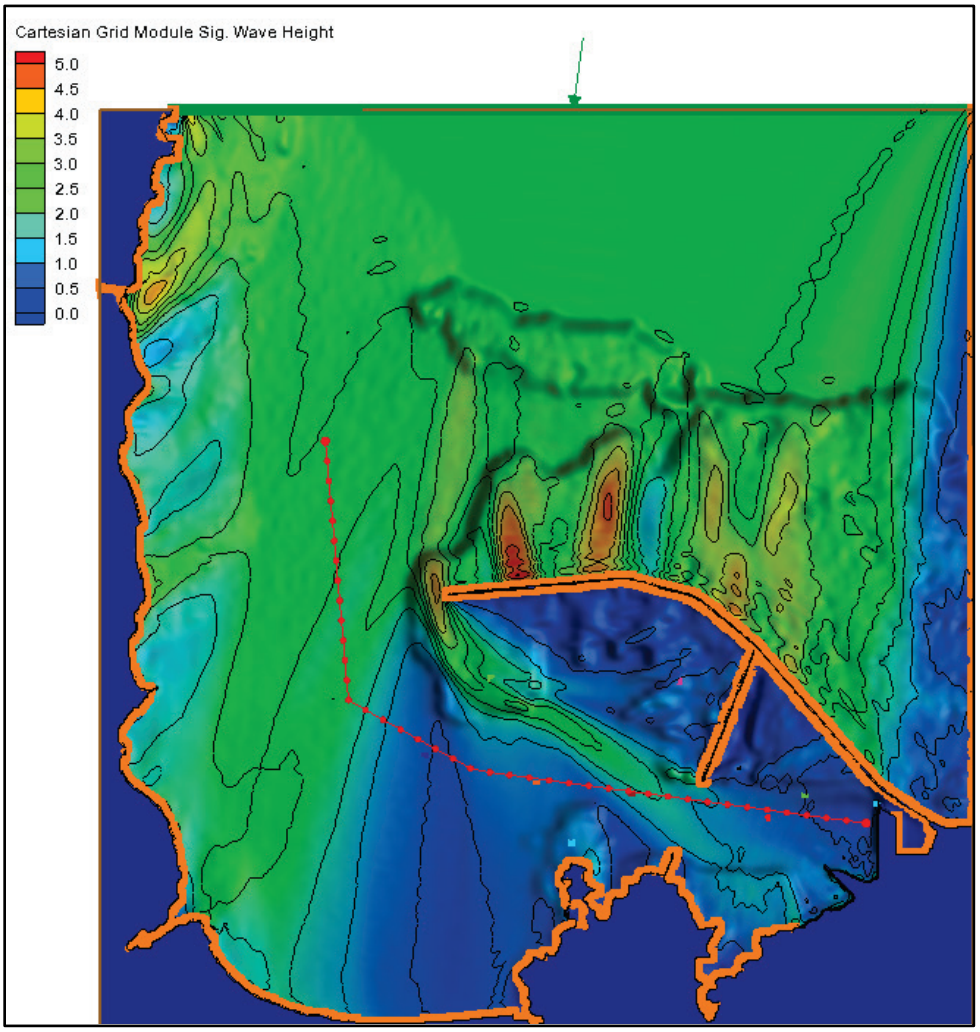

Alt-4 had a 2,300 ft (700 m) long spur attached to the west end of the Federal breakwater. It was oriented in the southwest direction and extended toward the navigation channel, ending at a 23 ft (7 m) depth. This structure posed no risk to ships in the channel amongst all structures considered because it was not close to the channel edge. Results in Figure 4-53 indicate Alt-4 was the most effective Alternative because it reduced waves almost everywhere in the harbor, including the turning basin and Piers 1 and 2 areas.

Figure 4-53. Wave height variation along the navigation channel for Alt-4.

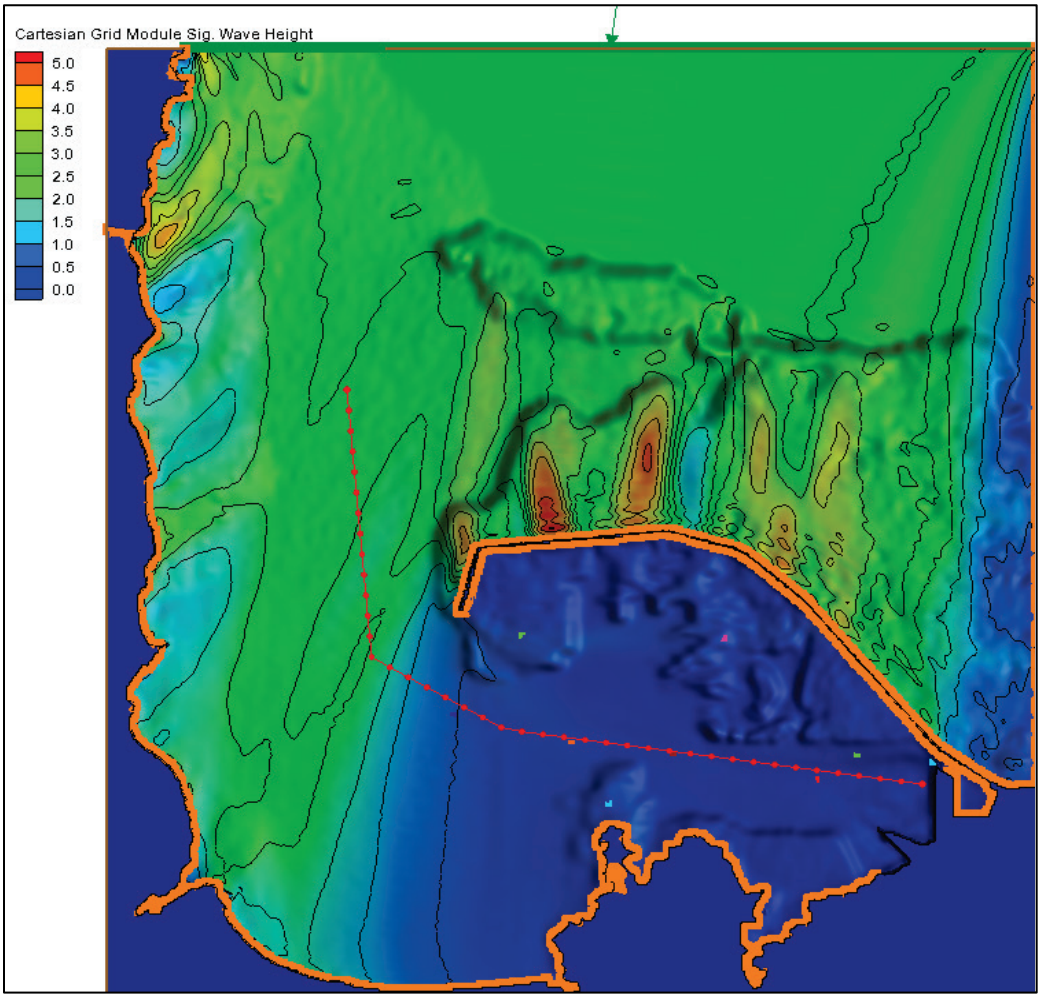

The wave heights for five Alternatives in Figures 4-49 through 4-53 show model results in the entire computational domain. The details of wave height change along the channel centerline were now used to evaluate the Alternatives. Since the channel centerline passed through the turning basin and ended at the Pier 1, this information was used for a selected segment of the channel and areas around it to assess the consequences of each Alternative. The statistics of waves over the entire 2.2-miles (4 km)-long channel transect are first described in Figures 4-54 to 4-56.

Figure 4-54 provides a direct comparison of wave heights for each Alternative and results of Alt-0 (i.e., existing harbor or no project). Figure 4-55 shows the percent change in wave height relative Alt-0. Figure 4-56 shows the wave height difference (bias) between Alternatives and Alt-0. The relative percent wave height change is defined as % Change = ([Alternative – Existing)/Existing] × 100), which varies between -100 and

+100 depending on the relative values of wave heights for an Alternative and Existing (Alt-0). The wave height difference (bias) is defined as Difference = (Alternative – Existing). The wave height statistics for the entire channel transect are summarized in Table 4-6.

Table 4-6. Statistics of wave height in navigation channel for comparison of Alternatives.

Wave Height Statistics	Alt-0	Alt-1	Alt-2	Alt-3	Alt-4
Average (m)	1.25	1.21	1.28	1.22	0.90
Maximum (m)	2.42	2.44	2.43	2.42	2.44
Minimum (m)	0.34	0.25	0.37	0.32	0.07
Ave diff (m)		-0.04	0.04	-0.03	-0.35
Max diff (m)		0.02	0.02	0.0	0.02
Min diff (m)		-0.09	0.04	-0.02	-80.42

Figure 4-54. Comparison of wave height variation by Alternatives in the navigation channel.

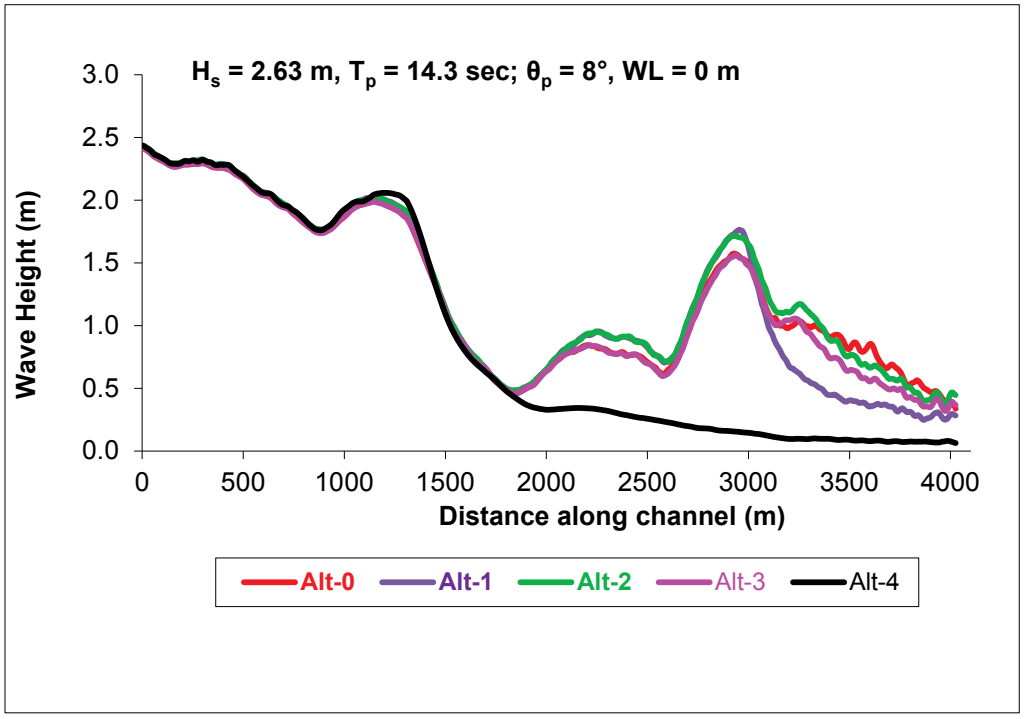

Figure 4-55. Percent change in wave height along channel centerline.

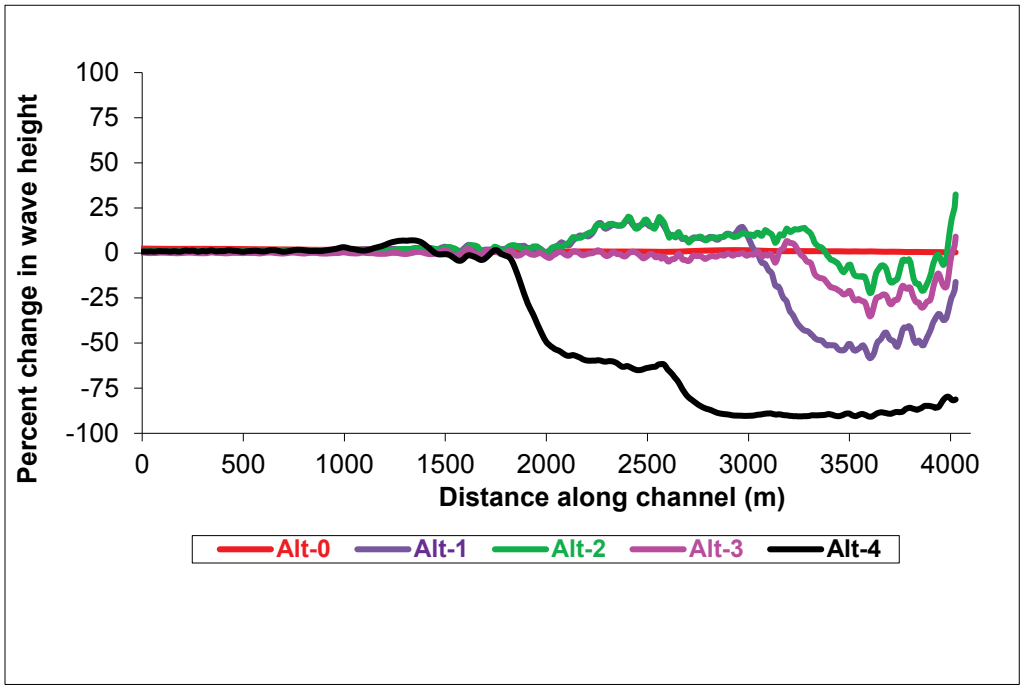

Figure 4-56. Wave height difference along channel centerline by Alternatives.

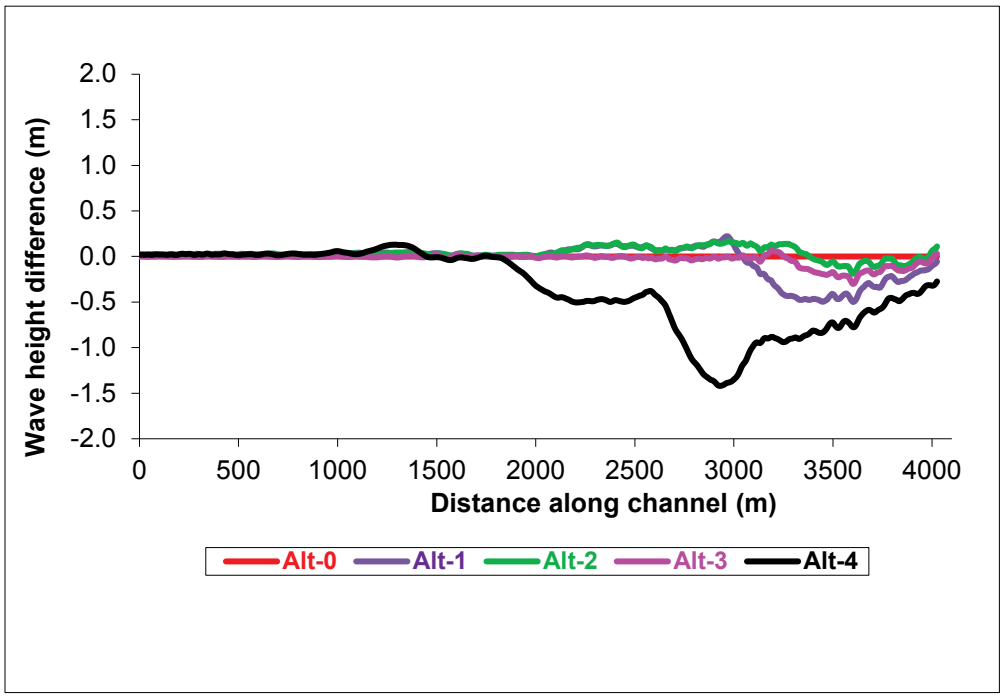

The last 0.5 mile (1 km) of channel transect passes through the turning basin, and the last three end points are situated near the face of Pier 1. Figure 4-57 shows the variation of calculated wave heights for each

Alternative in turning basin and Pier 1 areas. The summary of results for Alternatives is provided in Table 4-7.

Figure 4-57. Comparison of Alternatives based on calculated wave height in turning basin.

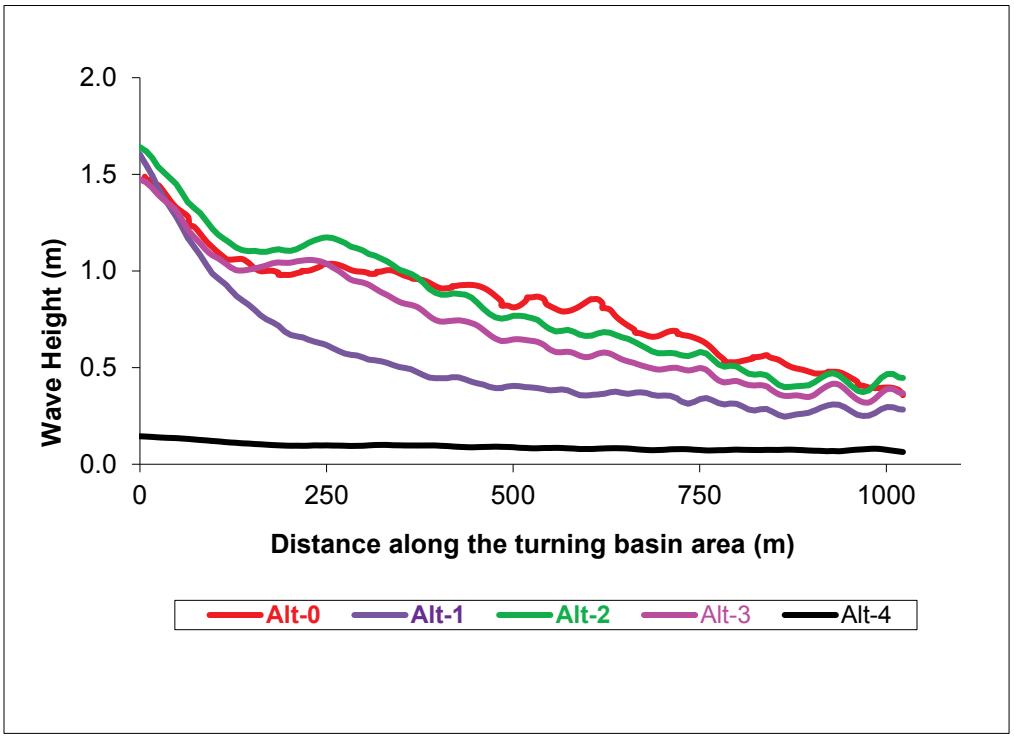

Table 4-7. Comparison of Alternatives based on wave height statistics in turning basin and Pier 1 area.

Wave Height Statistics	Alt-0	Alt-1	Alt-2	Alt-3	Alt-4
Average (m)	0.83	0.53	0.83	0.73	0.90
Maximum (m)	1.49	1.60	1.64	1.47	0.15
Minimum (m)	0.34	0.25	0.37	0.32	0.06
Ave diff (m)	0	-0.30	0.0	-0.11	-0.74
Max diff (m)	0	0.11	0.15	-0.02	-1.34
Min diff (m)	0	-0.09	0.04	-0.02	-0.27

In summary, the analysis of results provided in Figures 4-54 through 4-57 indicates Alt-4 is the best Alternative for providing the most wave energy reduction in the entire navigation channel and at the turning basin and Pier 1. Alt-4 outperformed other Alternatives with an average wave height reduction of 28% and 89%, respectively, in the channel and turning basin. Alt-1, Alt-3, and Alt-2 follow Alt-4 in the ranking of Alternatives. Note that the second-ranked Alt-1 achieves only 3% and 36% reduction in the entire navigation channel and turning basin, respectively. Alt-2 with a longer interior north structure and a shorter structure south of channel performed poorly. An earlier version of Alt-2 with only the structure on the north of channel had a similar performance. This was due to increased wave diffraction and reflection caused by longer structures that caused a significant increase in wave height near the structure. The reason Alt-4 achieved such a dramatic reduction in waves was its ability to control waves coming through the entrance. Alt-4 with the spur at the tip of the Federal breakwater is able to intercept and redirect waves toward the southwest side of harbor. The east and southeast sides of interior harbor (e.g., turning basin and Piers 1 and 2) benefited greatly from this diversion of waves, resulting in greater than 80% wave reduction at two piers and turning basin areas.

4.6.3 Permeability of breakwater

The modeling for investigation of the Federal breakwater permeability is discussed in this section. No field measurements of water levels, waves, and currents were available to assess the potential transmission of waves, currents, and sediments passing through the core of breakwater structure. Consequently, simulations were performed with conditions selected from Tables 4-2 and 4-3. The calculated wave estimates on the seaward side of the structure were compared to those in the lee (harbor side) of the structure. Figure 4-58 shows the section of breakwater selected for investigation. Model results were saved along two transects, each approximately 2,000 ft (600 m) long. The outside transect (T1) and inside transect (T2) were positioned slightly beyond the toe of structure.

Three storms were simulated to examine structure permeability. Results for the storm on 18 March 2014 at 1600 UTC are described first. The parameters for this storm were H_s = 10.8 ft (3.3 m), T_p = 13.3 sec, and θ_p = 25°. Figure 4-59 shows wave height estimates along the two transects, starting from the west tip (0 ft [0 m]) to the east end (2,000 ft [600 m]) of these transects. Along the outside transect, the larger wave heights

gradually decrease from west to east along T1. The wave heights along T2 in the lee of the structure remain essentially constant for the three levels of breakwater permeability investigated. The permeability of the breakwater assumed wave transmission occurred through a porous layer of structure below MSL (e.g., submerged height of structure). In addition, wave transmission would also occur over the exposed part of structure. Additional transmission would occur due to wave runup/ overtopping over the low crest elevation of the structure above MSL. Results for three porous layers (3.3 ft [1 m], 6.6 ft [2 m], and 9.8 ft [3 m]) indicate the transmitted wave height varies between 0.7 ft (0.2 m) to 1.3 ft (0.4 m), so it is approximately 10% of the wave height outside the breakwater. The high crest elevation of the structure (~11.5 ft [3.5 m]) above MSL prevented wave runup/overtopping of the breakwater section investigated. This is the main reason for the low transmitted wave heights calculated along T2.

Figure 4-58. Outer and inner transects for breakwater permeability testing.

Figure 4-59. Estimates of wave height for assumed permeability of the breakwater.

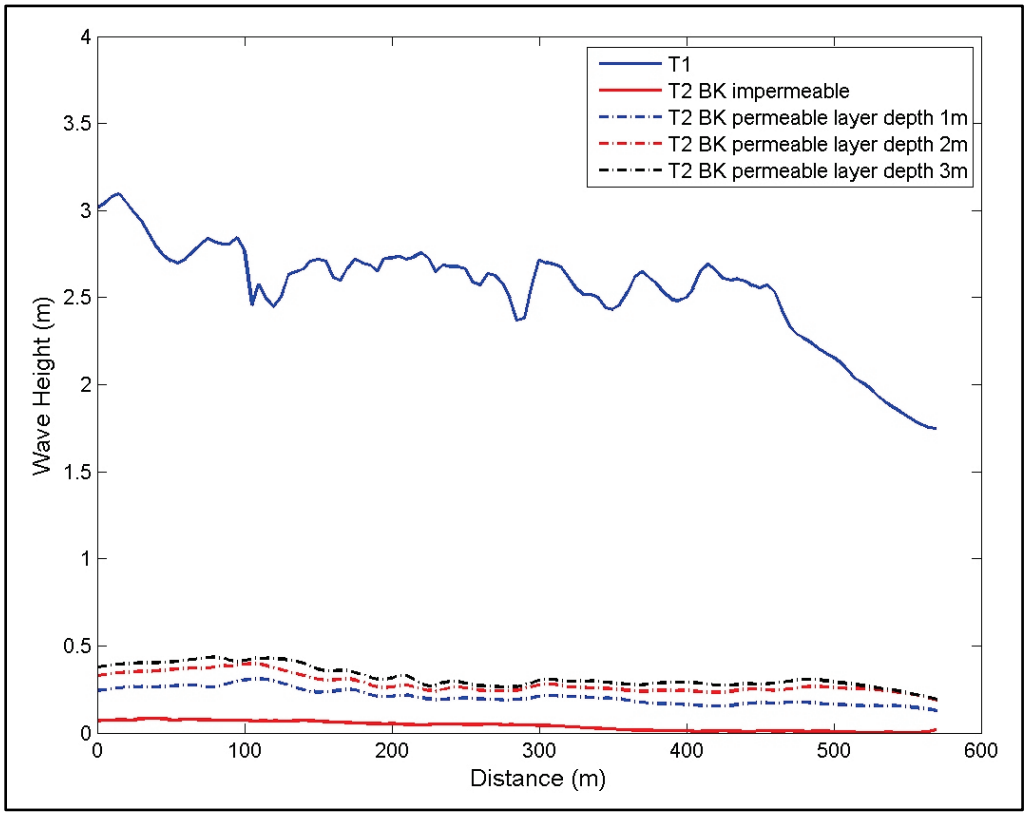

Wave runup/overtopping of the breakwater were investigated using one-dimensional (1D) and 2D modeling approaches. These two approaches were used to determine sensitivity of estimates to asses impacts of reducing computational domain size and run time. A finer grid resolution was used to better describe the physical attributes of breakwater. The 1D modeling with a very fine grid resolution cell size (as small as 1.6 ft [0.5 m]) allowed for representation of structure side slopes including the toe to crest and top width of the structure. Narrow 1D and 2D strips used much smaller cell sizes, with 1.6 ft (0.5 m) for 1D strips and 6.6 ft (2 m) for 2D strips, as compared to a 26.2 ft (8 m) cell size used in regular larger domain grids. These refinements not only greatly improved the representation of the structure but also helped to reduce the computational time of simulations.

Figure 4-60 shows the 1D grid domain. Figure 4-61 is a zoomed image depicting details of the structure. Figure 4-62 shows wave height variation through the center of the 1D strip. Figure 4-63 depicts the model domain for a 2D strip. In Figure 4-63, bathymetry changes along the 1D strip (x-direction) from the ocean side (blue) to the end of the strip inside the

harbor (red). The structure is shown in brown. The bathymetry is constant along the width of strip. Wave shoaling over the center of the strip is apparent from calculated wave heights in Figure 4-62. The 8.2 ft (2.5 m) wave height at the wavemaker boundary increases, reaching 9.8 ft (3 m) prior to waves reflecting from the structure. Due to scattered waves (backward reflected waves) from the structure, wave height increases to approximately 10.8 ft (3.3 m). There is a rapid decrease in wave height when wave becomes unstable and breaks, resulting in a sharp drop in wave height. The wave height reduces to 1.6 ft (0.5 m) but increases to 2.5 ft (0.75 m) with wave runup over the seaward face of structure. Because of high crest elevation of the structure (~11.5 ft [3.5 m]), wave runup reaches its maximum elevation along the side slope, and water recedes subsequently, and wave height reduces to zero. No overtopping occurred for the storm of 18 March 2014 at 1600 UTC (H_s = 10.8 ft [3.3 m], T_p = 13.3 sec, θ_p = 25°).

Figure 4-60. Calculated wave runup/overtopping for a 1D strip.

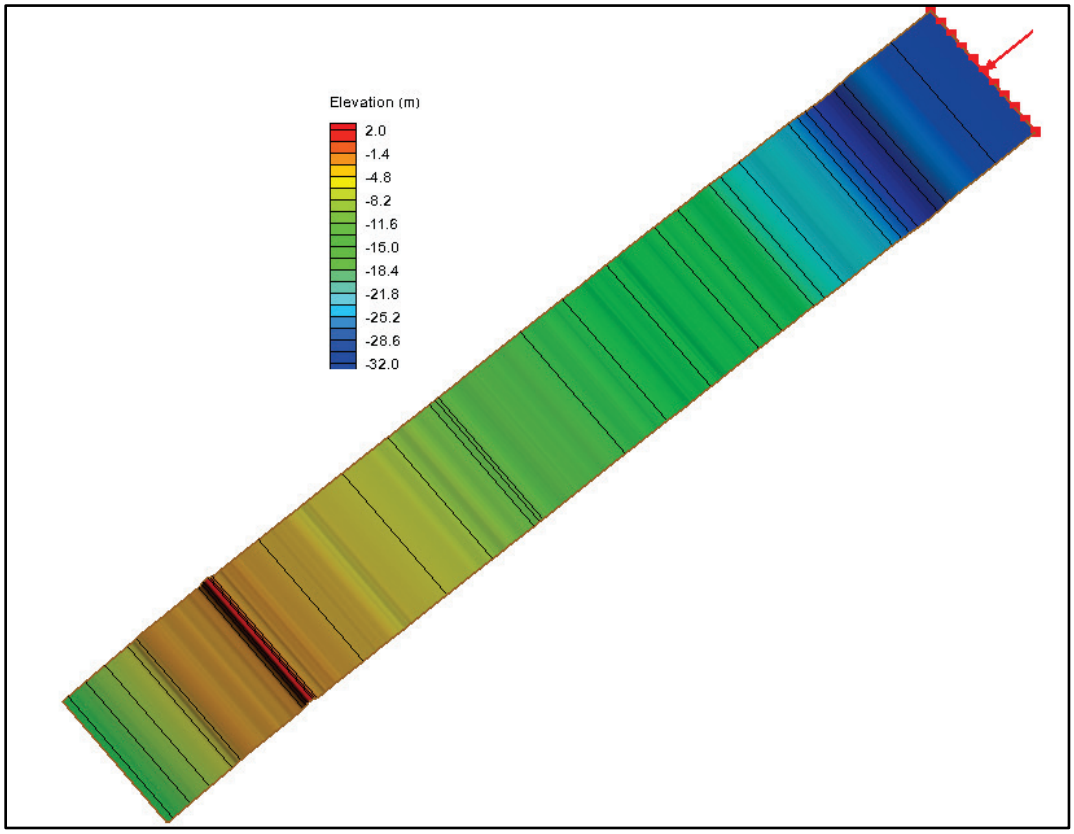

Figure 4-61. Zoomed image depicting details of the structure for 1D strip.

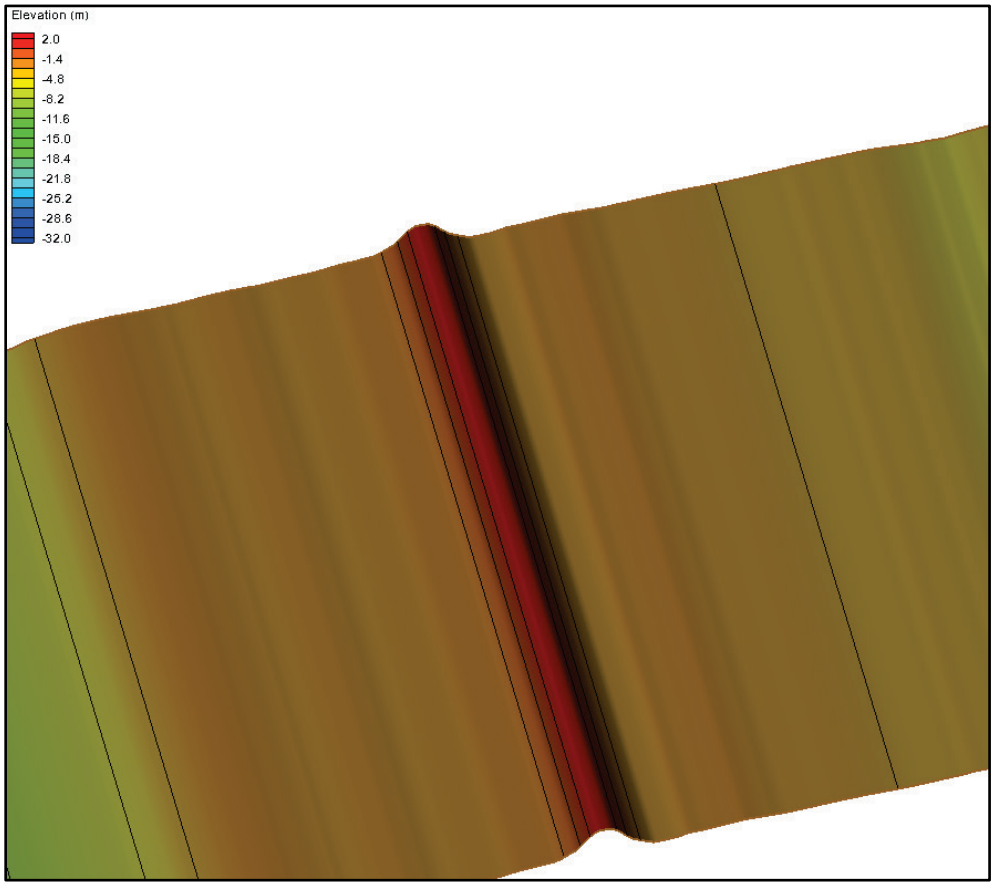

Figure 4-62. Wave height variation through center of 1D strip.

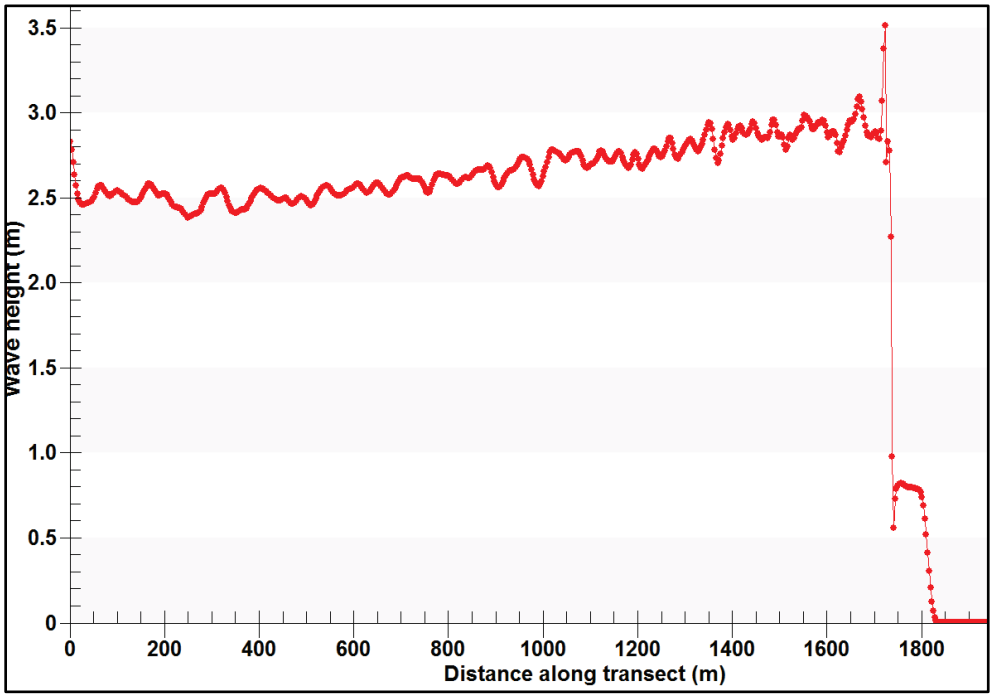

The storm of 18 March 2014 at 1600 UTC with parameters H_s = 10.8 ft (3.3 m), T_p = 13.3 sec, and θ_p = 25° was also simulated using a 2D grid of the finite strip shown in Figure 4-63. The bathymetry of this 2D grid for narrow strip changes both in the *x*- and *y*-directions. Model results were examined along five transects depicted in Figure 4-63. Wave heights along these transects were similar, with a maximum difference of approximately 10%. Wave height estimates along the center transect were quite similar to 1D model results (Figure 4-62). Therefore, computationally resource-demanding 2D modeling with numerically challenging runup/overtopping was not pursued for two additional storms described later in this section. The 1D simulations were sufficient for the analysis.

Figure 4-63. Model domain for a 2D strip.

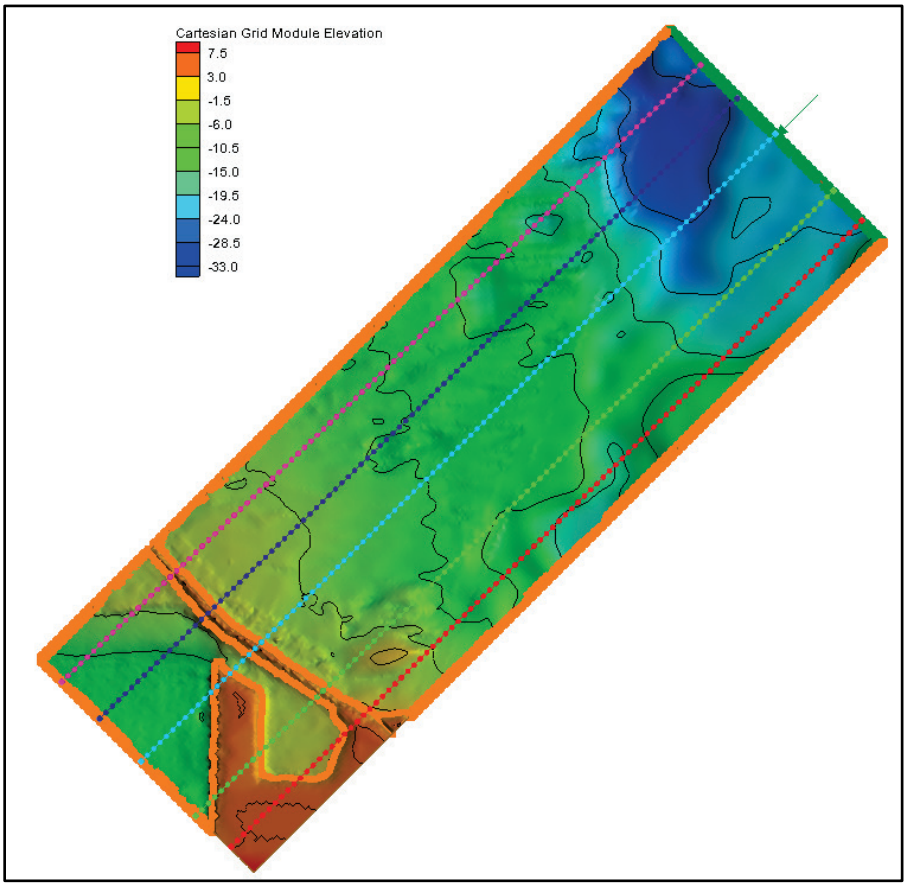

The second storm simulated was the 5 January 2014 at 1600 UTC event, and had deep-water wave parameters of H_s = 10.8 ft (3.3 m), T_p = 14.3 sec, and θ_p = 0°. This is a wave from true north having similar parameters as the first storm which was 25° oblique from the northeast. Results for this storm are presented in Figure 4-64, showing wave height trends along transects T1 and T2. The variation of wave height outside the breakwater

(T1) and inside the harbor (T2) for this storm was similar to the trend for the first storm in Figure 4-59. Larger wave heights outside were obtained on the west side of T1, and heights decrease toward the east part of transect. A negligible variation in wave height was obtained along T2 inside the harbor for the three values of breakwater permeability investigated.

Figure 4-64. Estimates of wave height for assumed permeability of the breakwater (H_s = 10.8 ft [3.3 m], T_p = 14.3 sec, θ_p = 0°).

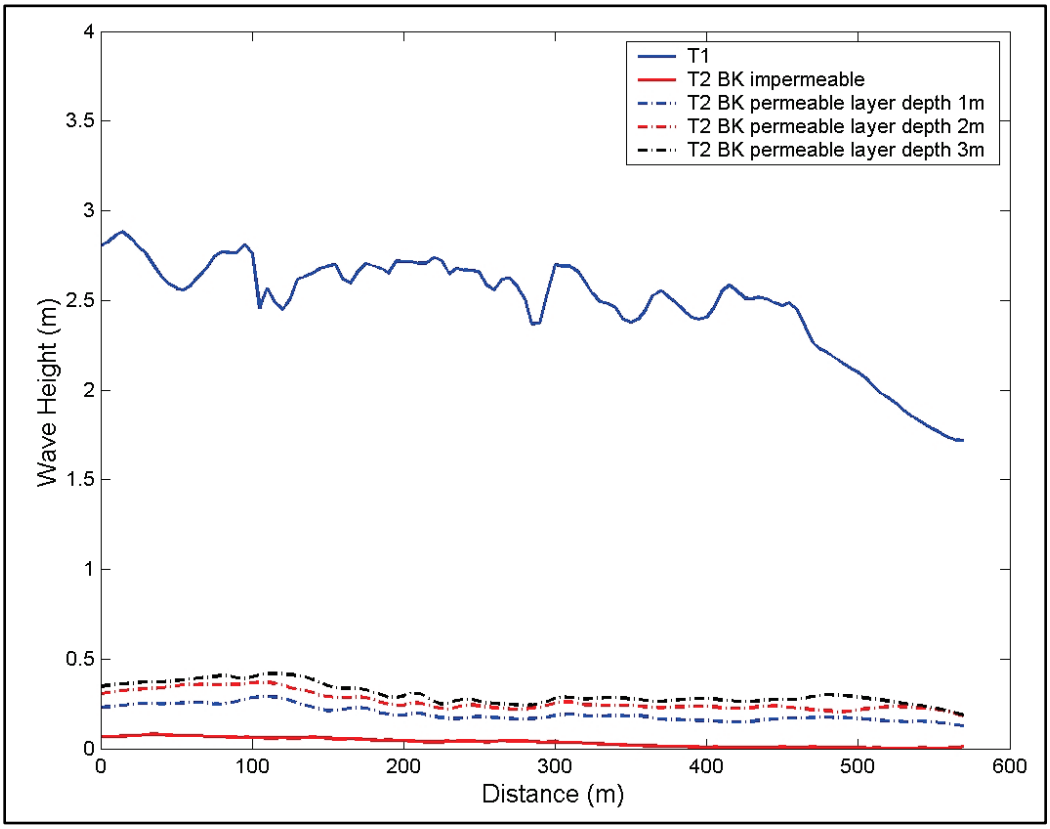

The third storm simulated occurred on 23 January 2014 at 0700 UTC and had the largest deep-water wave height (H_s = 16.4 ft [5 m], T_p = 14.3 sec, θ_p = 345°) among the three simulated storms. Furthermore, this storm from the northwest represents swells coming from Japan that affect the Hawaiian Islands. The estimate of wave height along transects T1 and T2 for this storm are presented in Figure 4-65. The trends in wave height change outside the breakwater (T1) and inside the harbor (T2) are similar to the trends for the other two storms. Although larger waves are calculated seaward of the breakwater along T1, wave heights along T2

Figure 4-65. Wave height estimates for assumed permeability of breakwater (H_s = 16.4 [5 m], T_p = 14.3 sec, θ_p = 345°).

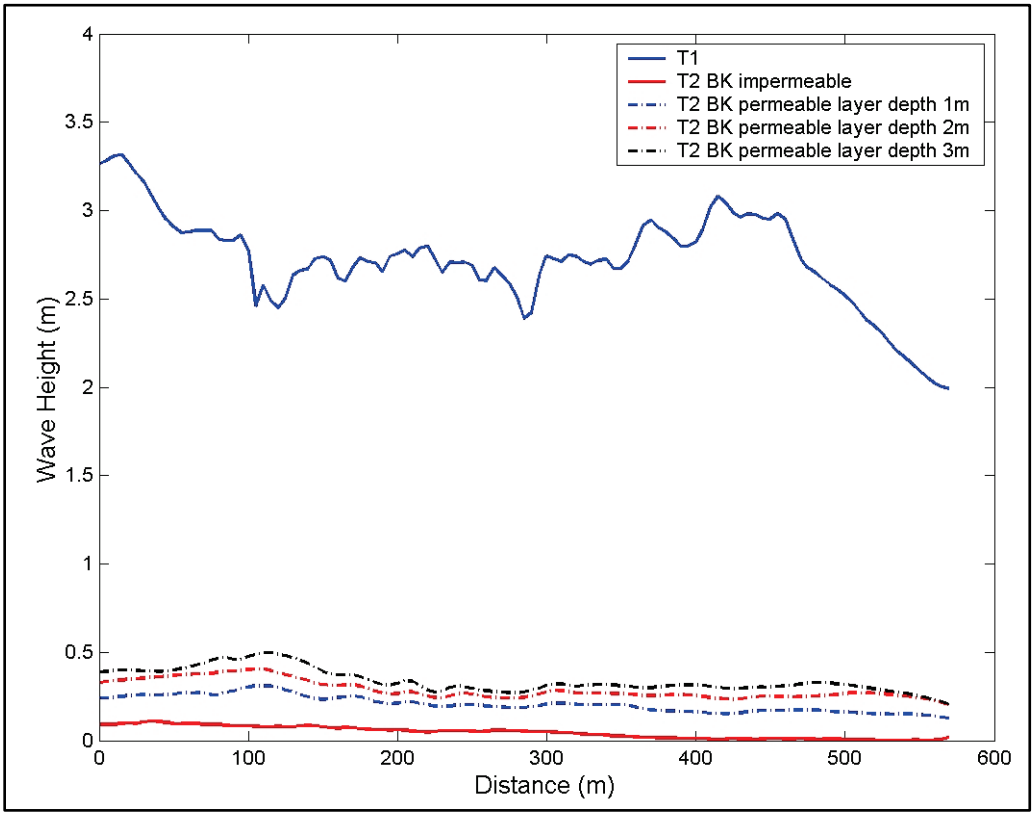

inside the harbor are less than 1.6 ft (0.5 m). The breakwater permeability has a weak effect on waves calculated inside the harbor.

A percent reduction in mean wave height inside the harbor at transect T2 can be defined as (T2-T1)/T1 × 100, using the mean wave heights (m) along T1 and T2. The mean wave heights at T1 and T2 and calculated percent reductions for three incident wave conditions are provided in Table 4-8. The percent reductions are provided in parentheses. These calculations are provided for impermeable and permeable breakwaters for three porous layer thicknesses. Included are the estimates for a breakwater with wave runup/overtopping.

The calculations are performed for three deep water waves incidents from 0°, 25°, and 345°. The nonzero wave heights for an impermeable breakwater include waves coming in through the harbor entrance plus waves that wrap around the tip of breakwater that reach transect T2 in the southeast corner of the harbor. The mean wave height reduction ranges

from 0.13 ft (0.04) m to 1.05 ft (0.32 m), and the percent reduction of mean wave height ranges from 87% to 99%.

Table 4-8. Estimates of mean and percent wave reduction in harbor.

Transect	Characteristic of Breakwater	Offshore Incident Waves			Mean
		Dir = 0° Hs = 3.4 m Tp = 14.3 sec	Dir = 25° Hs = 3.3 m Tp = 13.3 sec	Dir = 345° Hs = 5.0 m Tp = 14.3 sec	
T1		2.49	2.54	2.72	2.58
T2	Impermeable	0.04 (99%)*	0.04 (99%)	0.04 (98%)	0.04 (99%)
	Permeable layer (1 m)	0.19 (92%)	0.21 (92%)	0.21 (92%)	0.20 (92%)
	Permeable layer (2 m)	0.26 (89%)	0.28 (89%)	0.29 (89%)	0.28 (89%)
	Permeable layer (3 m)	0.30 (88%)	0.32 (87%)	0.34 (88%)	0.32 (88%)
	Wave runup	0.19 (93%)	0.20 (92%)	0.21 (92%)	0.20 (92%)

* Percent reduction of mean wave height on T2 in parentheses.
Wave height estimates on T1 and T2 are in meters.

5 Summary and Conclusions

Concerns about the so-called *surge* problem at Piers 1 and 2 and at the mooring/turning basin in Hilo Harbor, and potential wave transmission through the Federal breakwater, were investigated in this numerical modeling study. This study also provided wind, wave, and hydrodynamic forcings for a ship simulator training study conducted in December 2014 at CHL for two teams consisting of ship captains, pilots, harbor master, State of Hawaii DOT personnel, and U.S. Army Engineer District, Honolulu, engineers. Several infrastructure modifications were investigated to improve the overall usage of the harbor. The focus of this study was on improvement of wave conditions at the mooring/turning basin and Piers 1 and 2. Wave estimates at these areas and other parts of the interior harbor were developed using the latest available bathymetric surveys and field-monitoring data. The effects of proposed structural modifications on waves in the navigation channel and two areas of interest were evaluated and quantified. Wave estimates are provided at the harbor entrance, along the navigation channel, and at the two areas of primary concern.

Two wave models, CMS-Wave and B2D, were used to develop wave estimates inside Hilo Harbor. CMS-Wave, a large-domain spectral wave model, provided incident-wave input conditions for the ship simulator study and for detailed B2D wave modeling outside and inside the harbor. B2D is a time-domain, nonlinear wave model designed specifically for ports and harbor applications. This small-domain nearshore wave model was used to develop wave estimates inside the harbor and evaluate the proposed structural modifications.

Project-specific improvements to CMS-Wave were made to develop necessary inputs for B2D and the ship simulator training study. A number of R&D developments were necessary to enhance predictive capabilities of CMS-Wave, which were funded by the CIRP. These included (a) simulations in a full-plane mode with a combination of strong trade winds, storms, and nonstorm wave conditions offshore for both parent-child grid capability of CMS-Wave, (b) modeling of combined seas and swells from different directions, (c) development of incident wave parameters (height, period, direction) and wave spectra (2D) at the offshore boundary of B2D model, (d) validation of the model with the NOAA buoys and CDIP gauges

near the project site for improving the deepwater wave generation/growth capability of CMS-Wave, (e) development of custom pre- and post-processing analysis codes for preparing inputs for B2D setup, (f) development of Fortran and Matlab utilities to facilitate analysis of field data and the coupling of two wave models, and (g) development of utilities to process CMS-Wave and CMS-Flow results for input to the ship simulators.

A 2-week training study was conducted in two CHL ship simulators during the first 2 weeks of December 2014. Two separate groups attended these trainings, each for 1 week. A set of training conditions was identified for ship simulation training in close coordination with U.S. Army Engineer District, Honolulu, including duration of simulations, water levels, wind forcing, deep water incident wave parameters, design ships, and vessel tracks. Each selected condition was simulated for two harbor configurations: (a) existing harbor (without mooring/turning basin dredged) and (b) with the dredged mooring area. Two river discharges were included in test runs to assess the effect of river flows on waves and currents inside the interior harbor. Modeling results at the time of peak flood/ebb current with corresponding winds were extracted from the CMS solution files. Spatially varying winds, wave parameters, water levels, and current components were provided to the ship simulator. Estimates of maximum current fields, winds, and wave heights were developed for the existing bay configuration and proposed dredge area to expand and deepen the turning basin. Calculated maximum current magnitude in Hilo Bay along the navigation channel was less than 0.66 ft/sec (20 cm/sec), and maximum wave height was 6.6 ft (2 m). In the turning basin and at Piers 1 and 2, the maximum current was less than 0.33 ft/sec (10 cm/sec), and maximum wave height was less than 1.6 ft (0.5 m). The effect of wind on navigation in the interior harbor was very important for ships maneuvering and moorings at the Piers 1 and 2 and turning basin.

Wind and water-level effects were included in the transformation of deep-water storm and nonstorm conditions using CMS-Wave. Model results saved along the offshore boundaries of three B2D grids (north, north-northeast, northeast grids) were used to model nearshore waves over reefs outside the breakwater, in the harbor entrance and navigation channel, and throughout the inner harbor. Data from two field studies obtained in 2007 and 2013–14 were used to calibrate and validate numerical models. In these model tests, the largest waves in the harbor were obtained for

waves incident from north and ±10° around true north. These wave directions were used in the evaluation of Alternatives.

One severe storm event (H_s = 8.6 ft [2.63 m], T_p = 14.3 sec) from three directions ($\theta_p = 0^0, \pm 8^0$) was selected for investigation of harbor surging. 2D color contour plots of wave height were generated for each Alternative to determine (a) spatial variation of waves over the full modeling domain, (b) low and high wave energy areas outside and inside the harbor, and (c) changes in waves through the navigation channel and adjacent areas, and at the turning basin and two piers.

In comparing the Alternatives, special attention was paid to the last 0.62 n.m. (1 km) of navigation channel that passes through the turning basin. The calculated wave height variation along a transect through the turning basin was used to assess impacts of proposed structural modifications on waves at the turning basin and piers. The benefits (usefulness) of an Alternative is based on reduction of wave energy achieved in the turning basin and Piers 1 and 2. The wave height difference and percent wave height change relative to Alt-0 (i.e., existing harbor or no project) are used in the ranking of Alternatives. Alt-4, with a spur attached to the west tip of Federal breakwater, greatly outperformed other Alternatives. Alt-4 provided an average wave height reduction of 28% and 89%, respectively, at the turning basin and Pier 1, the two areas of interest. None of the Alternatives with structural modifications positioned inside the harbor close to the turning basin could outperform Alt-4. A significant increase in local wave height near these structures was due to diffraction and reflection effects from the added structures. For Alt-4, a dramatic reduction in the wave energy was achieved by the added spur that successfully intercepted and redirected waves toward the southwest side of harbor. The spur greatly reduced waves that otherwise would be heading to the interior harbor, moving through the channel to arrive at the turning basin and Pier 1. This diversion of waves with Alt-4 greatly benefited the east and southeast sides of the interior harbor, resulting in more than an 80% reduction of wave energy at the two piers and turning basin areas.

For assessment of the surge problem, model results at the UH gauge location north of the Pier 1 were analyzed to check for the presence of IG waves. These long-period waves are often the primary cause of harbor surging phenomenon, ship moorings, and onloading/offloading problems in harbors. For incident waves from ±10° of true north, model results

showed some wave energy in the low-frequency tail of wave spectra. Energy in the IG frequency band was negligible for highly oblique waves from the northeast and northwest directions. Evidence of ship accidents and data on ship maneuvering, responses, and moorings is required to correlate IG waves to one or more of these navigation problems. However, the existence of IG waves with periods close to natural periods of the harbor in the southeast corner of the harbor is a strong indication and cause of concern for the occurrence of harbor oscillations (surging).

For assessment of breakwater permeability, wave heights along a transect in the lee of structure were compared to the wave heights on a transect on the ocean side of breakwater segment east end in the Puhi Bay. Model results showed waves in the lee of the breakwater remaining essentially constant for three levels of breakwater permeability investigated. Calculations for permeability of the breakwater assumed that wave transmission occurs through a porous layer of structure below MSL as well as over the exposed part of structure. Wave runup and overtopping over the low crest elevation of the structure above MSL were considered in these simulations. Results for three porous layers (3.3 ft [1 m], 6.6 ft [2 m], and 9.8 ft [3 m]) indicated that the transmitted wave height was less than 1.3 ft (0.4 m), or approximately 10% of the wave height outside the breakwater. The high crest elevation of the structural segment investigated (~11.5 ft [3.5 m] above MSL) did not permit wave runup/overtopping, ensuring low transmitted wave heights in the lee of the breakwater. Model results suggested that wave transmission through the structure was negligible and that wave runup/overtopping could happen under certain severe storm conditions s (e.g., excessive water piling up in the Puhi Bay that can lead to runup/overtopping of parts of the east side of the breakwater).

In summary, the proposed modifications (Alternatives) have been ranked based on calculated average wave-height statistics along the navigation channel, with special emphasis on wave reduction offered by each Alternative at the turning basin and Pier 1. Generally, incident waves coming from north and northwest penetrated most into the interior of the harbor, affecting the east side of the inner harbor. The top-ranked Alt-4 offered the highest reduction of wave energy in the channel, at the turning basin, and at Piers 1 and 2. It is not only the efficiency of Alt-4 that makes it an excellent potential long-term solution to improving the conditions inside the existing harbor, but also Alt-4 achieves this objective by not

increasing the risk to navigation. In contrast, all other Alternatives involved placing certain structural modifications on either side of the navigation channel in an attempt to improve conditions at the turning basin and Piers 1 and 2. However, for these modifications to be effective, structures had to be placed as close to the navigation channel as possible. Doing so would increase the risk to vessels transiting, moored, or maneuvering in the turning basin. Furthermore, potential adverse effects of interior structures on water quality, reefs, submerged aquatic vegetation, and food chain have to be addressed. None of these issues are of concern for Alt-4. In conclusion, each of the Alternatives that most efficiently can address the current problems will require further consideration to fully evaluate the trade-offs between the improvements and the implications that would result from their implementation.

References

B2D references

Demirbilek, Z., A. Zundel, and O. Nwogu. 2005a. *BOUSS-2D wave model in SMS: I. Graphical interface*. ERDC/CHL CHETN-I-69. Vicksburg, MS: U.S. Army Engineer Research and Development Center.

Demirbilek, Z., A. Zundel, and O. Nwogu. 2005b. *BOUSS-2D wave model in SMS: II. Tutorial with examples*. ERDC/CHL CHETN-I-70. Vicksburg, MS: U.S. Army Engineer Research and Development Center.

Demirbilek, Z., L. Lin, and A. Zundel. 2007. *WABED model in the SMS: Part 2. Graphical interface*. ERDC/CHL CHETN-I-74. Vicksburg, MS: U.S. Army Engineer Research and Development Center.

Demirbilek, Z., and O. G. Nwogu. 2007a. *Boussinesq modeling of wave propagation and runup over fringing coral reefs, model evaluation report*. ERDC/CHL TR-07-12. Vicksburg, MS: U.S. Army Engineer Research and Development Center.

Demirbilek, Z., O. G. Nwogu, and A. K. Zundel. 2007b. *Infra-gravity wave input toolbox (IGWT): User's guide*. ERDC/CHL CHETN-I-73. Vicksburg, MS: U.S. Army Engineer Research and Development Center.

Demirbilek, Z., O. G. Nwogu, D. L. Ward. 2007c. *Laboratory study of wind effect on runup over fringing reefs. Report 1: Data report*. ERDC/CHL TR 07-4. Vicksburg, MS: U.S. Army Engineer Research and Development Center.

Demirbilek, Z., L. Lin, and O. G. Nwogu. 2008. *Wave modeling for jetty rehabilitation at the mouth of the Columbia River, Washington/Oregon, USA*. ERDC/CHL TR-08-3. Vicksburg, MS: U.S. Army Engineer Research and Development Center.

Demirbilek, Z., O. G Nwogu, D. L. Ward, and A. Sanchez. 2009. *Wave transformation over reefs: Evaluation of one-dimensional numerical models*. ERDC/CHL TR-09-1. Vicksburg, MS: U.S. Army Engineer Research and Development Center.

Demirbilek, Z., L. Lin, O. G. Nwogu, W. C. Butler, K. K. Hathaway, and T. D. Smith. 2015a. *Kikiaola light draft harbor monitoring plan part 2: Numerical wave modeling for evaluation of structural alternatives*. ERDC/CHL TR-14-9. Vicksburg, MS: U.S. Army Engineer Research and Development Center.

Demirbilek, Z., L. Lin, O. G. Nwogu, J. A. Goo, and T. D. Smith. 2015b. *Infrastructure modification for improving navigation at Faleasao Harbor in American Samoa*. ERDC/CHL TR-15-15. Vicksburg, MS: U.S. Army Engineer Research and Development Center.

Demirbilek, Z., and C. L. Vincent. 2015. Water wave mechanics. Chapter 1, EM 1110-2-1100 Part 2, *Coastal Engineering Manual*. Vicksburg, MS: U.S. Army Engineer Research and Development Center.

Demirbilek, Z., and J. Rosati. 2011. *Verification and validation of the Coastal Modeling System, Report 1: Summary report*. ERDC/CHL TR-11-10. Vicksburg, MS: U.S. Army Engineer Research and Development Center.

El Asmar, W., and O. Nwogu. 2006. Finite volume solution of Boussinesq-type equations on an unstructured grid. In *Proceedings, 30th International Conference on Coastal Engineering*. Coastal Engineering Conference, vol. 30, no. 1, American Society of Civil Engineers, 73–85. San Diego, CA.

Nwogu, O. 1993a. On the generation of infragravity waves by shoaling multidirectional waves. In *Proceedings, 2nd International Symposium on Ocean Wave Measurement and Analysis*. American Society of Civil Engineers. New York, NY.

Nwogu, O. 1993b. Alternative form of Boussinesq equations for nearshore wave propagation. *Journal of Waterway, Port, Coastal and Ocean Engineering, ASCE* 119(6):618–638.

Nwogu, O. 1994. Nonlinear evolution of directional wave spectra in shallow water. In *Proceedings, 24th International Conference on Coastal Engineering,* ASCE, 1, 467–481. Kobe, Japan.

Nwogu, O. G. 1996. Numerical prediction of breaking waves and currents with a Boussinesq model. In *Proceedings, 25th International Conference on Coastal Engineering,* ASCE, 4, 4,807–4,820. Orlando, FL.

Nwogu, O. G. 2000. Time domain simulation of long-period oscillations in harbors. In *Proceedings, 27th International Conference on Coastal Engineering,* 4, 3,643–3,654. Sydney, Australia. http://dx.doi.org/10.1061/40549(276)284

Nwogu, O. 2006. Boussinesq modeling of landslide-generated waves and tsunami runup. In *Advanced Numerical Models For Simulating Tsunami Waves And Runup Advances in Coastal and Ocean Engineering*. Edited by P.L.-F Liu, H. Yeh, and. C. Synolakis, 10, 273–278. Singapore: World Scientific Publishing Company.

Nwogu, O. 2007. Numerical modeling of waves generated by high-speed vessels in shallow water with a coupled Boussinesq-Panel method. In *Proceedings, 9th International Conference on Numerical Ship Hydrodynamics*, 331–343. Ann Arbor, MI.

Nwogu, O. G. 2009. Interaction of finite-amplitude waves with vertically sheared current fields. *Journal of Fluid Mechanics* 627:179–213. http://dx.doi.org/10.1017/S0022112009005850

Nwogu, O. G., and Z. Demirbilek. 2001. *BOUSS-2D: A Boussinesq wave model for coastal regions and harbors*. ERDC/CHL TR-01-25. Vicksburg, MS: U.S. Army Engineer Research and Development Center.

Nwogu, O., and Z. Demirbilek. 2004. Numerical modeling of ship-induced currents in confined waterways. In *Proceedings, 29th International Conference on Coastal Engineering,* 256–268. Lisbon, Portugal.

Nwogu, O., and Z. Demirbilek. 2006. Nonlinear wave interaction with submerged and surface-piercing porous structures. In *Proceedings, 30th International Conference on Coastal Engineering,* 287–299. San Diego, CA.

Nwogu, O., and Z. Demirbilek. 2008. Nonlinear wave transformation and runup over fringing coral reefs. In *Proceedings, 31st International Conference on Coastal Engineering*. Hamburg, Germany.

Nwogu, O., and Z. Demirbilek. 2010. Infragravity wave motions and runup over shallow fringing reefs. *Journal of Waterway, Port, Coastal, and Ocean Engineering, ASCE* 36(6). http://ascelibrary.org/doi/abs/10.1061/(ASCE)WW.1943-5460.0000050

CMS-Wave references

Lin, L., and Z. Demirbilek. 2005. Evaluation of two numerical wave models with inlet physical model. *Journal of Waterway, Port, Coastal, and Ocean Engineering, ASCE* 131(4):149–161.

Lin, L., Z. Demirbilek, H. Mase, and F. Yamada. 2008. *CMS-Wave: A nearshore spectral wave processes model for coastal inlets and navigation projects*. ERDC/CHL TR-08-13. Vicksburg, MS: U.S. Army Engineer Research and Development Center.

Lin, L., Z. Demirbilek, and H. Mase. 2011. Recent capabilities of CMS-Wave: A coastal wave model for inlets and navigation projects. In *Proceedings, Symposium to Honor Dr. Nicholas Kraus. Journal of Coastal Research*, Special Issue 59. Fort Lauderdale, FL.

Lin, L., Z. Demirbilek, R. Thomas, and J. Rosati. 2011. *Verification and validation of the Coastal Modeling System, Report 2: CMS-Wave*. ERDC/CHL TR-11-10. Vicksburg, MS: U.S. Army Engineer Research and Development Center.

Lin, L., and Z. Demirbilek. 2012. *Coupled BOUSS-2D and CMS-Wave modeling approach for harbor projects*. ERDC/CHL CHETN-IV-84. Vicksburg, MS: U.S. Army Engineer Research and Development Center.

Sanchez, A., W. Wu, T. M. Beck, H. Li, J. Rosati III, R. Thomas, J. D. Rosati, Z. Demirbilek, M. Brown, and C. Reed. 2011a. *Verification and validation of the Coastal Modeling System, Report 3: Hydrodynamics*. ERDC/CHL 11-10. Vicksburg, MS: U.S. Army Engineer Research and Development Center.

Sanchez, A., W. Wu, T. M. Beck, H. Li, J. D. Rosati, Z. Demirbilek, and M. Brown. 2011b. *Verification and validation of the Coastal Modeling System, Report 4: Sediment transport and morphology change*. ERDC/CHL TR-11-10. Vicksburg, MS: U.S. Army Engineer Research and Development Center.

Thompson, E. F., L. Lin, L. Hadley, and J. M. Hubertz. 1998. *Wave response of Kikiaola Harbor, Kauai, Hawaii*. Miscellaneous Paper CHL-98-5. Vicksburg, MS: U.S. Army Engineer Research and Development Center.

Appendix A: Description of CMS

The CMS-Wave module of the Coastal Modeling System (CMS) was used for the numerical modeling estimates of waves at Hilo Harbor. A brief description of the CMS is provided here for completeness.

As shown in Figure A-1, the CMS is an integrated suite of numerical models for waves, flows, sediment transport, and morphology change in coastal areas. This modeling system includes representation of relevant nearshore processes for practical applications of navigation channel performance and sediment management at coastal inlets and adjacent beaches. The development and enhancement of CMS capabilities continues to evolve as a research and engineering tool for desktop computers.

CMS uses the Surface-water Modeling System (SMS) interface for grid generation and model setup as well as for plotting and post-processing. The Verification and Validation (V&V) Report 1 (Demirbilek and Rosati 2011) and Report 2 (Lin et al. 2011) have detailed information about the CMS-Wave features and evaluation of model's performance skills in a variety of applications. The Report 3 and Report 4 by Sanchez et al. (2011a,b) describe coupling of wave-flow models, hydrodynamic and sediment transport, and morphology change aspects of CMS-Flow. The performance of the CMS for a number of applications is summarized in Report 1. Details are described in the three companion V&V Reports 2, 3, and 4.

Figure A-1. The CMS framework and its components.

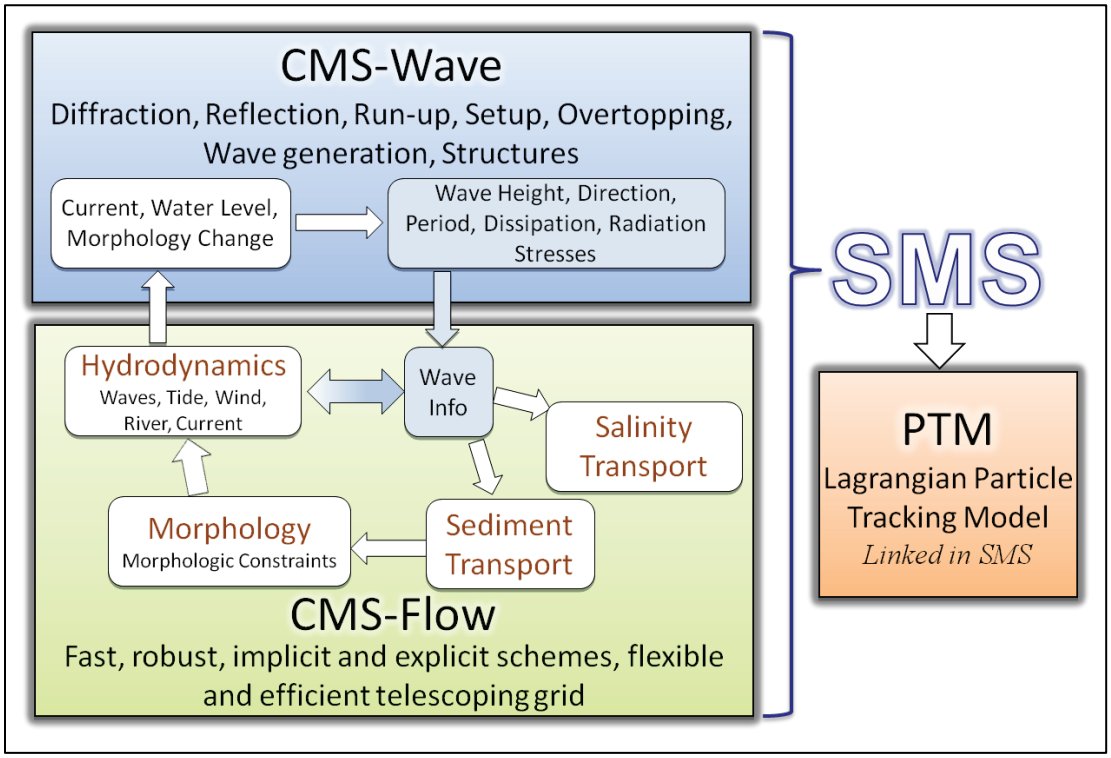

The CMS-Wave, a spectral wave model, is used in this study given the large extent of modeling domain over which wave estimates were required. Details of the wind-wave modeling are described in Chapter 3 of this report. The main wave processes included in the CMS-Wave are wind-wave generation and growth, diffraction, reflection, dissipation due to bottom friction, white-capping and breaking, wave-current interaction, wave runup, wave setup, and wave transmission through structures. The height and direction of waves approaching the Hilo Bay change due to wave shoaling, refraction, diffraction, reflection, and breaking. Waves propagating over the reefs outside the Federal breakwater and through the entrance interact with bathymetry, surrounding land features, currents, and coastal structures. These bathymetric and land features affect waves propagating into the navigation channel and interior of harbor.

CMS-Wave model solves the steady-state, wave-action balance equation on a nonuniform Cartesian grid to simulate steady-state spectral transformation of directional random waves from buoys or wave hindcast stations in deep water to the Hilo Bay. CMS-Wave is designed to simulate wave processes with ambient currents in navigation channels, coastal inlets, and harbors. The model can be used either in half-plane or full-plane mode for spectral-wave transformation (Lin and Demirbilek 2005;

Lin et al. 2008: Demirbilek et al. 2007b). The half-plane mode is default because in this mode CMS-Wave can run more efficiently as waves are transformed primarily from the seaward boundary toward shore. Lin et al. (2008 and 2011) describes features of the model and provides step-by-step instructions with examples for application of CMS-Wave to a variety of coastal inlets, ports, structures, and other navigation problems. Publications listed in the V&V reports and this report provide additional information about the CMS-Wave and its engineering applications. Additional information about CMS-Wave is available from the CIRP website: http://cirp.usace.army.mil/wiki/CMS-Wave.

The CMS-Flow model was not used in this study. Brief information regarding CMS-Flow is provided. CMS-Flow is a 2D shallow-water wave model that can be used for hydrodynamic modeling (calculation of water level and current). Both the explicit and implicit versions of flow (circulation) model are available to provide estimates of water level and current given the tides, winds, and river flows as boundary conditions. CMS-Flow calculates hydrodynamic (depth-averaged circulation), sediment transport and morphology change, and salinity due to tides, winds, and waves.

The CMS-Flow hydrodynamic model solves the conservative form of the shallow water equations that includes terms for the Coriolis force, wind stress, wave stress, bottom stress, vegetation flow drag, bottom friction, wave roller, and turbulent diffusion. Governing equations are solved using the finite volume method on a nonuniform Cartesian grid. Finite-volume methods are a class of discretization schemes, and this formulation is implemented in finite-difference for solving the governing equations of coastal wave, flow, and sediment transport models. See the V&V Reports 3 and 4 by Sanchez et al. (2011a,b) for the preparation of the flow model at coastal inlet applications. Additional information about CMS-Flow is available from the CIRP website: http://cirp.usace.army.mil/wiki/CMS-Flow.

Although hydrodynamic, sediment transport, and morphology change modeling were not considered in this study, it is noted for future reference that there are three sediment transport models available in CMS-Flow: (a) a sediment mass balance model, (b) an equilibrium advection-diffusion model, and (c) a nonequilibrium advection-diffusion model. Depth-averaged salinity transport is simulated with the standard advection-

diffusion model and includes evaporation and precipitation. The V&V Report 1, Report 3, and Report 4 describe the integrated wave-flow-sediment transport and morphology change aspects of CMS-Flow. The performance of CMS-Flow is described for a number of applications in the V&V reports.

Appendix B: Description of BOUSS-2D (BD2)

The Boussinesq wave model BOUSS-2D (B2D) is an advanced modeling approach for nonlinear wave propagation nearshore (Nwogu and Demirbilek 2001). This technology was developed and implemented in the Surface-water Modeling System (SMS) in 1990s through early 2000 and has since been used by Districts for navigation channels, inlets, harbors, coastal structures, moored vessels, floating breakwaters, and wave runup and overtopping on revetments, shorelines, and levees. Recent publications describe different applications of B2D model (Demirbilek et al. 2005a,b, 2007a,b,c, 2008, 2009; Nwogu and Demirbilek 2010). Additional information about B2D is available from these and other related publications in the References section of this report.

Types of problems for B2D application

The list below shows types of wave problems which can be simulated using Boussinesq wave models.

- Harbor/port/marina problems: harbor resonance, harbor and marina infrastructure modifications
- Generation of wave sub- and superharmonics
- Wave dissipation over porous media
- Wave reflection and diffraction from structures, shorelines, and variable surfaces
- Wave-wave interactions in shallow water
- Channel deepening/widening/realignment
- Wave-structure interactions: levees, flood walls, barriers, revetments, seawalls, groins, and breakwater design and repair (coastal and inland)
    - Wave runup/overtopping
    - Structure loading (wave forces)
    - Structure freeboard requirements
    - Frictional dissipation (i.e., waves on vegetated surfaces)
    - Wave interaction with array of structure types

    - Embankment stability
    - Wave interaction with complex geometries of levees, navigation channels, canals, ports/harbors, etc.
- Inundation mapping–overland propagation and runup
- Bore propagation through rivers and canals
- Transient waves (tsunamis, sneaker waves)
- Vessel-generated waves and ship wakes
    - Vessel-generated waves and effect on shorelines
    - Vessel-generated bed velocities and shear stresses
    - Vessel interactions with other vessels and with locks and dams

A few example applications are shown at the end of Appendix B.

Background

B2D model was used for numerical modeling of waves at Hilo Harbor, covering the nearshore part Hilo Bay between approximately 40 ft depth contour and the shorelines. Included in the modeling were the fringing reefs outside the Federal breakwater, the breakwater, harbor entrance, navigation channel, reefs to the north and south of the channel and interior harbor, the mooring and turning basin, and the Piers area. Chapters 1 through 3 described the study plan, purpose of numerical modeling, and implementation details of the modeling tasks including modeling performed to support the ship simulator study. Only a brief description of the B2D features is provided here because details of model theory, numerical methods used to solve the governing equations, and examples are available from the references listed.

Note that Boussinesq models are essentially shallow-water wave equations (SWWE) models with some extra dispersive and nonlinear terms. Models in this class excel under conditions of nonlinearity (large and/or long waves in shallow depths). Nearshore wave processes modeled extremely well by Boussinesq models include nearshore wind-wave propagation, harbor resonance, nonlinear shoaling, runup and inundation, nearshore circulation, tsunamis, and wave-structure and wave-ship-bank

interactions. Because Navier-Stokes models are not practical for field-scale problems, Boussinesq models presently are the preferred computational tools for calculating runup and overtopping of vertical or near-vertical walls and impulsive forces on structures. Boussinesq models can propagate vessel-generated waves if a source term is added for generation (i.e., moving pressure source or internal boundary). Boussinesq models are much better at this than shallow-water models because they include both short and long waves whereas SWWEs can only represent the long-wave component of the vessel-induced disturbances.

The B2D computes changes to waves caused by shoaling and refraction over variable bathymetry, reflection and diffraction from shorelines and structures, and nonlinear wave-current and wave-wave interactions. The internal Boussinesq equations defining the B2D do not contain adjustable parameters. Potential errors are introduced in numerical discretization of mathematical equations, imperfect boundary conditions, and physical processes that contain process-specific parameters such as wave turbulence, dissipation, bottom friction, and boundary reflectivity. The B2D needs field data because it can simulate processes that cannot be properly scaled in physical models, and consequently, these B2D model parameters are best calibrated with field data since they may not be estimated well by physical models (i.e., laboratory experiments) due to scaling effects. In the absence of field data, physical model data (if available) could be used in B2D for validation and calibration of boundary conditions, material parameters, and numerical algorithms. Generally, errors in the nearshore wave estimates come from two sources: (a) the model itself and (b) input to the model, including errors in the incident-wave conditions, bathymetry, and boundary specifications. The largest errors are associated with the specification of incident-wave parameters, simplification of wave breaking, dissipation processes, and contamination from model boundaries.

The B2D provides spatially and temporally varying wave, current, and water-level parameter estimates for engineering problems. Estimates include significant wave height, peak period and direction, wave spectrum, time-series of surface elevation, velocity and pressure, and wave-induced circulation. B2D model interface is operational in the SMS for grid generation and visualization of model results. The custom-built SMS interface of B2D allows users to setup and run the model in an intuitive

manner with built-in safeguards (Demirbilek et al. 2005a,b). The B2D can be run on PCs, workstations, and supercomputers.

The B2D consists of a set of comprehensive numerical modeling systems based on a time-domain solution of Boussinesq-type equations for simulating waves (wind-waves and vessel-generated waves) and their propagation in coastal regions, harbors, and waterways. The B2D represents most of wave phenomena of interest in the nearshore zone for navigation projects, inlets, harbors, levees, structures, reefs, wetlands, ship-wakes, wave-ship-bank interactions, and wave-current-structure interactions. The B2D-based engineering analysis systems may be used in navigation infrastructure design with a risk-based, probabilistic-design approach to evaluate life-cycle cost of Alternatives, operation, and maintenance of coupled systems in deciding the benefit or negative consequences of structures in projects. The B2D has capability of replacing considerably more expensive physical models with flexibility and generality for extension to sediment transport and morphology change, channel infilling, and water-quality issues. The USACE Operations and Maintenance (O&M) budget for dredging navigation channels and expansion of ports/harbor economic capacity will continue to increase with calls for deepening and widening of channels and harbors to accommodate future fleets of larger and faster vessels with greater width and draft. Vessel-to-vessel and vessel-to-bank interactions and risk of accidents will also increase with these demands. Aging and natural deterioration of navigation structures increase vessel transit and maneuvering risks along the high-traffic shipping routes, channels, and ports.

Numerical models that solve Boussinesq-type water-evolution equations are commonly used to investigate surface-wave propagation and transformation in coastal regions. Most of the models use finite-difference schemes to discretize the equations over uniformly spaced rectangular grids (Nwogu and Demirbilek 2001). The popularity of finite difference schemes is largely based on their simplicity and ease of implementation. However, the use of structured grids can severely restrict the potential application of such models to complex boundary problems such as coastal flooding over complex topography, wave propagation in curved channels, wave interaction with coastal structures of arbitrary shape, and wave agitation in harbors of arbitrary shape. Because unstructured grids provide users the flexibility of modeling complex geometries, and the grid

resolution can be refined where needed such as near structures or in shallow regions, it was therefore highly desirable to develop an unstructured-grid version of the finite-difference B2D model used in civil and military works. The development of an unstructured-grid, finite-volume version of B2D has been completed. This new model is being tested on supercomputers, and its interface in SMS is presently under development.

The B2D is designed to simulate wave processes with ambient currents at coastal inlets and in navigation channels. The model can be used for spectral-wave transformation. Lin and Demirbilek (2012, 2005) provide step-by-step instructions with examples of coupled B2D and CMS-Wave modeling application to harbor projects, coastal inlets, ports, structures, and other navigation problems. Nwogu and Demirbilek (2001), Demirbilek et al. (2005a,b) and other pertinent publications listed in the References provide further information about the B2D and example engineering applications. Additional information about B2D is also available from these websites:

http://cirp.usace.army.mil/wiki/BOUSS-2D

http://www.xmswiki.com/xms/SMS:BOUSS-2D.

In this study, the coupled B2D model was used for wave modeling nearshore to evaluate merits of eight proposed Alternatives to improve conditions inside the existing harbor. Details of this B2D modeling are described in Chapter 4 of this report.

Example applications

The images in Figures B-1 through B-10 show some recent examples of B2D model applications. See References for other types of applications.

Figure B-1: BOUSS-2D calculated wave-induced current field for Pillar Point Harbor, CA.

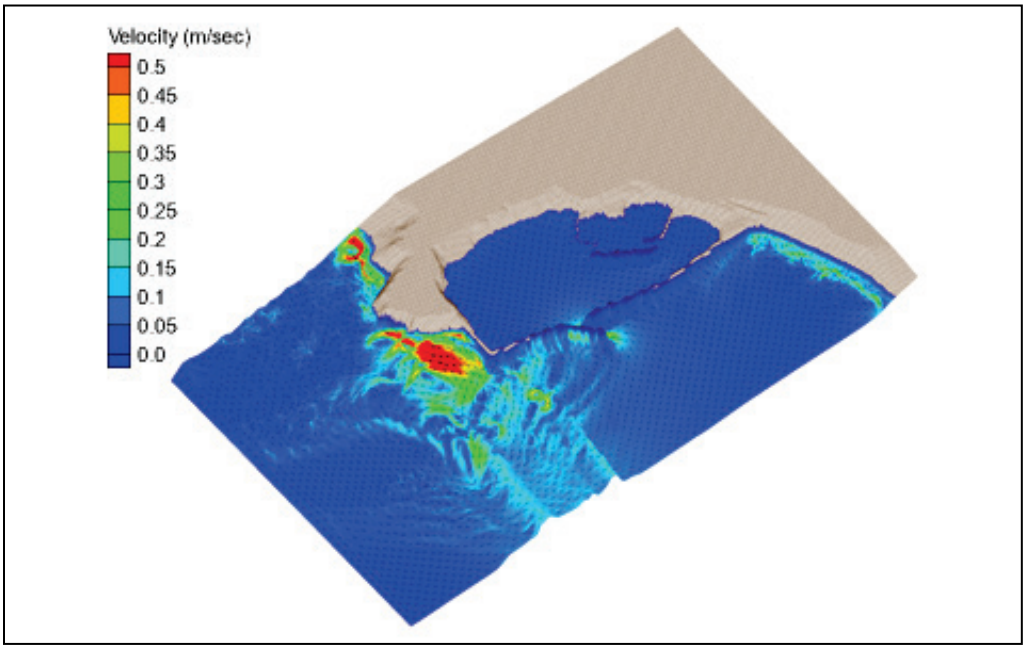

Figure B-2: Calculated wave fields by (a) BOUSS-2D and (b) CMS-Wave at Point Judith Harbor, RI, for incident wave from south-southeast.

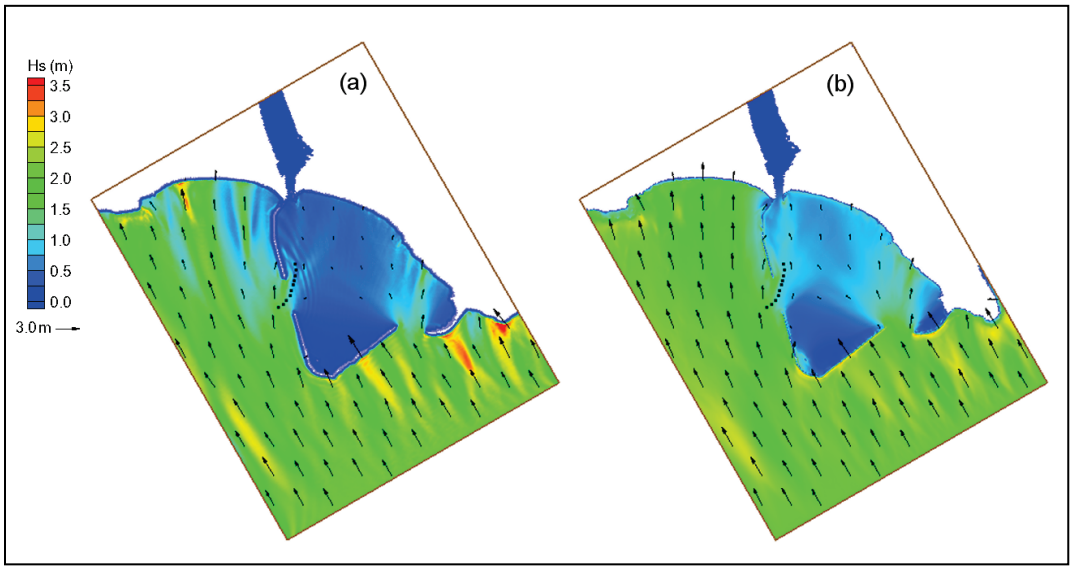

Figure B-3. Wave propagation inside a bay.

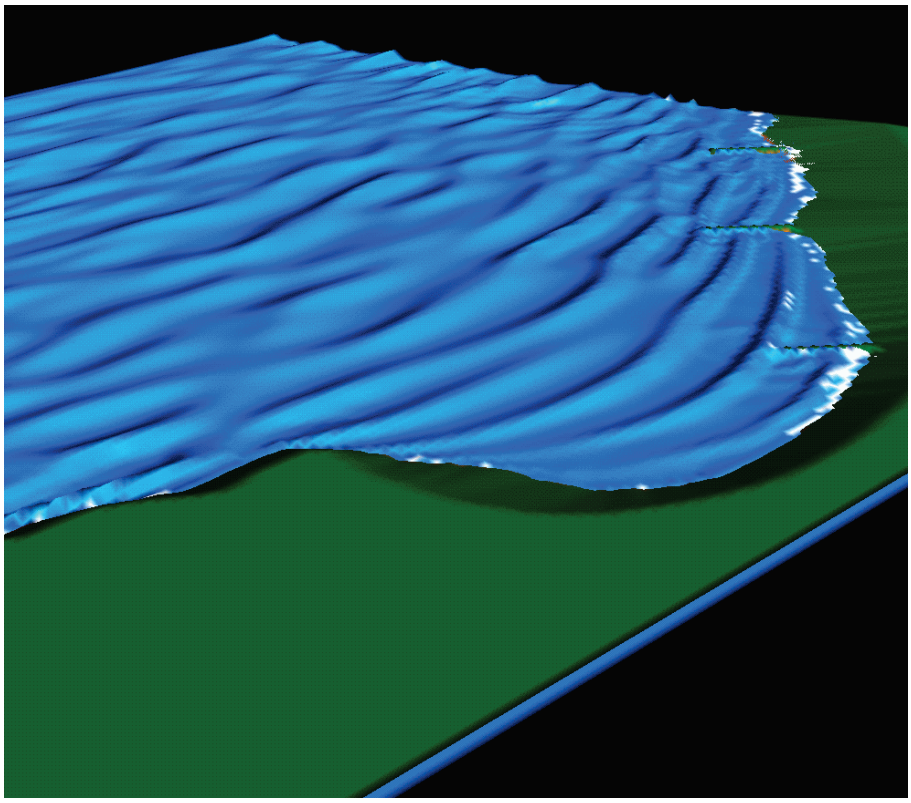

Figure B-4. Wave field around a detached breakwater.

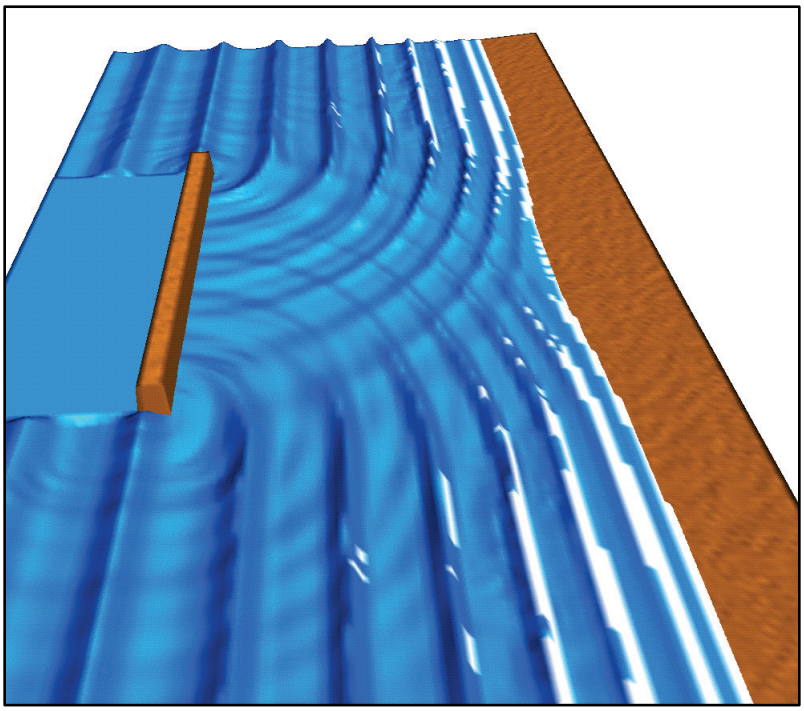

Figure B-5. Waves, wave-induced current, and circulation near a reflective jetty of an inlet.

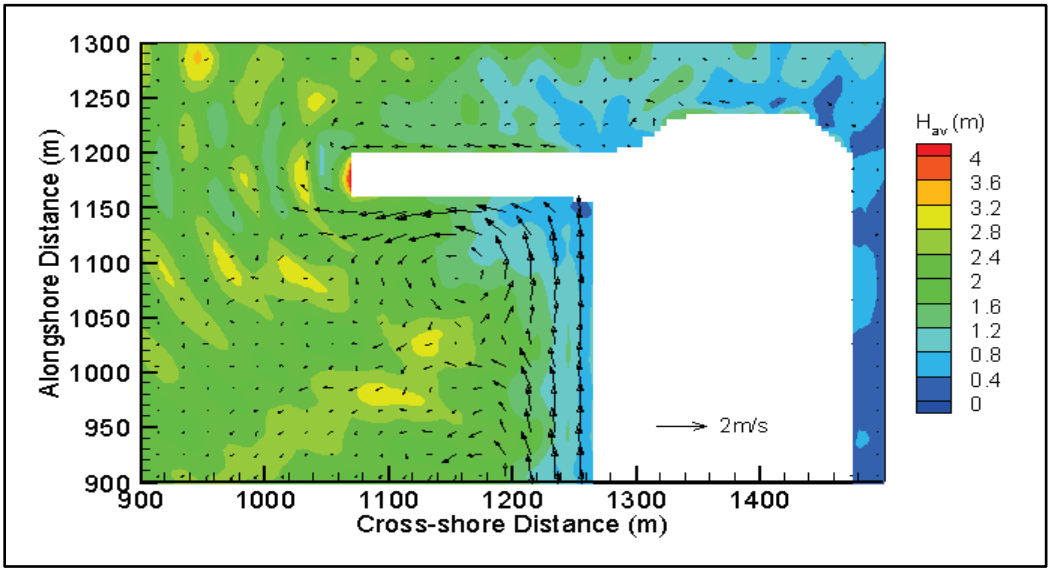

Figure B-6. Wave-induced current field developed between two groins placed on a beach.

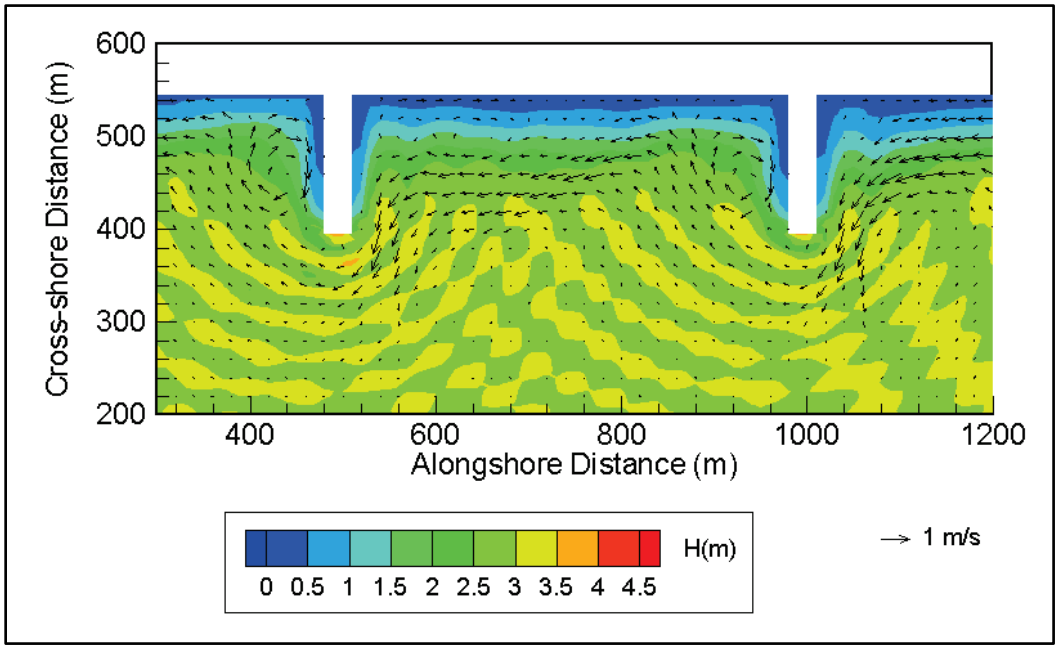

Figure B-7. Multiple ships moving (in transit) in a harbor.

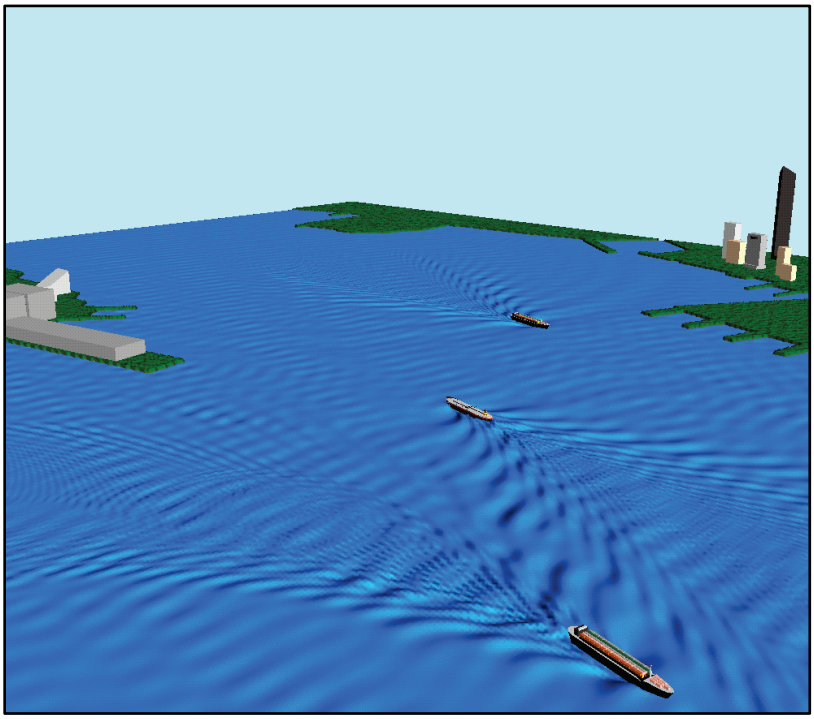

Figure B-8. BOUSS-2D domain for the Oyster Pt, CA, entrance and east marina.

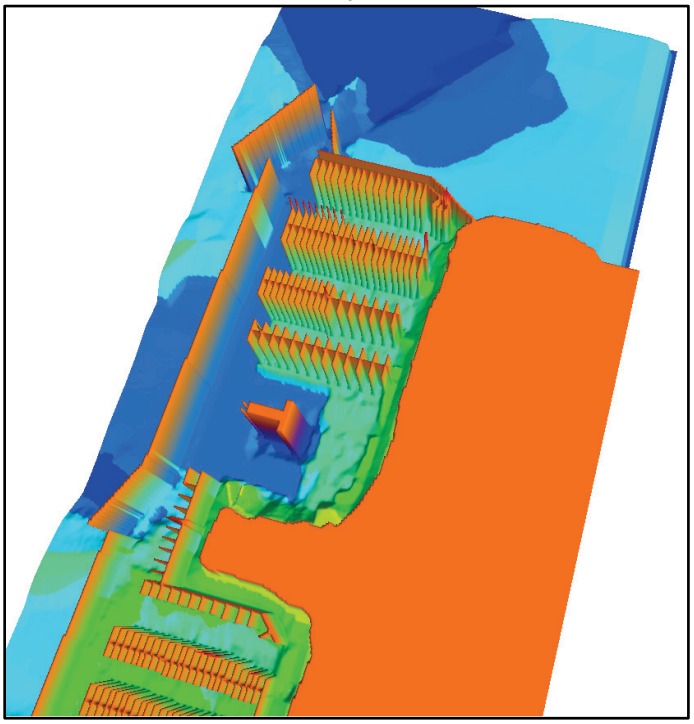

Figure B-9. BOUSS-2D grid for changes to entrance of Diversey Harbor, MI.

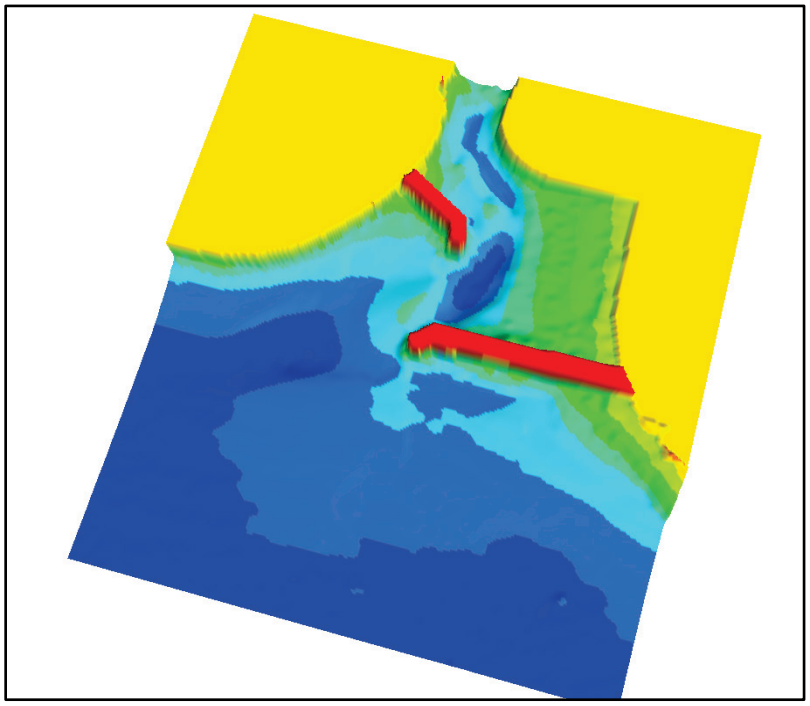

Figure B-10. BOUSS-2D runup/overtopping toolbox in SMS for a fringing reef application.

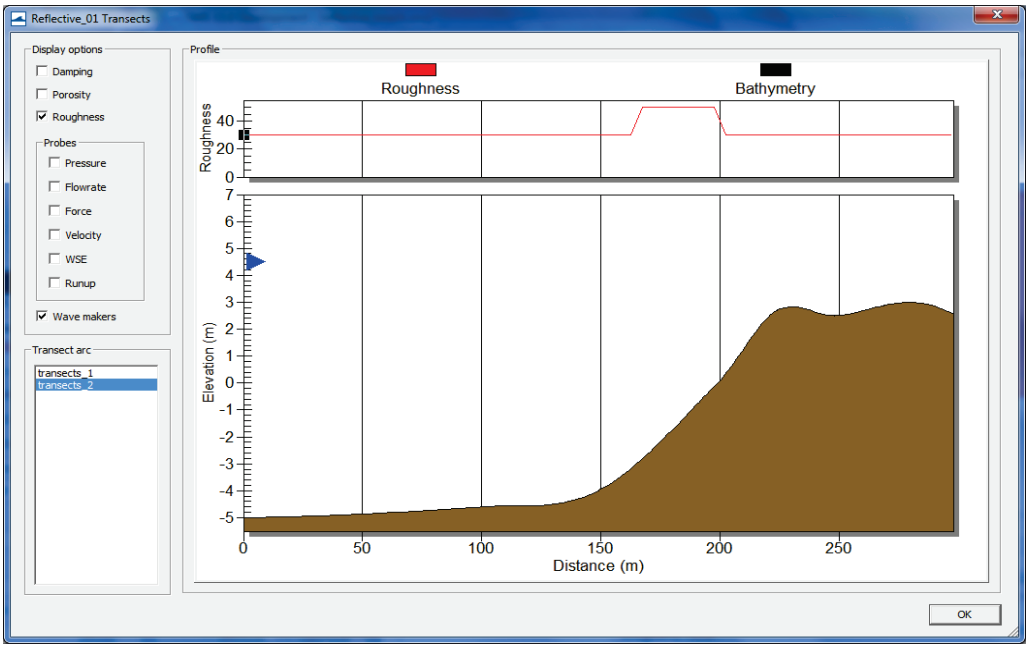

REPORT DOCUMENTATION PAGE

Form Approved
OMB No. 0704-0188

1. REPORT DATE *(DD-MM-YYYY)*	2. REPORT TYPE	3. DATES COVERED *(From - To)*
June 2016	Final	

4. TITLE AND SUBTITLE
Assessment of Modifications for Improving Navigation at Hilo Harbor, Hawaii

5a. CONTRACT NUMBER

5b. GRANT NUMBER

5c. PROGRAM ELEMENT NUMBER

6. AUTHOR(S)
Zeki Demirbilek, Lihwa Lin, Okey G. Nwogu, Kent K. Hathaway, William C. Butler, Jessica H. Podoski, and Thomas D. Smith

5d. PROJECT NUMBER
454634

5e. TASK NUMBER
A1100-FY16 Rosati

5f. WORK UNIT NUMBER
58F268

7. PERFORMING ORGANIZATION NAME(S) AND ADDRESS(ES)
U.S. Army Engineer Research and Development Center
Coastal and Hydraulics Laboratory
3909 Halls Ferry Road
Vicksburg, MS 39180-6199

8. PERFORMING ORGANIZATION REPORT NUMBER
ERDC/CHL TR-16-9

9. SPONSORING / MONITORING AGENCY NAME(S) AND ADDRESS(ES)
U.S. Army Engineer District, Honolulu
Building T223
Fort Shafter, HI 96858

10. SPONSOR/MONITOR'S ACRONYM(S)
POH

11. SPONSOR/MONITOR'S REPORT NUMBER(S)

12. DISTRIBUTION / AVAILABILITY STATEMENT
Approved for public release; distribution is unlimited.

13. SUPPLEMENTARY NOTES

14. ABSTRACT

Numerical wave and flow modeling studies were conducted to evaluate modifications to improve navigation at Hilo Harbor, HI. Analysis of field data, hydrographic surveys, and numerical and ship simulation modeling calculations are described in this report. The existing mooring and turning basin area adjacent to the Federal channel cannot safely accommodate the size of vessels presently using the harbor. A second issue affecting navigation in Hilo Harbor is the surge problem, which occurs mostly during winter swells when ships are in the berthing areas, describing a pulling away of ship movement from the piers, a form of long-period wave phenomenon commonly known as harbor oscillation.

CMS-Wave and BOUSS-2D models were used to investigate potential Alternatives to address navigation conditions in Hilo Harbor, with field data from 2007 and 2013–14 for calibration of the numerical models. Alternatives considered included modifying the breakwater, incorporating structures in the interior harbor, and deepening and expanding the mooring basin to provide more space for safe mooring and maneuvering of ships. Results of this study indicated that the addition of a spur to the western-most tip of breakwater would provide the greatest reduction in wave and currents in the harbor.

15. SUBJECT TERMS
hydrodynamics, models (mathematical), hydraulic structures (design and construction), Hilo Bay, HI (navigation), Hilo Bay, Hawaii

16. SECURITY CLASSIFICATION OF:			17. LIMITATION OF ABSTRACT	18. NUMBER OF PAGES	19a. NAME OF RESPONSIBLE PERSON Zeki Demirbilek
a. REPORT	b. ABSTRACT	c. THIS PAGE			19b. TELEPHONE NUMBER *(include area code)*
Unclassified	Unclassified	Unclassified	SAR	160	601-634-2834